IMPULSE BREAKDOWN OF A POINT-PLANE GAP IN SF_6 AND SF_6/N_2 MIXTURES

Thesis submitted in accordance with the requirements
of the University of Liverpool for the degree of
Doctor in Philosophy

by

HORATIO RODRIGO

December, 1982

BEST COPY

AVAILABLE

Poor text in the original thesis.
Some text bound close to the spine.
Some images distorted

ABSTRACT.

A dual photomultiplier system and a field probe has been used to study the optoelectrical phenomena is commercially pure SF_6 and mixtures of SF_6 with oxygen free N_2, under positive impulse voltages in a point plane gap. The luminous extension of the predischarge, the electric field at the cathode, and where possible the velocity of discharge propagation has been measured. An extrapolation technique has been used to estimate the critical pressure, and the results have been compared with those of other recently published work. An attempt has been made to establish the different regimes of operation with regard to leader formation both prior to and after streamers cross the gap. This has been done with particular emphasis on the d/r ratio and the field variation with increment in voltage. The cloud model has been shown to be inoperative under impulse voltage conditions such as in this thesis. Comparisons have been made of critical pressure determined under d.c. conditions with any available results obtained using impulse voltages. An attempt has been made to explain the large discrepancy particularly in SF_6 between the calculated and experimentally determined values of V_i, the corona initiation voltage. The internal electric field and the electrostatic radius of the discharge channel has been estimated. The analysis of the experimental results has been carried out for the stem and leader stages of the discharge development using an electrostatic model, prior to the streamers crossing the gap and reaching the cathode. By comparing the results with those of other authors, it has been shown that : the results of the leader internal electric field are in reasonable agreement with the work of others.

ACKNOWLEDGEMENTS

I would like to thank Professor J.D. Craggs and Professor J.H. Leck for the provision of the laboratory facilities.

I would like to express my sincere thanks to Dr. P.A. Chatterton, my supervisor, for the interest and the enthusiasm with which he has directed the work, and for many hours of most fruitful discussion on this investigation.

I am also most grateful to the Technical Staff of the Department for their willingness to co-operate and above all their forbearance with me.

I would like to acknowledge with thanks the financial support of the General Electric Company, over the past two years. It was their funds that made the work discussed in this thesis a reality.

The continued interest shown by Professor J.K. Nelson and Professor J.M. Meek is much appreciated.

Thanks are also due to Dr. A.G. Leaver, Warden of Rankin Hall for appointing me as a Tutor in Rankin Hall and continuing the tenure over the last three years.

For early encouragement and continued interest I would like to express my thanks to the staff of the Department of Electrical Engineering, Royal Melbourne Institute of Technology. In particular I would like to thank Dr. J. Hulanicki, Dr. S. Shihab and Dr. L. Doukas.

Finally, I would like to thank Miss Brenda Caldwell for typing this thesis.

CHAPTER 1

1.0 INTRODUCTION

The conduction of electricity through gases and the electrical breakdown of gases are of interest from both a purely scientific and a technological sense. From studies of the phenomena in gaseous media it is possible to increase our knowledge of fundamental physical processes, and the earliest experiments were carried out with this object, however, technological applications are equally important. For example, gases are used widely as insulating media in equipment ranging from Geiger tubes where the voltages range from 1 to 3 kV to switch gear, gas insulated cables, gas insulated transformers and metal clad sub-stations which operate at voltages of several hundred kV.

Under normal conditions a gas is an almost perfect insulator. If, however, stressed by a sufficiently high electric field its insulating properties fail and it becomes an almost perfect conductor. The transition to a conducting state is called "electrical breakdown" of the gas. This transition between the states can be exceedingly fast, so the electric spark has many uses in switching circuits, but in other applications the insulating properties are employed. For example, overhead power transmission lines are insulated by atmospheric air - and in such cases it is imperative to have adequate information about the breakdown strength of the gas under the conditions of use.

It is very rarely, or never, that one encouters a uniform field situation in an industrial or scientific application. A large volume of work has been carried out over a considerable period into the study of compressed

gaseous insulation. Some of this work will be reviewed in the next Chapter, with particular emphasis on non-uniform field studies in compressed SF_6 and its admixtures with other gases. In addition, the review will include work done on long gaps in atmospheric air under impulse voltage conditions.

The mechanisms of breakdown under highly non-uniform field conditions can be explained by the streamer theory. In the original streamer theory put forward independently by Meek (1940), Loeb and Meek (1941) and Raether (1940), it was proposed that a single avalanche to streamer transition would occur when the primary avalanche attained a critical size, but it was later suggested that a similar transition could also occur when the critical space charge of positive ions was built up by generations of avalanches. In this case the breakdown threshold is set by the Townsend Criteria, and so it is not possible to detect the change in the breakdown mechanism by steady state measurements of breakdown voltages and pre-breakdown currents alone. Measurements of formative time lags, along with the results of steady state investigations, provide information about the processes which occur in the discharge and, consequently, about the breakdown mechanism. The formative time lag is : the interval of time which elapses between the initiation of discharge by a primary electron and the collapse in voltage across the gap which is taken to indicate breakdown.

In the following sections various important concepts necessary for discussion of gas discharge problems are introduced and defined.

1.1 IONIZATION AND DECAY PROCESSES IN GASES

1.1.1 Ionization by electron collision

Ionization by electron impact is about the most important process in the breakdown of gases. The effectiveness of the electron impact ionization depends upon the electron energy. If an electron moving in an electric field collides with a gas atom, or molecule, then depending on the energy of the electron, the molecule may be ionized, which means that one or more of its electrons are raised to a level of energy which enables the electrons to be separated from the molecule. The molecule is then changed to a positively charged ion. The electrons thus liberated are then accelerated by the electric field and may themselves collide with other molecules, giving rise to a cumulative effect, which is manifested by an increase in current due to ionization. The electron energy distribution function determines the effectiveness of electrons to ionize the gas. Normally the mean energy of the electrons tends to increase with (E/p).

The increase in current was explained by Townsend (1915) by introducing a quantity α known as Townsend's first ionization coefficient. If an electron moving through a distance of 1 cm in the direction of the applied field produces by impact α new electrons, then the increase in the number of electrons over a small distance dx in the electrode gap is given by :

$$dn = \alpha \cdot n \, dx$$

integrating this expression over the gap length d

$$n = n_0 \, e^{\alpha d}$$

Hence

$$i = i_o e^{\alpha d} \qquad (1.1)$$

where, i_o is the current leaving the cathode and i the current at the anode. Experiments have suggested that the coefficient α depends on the gas pressure p as well as on the electric field strength E.

In travelling through a free path λ in the direction of an electric field E, an electron gains energy equal to λeE. If $\lambda eE \geqslant e V_i$, where V_i is the ionization potential of the gas, the electron will ionize the gas. The chance that an electron will ionize is governed by the probability of occurrence of free paths λ that are greater than or equal to λ_i, where $\lambda_i = \frac{V_i}{E}$.

It has been shown from the Kinetic theory that the number of electrons that will have free paths of length greater than λ_i is given by :

$$n = n_o e^{-(\lambda i / \lambda m)}$$

where n_o is the number of electrons starting out on free paths and λ_m is the mean free path, the number α of ionizing collisions per cm of path, which is equal to the number of free paths multiplied by the chance of a free path being longer than the ionizing length λ_i so that

$$\alpha = \left(\frac{1}{\lambda_m}\right) e^{-(\lambda_i / \lambda_m)}$$

$$= \left(\frac{1}{\lambda_m}\right) e^{-\left(\frac{V_i}{\lambda_m E}\right)}$$

but $\frac{1}{\lambda_m} = A p$, A being a constant

$$\frac{\alpha}{p} = A e^{-\left(\frac{A V_i p}{E}\right)}$$

$$= A e^{-\left(\frac{B p}{E}\right)}$$

Hence

$$\frac{\alpha}{p} = f(E/p) \qquad (1.2)$$

Thus, α is a function of E and p . It must be pointed out, however, that in the derivation of equation (1.2) above a number of simplifying assumptions were made. For instance, it was assumed that the probability of ionization is zero if an electron has energy less than $e V_i$ and is unity if the energy exceeds this value. This may not always be true. However, there is good agreement between the experimentally determined values of α and those calculated from equation (1.2). More exact methods of deriving the equation are discussed by Meek and Craggs (1953). Meek and Craggs have also given a summary of α determinations obtained by a number of workers.

1.1.2 Excitation

Electrons in transit through a gas will undergo excitation collisions with gas molecules. This is analogous to ionization collisions. However, due to the lower energy of some electrons they may collide with gas atoms and excite them to a higher energy state, which is less than that required to eject electrons off the atoms. The atoms so excited, recover to their normal state in 10^{-7} to 10^{-10} sec and in doing so release a quantum of energy or photons.

1.1.3 Photoionization

The photons that may be released due to excitation could ionize another atom whose ionization potential is equal to or less than that of the photon. This process is known as photoionization, and may be represented as

$$A + h\nu \longrightarrow A^{+} + e^{-}$$

A being a neutral atom and $h\nu$ the photon energy. For ionization to occur

$h\nu$ must be greater than or equal to $e V_i$ of the atom or molecule. If the quantum of energy $h\nu$ is greater than $e V_i$ then the excess energy may be imparted to the released electron as kinetic energy. The probability of an atom or molecule being photoionized depends upon the quantity ($h\nu - e V_i$). The larger this quantity is the greater the probability. If, however, the photon energy is less than $e V_i$ it may still be absorbed by the atom and raise the atom to a higher energy level. This process is known as photoexcitation.

Photoionization is a secondary process, and appears essential in the streamer breakdown mechanism.

1.1.4 Photoabsorption (μ)

Photoabsorption could be considered to be a special case of photoionization. Photons may be absorbed in their transit through a gas. This depends on the nature of the gas. In the process of absorption the photon disappears and the absorbed energy goes into excitation of the molecules with which they interact. Exactly as an excited atom emits a photon when the electron returns from a higher to a lower orbit, a similar process can take place when an atom absorbs an incident photon by letting an electron move to a further orbit. This reversible process can be expressed symbolically as

$$h\nu + A \rightleftharpoons A^*$$

An atom will absorb a photon if the lowest excitation energy of the atom is greater than the energy of the photon.

1.1.5 Ionization by Metastables

The lifetimes of some excited electronic states extends to long times, of the order of hundreds of milliseconds to seconds. The atoms that remain in this state are called metastables. If the energy of the metastable exceeds

the ionization energy V_i of another atom then on collision ionization may results. It can be represented thus

$$A^m + B \longrightarrow A + B + e$$

where A^m is a metastable atom. The energy of metastable A^m is denoted by V_m.

If, however, $V_m < V_i$ then the atom B will be excited on collision with A. This may be represented by

$$A^m + B \longrightarrow A + B^*$$

Another way the ionization reaction may proceed is as follows :

$$A^m + 2A \longrightarrow A_2^* + A$$

$$A_2^* \longrightarrow A + A + h\nu$$

The photon $h\nu$ released in the last reaction is of too low energy to cause ionization in the gas, but it may be able to release electrons from the cathode.

1.1.6 Thermal Ionization

As the temperature of a gas is raised to a high enough value the neutral atoms will acquire sufficient energy to ionize the atoms they impinge upon. Usually the term thermal ionization is applied to the ionizing action of molecular collisions, radiation and electron collisions that take place in gases at high temperature.

1.1.7 Electron Attachment - Negative Ion Formation

Electronegative gases such as oxygen, sulphur hexafluoride, some halogens and hydrocarbons have the property of attaching free electrons to neutral molecules to form stable negative ions. Negative ion formation is an extremely important process for gases of high dielectric strength. The

negative ions may be formed by (a) a direct electron capture, (b) dissociation or (c) a pair production process.

(a) $AB + e \longrightarrow (AB^-)^* \longrightarrow AB^- + h\nu$

(b) $AB + e \longrightarrow A + B^-$

(c) $AB + e \longrightarrow AB^* + e \longrightarrow A^+ + B^- + e$

In general electron capture processes occur at much lower electron energies than pair production processes.

By analogy with α, the Townsend first ionization coefficient, an attachment coefficient η may be defined.

η is the number of attachments produced in the path of a single electron in moving through a distance of 1 cm in the direction of the applied field. The loss of electron current over a distance dx due to attachment is

$$di = - i \eta \quad dx$$

hence $i_2 = i_1 e^{- \eta x}$

If E/p is sufficiently high, both ionization and attachment take place.

In this case the change in the number of electrons (n_x) over a small distance dx is

$$dn = n_x \alpha \, dx - n_x \eta \quad dx$$

$$= n_x (\alpha - \eta) \, dx$$

Integrating:

$$n_x = n_o e^{(\alpha - \eta)x}$$

The change in the number of negative ions over the distance dx is

$$dn' = n x \eta \quad dx$$

$$dn' = n_o \eta \, e^{(\alpha - \eta)x} \, dx$$

Integrating :

$$n = n_o \quad \frac{\eta}{(\alpha - \eta)} \quad (e^{(\alpha - \eta)d} - 1)$$

Thus the total current measured is given by

$$i = i_o \left[\frac{\alpha}{(\alpha - \eta)} \quad e^{(\alpha - \eta) d} \quad - \quad \frac{\eta}{(\alpha - \eta)} \right] \qquad (1.3)$$

where d is the gap length and i_o is the photoelectric emission current.

It may be seen that in the absence of attachment, i.e. $\eta = 0$, equation (1.3) reduces to equation (1.1).

1.1.8 Electron Detachment

Electrons may become detached from negative ions to give a neutral atom or molecule and an electron. The associative detachment process which is the inverse of dissociative attachment can be represented thus :

$$A^- + B \longrightarrow AB + e$$

Several authors have studied the reaction rates in gases such as Oxygen and Carbon Dioxide and Rees (1978) has made a survey of their work.

1.1.9 Recombination

This process can be thought of as the reverse of photoionization. When positive ions and electrons are present in a gas, collisions are likely to occur between them (Rees, 1978). If an electron on collision with a positive ion is captured by the ion, then the electron loses kinetic energy which is either emitted as a quantum of radiation, represented by

$$A^+ + B^- \longrightarrow AB + h\nu$$

(In this expression B^- may be an electron or negative ion). Or, alternatively,

a third body **C** may be involved and may absorb the excess energy. At low pressures the walls of the vessel containing the gas usually act as the third body, and as such there is hardly any recombination within the volume of gas, but at higher pressures three body collisions can occur and recombination in the gas itself takes place.

The rate of recombination is directly proportional to the concentrations of positive and negative ions and electrons. If there are n_+ positive ions and n_- negative ions per unit volume of gas then

$$\frac{dn_+}{dt} + \frac{dn_-}{dt} = - R\, n_+\, n_-$$

where R is the recombination coefficient.

In general,

$$n_+ = n_-$$

hence

$$\frac{dn}{dt} = - R\, n^2$$

1.2 ELECTRODE PROCESSES

The electrodes, certainly in uniform fields, play an important part in a gas discharge. By irradiating the cathode primary electrons can be supplied to start the discharge and secondary electrons are produced at the cathode to sustain it. Under normal conditions electrons are held within a solid material by electrostatic forces, and a minimum amount of energy $e\phi$ is required to release an electron. The work function ϕ is dependent on the material. The work function could be looked upon as a potential barrier which has to be overcome to release electrons. The energy required for the

release of electrons can be supplied to the cathode in several ways.

1.2.1 Photoelectric Emission

Photons that arrive at the cathode surface with energy equal to or greater than eø , the work function, can cause electrons to be released from the cathode. When the energy of the impinging photons exceeds eø the excess energy is used up by the electrons in acquiring kinetic energy. The photons themselves can be produced by radioactive sources and ultraviolet light.

1.2.2 Electron Emission Due to Positive Ion Impact

When a metal surface is bombarded with positive ions electrons are released from the surface depending on the energy of the positive ions. If the ionization energy of the positive ion is greater than twice the work function, eø, of the metal, then electrons are ejected from the metal, this is termed potential ejection (McDaniel, 1964). Metastable atoms which collide with the cathode can also cause electron emission, as can neutral atoms or molecules if they have sufficient energy. The various methods of electron emission due to particle impacts at the cathode are described by Loeb (1960), and McDaniel (1964).

1.2.3 Field Emission

Electrons can be liberated from the surface of a metal by an intense electric field as is associated with extreme non-uniform field situations such as fine wires and needle points. Under uniform field conditions it can occur if the electrode separation is small and the gas pressure high. The condition necessary here is the existence of an exceedingly high electric field.

1.3 BREAKDOWN PROCESSES IN GASES

1.3.1 Introduction

The processes that lead to breakdown in a gaseous medium will be presented and discussed in the rest of this Chapter. The first half will deal with the uniform field cases. However, reference will be made to the non-uniform field case from time to time in this half. The non-uniform case will be discussed in the second half. All the definitions given in Section 1 will be used freely throughout.

1.3.2 The Electron Avalanche

As was shown earlier when an electron leaves the cathode in a parallel plane electrode system, the number of electrons which arrive at the anode is given by equation (1.1)

$$n = n_o e^{\alpha d}$$

Thus, a single electron starting at the cathode grows exponentially to a very high number of electrons arriving at the anode. This collection of electrons is termed an electron avalanche.

In a non-uniform field situation, where the electric field E is dependent on the distance x, the electron number produced by collision is given by

$$n = e^{\int_{x_1}^{x_2} \alpha \, dx}$$

this too is called an electron avalanche. The electron avalanche is the fundamental building block of all gas discharge manifestations. The discharge growth will be affected by whether the electron avalanche is advancing in a convergent or divergent field.

1.3.3 Space Charge Field of an Avalanche

In non-uniform fields the discharge can be locally contained. These contained discharges are distinctly different from those predicted by the Townsend mechanism, and hence another process must be operational. The ionization channels are filamentary and branched. They can be started at relatively low voltages and are capable of travelling long distances. This phenomenon is known as a "streamer" because of its filamentary nature. Even under uniform field conditions, the field becomes distorted when the local space charge field attains a value equal to the applied field. The Townsend mechanism disregards the effect of the space charge on building up locally high fields.

The electric field around an avalanche is depicted in figure 1. The field behind and ahead of the avalanche is increased by the space charge that is generated, and reduced to a value less than the applied field, E, between the electron and ion cloud. The mechanism of streamer development in a uniform field geometry will be discussed now: it is appropriate to consider the simplest case, the parallel plate electrode system. When an electron, liberated from the cathode, undergoes the transition to an electron avalanche and reaches the anode, the electrons due to their high mobility are swept away and the positive ions, which are much slower, are left behind in a nearly conical channel with the head at the anode. Since the avalanche develops in an exponential manner the density of ions will be greatest near the anode. The positive ion charge will produce field distortion in both the radial and axial directions. Photoelectrons are formed in the surrounding gas which are capable of initiating auxiliary avalanches which will be directed towards

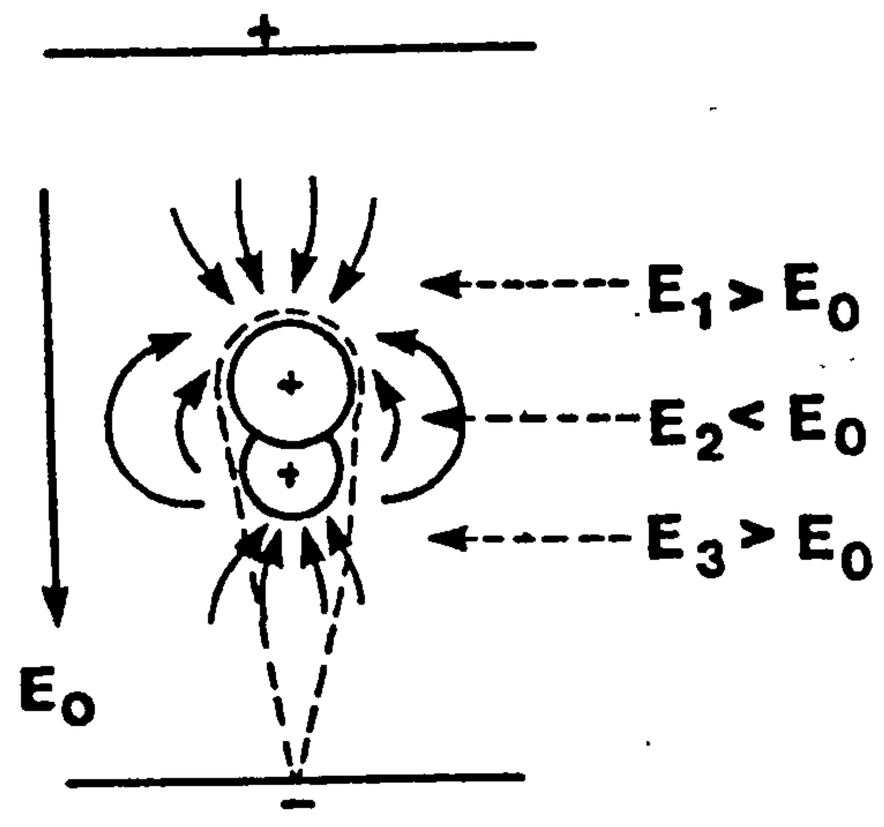

Figure 1 : Effect of space charge of an avalanche (Raether, 1964)

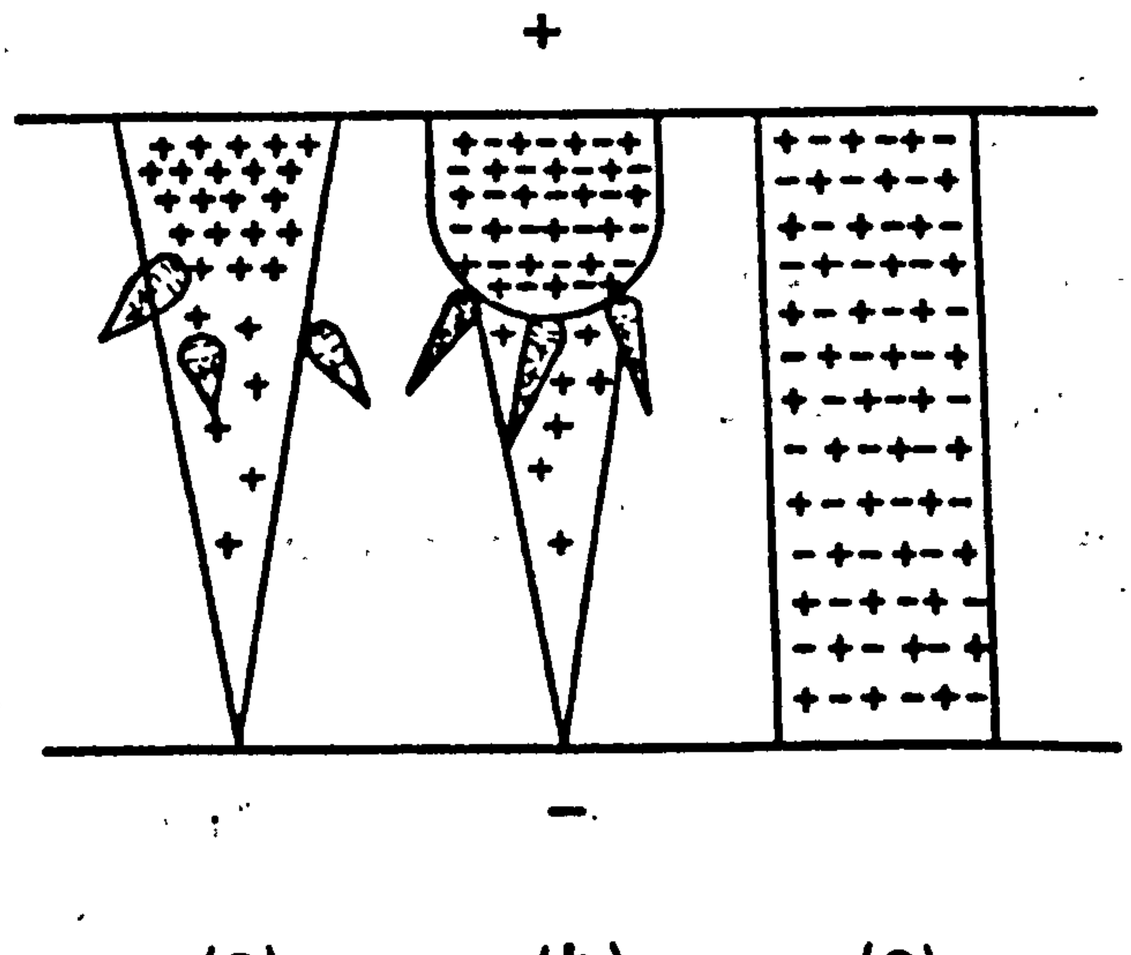

Figure 2 : Transition from an electron avalanche to a streamer and subsequent growth of a streamer across the gap (Meek and Craggs, 1953)

the stem of the original avalanche, if the space charge field developed due to the original avalanche is of the same order of magnitude as the externally applied field. The space charge field is greatest along the axis of the primary avalanche and hence the largest concentration of the auxiliary avalanches occur along the axis. Positive ions left behind these avalanches lengthen and increase the intensity of space charge of the primary avalanche in the direction of the cathode, theprocess develops into a self propagating streamer. The successive stages of development of a conducting channel are shown diagramatically in figure 2.

1.3.4 Townsend Criterion

The current in a spark gap increases as the applied voltage is increased according to the expression

$$i = \frac{i_o e^{\alpha d}}{1 - \gamma (e^{\alpha d} - 1)}$$

where γ is called the second Townsend ionization coefficient and represents secondary processes at the cathode. When the discharge becomes self-sustained the current rises to an indeterminate quantity, when the denominator of this equation becomes zero,

$$1 - \gamma (e^{\alpha d} - 1) = 0$$

since $e^{\alpha d} >> 1$

$$\gamma e^{\alpha d} = 1$$

Townsend defined this condition as the onset of a spark. Loeb (1961) has treated Townsend's theory in the following manner :

If $\gamma e^{\alpha d} < 1$ the discharge is not self sustaining and it ceases if the source of primary electrons is removed.

If $\gamma e^{\alpha d} = 1$ is defined as the sparking threshold which means that the number of ion pairs created are sufficient to cause one secondary electron and so cause a repetition of the avalanche process. The discharge is then self sustaining and can continue in the absence of the source producing i_o.

If $\gamma e^{\alpha d} > 1$ the ionization produced by successive avalanches is cumulative. The discharge grows rapidly until breakdown occurs.

1.3.5 The Streamer Theory

At low pressures the Townsend theory and the breakdown criterion are in agreement with experimental observations. This, however, is not the case for long gaps at pressures equal to and above atmospheric. The Townsend theory stipulates that the formative time for breakdown of a gap should be not less than the positive ion transit time, but it was shown by experimental observations that at atmospheric pressure the formative times are about 100 times less than the electron transit time. This observation alone does not prove that the Townsend theory is invalid, since a Townsend mechanism could still be operational with a rapid secondary process. Early measurements, however, of ionization currents in air showed that the variation of currents in the gap (which were logarithmetic due to the exponential nature of their increase) with gap length were linear even up to breakdown, from which it was concluded that no significant secondary process was active to any significant extent. It was also shown that at atmospheric pressure the breakdown voltage was independent of the cathode material, even further doubt was cast upon the existence of a cathode based secondary process.

As a consequence of many experimental observations, particularly those of Raether in cloud chambers, Meek (1940) and Raether (1940) independently proposed a "streamer" (or "kanal") theory of breakdown. This theory is based upon the considerations of individual electron avalanches, their transition to streamers, and the mechanism of streamer advance. It invokes processes in the gas such as electron avalanche formation according to the Townsend mechanism, photoionization, and space charge effects brought about by avalanches and streamers. As was stated earlier, the essential condition necessary for streamer formation is that the radial space charge field generated by the electron avalanche has to attain the same order of magnitude as the applied field. Unless this condition is fulfilled, there will not be any appreciable enhancement of ionization in the vicinity of the avalanche or diversion of auxiliary avalanches to the primary one.

To calculate the approximate magnitude of the space-charge field it is assumed that the positive ions are contained in a spherical volume of radius r at the head of the avalanche. The radial field E_r produced by this space charge, at the radius r is given by :

$$E_r = \frac{4}{3} \pi r N \epsilon$$

where N is the ion density and ϵ the electric charge. In moving along a small path length dx at the end of a distance x, the number of ion pairs produced will be given by $\alpha . e^{\alpha x} dx$, and hence,

$$N = \frac{\alpha e^{\alpha x}}{\pi r^2}$$

so that $$E_r = \frac{4 \epsilon \alpha e^{\alpha x}}{3 r}$$

where r is the radius of the avalanche head after moving a distance x ;

the value of r is dependent on the diffusion coefficient D and the temperature of the gas, T.

$$r = \sqrt{(2\,D\,T)}$$

therefore

$$E_r = \frac{4\,\varepsilon\,\alpha\,e^{\alpha x}}{3\sqrt{2D(x/v)}}$$

where v is the velocity of the avalanche and hence the electrons in the applied field E, if the mobility of the electrons is k ,

$$E_r = \frac{4\,\varepsilon\,\alpha\,e^{\alpha x}}{3.\sqrt{(2D/k)\,(x/E)}} \qquad (1.4)$$

For Air the value of $\frac{D}{k}$ is known, so that equation (1.4) becomes :

$$E_r = 5.27 \times 10^{-7}\ \frac{\alpha\,e^{\alpha x}}{(x/p)^{\frac{1}{2}}}\ \ V\ cm^{-1}$$

The criterion for inception of a streamer is that

$$E_r = k\,E$$

where $k \simeq 1$.

Substituting E for E_r and d for x in the above equation, and taking the logarithm,

$$\alpha d + \ell n\,(\alpha / p) = 14.66 + \ell n(E/p) + \ell n(d) - \tfrac{1}{2}\,\ell n\,(p\,d) \qquad (1.5)$$

Equation (1.5) is Meek's sparking criterion. Given the values of $(\frac{\alpha}{p})$, p , d and V_s , the sparking potential can be calculated, thus V_s for other values of p d can be obtained.

Raether suggested that for the transition from avalanche to streamer

to take place αd had to attain a critical value N. Since the values of α are known for a number of gases, it is possible to calculate values d_s, the breakdown gap length. By following this procedure it was found that the criterion for streamer formation was when

$$\alpha d \simeq 18 \text{ to } 20 \qquad (1.6)$$

The criteria proposed by Meek and Raether predict values for V_s which are in good agreement with those obtained experimentally.

Although the foregoing discussion was mainly confined to air, they can be extended to other gases and pressures other than atmospheric, provided the various constants for the different gases are known.

1.4 BREAKDOWN IN NON UNIFORM GAPS

The breakdown for gaps in which the field is non-uniform like point plane, cylindrical geometries, and sphere gaps is somewhat different and will be considered here in the light of the streamer theory.

Meek (1940) studied a gap between two spheres in terms of the streamer theory. In this case the number of ions pairs crossing the gap is given by an integral of the exponential of α across the gap. The criterion given by Meek (1940) for streamer formation under these conditions is :

$$E_r = 5.27 \times 10^{-7} \frac{\alpha_x \, e^{\int_0^x \alpha \, dx}}{(x/p)^{\frac{1}{2}}} \quad V \text{ cm}^{-1} \qquad (1.7)$$

where α_x is the value of α corresponding to the external field at the avalanche head. The assumption made in calculating the minimum breakdown voltage of the gap is that the transition from an avalanche to streamer occurs at the anode. The radial field E_r is then equal to the applied field at the

surface of the anode. For long gaps between spheres the field in the mid gap may fall to values where α would reach negligible values, thus making avalanche formation impossible. In this case the ionization will be confined to the region near the surface of the high voltage sphere (electrode). Under these circumstances Meek (1940, 1942) has suggested that electron avalanches do not cross the whole gap but that streamers are initiated by avalanches growing across the high field region enclosing one of the spheres, namely ; the highly stressed one. In this case the number of ion pairs in an avalanche is given by the exponential of the integral of α across one half of the gap only.

From the foregoing considerations Meek (1940, 1942) has calculated the sparking voltage at different gaps between spheres of different diameters. The resultant curves are shown in figure 3. In this the full curve is that measured. The dashed curves have been calculated on the assumptions (I) that the electron avalanche crosses the entire gap and (II) that the electron avalanche crosses only the high field region in the vicinity of the high voltage electrode. In the first case E_r as given by equation (1.7) includes the term $e^{\int_0^d \alpha dx}$ where d is the gap length, and in the second case, E_r includes the term $e^{\frac{1}{2}\int_0^d \alpha\, dx}$.

In highly divergent fields such as point plane gaps, the transition from an avalanche to a streamer defines the corona inception, and not the spark over voltage.

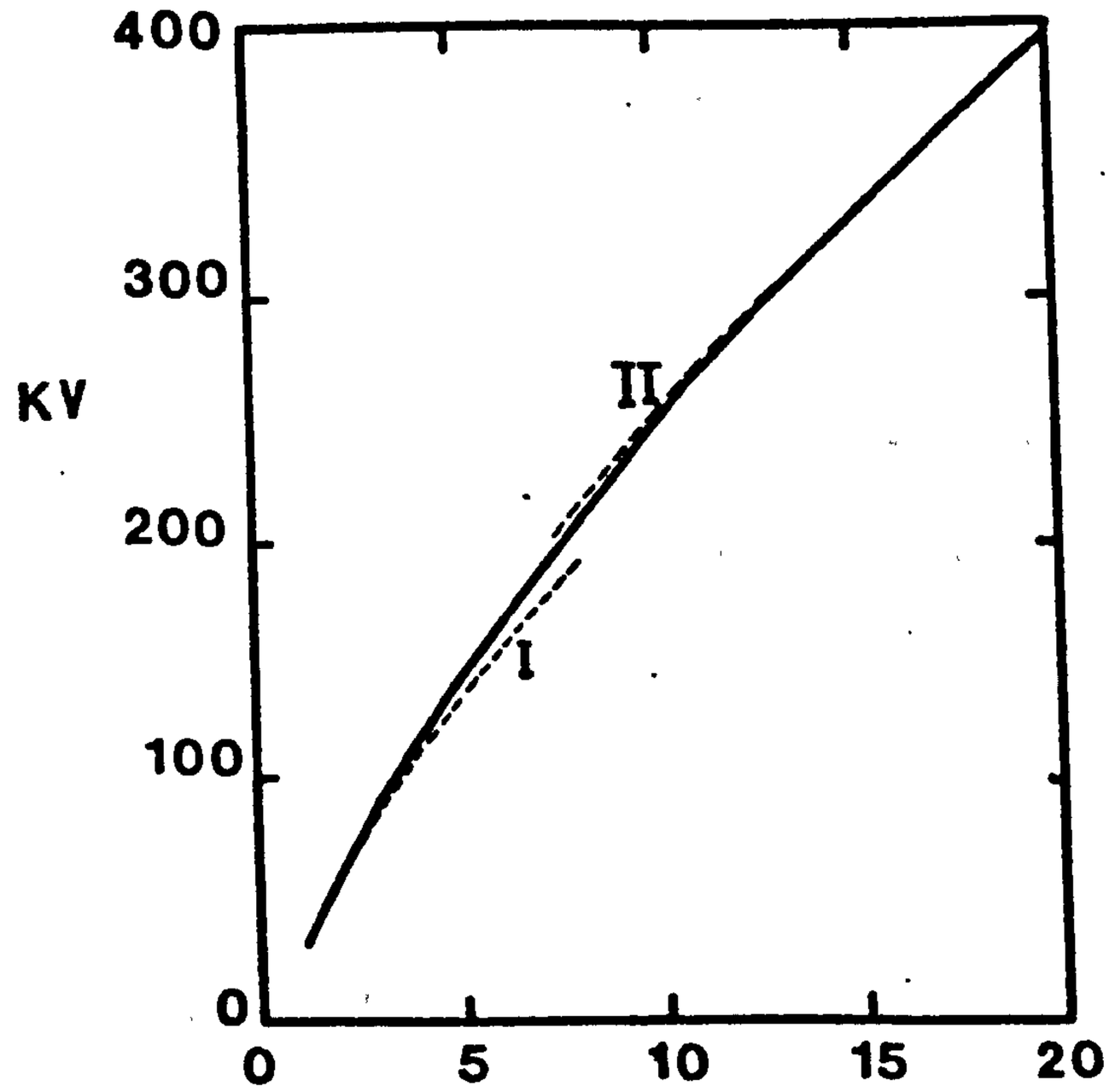

Figure 3 : Calculated and observed curves for the breakdown voltage between two spheres of equal diameter.

-------- calculated

———— observed

(Meek, 1942).

1.5 PARTIAL BREAKDOWN OR CORONAS

Partial breakdown or coronas are almost exclusive to non-uniform field geometries. Most of the analytical derivations made for the uniform field case do not apply, therefore, to the case when E and consequently α are functions of the position in space. However, the general concepts and the picture obtained can be applied in many instances to the non-uniform case. The differences between the two situations will be evident in the following discussions.

1.6 ANODE CORONAS

The discussions to follow will be to deal with positive point coronas, because the aim of this thesis is the study of positive point breakdown and pre-breakdown phenomena. However, negative corona will be encountered at a later stage and so some mention of their existence will be made, but a detailed analysis of them will not be given.

1.7 PRE-ONSET BURST PULSE CORONA

As their name implies; this mode of operation is intermittent and non self sustained. Its appearance is a tight velvety blue glow over much of the anode surface. As would be expected the intensity of the glow increases with the increase in current. The duration of this type of burst corona pulses ranges from of the order of nanoseconds to microseconds. Each new burst of corona is triggered by the arrival of an external electron. Each burst pulse can be resolved into a number of current pulses or bursts : a primary burst followed by a regular sequence of secondaries usually of smaller magnitude. The primary burst can be initiated by a naturally occurring or artificially created free electrons. These primary electrons, depending on

their energy, produce photons which ionize the surrounding gas by photo-ionization. When each burst is localized on the anode, the complete burst pulse represents the lateral spread of the discharge along the surface of the anode.

1.8 ONSET POSITIVE STREAMER

The initial form of anode corona is always the burst pulse. As the voltage is increased further, depending on the field configuration, the primary burst could develop into a cathode directed streamer. Field enhancement takes place as the primary streamer advances, due to the positive space charge, new avalanches formed due to photoionization accelerate towards the high field region at the centre of the positive space charge. The auxiliary avalanches add more positive space charge thus further strengthening the field and extending a discharge channel out from the anode. Branching of the streamer channel is brought about because new secondary avalanches start from random locations within the surrounding volume that comes under the influence of the positive ion space charge. Figure4 depicts the processes that take place.

In general onset streamers in divergent field geometries do not lead to spark breakdown. They tend to die out due to the low fields prevalent in the mid gap region. These streamers, however, are self propagating due to their mechanism and travel into the interelectrode space at velocities of the order of 10^8 cm s^{-1}.

The mechanism of onset streamers in non-uniform fields under impulse voltages will be discussed below. The groundwork for this has been established in the preceding sections, although the essential mechanisms are similar,

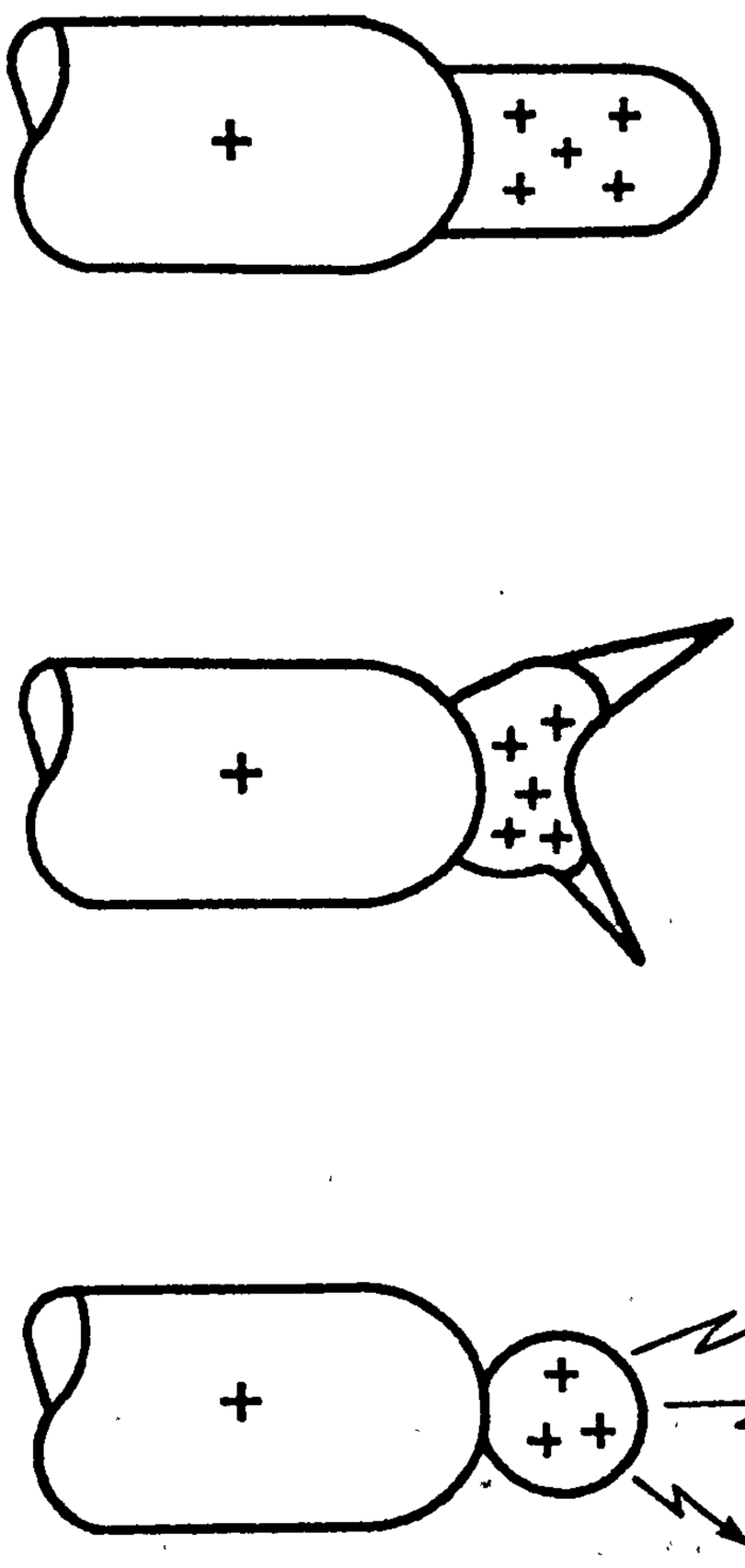

Figure 4 : Growth of the cathode directed positive streamer (Beattie, 1975).

there are definite differences.

When a non-uniform gap such as a point plane system is stressed by an impulse voltage waveform whose rise time is of the order of 0.1 μs to 1.0 μs and fall time of the order of 10's of μs the gap does not contain any appreciable accumulation of space charge even at threshold of detectable ionization. The detection of onset of ionization under such conditions is exceedingly difficult. The first detectable ionization in a point plane gap when a positive impulse voltage is applied is a glow cloud plus branched streamers emanating from the anode. Fast sensitive photomultipliers are used to detect the onset of these streamers, in addition image converter and intensifier photography enable the study of the onset streamers visually. Under impulse voltage conditions the streamers become highly branched and the branches increase in diameter indicating new growth beyond the preceding stage. It is also supposed that only the advancing tips have ionizing activities and hence are luminous, the rest of the channel is only weakly ionized and hence no radiation is emitted from them. The major difference between the uniform field case and the one considered is that the magnitude of α has to rely more on local field augmentation by positive ion concentrations of previous avalanches.

1.9 NEGATIVE STREAMERS

When a negative impulse voltage is applied to the cathode of a non-uniform gap (the geometry is not critical) the ionizing process that develops is not distorted by space charge accumulations. The negative streamer grows as a result of successive avalanches developing away from the streamer tip. The electron avalanches rapidly come into lower fields. In addition

they leave behind immobile positive ions. These produce secondary electrons when they strike the electrode with high enough energy; these electrons again move outwards and form more positive ions near the cathode. Observations show that positive and negative corona occur at about the same voltage, the positive corona already exhibits streamers, whereas the negative point shows a diffused glow before streamers of a feathered nature are formed. It has been shown by Licternberg figure studies that whilst the positive streamers show distinct branches, the negative streamers exhibit a feather like structure (Nasser, 1971).

1.10 STEM FORMATION AND LEADER INCEPTION

When the streamers are not capable of reaching the cathode and giving rise to a return stroke, a very high density of ionization may develop near the anode when the concentration of the streamers becomes excessive. Under these conditions a highly conducting channel of ionization forms at the anode, or very close to it. This channel is essentially stationary, and the corona filaments branch out from it. This highly ionized channel is termed a stem. When the voltage is raised beyond this point, where the stem forms the corona filaments become narrower and develop in a more radial direction. These filamentary corona filaments are very intense and they give rise to the leader which extends the stem and begins to propagate into the interelectrode space. The velocity of propagation of the leader in general is about two orders of magnitude less than that of the streamers. The formation of the leader in itself is not a sufficient condition for break-down of the gap.

1.11 FORMATION TIME OF SPARK DISCHARGE

The formation time of a spark is dependent on the ionization coefficient, which is dependent on the electric field. Several theoretical calculations of formative time have been done and these are described by Meek and Craggs (1953). Dutton (1978) has made a review of formative time lag measurements, which have been carried out in several gases.

The formation time of a spark has been calculated by Raether's Criterion. It is assumed that the time taken for the discharge to develop to breakdown is approximately equal to the time taken to attain the critical amplification where $\alpha x = 20$. The development of the subsequent streamer is exceedingly rapid. In this case

$$t_f = \frac{x}{V}$$

where V is the drift velocity of electrons,

hence

$$t_f = (20 / \alpha V)$$

A very much more rigorous approach to the problem has been carried out by Fletcher (1949). In this treatment the space charge distribution in the avalanche has been considered.

1.12 A COMPENDIUM OF BREAKDOWN MECHANISMS

The streamer (or kanal) theory was proposed because the Townsend theory was unable to explain some outstanding fundamental aspects leading to spark breakdown. Some of the factors that led to an alternative explanation were :

(a) The very short formative time lags were inconsistent with the secondary processes at the cathode by positive ion impact

(b) Spark breakdown was independent of the cathode material.

(c) The filamentary nature of the spark at high values of pd was visually different from that at low values of pd.

The formation of a narrow spark channel brought about by photoionization of the gas, due to the space charge created by an electron avalanche, was first proposed by Loeb and Meek as a qualitative idea. Raether was prompted into the 'kanal' theory by his cloud chamber experiments that gave him a clear idea of what an electron avalanche looked like. It has since been thought that photoionization is not likely to occur in pure gases. However, in air, which is a mixture of mainly oxygen and nitrogen, an electron could excite a nitrogen molecule to about 15 eV, and the photon so produced could then ionize an oxygen molecule with an ionization potential of about 12 eV. In a pure gas, ion excitation or recombination would be able to produce photons which could then photoionize other molecules, provided of course that the photons so produced are of high enough energy. Llewellyn Jones (1957), however, has pointed out that these processes would, if predominant, make the current markedly dependent on i_o, which is not found experimentally.

A later suggestion by Loeb (1951, 1961) and Raether (1964) is that in long gaps the mechanism of breakdown is not simply a streamer type or a Townsend type, but a combination of the two. At a static breakdown threshold the space charge is built up by a Townsend process of successive avalanches, and, with increase in voltage (application of over voltage) less generations of avalanches are required to build up the same space charge, until in a highly overvoltagesituation the transition from avalanche to streamer could take place during the passage of the very first avalanche. According to the foregoing, the static breakdown threshold is set by the

Townsend Criterion. In addition, the formative time lags would decrease with increase in overvoltage. However, the scarcity of experimental data make it difficult to substantiate these statements.

The ideas expressed in the foregoing sections are not necessarily those of the author, they have been drawn mostly from Loeb (1965) and his collaborators.

1.13 PURPOSE OF THIS STUDY AND SEQUENCE TO BE FOLLOWED

The work undertaken in this thesis has concentrated on the study of discharge development and prebreakdown phenomena in compressed SF_6 and mixtures of SF_6/N_2. The problems studied here are common to those in gas insulation cables, transformers and other gas insulated systems. It is hoped that this work will contribute towards the understanding of the physical phenomena that take place within the gaseous medium. A dual photomultiplier and a field probe in the cathode has been used to study a number of optoelectrical properties, and an attempt is made to use these in order to understand the phenomena of conduction within the discharge channel and the critical pressure in SF_6 and its mixtures with N_2.

Chapter Two deals with a review of previous work in long air gaps and breakdown in SF_6 and its mixtures with other gases. Some of the ideas, and problems associated with this kind of work, as experienced by other workers, will be discussed in order to bring the work in this thesis into perspective. Chapter 3 gives a description of the apparatus and experimental techniques used. Chapter 4 is a presentation of the results obtained during the course of this project. Chapter 5 gives a discussion of these results and their implications. Also, the conclusions and suggestion for future work are given there.

CHAPTER 2

REVIEW OF PREVIOUS WORK

2.1 BREAKDOWN IN LONG AIR GAPS

2.1.1 Introduction

The breakdown in long air gaps will be treated in the following sections. The idea of making such a survey is because the breakdown of long air gaps have been compared to the breakdown of short gaps in SF_6 under similar non-uniform field conditions. Although these similarities between the breakdown of long non-uniform gaps in air and those in compressed SF_6 cannot be made without considering the different parameters involved, such as, pressure and gas composition. An understanding of the basic physics is what the author will be endeavouring to achieve. This part of the review, which will deal with the mechanisms of long air gap breakdown, will by no means be a comprehensive review of the state of the art regarding atmospheric air insulation. Rather, it will be a critical analysis of the situation with special reference to basics, with a view of obtaining a more complete understanding of the breakdown processes operational in compressed gaseous insulation. The reasons for this study of breakdown processes in long air gaps are firstly as stated above; the similarities of discharge development in the two different media, and secondly the vast volume of theoretical and experimental work that one can draw on makes air insulation a good starting point for the study of insulation properties in any other gaseous medium.

2.2 BREAKDOWN VOLTAGE OF NON-UNIFORM GAPS

2.2.1 Physical Phenomena

The physical phenomena associated with the development of discharge and breakdown in long air gaps, when subjected to an impulse voltage can be separated into a number of constituent phases. Figure 2.1 shows diagramatically, the different aspects of a positive discharge.

The first observable light after the application of voltage occurs at time T_i when the voltage attains a value U_i, this is called the corona inception voltage. The photomultiplier records this light pulse, as shown in figure 2.1(c). After this there is no observable phenomenon for a period until a second burst of corona occurs, the intervening period is the primary dark period. At time T_i a short highly luminous channel is formed, this channel is called the stem. The corona streamers at the edge of the stem continue on making the conditions right for the leader to form. After a further dark period the leader forms from the stem with almost instantaneous increase in length, this phenomenon, depending on voltage waveform, may repeat itself. When the elongation of the leader channel begins to be continuous the stage of secondary dark periods ceases. The time T_c, and voltage U_c, at which this occurs, are the continuous leader inception time, and continuous leader inception voltage respectively. During its propagation the leader is preceded by edge streamers, the lengths of these streamers increase as the leader propagates into the interelectrode space. When these edge streamers reach the plane (cathode) at time T_f, the velocity of the leader tip increases exponentially, and, in a very short space of time, the leader tip itself reaches the plane at time T_B, thus completing the insulation breakdown of the gap.

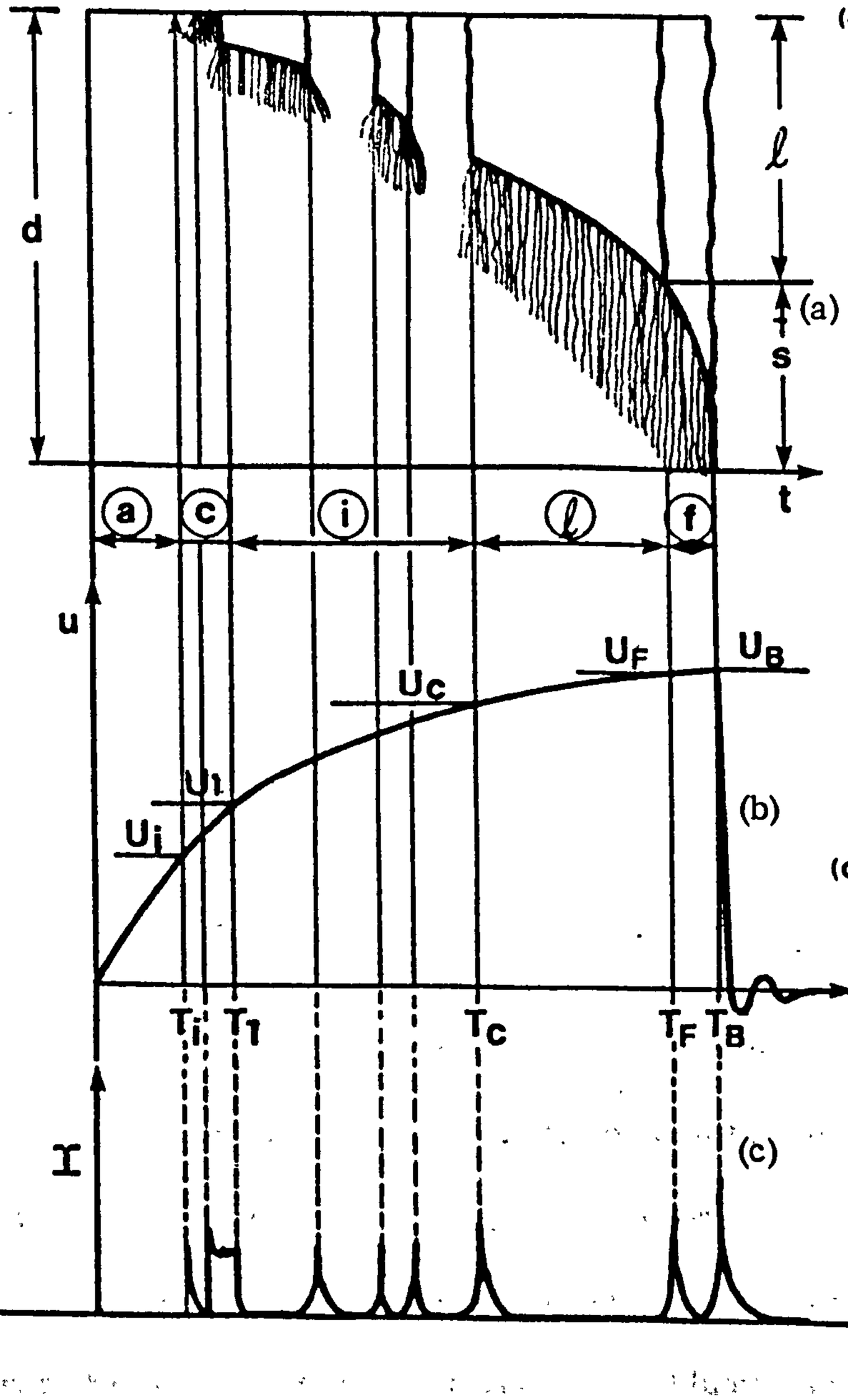

(a) Image converter picture of a discharge of a gap of length d.

(a) absence of phenomena
(c) corona, primary dark period
(i) stem/leader secondary dark periods
(l) leader continuous propagation
(f) final jump.

T_i, U_i = corona inception

T_i, U_i = stem formation

T_c, U_c = continuous leader inception

T_B, U_B = breakdown

(c) Photomultiplier signals at electrode tip.

Figure 2.1 : (Carrara and Thione, 1976)

The foregoing is a phenomenalistic discussion of the discharge development taken chronologically. This sequence of events could change in so far as the dark periods are concerned, depending on the impulse voltage waveshape. Under lightning impulses of the 1/50 μs type the secondary dark periods may be absent altogether. Thus, for impulse voltages of this type the duration of the voltage may be too short and the leader once formed would only propagate a small fraction of the gap length. Thus, it is important to realise that leader formation alone is not a sufficient criterion for breakdown (Gallimberti, 1979). The last phase of breakdown in all cases, however, is the final jump.

2.3 STREAMER FORMATION AND PROPAGATION

The streamer mechanism theory, as was first proposed by Meek (1940), Reather (1940) and Loeb and Meek (1941) arose out of the fact that the time lags to breakdown are an order of magnitude less than the time taken by an electron to drift from the cathode to anode. In addition, for the case of a point plane gap, the applied field is only high near the anode so that ionization cannot occur far from the point without the help of space charge distortion (Marode, 1975a). The importance of streamer channel conductivity has to be emphasised. This may be specially true in long gaps under breakdown conditions. The increase in velocity and luminosity as the streamers approach the cathode, and other streamer properties have all been attributed to the conductivity of the channel. Once the primary streamers cross the gap, the flow of electrons up to the channel will make it more conducting near the anode.

The passive region of the streamer is the filamentary weakly

conducting channel left behind the highly ionized head. It has been shown by various experiments and theoretical simulations that the current flowing in this passive region is essentially an electronic conduction current (Marode, 1975 (a) and (b), Gallimberti, 1972 and Suzuki, 1971).

Marode (1975a) has divided this into three different phases (a) the primary streamer, (b) compensation and (c) resistive. From this it has been shown that the filament is built up of the primary streamers, and that there is left behind an accumulation of negative charges as the streamers reach the cathode, and finally, that there is current continuity in the cathode region.

The roles of secondary mechanisms, such as cathode photoemission and photoionization are important processes in streamer propagation and indeed their formation. However, there is sparse experimental and theoretical information available. Early observations of anode and cathode directed plasma propagation were qualitatively explained by Loeb and Meek (1940), on the basis of a combination of secondary electron production by gas photo-ionization and enhanced ionization in the space charge distorted field. In this the onset of space charge dominated phase of discharge development, filamentary discharges will occur when the total number of electrons in the avalanche reaches 10^8. There is good agreement between the experimental values of Chalmers et al (1972) and the theoretical predictions of Kline (1974).

Loeb (1965) has suggested that anode and cathode directed luminous waves, propagate by means of the enhanced ionization which must accompany the observed luminosity. The electron cloud advancing towards the anode leaves behind it a cloud of relatively immobile positive ions. If the volume

within which these two clouds are created is small enough, the field of the space tip of the electron cloud is such that, when it is added to the imposed field, the negatively charged cloud enters the anode, or from mid-gap advances towards the anode by photoionization in advance, and by electron multiplication in the combined field. The space-charge field of the positively charged cloud draws into its tip photoelectrons created by photons in the initial avalanche head and advances towards the cathode, either from the anode or from mid-gap. The speeds of both these streamers, because of photoionization in advance and the distortion of the field are greater than the speed of the initial avalanche. Detailed analytical theories have been derived by Klingbeil et al (1972), Loeb (1965), Wright (1964). Klingbeil et al were among the first to include photoionization and predict equal anode and cathode directed wave velocities in a co-ordinate system moving at the electron drift velocity. The view expressed by Wright (1964), Klingbeil et al, has been that the streamer channel is strongly conducting with almost equal densities of positive ions and electrons, with negligible attachment rate. The anode potential, they claim, is maintained at the tip of the active region and the high electric field in this region is ascribed to the geometry. Also, the propagation of the streamers takes place due to photoionization of the gas ahead and collisional multiplication.

As against this view point Dawson and Winn (1965), and Gallimberti (1972) argue that the streamer is an isolated spherical volume of space charge that leaves behind a weakly conducting trail as it propagates. In this model the conducting channel plays little or no role in the propagation of the streamer. It is suggested that the streamer moves in steps from

avalanches that are triggered by photoionization and grow in the fields produced by the combination of space charge and the applied fields.

The basis of almost all theoretical predictions of streamer propagation is the solution of continuum equations. These equations have been solved by several authors, Ward (1965), Davies et al (1971), and Reininghaus (1973), using numerical techniques. According to Davies et al and Reininghaus photoionization is not an essential condition for streamer propagation. Instead they include a coefficient for photoemission, and make the assumption that all the photoelectrons are released near the axis of the discharge. On the other hand Kline and Siambis (1971) have shown by using a photoionization coefficient measured by Penney and Hummert (1970) that streamer propagation can take place by gas photoionization alone. The treatment of Kline and Siambis is a very fundamental microscopic one using a monte carlo approach. Kline (1974) has shown that streamers propagate due to the presence of electrons, ahead of the ionizing wave. These electrons are supplied by photoionization, photoemission, or both depending on the experimental conditions. By using the above ideas and detailed mathematical analysis, Kline has obtained remarkable agreement with the streak photographs of Koppitz (1973).

2.4 LEADER PROPAGATION AND PROPERTIES

The mechanism of corona initiation and streamer propagation in the interelectrode space in a gaseous medium is now fairly well understood, although there is still a lot to be learned. One of the most important facts that has emerged from the studies of corona inception and streamers is that the corona streamers do not themselves cause voltage collapse, even

when bridging the gap; the leader channel on the other hand, is sufficiently conducting after completion of its propagation through a certain part of the gap to initiate the final jump phase. The length of the leader before final instability depends on how energetic the edge streamers are. The diameter of the leader channel and the electric field at the head of the leader are important parameters, in the physical interpretation and modelling.

Ross (1977), has used a time resolved Schlieren technique to measure the leader diameter in a 1.5 m rod-plane gap, subjected to positive impulses of 30 and 100 μs time to crest. The accuracy of measurement of the thermal channel diameter is $\pm$ 0.1 mm, and was observed to expand subsonically, the velocity of expansion being less than 100 m sec^{-1} in all cases ; the absence of a strong shock wave indicated pressure within the leader remains at the ambient value. Ruhling (1977) has measured the diamter of the light emitting leader core using a microdensitometer. He has found that for a 1.5 m and a 10 m gap, the diameters lay in the range 1-2 mm, and 4-8 mm respectively. The luminosity of the leader channel bears a direct relationship to the current injected into the gap during discharge development. Ruhling (1977) has shown that by measuring the current density the electron density can be calculated. The fluxmeter measurements of Waters (1977) show that the total energy supplied is approximately divided between the energy stored in the redistributed electrostatic field and that dissipated in the discharge process. A small proportion of the total energy is lost by way of radiation. It has been shown by Pigini et al (1977) using photomultipliers, slits and filters that the leader light output is predominantly in the visible red, whereas the leader corona emits almost exclusively in the ultra violet. However, it must

be pointed out that the results of the Les Renardieres group (Electra, No. 53, 1977) are in contrast to those of their previous studies on long air gaps (Electra, No.35, 1974), with regard to the spectrum of light emission of the leaders.

The spectrum of the leader corona in the blue region is predominantly due to nitrogen second positive band (Electra, 1974). The relative intensities of these bands can be calculated as described by Gallimberti et al (1974). Jones and Ross (1976) have measured the value of the peak emission of the second positive band in a 2 m rod-plane gap. These results are in good agreement with those obtained by the Les Renardieres group (Electra, 1977).

Although the transition from a corona phase to a leader are fairly well defined from a phenomenalistic view point, the physical processes causing this transition are uncertain. These processes it is envisaged cause gaseous heating with the corona streamer channels which consequently give rise to a large increase in the conductivity. Aleksandrov (1966) has shown that by considering the transition mechanism that thermalisation is a distinct and pertinent possibility. He considers a group of streamers, containing a total of N_e electrons, in which the electric field gradient is G_s. If the kinetic energy of these electrons is converted completely to gaseous heating with the channel of radius r, then the temperature rise ΔT will be given by

$$\Delta T = \frac{N_e \; e \; G_s}{(Z/2) K n \pi r^2}$$

where n is the gas number density, and the number of degrees of freedom Z = 5 for a diatomic molecule. Then, for example, a charge of 2 μc in the corona streamers, and a potential gradient of 20 kV cm^{-1} will cause a

temperature rise of 5.5×10^3 K within the leader channel of radius 0.5 mm. One possible feature of the transition region at the tip of the ionized wave has been considered to be associated with a hypersonic shock wave caused by the rapid thermalisation of the electrons in the corona streamers (Kekez and Savic, 1974). As an extension of this Kekez and Savic (1980) have studied the channel expansion in detail using a Schlieren technique. They have also derived the following expression for specific internal energy at the front :

$$\epsilon = \frac{\gamma}{(\gamma^2-1)(\gamma+1)} v^2$$

where ϵ is the specific internal energy at the front, γ the adielectric index and v the detonating speed.

It may be interesting to note that the laser supported detonation of Ramsden and Savic (1964) and the electrically supported detonation of Kekez and Savic (1974) both use the above equation, and that both detonations are based on the same (Joule heating) effect to supply the energy for the shock. The energy transfer to heavy particles is done in the rear of the shock wave in both cases (Kekez and Savic, 1980). Savic and Kekez (1980) have discussed the presence of a second shock wave, under certain circumstances, which turns back and proceeds towards the anode, producing a high pressure region and elevated temperatures.

2.5 BREAKDOWN MODELS

2.5.1 The Aims of Modelling

The primary aim of any breakdown model is to ascertain the factors governing the processes that take place before, and during, when the gap is

rendered conducting. Reasons for statistical variations are of particular concern, and are normally delved into in detail so as to make the model useful and reliable. Although the ultimate goal of any model is to reduce the need for extensive experimentation, it seems, at least presently, that the day of the experimentalist is far from over. Despite this there is considerable drive towards the development of mathematical models.

2.5.2 Jones Model

This is a basic model which examines the factors necessary for the propagation of the discharge. The developing discharge is represented as a cylindrical column. This column is not necessarily bounded by the leader corona cloud. The leader/leader-corona system is represented by a uniform charge of q c m^{-1}, distributed along the cylindrical column so that the surface field strength is just too low to support further ionization. If the length of the column at any given instant is yd ($0 \leqslant y \leqslant 1$), and the anode potential V, then the potential P at the tip of the advancing column will be given by

$$P = V - g\,y\,d \qquad (2.1)$$

where g is the electric field gradient at each point along the length of the column. In general g will be time dependent and will reach a final value g_o, which is a function of current.

The rate of growth of the column can be obtained by differentiating equation (2.1) w.r.t. time

$$\frac{dP}{dy}\,\frac{dy}{dt} = \frac{dV}{dt} - gd\,\frac{dy}{dt} - yd\,\frac{dg}{dt}$$

$$v = \frac{(d\,V/dt) - yd\,(\frac{dg}{dt})}{g + (\frac{1}{d})\,\frac{dP}{dy}} \qquad (2.2)$$

where $v = \frac{dy}{dt}$ the velocity with which the column propagates.

The propagation of the column will be interrupted if the numerator of equation (2.2) becomes zero. This will be dependent upon the rate of change of voltage, and the characteristics of the column: namely, low conductivity of the column. As against this if the denominator of equation (3.2) tends to zero then the propagation velocity will tend to a very high value. This is the mathematical representation of the large acceleration of the leader channel at the onset of the final jump, thus it is the criterion for breakdown of the gap.

As the value of y tends to unity, the length of the gap unbridged by the column reduces. Jones (1973) points out that since g is always greater than zero, the value of P required for continued column propagation is such that $\frac{dP}{dy}$ has to be negative. Breakdown will then depend on g becoming sufficiently small. By analogy with the switchgear arc, the heating process within the column is regarded as having an inverse current-voltage characteristic having a heating time constant τ. The temporal variation of gradient g is expressed empirically by :

$$\frac{dg}{dt} = \frac{g_o - g}{\tau} \qquad (2.3)$$

an expression for g can thus be obtained from equation (2.3) above provided g_0 is a constant, which implies a constant discharge current. It has been shown that after a time t of uniform column growth

$$g(t) = g_o + \frac{\tau}{t} \left\{ g\,(t = 0) - g_o \right\} \left\{ 1 - \exp\,(-t/\tau\ ) \right\} \qquad (2.4)$$

By comparing the behaviour of g(t) to the voltage U curve, and adopting a best fit approach, Jones has derived :

$$g_o = i^{-0.4} \text{ kV cm}^{-1} \tag{2.5}$$

this is the static gradient - current characteristic, a value of 50 μs is assumed for τ and g (t = 0) is taken as 5 kV cm^{-1} .

2.6 ALEKSANDROV MODEL

The semiempirical model for breakdown voltage of very long air gaps developed by Aleksandrov (1969 a+b) is based on the premise that : when the leader channel develops, it is surrounded by space-charge arising from streamers developing in the leader corona. It has been shown (Aleksandrov (1969a) that the potential increase in the gap necessary to distort the field near the electrode so that a discharge develops is not proportional to the gap width. In fact the wider the gap the smaller the required potential increase because the region with the progressively weakening field gets larger.

For the purpose of calculating the electric field strength E_m at the head of the developing discharge, the space charge boundary is considered to be a hyperboloid of revolution. The maximum field intensity in the vertex of the hyperboloid is determined by the formula

$$E_m = \frac{U}{\rho(1 - \rho/d)^{0.5} \tanh^{-1}(1 - \rho/d)^{0.5}} \tag{2.6}$$

where U is the voltage across the discharge gap, ρ the radius of curvature of the tip.

In an attempt to estimate the radius of curvature ρ, Aleksandrov (Loc. cit.)

has considered the space charge volume as a cylindrical column of radius ρ terminated in a hemispherical cap.

Measurement of leader current during spark discharges in the laboratory gives a value of 10^{-4} coulombs for q_i : and the radial field $E(r) = 20$ kV cm^{-1}, from this the value of ρ has been calculated as 0.9 m. This radius can be taken as an estimate of the hemispherical boundary of the leader space charge facing the plane. Using the breakdown voltage of 1.55 MV for a 5 m point-plane gap under a 50 Hz voltage waveform, Aleksandrov (Loc. cit.) has calculated E_m to be 12 kV cm^{-1}. He points out that this voltage waveform is the same as a positive pulse with a rise time of several thousand microseconds. Equation (2.6) is used to estimate the breakdown voltage as shown below :

$$U_d = 1260\, \rho\, (1 - \rho/d)^{0.5}\, \tanh^{-1} (1 - \rho/d)^{0.5} \quad KV \qquad (2.7)$$

Aleksandrov (1969a) by drawing on the data presented on lightning discharges of other authors suggests $q_i = 10^{-3}$ Cm^{-1} for lightning channels of length 3 km. With these data and the dependence of the linear charge density per unit length of discharge gap, measured in laboratory spark gaps, he proposes the simple relationship :

$$q_L = 100 + 0.3\, d\, \mu c\ m^{-1} \qquad (2.8)$$

2.7 CORONA CLOUD MODELS

In this type of development the minimum conditions under which electron avalanches can grow are of interest. Under divergent field conditions, depending on factors such as crest voltage and the rate of rise of voltage and humidity and other atmospheric conditions, breakdown could occur without

the appearance of corona. In such cases it has been assumed that breakdown of the gap takes place when the space charge limited corona avalanche occurs (Hepworth, Klewe and Tozer, 1971). The electron avalanche growth have been computed by Hepworth et al (1971) in air around cylinders and spheres. In these cases the data of Harrison and Gaballe (1953) have been expressed as :

$$(\alpha - \eta) = 50 \exp (1.1\ E) - 750 \qquad (2.9)$$

It had been assumed that there were initiatory electrons always present and they had neglected secondary processes.

Hepworth , Klewe and Tozer (1972) have extended their electron avalanche calculations to obtain sparkover criterion for non-uniform field gaps where corona precedes breakdown. In this model they assume that many electron avalanches grow about the surface of the highly stressed electrode giving rise to a corona cloud behind them. This could then be represented by a spherical cloud, the conductivity of this cloud, although not as strong as that of a plasma, nevertheless can be treated as perfectly conducting. The theory was first proposed for a concentric sphere geometry of inner and outer radii a and b , the corona cloud is thought to expand through avalanche growth at the surface of the inner more highly stressed electrode until its radius c satisfies the condition :

$$Zc = \frac{1}{(\alpha - \eta)}$$

Z is the fraction of the radius of the stressed inner sphere, and is independent of the outer radius. The value required for positive and negative polarities are different.

The authors have compared this model with the work of other workers and point out that there is no satisfactory quantitative model to explain

the transition from corona to breakdown in a divergent field. In their model the authors consider the dimensions of the corona cloud to grow an extent that brings about an instability,

$$\text{i.e.} \quad c \geqslant 0.5b$$

further expansion of the corona cloud is brought about by increasing voltage. The applied voltage V is related to the electric field at the surface of the corona sphere by

$$E = \frac{V\,b}{(b-c)c} \tag{2.10}$$

The authors have shown that for negative impulses the field strength at sparkover is,

$$E_{(-)} = 0.23 \ \ell n \left(14 + \frac{0.027}{Z_{(-)}b} \right) \tag{2.11}$$

The breakdown condition for positive impulses has been derived using the experimental condition $c \geqslant 0.09b$ as :

$$E_{(+)} = 0.082 \ \ell n \left(14 + \frac{0.15}{Z_{(+)}b} \right) \tag{2.12}$$

They have extended the foregoing to the more practical configurations of sphere-plane and rod-plane gaps. The assumptions that have been made are (a) that the corona cloud remains spherical in shape and (b) introducing a numerical factor f(a/b). The latter has been introduced to account for the higher voltage required to produce a given electric field strength in a sphere plane gap, than in a concentric sphere gap, these values of f(a/b) have been taken from Mattingly and Ryan (1971). This results in the following equations for the average field strength at breakdown.

Convergent fields (a $\leqslant$ d) for small sphere

$$E_{(-)} = 1.13 \left(0.23 \frac{a+d}{d} \right) \ell n \left[14 + \frac{0.27}{Z_{(-)}(a+d)} \right] \qquad (2.13)$$

for very large spheres (a $\geqslant$ d) convergent field

$$E_{(-)} = 0.91 \frac{a}{a+d} \ell n \left(14 + \frac{0.013}{Z_{(-)}a} \right) f(a/b) \qquad (2.14)$$

for divergent fields (a $\leqslant$ 0.1 d)

$$E_{(+)} = 1.05 \left(0.065 \frac{a+d}{a} \right) \ell n \left(14 + \frac{0.15}{Z_{(+)}(a+d)} \right) \qquad (2.15)$$

divergent fields (a $>$ 0.1d)

$$E_{(+)} = 0.91 \left(\frac{a}{a+d} \right) \ell n \left(14 + \frac{0.013}{Z_{(+)}a} \right) f(a/b) \qquad (2.16)$$

It has been suggested by the authors that a transition to uniform fields when the field at the cathode reaches 2.4 M V m^{-1} and the avalanche growth can begin from the cathode, this occurs for

$$\frac{V}{d} = E \geqslant \frac{2.4\,b}{a} \qquad (2.17)$$

when this point is reached secondary ionization at the cathode become important. It has been shown that $\gamma = 10^{-5}$ under such uniform field conditions, the breakdown field strength is thus given by

$$E = 0.079 \ \ell n \left(14 + \frac{0.15}{d} \right) \qquad (2.18)$$

This model compares well with experiments for small concentric hemispheres where data are available. Also, it can be extended to rod-plane and sphere plane gaps. The fact that it can be applied to uniform fields

as well indicates the flexibility, and the breadth encompassed.

Kline (1977) has presented a corona cloud model to predict the breakdown voltage for a wide range of electrode geometries. The model also has been used to predict the gap factor for different geometries.

Several assumptions are made in the formulation of this model ; the corona cloud is a conductor, and its shape has been obtained from the image converter photographs of other workers. The corona cloud is assumed to grow from the positive high voltage electrode along the shortest path to the grounded or negative electrode. Using these assumptions Kline (Loc. cit.) has shown that the electric field at the tip of the corona cloud as a function of the corona cloud dimensions goes through a minimum point for a variety of gap geometries. The implication of this Kline suggests is that the actual electric field of the corona cloud tip remains constant as the applied voltage and the corona cloud length increase. It has to be borne in mind that this relates to the critical switching surge which gives the minimum critical breakdown voltage.

The gap factor for various electrode geometries has been predicted by making the following assumptions : (a) the breakdown occurs at the crest of the critical voltage surge, (b) the corona cloud length is equal to the critical cloud length corresponding to the minimum value of the field strength at the corona cloud tip and (c) the actual corona cloud tip field at breakdown is the same for every geometry considered, from the above

$$K = \frac{V_{s,\,ns}}{V_{s,\,rp}} = \frac{(E_{n,min})\,rp}{(E_{n',min})\,ns} \qquad (2.19)$$

In equation (2.19) K is the gap factor, and the subscripts (rp) and (ns) denote, respectively rod-plane geometry and any other geometry. E_n is the

calculated normalized field at the corona cloud tip.

Expressions for breakdown voltage have been derived. The gap factor is independent of the gap length and have been shown to be consistent with experimental observations.

$$V_s = K\,(500\,d^{0.6}), \quad d \leqslant 5\ m \tag{2.20}$$

$$V_s = K\left(\frac{3400}{1+8/d}\right), \quad d > 5\ m \tag{2.21}$$

The idea of a conducting corona cloud is an old and simple one. However, it is one that can be used to advantage, as has been depicted in the foregoing. The electric field at the leader corona tip and its relationship to the gap geometry could be said to be the most important single feature that has emerged in the presentation of the breakdown process in this manner.

2.8 THE HUTZLER MODEL

The model presented by Hutzler and Hutzler - Barre (1978) is based on the models of Aleksandrov, and Jones in the main. The leader tip potential is obtained by applying ohms law to the leader developing in the interelectrode space. It is expressed thus :

$$P(t) = U(t) - \int_0^{L(t)} g\,(M, t)\,d \tag{2.22}$$

where P(t) is the potential at the time (t), U (t) the applied voltage, L(t) is the effective leader length at time t and g (M, t) is the longitudinal electric field at a point in the interelectrode space at instant of time t.

The condition necessary for the propagation of the leader is that corona has to be maintained at the leader tip and the electric field has to

be fairly high. An interruption to the leader current which occurs because of a fall in tip potential P is considered to cause deionization of the leader core, so that the leader gradient increases according to the equation

$$g(t') = g(t_i) \exp (t'/\tau) \qquad (2.23)$$

where $t' = t - t_i$ is the time that elapsed since interruption of the discharge at $t = t_i$, τ' is the time constant of deionization and is taken as 500 μs. The leader propagation can only restart if $\frac{dv}{dt}$ is greater than the increasing leader gradient ; if $g(t') > g_s$ the leader is assumed to be permanently stopped. In order to simplify computational problems the gap geometry is taken into consideration. The leader propagation is considered to consist of straight successive steps of length ℓ which make an angle ϕ with the axis of the gap. The angle ϕ for each new element is defined as having a probability density given by

$$p(\phi) = \frac{\sin \phi}{a} \exp \left(- \frac{(1 - \cos \phi)}{a} \right) \qquad (2.24)$$

where a is given by

$$a = (1.5 \times R)^{-1} \left(0.8 + 10^{-10} \frac{dU}{dt} \right)^{-1} \qquad (2.24)$$

This simulates the observed variations in leader path with applied voltage waveform shape and gap geometry. R is the radius of curvature of the leader tip in the Laplacian field. The leader will either propagate or be arrested depending on the angle ϕ. If ϕ is so great that the field falls below E_c, the critical field, then the propagation will be stopped. On the other hand if the value of the tip field E is greater than E_c then propagation will

be maintained.

By taking $\phi = 0$ the minimum possible breakdown voltages are obtained. The simulations of current and leader growth are similar to those of other workers, and show a good representation of the constant leader propagation and discharge current at critical breakdown, and the discontinuous nature of growth under slow rising impulse voltages. The difference between maximum axial leader length at withstand and the leader length are also simulated.

2.9 BREAKDOWN MECHANISMS IN SF_6

2.9.1 Introduction

Due to the ever increasing growth of the usage of sulphur hexafluoride as a high voltage insulating medium, many experimental and theoretical investigations have been reported in the literature describing the breakdown behaviour of SF_6 and its mixtures under direct, alternating, and impulse voltages. In this review, the experimental results are discussed in the light of the theoretical statements. There are a whole host of aspects dealing with the various conditions of breakdown and corona initiation voltage. Obviously it would not be possible to cover all this ground in the space of a review of this nature. However, the author envisages that the aspects relating to the work in this thesis to be covered in reasonable detail. Some aspects that will be discussed in this section may not bear a direct relationship to the later chapters, however, they have been included for the sake of completion.

2.9.2 Discharge parameters in SF_6

In an electronegative gas such as SF_6 the prebreakdown current, under non-uniform field conditions has been expressed by Pedersen (1967, 1970) as follows :-

$$\frac{I}{I_o} = \frac{1 + \int_0^d \exp\left[\int_0^x (\alpha - \eta)\, dx\right] \alpha\, dx}{1 + \gamma\left[\int_0^d \exp \int_0^x (\alpha - \eta)\ dx\right] \alpha\, dx} \qquad (2.25)$$

where I_o is the initial photoelectric current, γ the secondary electrons produced per primary electron as a result of ionization processes such as electron emission from the cathode, toegether with photoionization in the gas caused by photon release from excited atoms or from recombination processes. From equation (2.25) the Townsend criterion for breakdown in non-uniform fields is derived as :

$$\gamma \int_0^d \exp\left(\int_0^x (\alpha - \eta)\, dx\right) \alpha\, dx = 1 \qquad (2.26)$$

equation (2.26) is a generalisation of the criterion derived by Geballe and Reeves (1953) for a strictly uniform field distribution. Equation (2.26) suggests that there will be an infinite current flowing as a result of electric breakdown of the insulating medium. However, the current limit will be determined by the circuit parameters. For a strictly uniform field equation (2.26) becomes

$$\frac{\gamma\alpha}{(\alpha - \eta)} \left\{\exp\left[(\alpha - \eta)\, d\right] - 1\right\} = 1 \qquad (2.27)$$

An important consequence of equation (2.27) for the Townsend type of breakdown in a uniform field is the existence of a limiting field strength below which breakdown cannot occur (Loeb and Meek, 1941).

When $(\frac{\alpha}{p}) > (\frac{\eta}{p})$, breakdown is possible for sufficiently large pd regardless of the values of $(\frac{\alpha}{p})$, (η/p) and γ. Under this condition the breakdown criterion always has a pd dependence. However, for $(\alpha/p) < (\eta/p)$ equation (2.27) approaches, with increasing pd, an asymptotic form which is independent of pd, i.e.

$$(\alpha/p) = (\eta/p) \tag{2.28}$$

Equation (2.28) is a condition dependent on (E/p) alone, and fixes a limit for this parameter $(E/p)_{lim}$, below which no sparking should be possible regardless of the magnitude of pd. If γ is negligible then the limiting condition is given by equation (2.28).

Bhalla and Craggs (1962), assumed the formation of negative ions, and consequently, values of α , η , γ and breakdown sparking distance d_s have been calculated in SF_6 by employing equations (2.25), (2.26), (2.27). The second Townsend coefficient γ is very sensitive to the condition of the electrodes and the purity of the gas, and it will only be defined under carefully controlled laboratory conditions. Measurement of γ so far has been possible only at pressures below 25 mm Hg. Bhalla and Craggs (1962) have suggested that the exponential decay of the ionization current may be due to photoabsorption in the ultraviolet end of the spectrum and also those due to photoabsorption in the ultraviolet end of the spectrum and also those due to cathode effects.

The predominant process of negative ion formation in SF_6, is the capture of slow electrons producing SF_6^- and SF_5^-, and of course the contribution due to secondary capture processes. Berg and Dakin (1956) have shown that at higher pressures, the electrons are equilibrated more rapidly in the gap and the attachment coefficient would be expected to increase. Hickman and Fox (1956) have shown using a monoenergetic electron source that the type of negative ions formed during the capture of electrons by neutral molecules in SF_6 depends entirely on the energy distribution among several modes of vibration or rotation that are prevalent. They have stated further, that to obtain better resolution of the ratio of SF_6 to SF_6^- that may be formed, a very precise monoenergetic electron source would have to be used.

2.10 MEASUREMENT OF DISCHARGE PARAMETERS

The current flowing in a uniform field gap has been expressed by Harrison and Geballe (1953) as follows :-

$$\frac{I}{I_o} = \frac{\alpha}{(\alpha - \eta)} \left[\exp (\alpha - \eta) d\right] - \frac{\eta}{(\alpha - \eta)} \qquad (2.29)$$

provided detachment and secondary processes are absent. The value of current in a uniform field gap at fixed values of (E/p) and variable gap length d has been measured. The values of α and η in equation (2.29) are obtained by fitting the measured values of (I/I_o) as a function of d to equation (2.29)

Ahearn and Hannay (1953) have shown that negative ion formation due to resonance capture of the form indicated by the equation below

$$e + SF_6 \longrightarrow (SF_6^-)^* \longrightarrow SF_6^- \qquad (2.30)$$

$$(SF_6^-)^* \longrightarrow SF_5^- + F \qquad (2.31)$$

$(SF_6^-)^*$ is a metastable state of the SF_6^- ion.

Ahearn and Hannary (1953) have further shown that these two products SF_6^- and SF_5^- are produced in approximately equal quantities and that the equations (2.30) and (2.31) are equally likely to be followed during the formation of these different species of ions.

Gabelle and Harrison (1953) and Bhalla and Craggs (1962) measured values of (α/p) and (η/p) as a function of (E/p). The values of (E/p) ranged between 90 and 160 V cm^{-1} mm Hg^{-1}. In the case of Gabelle and Harrison, they went up to 230 V cm^{-1} mm Hg^{-1}. The maximum pressure used was 230 mm Hg. The conclusion that was drawn by them was that up to about 410 mm Hg cm the breakdown in SF_6 was caused by the Townsend build up mechanism.

Dutton, Harris and Jones (1970) reported a strong pressure dependence of (α/p) and (η/p) for pressures up to 400 mm Hg and (E/p) equal to 118 V cm^{-1} $torr^{-1}$ they suggested that at such pressures one or more attachment process operates, which depend on the square of the pressure. However, Boyd and Crichton (1971) who carried out similar measurements over a range of $115 \leqslant (E/p) \leqslant 200$ V cm^{-1} $torr^{-1}$ at pressures up to 400 torr ruled out any dependence on pressure of (α/p) and (η/p) in the pressure range considered above. According to Boyd and Crichton (1971) (α/p) and (η/p) are only linear functions of (E/p). Subsequently, Maller and Naidu (1976) also did not find any dependence of (α/p) and (η/p) on pressure.

In order to obtain accurate values for α and η from prebreakdown current measurements, the variation in electric field measurements has to be kept within about 0.1%, consequently, the measurements of gap length have to be made to the same degree of accuracy (Karlsson and Pedersen,

1972, Boyd and Crichton 1971, Maller and Naidu 1976). The upper limit for pressure in these measurements has been put at 750 mm Hg (Boyd and Crichton, 1971). While the values of α and η are important at pressures of technical operating pressures, their determination has not been possible at such pressures. These limitations of pressure are due primarily to the lack of uniformity of the discharge gaps. As Karlsson and Pedersen (1972) have pointed out, the uniformity of the gap does not depend on the geometry of the gap alone, rather it depends also on the physical properties of the gas and the actual phenomena under investigation. The determination of uniform field breakdown is subject to less stringent criteria, an ultimate upper limit of pd is in this case a few thousand mm Hg cm, provided that the field strengths at the edges of the electrodes are sufficiently low.

Values of Townsend's second ionization coefficient γ have been determined experimentally (Bhalla and Craggs, 1962, Boyd and Crichton, 1971, Maller and Naidu, 1976) for pressures below 25 torr. The value of γ has been shown to have a strong dependence on the gap separation. Perlin (1972) has shown that an increase in the gap length from 0.1 cm to 8 cm for virtually constant electric field strength in the gap, γ decreased by a factor of 10^{-19}. He ascribes this to the effect of photon absorption in the gaseous medium. The coefficient of photoabsorption μ is proportional to the density of the gas or at constant temperature it is proportional to the pressure. Perlin (1972) has obtained values for the coefficient μ in SF_6 and nitrogen to be 6.0 cm^{-1} and 2.5 cm^{-1} respectively at a pressure of 1 atmosphere. Blair and Whittington (1970) have measured the photon absorption coefficient in oxygen, nitrogen and their mixtures in the range of wavelengths between 100 and 120 nm, using electrodes of various metals. They have observed that variation

of μ is linear for various values of (E/p). Also, it has been shown that photoabsorption increases with the increase in oxygen content. Blair, Macleod and Orr (1976) have in addition studied the absorption coefficient in nitrogen, oxygen and SF_6. They have reported that the heaviest absorption occurs at the low wavelengths in ultraviolet. A point of interest in their work is that the photon absorption in oxygen is higher than that in SF_6. This could be an important point when considering the initiation voltage measurements and other paramters related to luminous events in SF_6 and mixtures of SF_6 with other gases at these wavelengths in UV. Despite the limitations on the measurements of α and η , calculation of corona initiation voltages and breakdown voltages are made using them. These calculations are based on the Townsend or Streamer theories, depending on the experimental conditions. However, the validity of the usage of these measured constants, which are obtained under very carefully controlled laboratory conditions, may not be applicable in practical situations.

2.11 BREAKDOWN VOLTAGE IN NON-UNIFORM FIELDS

There is as yet no general model which can be used successfully to determine discharge voltages in SF_6. This may be at least partly due to the fact that discharge phenomena in compressed SF_6 is not fully understood. The existing methods can be broadly classified into two categories : those based on the streamer theory and those based on the Townsend mechanisms.

The streamer theory originally proposed by Meek (1940), Raether (1940) and Loeb and Meek (1941), has been modified by Pedersen (1967, 1970) and adopted for the case of SF_6. This is shown in equation (2.32) and is called the Pedersen criterion.

$$\int_0^x (\alpha - \eta)\, dx = K \qquad (2.32)$$

where K is a constant. Pedersen has shown that K works out to be about 18.

Attention, however, should be drawn to the fact that equation (2.32) can only be applied to SF_6. This is important, because the variation of α and η in other electronegative gases with field strength is unknown and may vary in a manner that is quite different from that in SF_6. Equation (2.32) gives the streamer criterion, and offers a promising approach for the solution of engineering problems. This criterion states that : the streamers are formed when the number of electrons in an avalanche attains a certain critical value. When this is reached it gives rise to total or partial breakdown of the insulating medium, depending on the degree of non-uniformity of the field in the gap. In the case of a uniform field gap geometry, streamer formation will lead to a breakdown directly, while in a non-uniform field gap it may not cause complete breakdown. The streamer criterion shown in equation (2.32) does not take into account the field distortion caused by the avalanche head. Because of the rapid variation of $(\alpha - \eta)$ with field strength, equation (2.32) is satisfied even for very small increments of field strength above the value corresponding to $(\alpha - \eta) = 0$ in SF_6. The essential result is that for non-uniform field gaps like rod-plane configurations, the critical avalanche length x is very small compared to the total gap length.

Blackett et al (1970) had used the Pedersen criterion to predict the corona threshold voltage and breakdown voltage in sphere - sphere arrangements. Their experimental values were within $\pm$ 10% of those predicted using the criterion of equation (2.32). Hazel and Kuffel (1976) had used the Pedersen

criterion and studied the breakdown and corona threshold voltages of a point plane gap in SF_6. The corona initiation voltage had been calculated using the equation proposed by Nitta and Shibuya (1971). Hazel and Kuffel (1976) had derived a semiempirical corona free breakdown criterion, they have shown that their predictions are in reasonable agreement with the experimental values obtained for a point plane gap in SF_6 under d.c. voltage conditions for corona free breakdown. The region of single corona pulse observed by Hazel and Kuffel (1976), is similar to the observations of Anis and Srivastava (1982) who reported their observations under switching impulses in SF_6. In both these cases the steady corona discharge voltage lies considerably above the theoretical corona onset voltage predicted by Nitta and Shibuya (1971).

When a non-uniform field gap in an electronegative gas such as SF_6 is subjected to a voltage, a pressure is reached above which no corona precedes breakdown. This pressure p_c is called the critical pressure ; at a lower pressure p_m the breakdown voltage reaches a maximum. The corona mechanisms that are active centre on the vicinity of intense field. With the build up of positive space charge the formation of electron avalanches are possible so long as $\alpha > \eta$, and hence the condition $(E/p)_{\alpha=\eta}$ should give the limiting value of the field at the highly stressed electrode for either onset of corona or breakdown (Howard, 1957). At the critical pressure p_c the value of (E/p) is denoted by $(E/p)_c$. Howard (1957) had obtained $(E/p)_c$ values from the experimental data of other workers and compared them with $(E/p)_{\alpha=\eta}$. Howard attributes the low value calculated for the results of Pollock and Cooper (1939) to the strong irradiation used in their experiments. There is generally good agreement for the data of Works and Dakin (1953). However, for some inexplicable reason the values for Foord's results (1953) have been found to be very high.

Works and Dakin (1953) have also studied the breakdown of a 5.08 cm point plane gap under d.c. and 60 Hz a.c. voltages at pressures up to 6 bar. They showed the existence of a negative slope of the V_s, p characteristics for both positive d.c. and alternating voltages. They had also determined the corona onset voltage although the method was not described in detail. The high breakdown voltage at p_m is attributed to corona stabilization, which is the modification of the field by a localised discharge, so as to inhibit the development of complete breakdown. Works and Dakin suggest that at pressures above p_m, corona streamer propagation across the gap is enhanced by positive ion diffusion and that photoionization is a more effective secondary process at the higher gas density. This could be the explanation for the observed decrease in breakdown voltage and the disproportionately low increase in breakdown voltage with gap length at higher pressures. The indirect spark paths observed by Foord (1950) were also observed by Works and Dakin and later by Hazel and Kuffel (1976). This effect has been ascribed to the build up of space charge close to the highly stressed electrode in electro-negative gases. This effect of curved sparks becomes more pronounced at higher pressures. Works and Dakin also studied the effect of 1.24/40 μs impulse waveform on a 5.08 cm rod-rod gap in SF_6, it was shown that the breakdown voltage maximum at p_m to be much less pronounced than in the case of d.c. or a.c. voltage. It is probable that the inhibiting positive space charge has insufficient time to form for such rapidly rising voltage waveforms. Berg and Works (1958) had found that a combination of a d.c. voltage bias above the corona initiation voltage and a superimposed voltage could produce a high breakdown voltage in SF_6. In this case, for SF_6 they have shown that,

above the corona initiation voltage, space charge causes the total voltage for breakdown to increase as the bias voltage. Below the corona initiation voltage, the total voltage versus bias voltage has been shown to be flat. This has been attributed to either the breakdown voltage being an insensitive function of pulse length, or that even with an impulse voltage, some space charge is created which raises the total breakdown voltage. Narbut et al (1959) have stated that, at low over voltages, the formative time lags to breakdown in SF_6 can be some hundreds of microseconds, reducing to about 1 μs at overvoltages of about 50 per cent.

A 5 cm point plane gap in SF_6 was studied by Klewe and Tozer (1970) up to a pressure of 14 bar, under impulse waveforms of 2/50 μs and 200/3000 μs. For positive voltage impulses both waveforms showed two critical pressure regions. The maximum voltage occurring at pressures of 2 bar and 9 bar. They have calculated the corona space charge region R using the criterion given by Howard (1957), viz $\alpha = \eta$ at the surface of the anode. The negative V, p regime has then been interpreted as the limit of corona development, since for a smaller radius R the condition $\alpha = \eta$ at that radius is satisfied at a lower applied voltage. A larger R was found for the higher breakdown voltage under the switching impulse voltage waveform, which is consistent with this model. Klewe and Tozer have estimated the velocity of the return stroke to be about 10^6 cm sec^{-1} using high speed framing photographs. The return stroke is preceded by a gradual brightening of the complete channel. Takuma et al (1972) obtained image converter photographs of leader growth in a 50 cm rod plane gap in SF_6 under lightning impulses of both polarities. In both polarities the leader channel grows in steps, each step being accompanied by a reillumination of the channel. The

velocity of the negative leader is about $3 \dot{x} 10^6$ cm sec^{-1}, and of the positive leader about 15×10^6 cm sec^{-1}. The pause time between leader steps is inversely proportional to the gas pressure. At 1 bar the time between the steps is about 1.5 μs, at 4 bar it appears that the channel grows continuously.

Watanabe and Takuma (1977) have examined the discharge extension in point plane gaps of length 30 and 50 cm under lightning impulses of the form 1·84/46 μs in SF_6, mixtures of SF_6/N_2 and SF_6/ air. The extension of the discharge path was studied using image converter and still cameras. They observed that with increase in content of SF_6 in mixtures with N_2 the extension of the leader to be stepped with a small region of corona streamers ahead of the leader channel. In SF_6 the corona region ahead of the leader shrinks, this shrinkage of the corona streamers is attributed to the decrease of the effective range where electrons can multiply by ionization before attachment. Figure 2.11.1 shows schematically the discharge patterns in SF_6 and N_2. Voss (1979) used an image converter camera and photomultipliers to study the discharge development in SF_6 and SF_6/N_2 mixtures of a point plane gap up to 80 mm, under a fast rising impulse voltage waveform 1.24/48 μs. Figure 2.11.2 shows the time resolved and still photographs obtained by Voss. In his experiments Voss varied the SF_6 content in the mixtures with N_2 between 2% and 100%, the whole study was conducted at 1 bar. The increase of SF_6 content leads to a strong spatial concentration of streamer growth. In pure SF_6 gradual development was not observed in the time integrated photographs, instead a filamentary branched discharge was observed. Again, this filamentary structure is ascribed to the high photoabsorption and low diffusion coefficient in SF_6. The observations of Voss confirm those

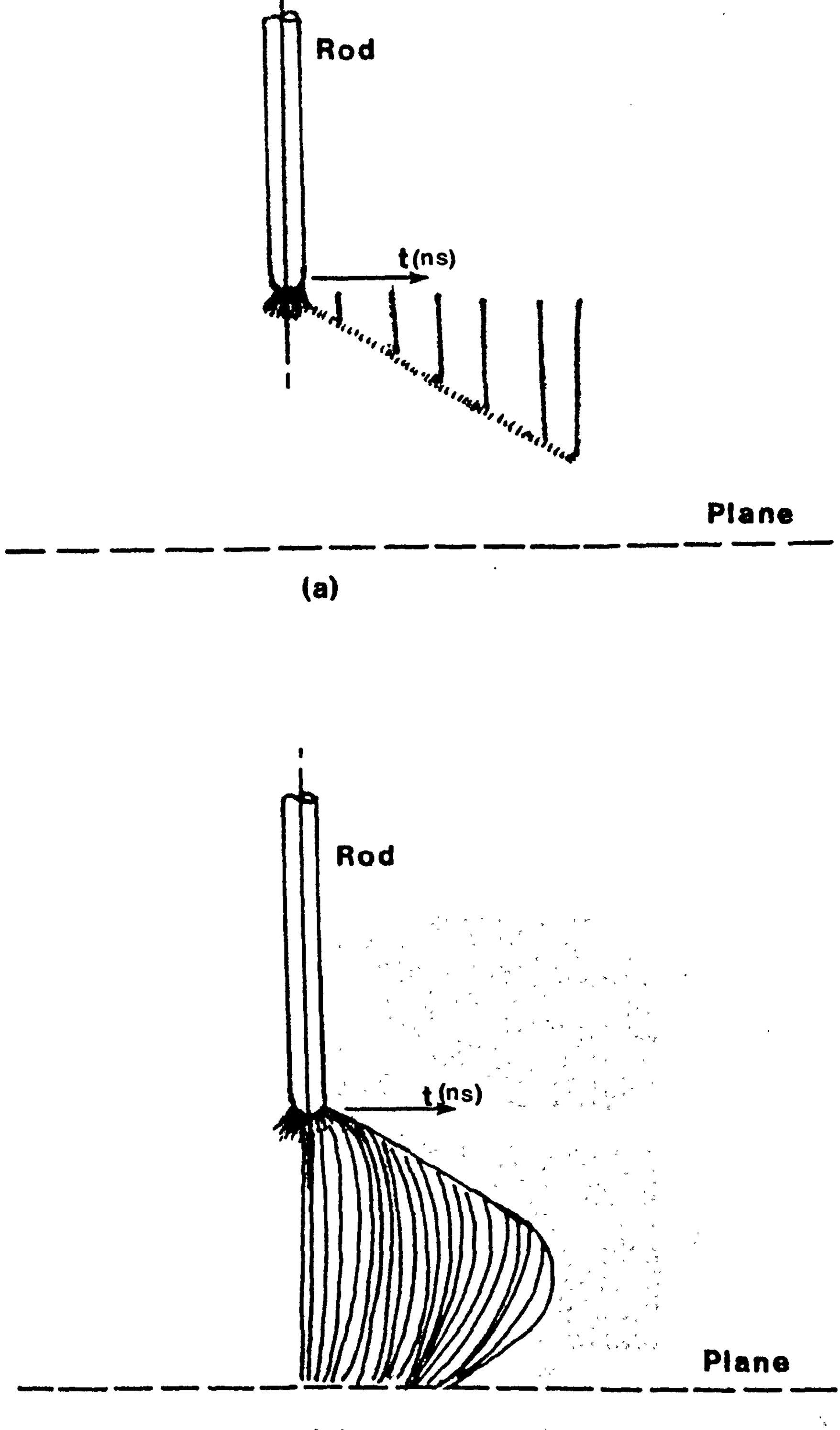

Figure 2.11.1 : Schematic of the streak photographs of the discharge in

(a) SF_6

(b) N_2

(Watanabe and Takuma, 1977)

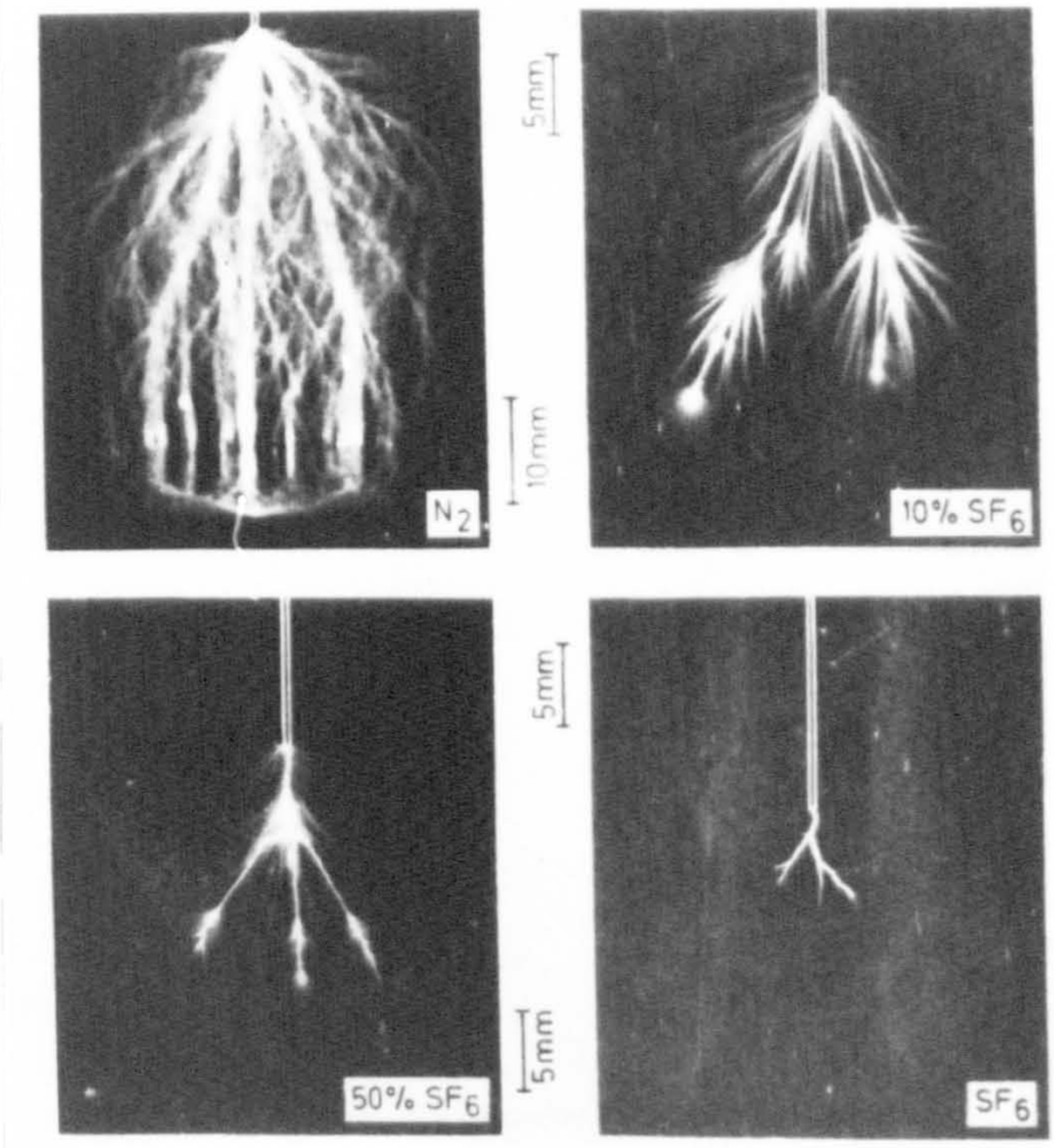

(a)

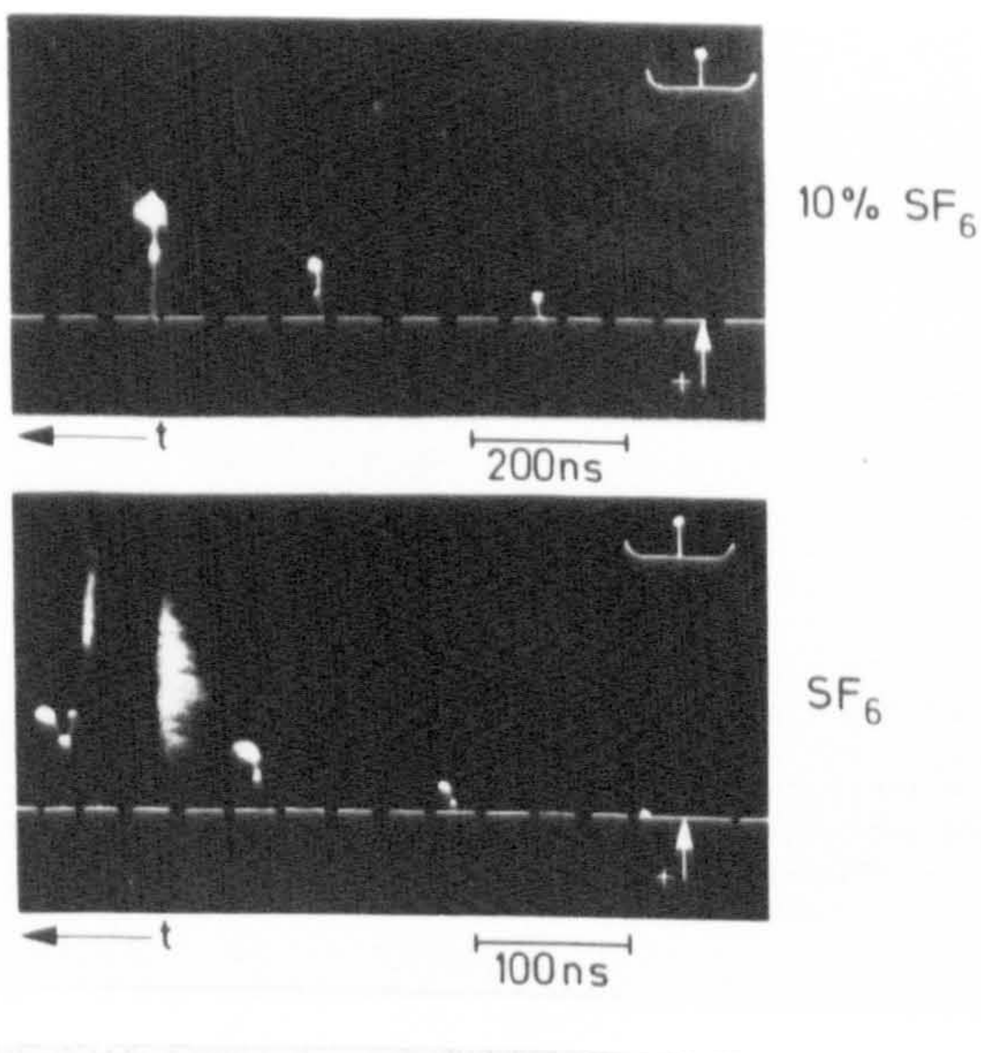

(b)

Figure 2.11.2 : The development of the discharge in SF_6 and mixtures of SF_6 with N_2

(a) still photographs (b) time resolved photographs

(VOSS 1979)

of Watanabe and Takuma (1977) regarding the stepped leader growth. In his experiments Voss reports that the duration of the steps change from 200 ns for 10% SF_6 in nitrogen to 70 ns in pure SF_6. Voss has proposed a model to predict the minimum breakdown voltage, by using measured values of streamer and leader electric fields together with the critical leader length. Chatterton (1979) has used a corona cloud model for impulse voltage breakdown where the cloud limits were determined by the absorption length and the critical avalanche length originally proposed by Farish et al (1977) to predict the critical pressure p_c at which corona free breakdown occurs in non-uniform fields. Nelson et al (1982) showed, using an optical multichannel analyser in 50% SF_6 50% N_2, under steep fronted impulse waveforms in non-uniform fields, that : the luminous extent is greater than is predicted by the cloud model advanced by Chatterton (1979).

In switching impulse tests of 30 cm rod-plane gaps in SF_6, Kurimoto et al (1975) showed that the effects of corona stabilization were greatest at subatmospheric pressures, thus for positive impulse voltages the critical pressures p_c were 800 torr and 400 torr for 1.9 cm and 6 cm diameter rods respectively. Farish et al (1978) have shown that in small point plane gaps of length between 2 and 20 mm, with point radii ranging from 0.2 to 2 mm in SF_6 under d.c. voltages, that in the negative slope region of the V_b, p characteristic widely differing results, for the same experimental conditions were prevalent. They observed the development of the discharge using an image intensifier. The discharge in SF_6 near p_c is highly filamentary, whereas in 50% SF_6 50% N_2 mixture at p_c the discharge exhibits a glow near the anode, also further in the gap the filaments terminate in a luminous spherical volume. Kurimoto et al (1978) attempted

to predict the critical pressure for rod-plane gaps in SF_6 and air. In this study a simplifying assumption that : the corona free breakdown conditions are satisfied when the photoabsorption mean free path for ionization radiation becomes equal to the radius of the critical avalanche head. They showed by studying a 30 cm rod plane gap in SF_6, with rods of diameter 1.9 cm and 6 cm, that the critical pressure reduces with field non-uniformity under switching impulse voltages. In addition, they showed that the filamentary channel crosses the gap when the average channel potential gradient becomes less than the average applied potential gradient (v/d) in the gap. Farish et al (1979) by studying a 20 mm point plane gap under d.c. conditions at pressures below 3 bar in SF_6 and mixtures of SF_6 with nitrogen showed the discharge to have many reilluminations even under d.c. conditions, figure 2.11.3 shows the discharge in 50% SF_6, 50% N_2. They concluded that, the breakdown in the rising part of the voltage pressure characteristic is determined by the space charge controlled field and that the minimum field required for streamer propagation could be estimated to lie between 39 and 47 kV cm^{-1} bar^{-1} depending on the pressure. Ibrahim and Farish (1980) studied the impulse breakdown and pre breakdown phenomena in SF_6 and mixtures of SF_6 with nitrogen, in gaps up to 20 mm using standard impulse waveforms. They showed that in pressures up to 3 bar, the corona stabilization process is less effective under impulse voltages than it is under d.c. Also, the initiatory electrons greatly influence the corona initiation characteristics. The time resolved records of the discharge at breakdown in 10% SF_6 90% N_2 show it to be diffused with few reilluminations, but it shows a distinct stepping mechanism. In 50% SF_6 50% N_2, however, the

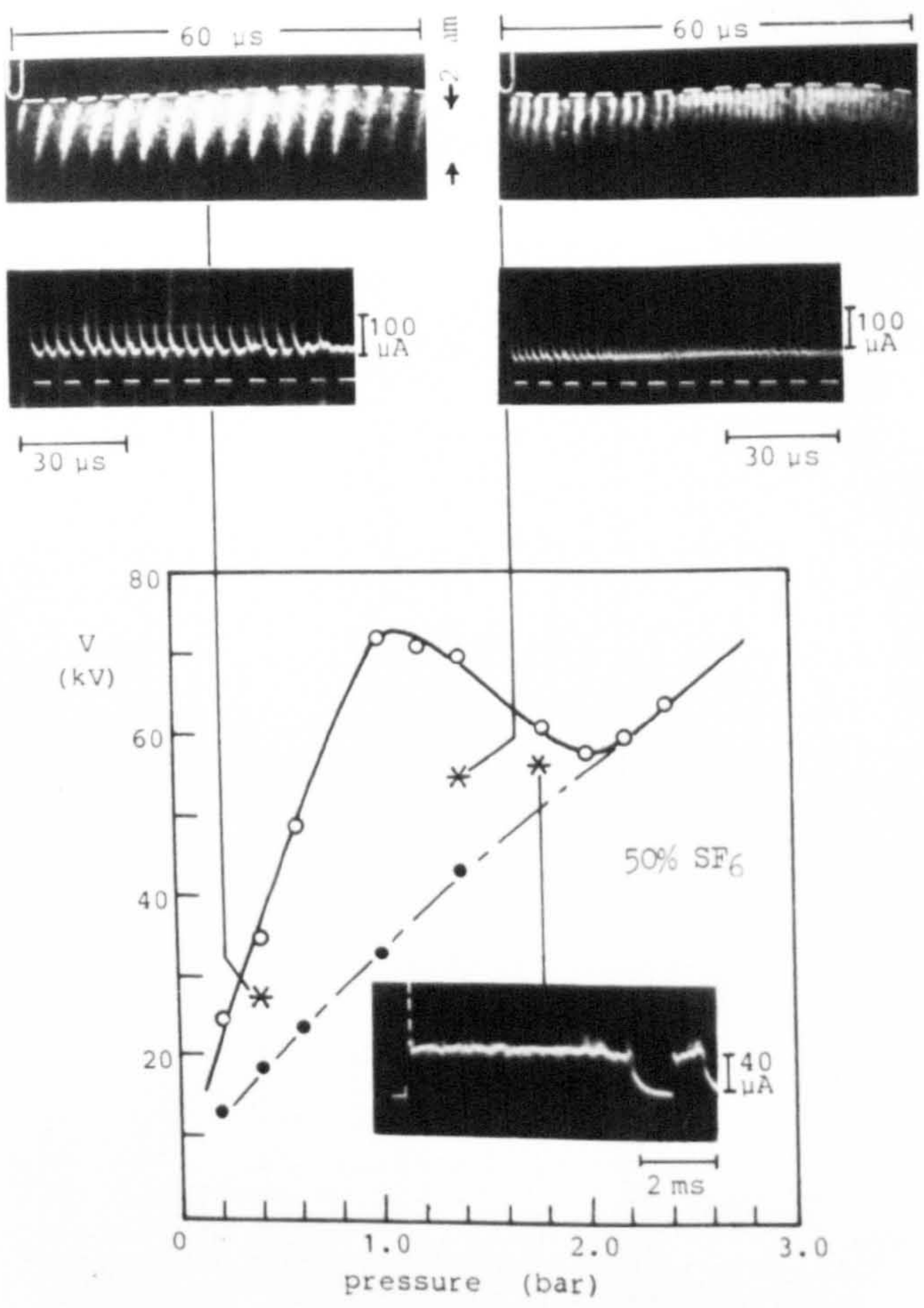

Figure 2.11.3 : The development of prebreakdown discharge under d.c. voltage (Farish et al, 1979).

time resolved photographs show the discharge to be very similar to those obtained by Voss (1979). Figure 2.11.4 shows the time resolved photographs of Ibrahim and Farish (1980). In the 50% SF_6 50% N_2 mixture Ibrahim et al (1980) also show distinct reilluminations and a stepped mechanism. It is seen that even in small gaps the discharge propagates in steps. Anis and Srivastava (1981) examined the types of discharge pulses in a rod plane gap under different impulse voltage waveforms. They have attempted to relate the random dispertion of discharge pulses to the rate of production of initiatory electrons near the anode. By these considerations they derived a relationship between the rate of production of electrons and the electric field strength. Anis and Srivastava (1982) have also studied the breakdown in a point plane gap under switching impulse voltages. An impulse breakdown threshold has been defined which is different from the 50% breakdown voltage. In this threshold case the probability of occurrence of breakdown is very much smaller than 50%. They argue that by analysing it in this manner, the effects of statistical formation could be deleted and the systematic corona stabilization could be singled out. Anis and Srivastava (1982) defined two values of critical pressure (1) p_{c1} is the pressure at which the corona onset voltage equals the impulse breakdown threshold and (2) p_{c2} is the pressure at which the impulse corona onset plus the breakdown threshold equals the static corona onset voltage. They have shown that both p_{c1} and p_{c2} increase with the ratio of gap length to radius of the point (d/r) and that they tend to reach a plateau at about d/r = 100.

The recent measurements of Pigini et al (1982) in long point plane gaps in SF_6 under switching impulse voltages have shown the development to be stepped with a large number of reilluminations. Figure 2.11.5 shows a

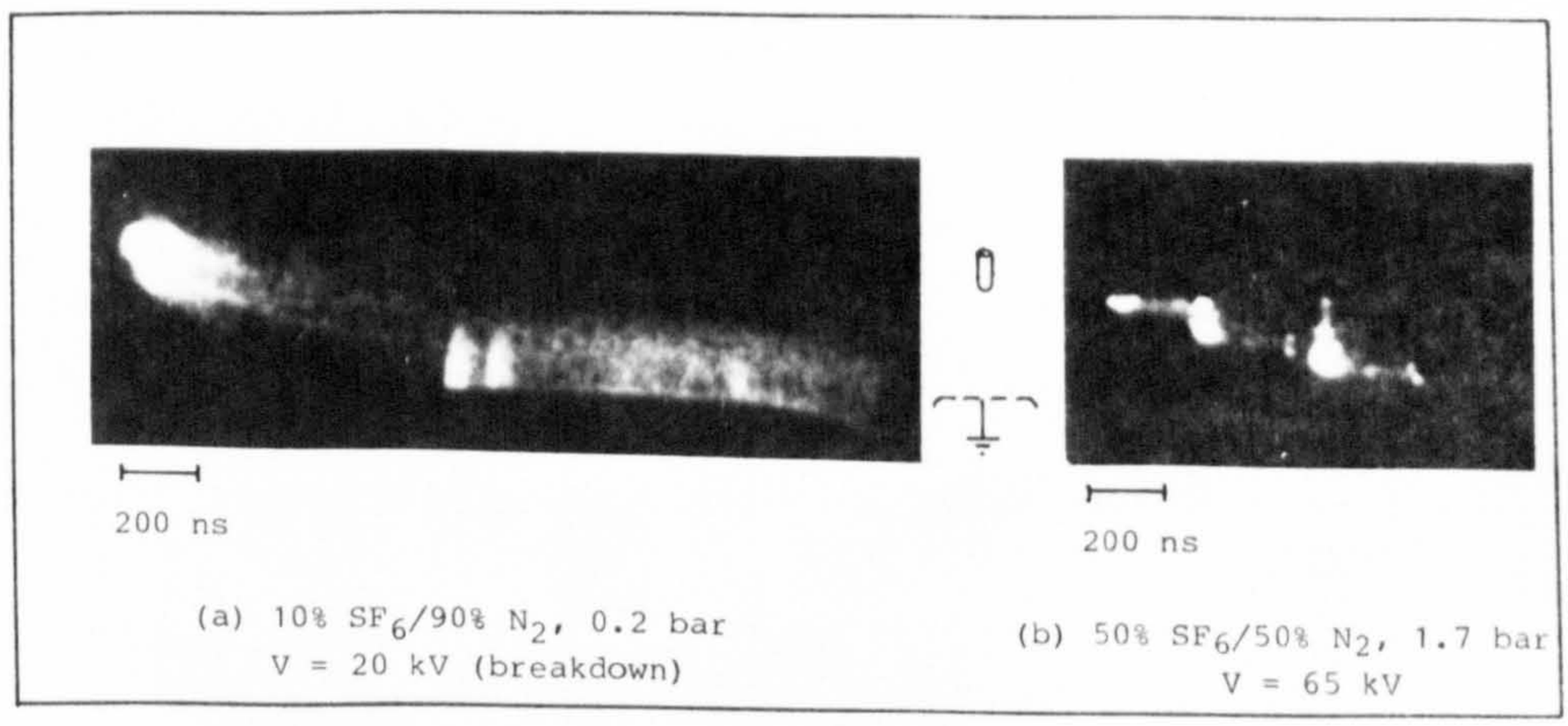

(a) 10% SF_6/90% N_2, 0.2 bar
V = 20 kV (breakdown)

(b) 50% SF_6/50% N_2, 1.7 bar
V = 65 kV

Figure 2.11.4 : Time resolved photographs of prebreakdown discharge development (Ibrahim and Farish, 1980).

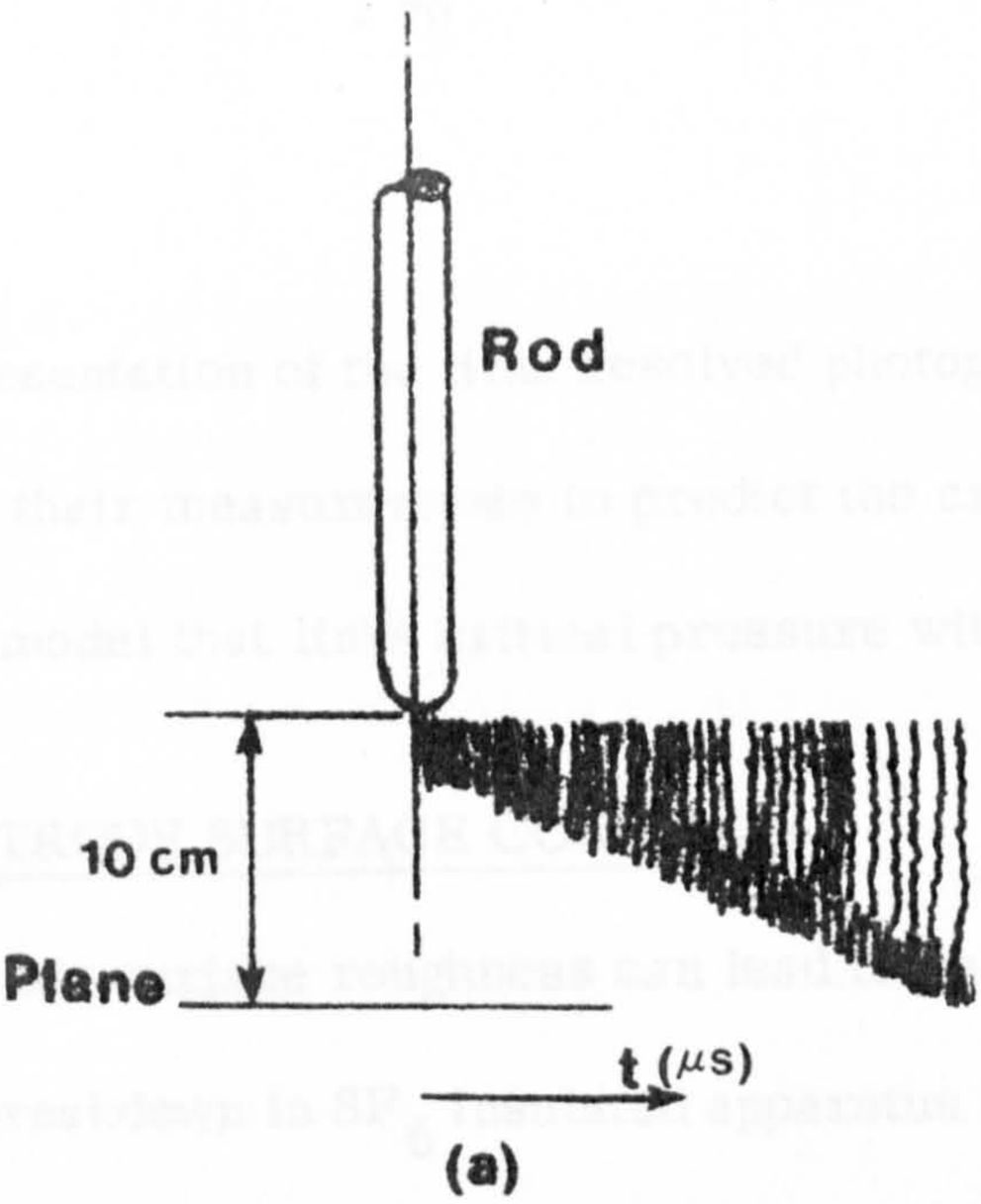

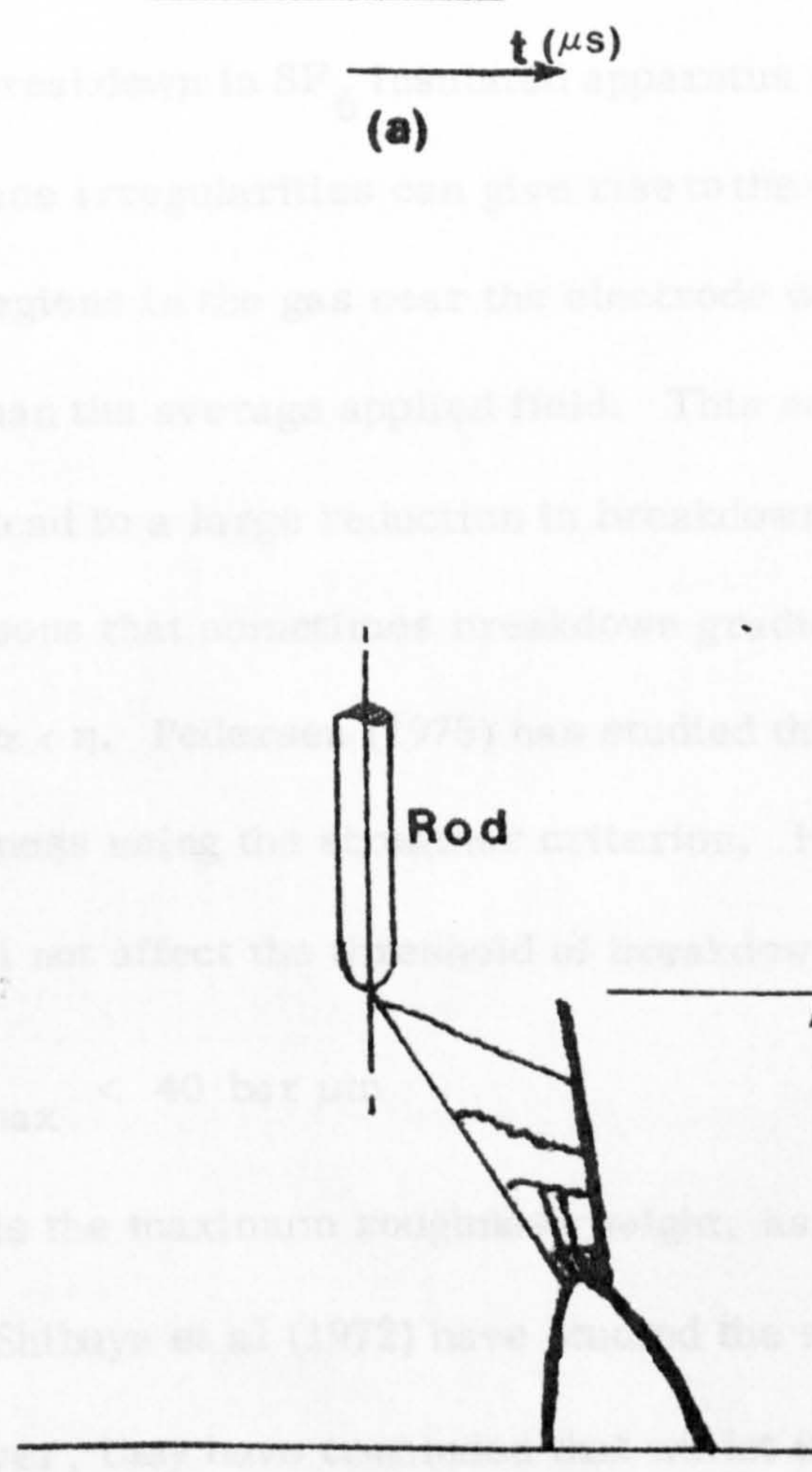

Figure 2.11.5 : Schematic diagrams of time resolved photographs obtained in SF_6 .

(a) withstand, streak mode at 3 bar

(b) breakdown, streak mode at 2.2 bar

(Pigini, et al 1982).

schematic representation of the time resolved photographs of Pigini et al. They have used their measurements to predict the critical pressure p_c using a simple model that links critical pressure with electrode radius.

2.12 ELECTRODE SURFACE CONDITION

Electrode surface roughness can lead to substantial reduction of the threshold for breakdown in SF_6 insulated apparatus where no particles are present. Surface irregularities can give rise to the existence of localised microscopic regions in the gas near the electrode with a field strength much higher than the average applied field. This condition depending on the pressure can lead to a large reduction in breakdown voltage. This could be one of the reasons that sometimes breakdown gradients in SF_6 are in the region where $\alpha < \eta$. Pedersen (1975) has studied the influence of the electrode surface roughness using the streamer criterion. He has showed that surface roughness will not affect the threshold of breakdown if

$$p\,R_{max} < 40 \text{ bar } \mu m \qquad (2.33)$$

where R_{max} is the maximum roughness height, assuming a hemispherical protrusion. Shibuya et al (1972) have studied the same effect using a different model, however, they have concluded that whilst it can be used to explain the growth of small currents in high pressure SF_6, it is unable to explain the rapid growth of current in high field regions. According to Cooke (1975), the breakdown voltage decreases when the product of gas pressure and protrusion height above the flat electrode surface exceed about 80 bar μm. Detailed investigations have been carried out to understand the effect of pressure, shape and size of electrode surface protrusions and the field configurations on the discharge characteristics of SF_6. Experimental

findings support the theoretical calculations to a reasonable degree as shown by several authors (Pedersen 1975, Bortnik and Cooke 1972, Berger 1976, Cooke 1975, Kawaguchi et al 1971). It has been reported that uneveness caused by machining which gives rise to undulations of up to 30 μm had only minimal effect on the breakdown of a coaxial system for a pressure of up to about 5 bar. However, contrary to this view point McAllister (1980) has shown that in a practical system the electrode surface roughness will always lead to a reduction in the insulation strength. McAllister has obtained a model for surface roughness associated with a non-uniform field geometry, including the macroscopic curvature of the high voltage electrode. He has said that most of the previous models may be in error due to the fact that they had not considered the macroscopic curvature of the electrode, this perhaps may be the reason for erroneously concluding that there is a lower limit to the effect of surface roughness upon the insulation strength.

2.13 ELECTRODE AREA

As the area of electrodes is increased, the breakdown voltage in SF_6 decreases until the electric field strength reaches about 100 kV cm^{-1} (Cookson, 1970). The figure 2.13.1 shows the 0.5% breakdown strength as a function of electrode area and pressure (Nitta et al 1974).

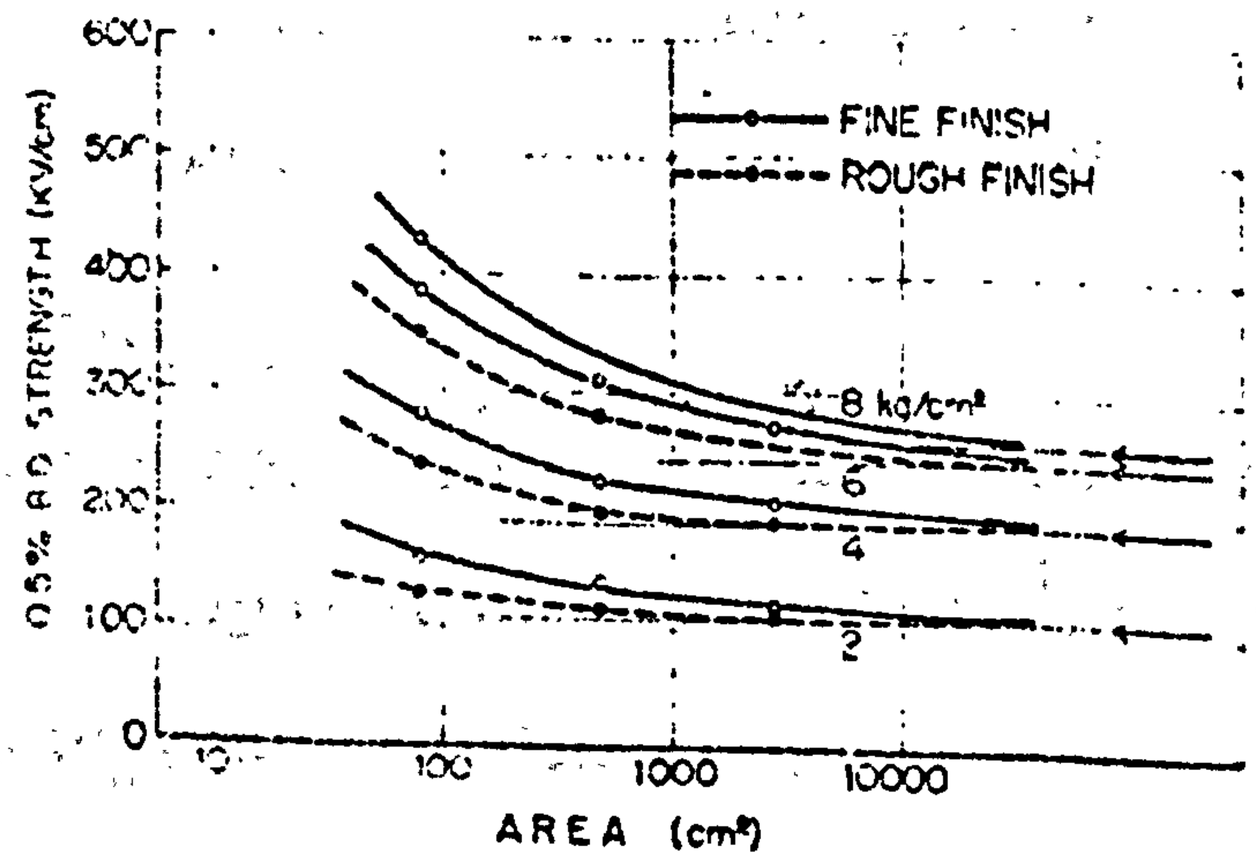

Figure 2.13.1 : (Nitta et al 1974)

Minimum Breakdown Field Strength as a Function of Electrode Area

The influence of electrode area is more pronounced at high pressure, and high electric fields. Nitta et al have proposed an extreme-value cumulative probability distribution for breakdown. Their results show a minimum value of field strength independent of the surface roughness. Masetti et al (1980) by using a modified version of the distribution used by Nitta et al have shown the absence of a minimum electric field strength with increase in area. The work of Rein et al (1977) is more in line with that of Nitta et al. Their observations confirm that the electric field strength decreases to a minimum with increase in the electrode area. The waveform and polarity also affect the electrode area. The negative switching impulse breakdown gradients are influenced to a lesser degree than those due to power frequency voltages. This could be ascribed to the different durations of the two voltage waveforms.

The breakdown of the gap in SF_6 is governed by the maximum potential gradient. The points at which the potential gradient is high is called a weak point because they are more susceptible to breakdown of the gap than other points. The number of these points increase as the gap and electrode area are increased. The weak points of the gap breakdown in an irregular pattern and thus the breakdown voltage changes by a conditioning effect. The number of conditioning sparks and the relative increase in breakdown voltage becomes larger as the electrode area is increased (Cookson, 1970).

2.14 ELECTRODE MATERIAL

The effect of field strength on electrode material does not show up into the field strength exceeds about 200 kV cm^{-1}, and pressure reaches about 3 bar in SF_6 (Goryunov 1975). At higher pressures similar dependences of breakdown voltage on electrode material have been reported, in other gases

and their mixtures with SF_6 (Cohen 1956, Cookson 1970). While under uniform field conditions in SF_6 the breakdown voltage is dependent on the electrode material, under certain experimental conditions no such dependence has been reported in non-uniform fields, such as coaxial arrangements up to about 4 bar (Kawaguchi et al 1970). The breakdown voltage is primarily dependent on the cathode material and the influence of electrode material. increases with increase in gas pressure, and electric field strength. However, Cookson (1970) has reported anode effects under other experimental conditions. McAlpine and Cookson (1970) showed that an insulating film on the anode affects the breakdown voltage in compressed SF_6. It has been known that the insulation strength increases significantly with an insulating film on the cathode. In general insulating coverings improve the breakdown strength characteristics. McAlpine and Cookson (1970) have observed that under uniform field conditions, with insulating coverings on the electrodes Paschen's law is obeyed for electric field strengths up to about 130 kV cm^{-1}.

2.15 SUMMARY

This study was undertaken to measure the critical pressure and electric field strength in SF_6 and mixtures of SF_6 with N_2, under lightning impulse voltages. These were unknown quantities at the time this study was first undertaken. However, recently, Anis and Srivastava (1982) and Pigini et al (1982) have reported their results relating to critical pressure and electric field strength in SF_6. As is evident from this review their experimental conditions were different from those of the author. In this thesis, the electrostatic radius of the discharge channel, and the internal field strength were estimated by fitting an electrostatic model to the experimental

results. Whilst the luminous radius of the discharge channel could be estimated by recourse to time resolved and still photographs of the discharge, the estimation of the electrostatic radius of the discharge channel would require a far more accurate electrostatic model. There is still a dearth of information regarding critical pressure under impulse voltage conditions, as such a lot more work is required to be carried out in order to obtain reliable experimental results. This would also help to a great extent the theoretical modelling of the critical pressure under impulse voltage conditions. Another quantity that has so far been sparsely studies is the determination of corona initiation voltage under impulse voltages, in SF_6 and mixtures of SF_6 with other gases. The differences that exist between the experimental results of corona initiation voltage (V_i) and the theoretical ones have yet to be explained to any degree of satisfaction. Although the lack of initiatory electrons has been advanced as a plausible arguement. A full discussion of the critical pressure and electric field strength will be given in Chapter 5. It is envisaged that the discussion to follow will bring out the possibilities of using these internal electric field strengths to predict the critical pressure and breakdown voltage.

CHAPTER 3

APPARATUS AND EXPERIMENTAL METHOD

3.0 EXPERIMENTAL APPARATUS

The high voltage source used was a fourteen stage Ferranti "Marx" generator. The circuit diagram of the impulse generator is shown in figure 1. The maximum charging voltage per stage is 100 kV. For this voltage the maximum stored energy is 11 kJ. The capacitance of each stage is 0.14 μF. Two stages of this generator were used for most parts of this experiment. However, occasionally four stages were used.

The wave shapes used were 1/50 μs and 1/10000 μs, the magnitudes of the various resistors used are shown in figure 1.

The load or the output capacitance is made up of two sections each of capacitance 800 pf, connected in series giving a total wavefront capacitance of 400 pf. This capacitor also formed the high voltage arm of the capacitance potential divider used for measurement of output voltage. The low voltage arm of the capacitance voltage divider consists of a 0.6196 μF capacitor whose loss resistance is 0.06 mΩ. The impulse voltage is divided up in the ratio 1 : 1550 by this divider. The signal at the oscilloscope was divided further by a factor of approximately 1 : 20 using a resistive network, consisting of two resistors of value 1 kΩ and 50 Ω. A 100 V neon connected across the 50 Ω resistor was used to protect the amplifier of the oscilloscope.

The power supply of the impulse generator is a 2 x 220 / 50,000 V transformer connected to the mains via a voltage stabiliser. The high voltage side of the transformer is connected to the charging resistor of the generator through a voltage doubler and polarity switch. A 100 kV resistance potentio-

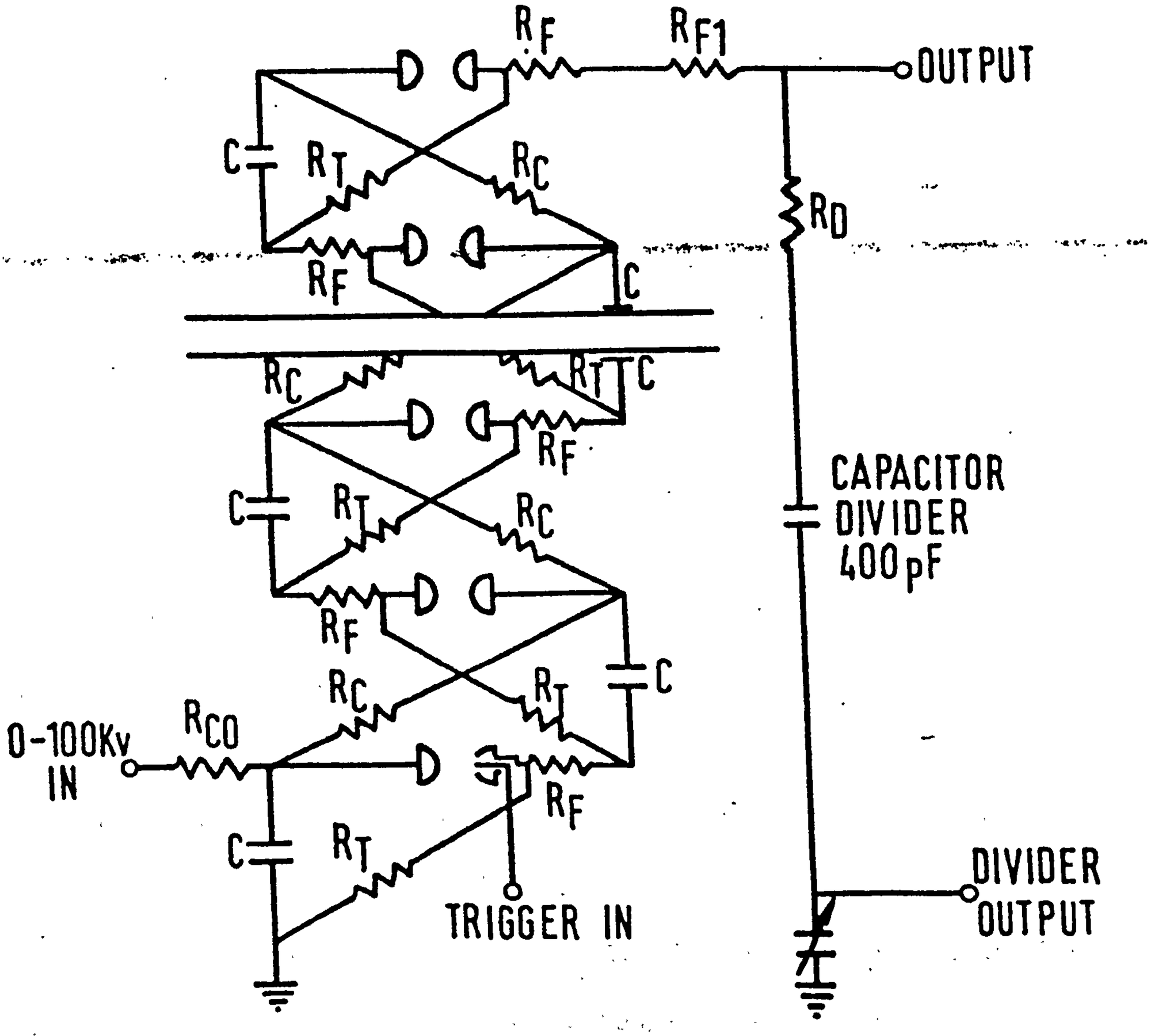

C = 0·14 μF 100Kv

R_C = 25·1 KΩ, 10MΩ

R_T = 495Ω, 10MΩ

R_{CO} = 538KΩ

R_F = 34·2Ω

R_{F1} = 500Ω

R_D = 100Ω

14- STAGE FERRANTI IMPLUSE GENERATOR.

Figure 1 : Circuit diagram of the impulse generator

meter is connected in parallel with the impulse generator. This provides the control signal for the voltmeter that measures the charging voltage per stage.

The stage voltmeter of the impulse generator was calibrated in terms of the output of the impulse generator, the output being measured by standard sphere gaps and capacitive voltage divider incorporating an oscilloscope.

3.1 METHOD OF REDUCING IMPULSE GENERATOR

The procedure adopted for reducing the impulse generator to two stages from fourteen stages is as follows. A bare conducting wire was placed from the very top stage to the desired second stage on the earthy side of the generator. The charging resistor connecting the second stage to the third stage was removed. This effectively reduced the generator to one of two stages, with a maximum output voltage of $\pm$ 200 kV. If, however, the wave-tail resistor is removed instead of the charging resistor, then the stage voltage appears at the output of the generator and hence on the anode of the experimental gap. This can be useful, if a glow discharge is required at the point electrode, to check the alignment of the optics, for instance.

In order to change the waveshape of the reduced, two stage generator, from 1/50 μs to 1/10,000 μs, three 10 MΩ high voltage resistors were utilised. Two of these resistors were used as wavetail resistors and the third replaced the 25.1 kΩ charging resistor.

When the long wavetail waveform was used a Tektronix X10 or a X100 voltage probe was used at the oscilloscope to display the impulse generator output voltage signals.

3.2 CALIBRATION OF THE IMPULSE GENERATOR

3.2.1 Determination of operating region of impulse generator

The operating region of the impulse generator was determined by obtaining the self triggering and no triggering regions. To obtain the self triggering region, the gaps were set at a particular value, and the voltage was raised gradually until the gaps flashed over spontaneously. Care was taken to ensure that enough time was given for the capacitors to charge to the appropriate value. The procedure adopted for obtaining the no trigger region was : having obtained a self triggering point the voltage was reduced in steps of about 5%, and after allowing time for settling the impulse generator was triggered. This was repeated until a value was reached below which flashover of the gaps was not possible. The foregoing was repeated for a series of gap settings encompassing the whole range of the impulse generator, Figure 2 shows the self triggering and no triggering regions, and the mean graph for the trigger characteristics of the two stage impulse generator.

3.2.2 Calibration using sphere gaps

The method of calibration described below applies to both waveforms, namely : 1/50 μs and 1/10,000 μs. Standard spheres of diameter 25 cms were used. In addition to the sphere gaps the oscilloscope (Tektronix 7633) was used to record the impulse waveform and the crest value of the applied voltage. The method adopted is called the up-down method, described in detail by Bakken (1967). Hertig and Ingmann (1965) have treated the determination of switching surge ratings from both a theoretical as well as from a practical point of view. The method of calibration is as follows : The voltmeter on the main console is graduated in voltage per stage. For a given value of voltage on this meter the output voltage depends on the number

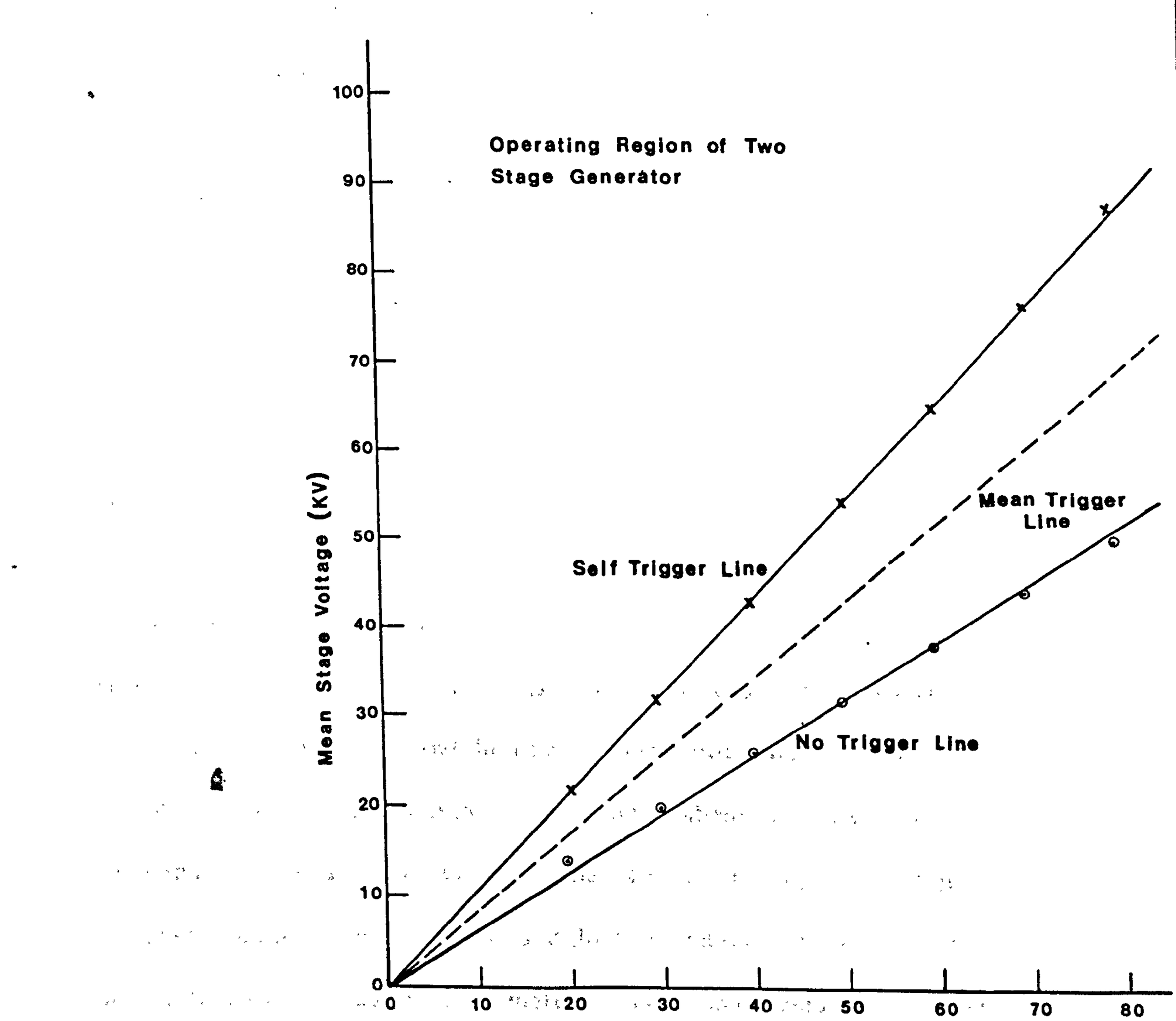

Figure 2 : Operating characteristics of impulse generator

of stages in use. The sphere gaps were placed such that the gap corresponded to a known flashover value, which was obtained from the IEC charts. Care being taken to make the appropriate connections for temperature and humidity as given by Kuffel and Abdulla (1979). A point depending on the applied voltage, was chosen from the operating chart of figure 2. The voltage corresponding to this value was placed on each stage of the reduced impulse generator. The generator was next triggered, if the gap flashed over, the voltage was reduced by an amount between 1 and 4 per cent of this flashover value. Having reduced the voltage the above was repeated. The voltage was then either decreased or increased depending on whether there was a flash-over or a withstand. If the first voltage setting gave a flashover of the gap, then the voltage was reduced by between 1 and 10 per cent until there was a withstand, this gave the region of interest (Bakken 1977). Having ascertained the voltage where there was a withstand, the voltage was increased by a few percent until there was flashover of the gap. This flashover voltage was taken as the starting point. The voltage was next reduced by about two per cent of the flashover value and the impulse generator triggered. This procedure was repeated, increasing the voltage whenever there was a with-stand and decreasing when there was a flashover. For any one setting of the sphere gap between twenty five and thirty impulses were applied and the 50% flashover voltage was estimated using the expression given below.

$$V_{50} = \frac{1}{N} \sum_{s=1}^{N} V_s$$

where N is the actual number of breakdowns.

Figures 3 and 4 show the calibration graphs for the two waveforms.

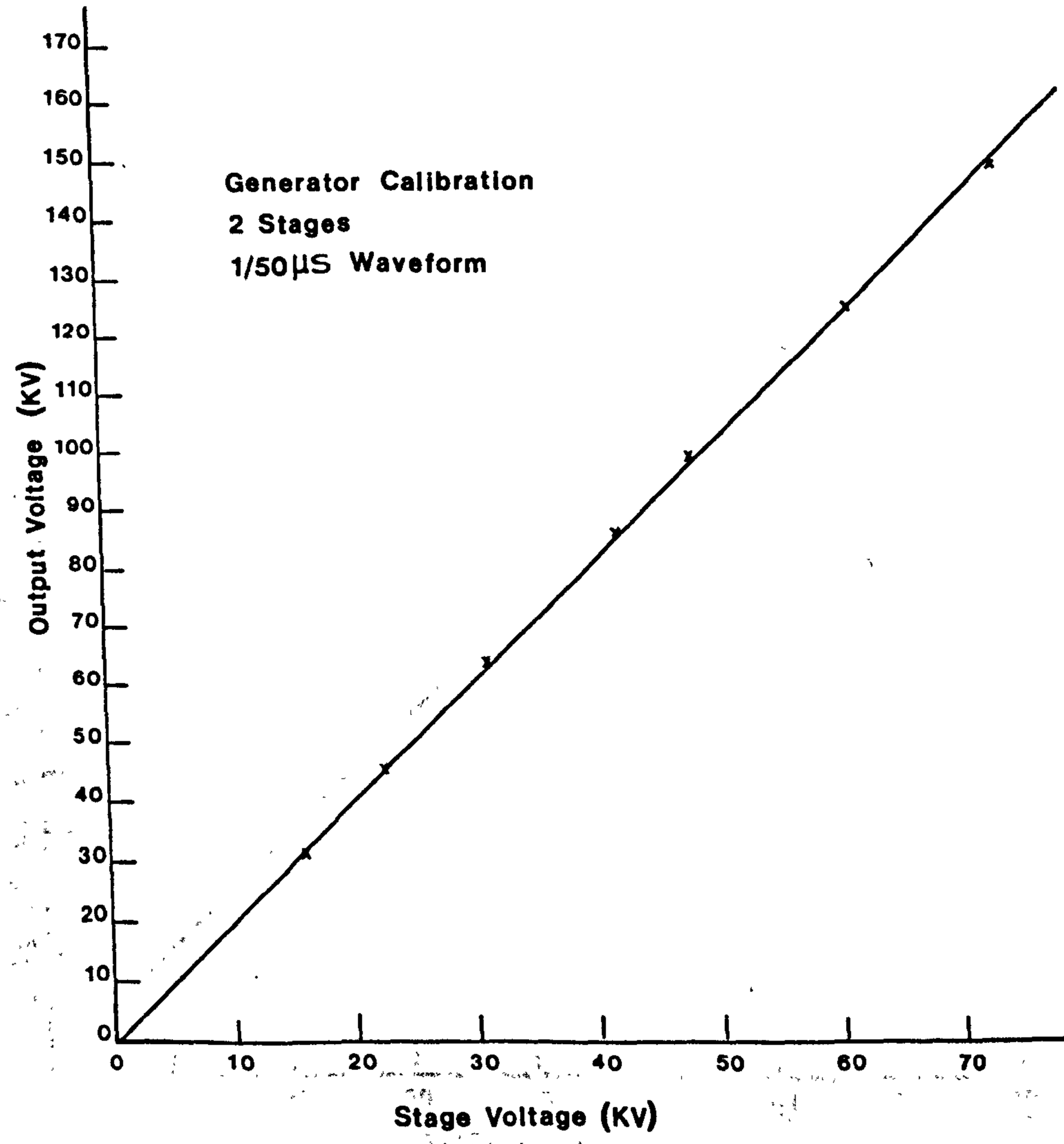

Figure 3 : Calibration graph of the two stage impulse generator for 1/50 μs voltage waveform.

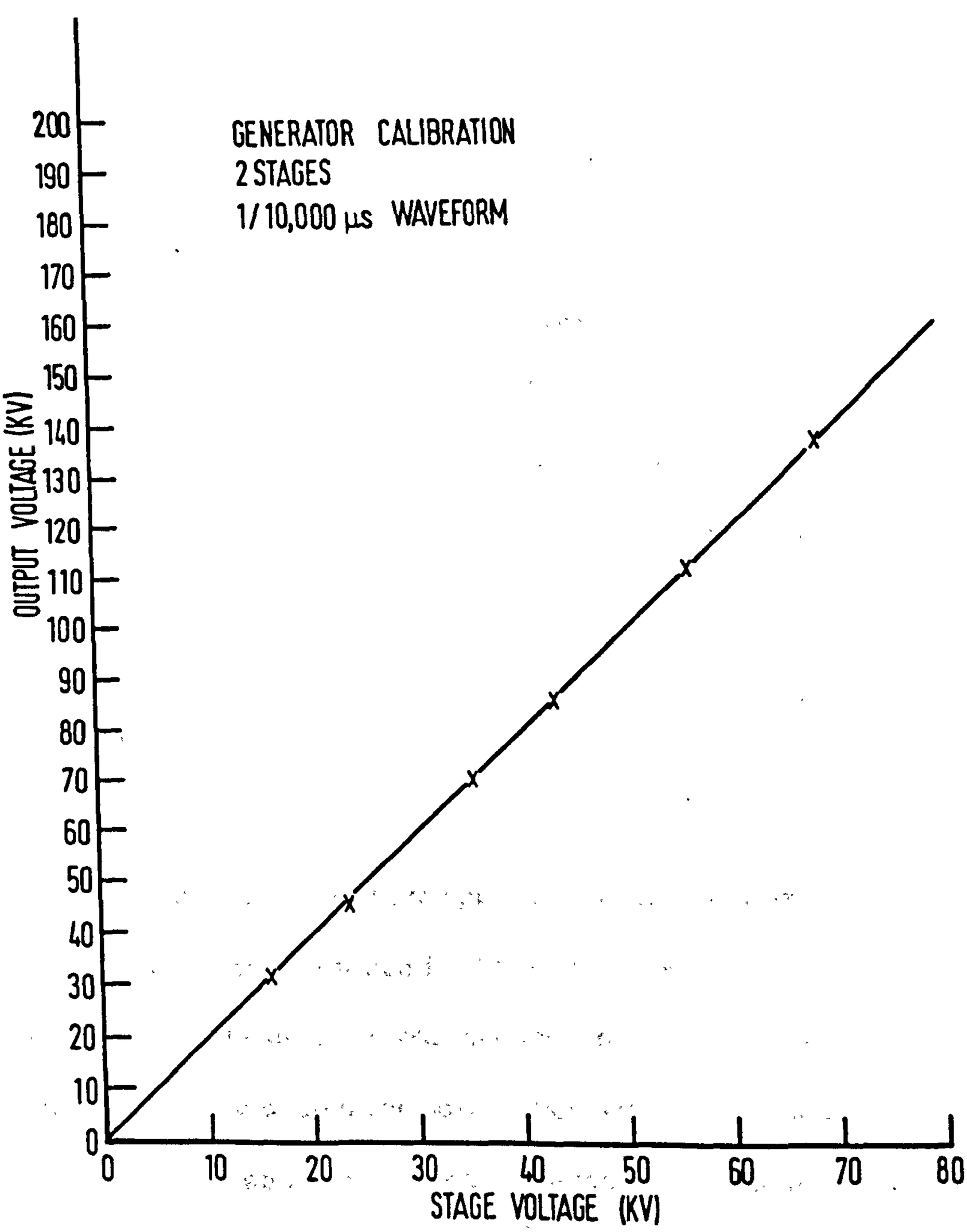

Figure 4 : Calibration graph of the two stage impulse generator for 1/10,000 μs voltage waveform

3.3 EXPERIMENTAL GAP

The experimental gap consisted of a cylindrical rod of Tungsten, with a hemispherical end. It was ground and polished to a finish of 3 μm using diamond paste. The plane consisted of a Rogowski profiled electrode of diameter 143.5 mm made of duraluminium. The plane electrode carried three field probes each diameter 1 mm (Meek and Collins 1965). The rod was the high voltage electrode and the plane was earthed. The gap length was fixed at 55 mm. The diameter of the rod electrode was 2 mm, giving the tip radius as 1 mm. The gap was set using an internal micrometer screw gauge which could be read to an accuracy of 0.01 mm. Figure 5 shows the electrode support assembly, the Rogowski profiled plane electrode could be moved up and down by using a linear motor drive, it could also be operated manually. In fact, all the gap settings throughout the experiment were carried out manually. The grinding and polishing of the electrodes was carried out by the staff of the Instrument Workshop.

3.4 EXPERIMENTAL CHAMBER

The experimental gap described in the previous section was housed in a chamber, a schematic diagram of which is shown in figure 6. The vessel was made of stainless steel and had an internal diameter of 40.6 cm, and an inside length of 72.4 cm. There were three observation windows, and a port for admission of gases. There was also a safety value that was set at a bursting pressure of 20 bar. Quick access to the inside of the chamber could be made through one of the viewing ports. The base plate of the experimental chamber could be unbolted and removed completely. The base plate carries the electrode assembly shown in figure 5. The base plate of the chamber also carries feed throughs for probes on the plane electrode.

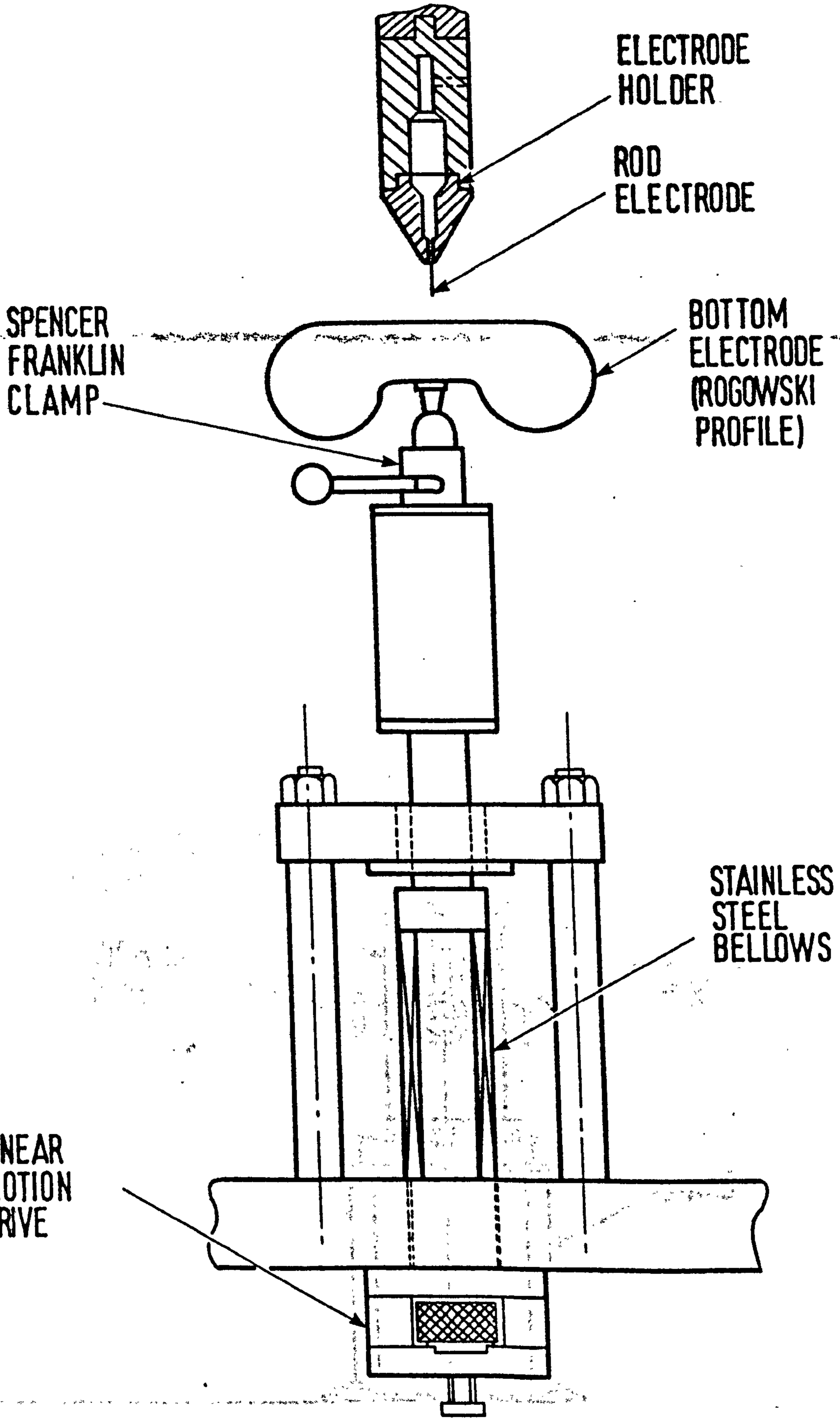

Figure 5 : ELECTRODE SUPPORT ASSEMBLY

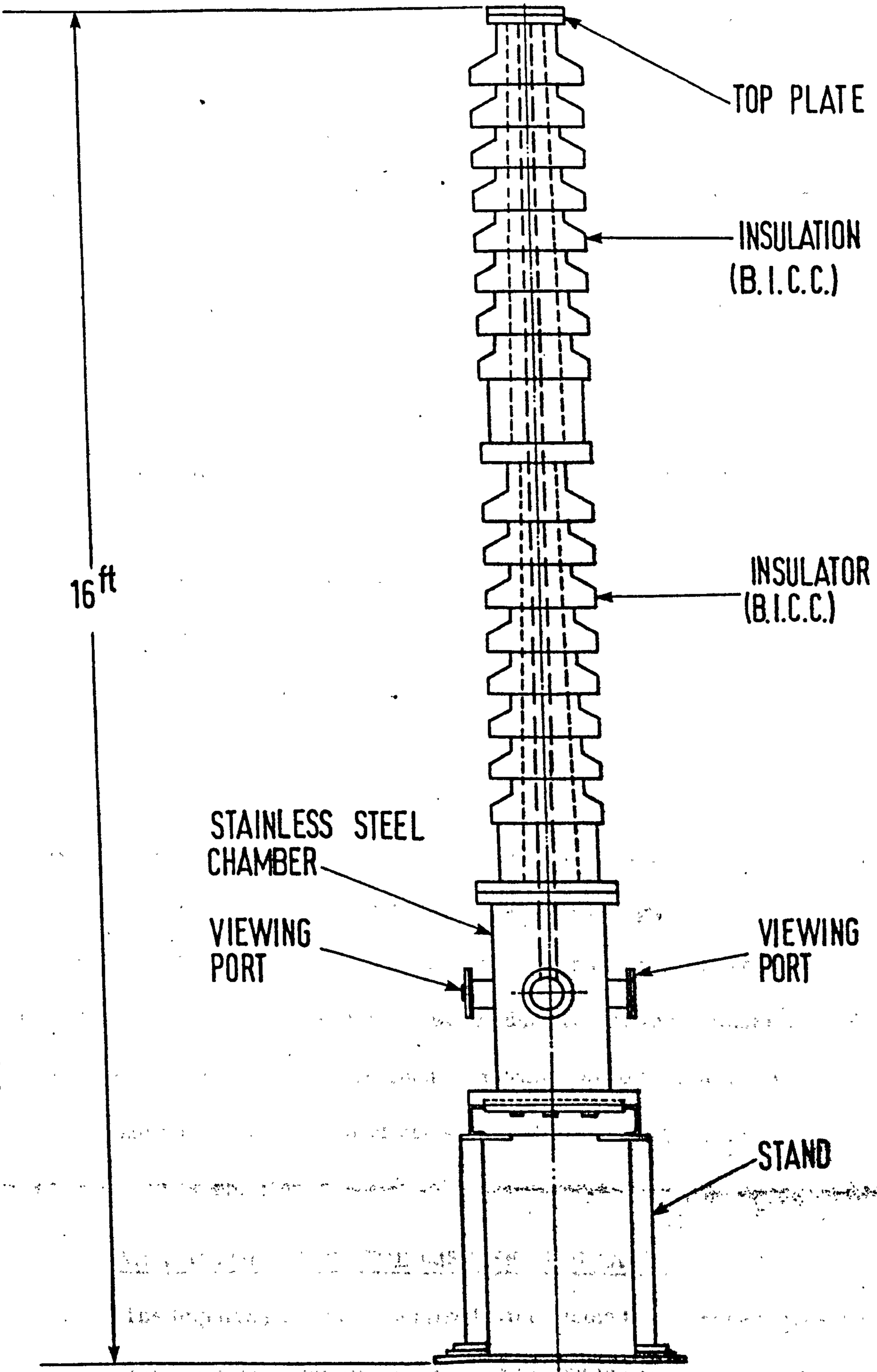

Figure 6 : GENERAL ARRANGEMENT PRESSURE VACUUM CHAMBER

The inside of the experimental chamber was painted with "Aquadag". This is a colloidal graphite which was diluted with distilled water. The purpose of blackening the inside was to ensure against reflections that may occur from the walls of the chamber during spark development. The inside of the base plate was similarly blackened. The experimental gap could be adjusted whilst the chamber was pressurised.

Two sections of B.I.C.C. porceline insulators each of length 1.61 m were connected together to form a composite insulator. This composite insulator was bolted to the top of the experimental chamber as shown in figure 6. The high voltage electrode was led into the experimental chamber through this insulator. The total assembly was carried on a steel stand that stood about 1 m above the laboratory floor. The experimental chamber could be evacuated to a pressure of 0.02 torr.

The pressure was measured using a Wallace and Tienan pressure gauge inat read the absolute pressure. It was graduated in steps of 0.5 p.s.i. The gases used were sulphur hexafluoride (SF_6) 99.66% pure, and oxygen free nitrogen (N_2) 99.9% pure. The cylinders of gas were supplied by the British Oxygen Company. The gases were admitted into the chamber through a filter to free them of dust. To ensure the gases were free of moisture and to absorb noxious spark products silica gel and activated alumina were placed inside the chamber.

3.5 METHOD OF FIRING THE IMPULSE GENERATOR

The impulse generator was fired from inside the screened measuring room (Faraday Cage). The problem that was faced in achieving this objective was one of earth isolation. The Faraday Cage was a completely isolated screened room made of copper. It was in position before the experiment was

started. The power supply to this room was obtained from the mains through an isolating transformer and mains filter. The Faraday cage was earthed through a copper tube to the bottom of the capacitor divider. All the instruments inside the screened room were earthed at this point, as such taking another earth inside it created an earth loop. When the impulse generator was fired under these circumstances, large circulating earth current flowed in the earth loop, thus generating spurious voltage drops. These spurious voltages were picked up by the measuring circuits, and were manifested as noise superimposed on the actual signals that were being measured. Due to these reasons their elimination was imperative.

In order to overcome this problem, an optical coupler which gave complete earth isolation, was designed and installed by the staff of the Electronics Workshop in close collaboration with the author. The figures 7 and 8 show the details of the optocoupler and firing circuit. Figure 9 shows a block diagram giving the essential parts.

A pulse generator (Type Farnell) placed inside the screened room provided a square pulse of about 10 V amplitude, and pulse width 2 μs. This pulse was received and converted to a light signal by a light emitting transistor. The light was transmitted through a perspex tube where it was received and converted to an electrical signal once again. This electrical signal was driven down a transmission line by a line driver. The pulse that was driven down the line triggered the gate of a thyristor, which provided a pulse into the triggertron of the impulse generator. The delay between providing the first pulse from the Farnell pulse generator, to firing of the impulse generator was 1.6 μs. Figure 10 shows the thyristor trigger arrangment.

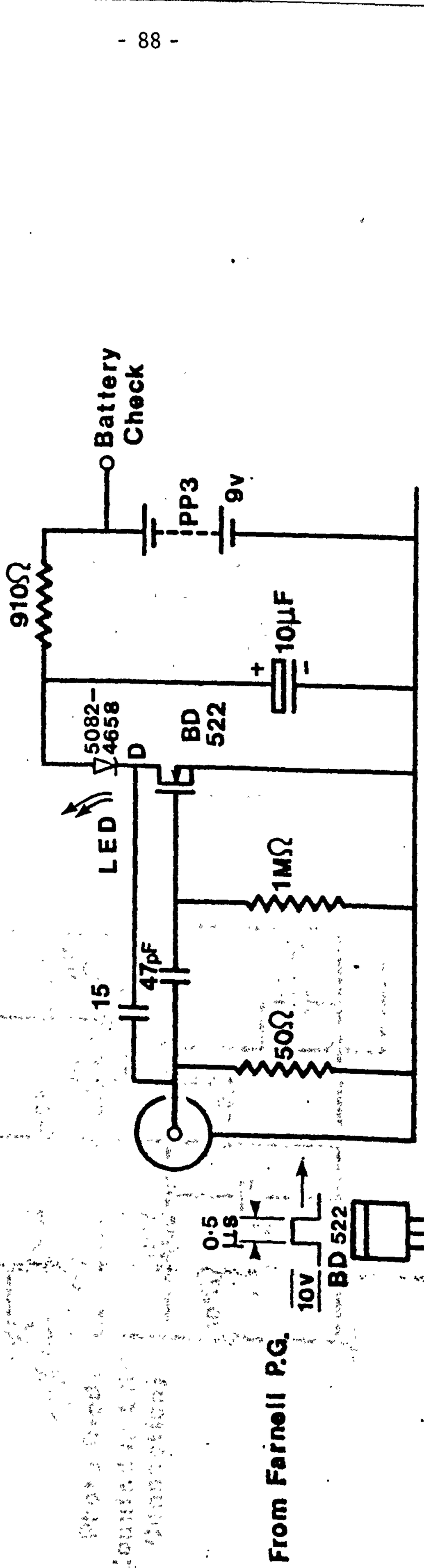

Figure 7 : Optical transmitter

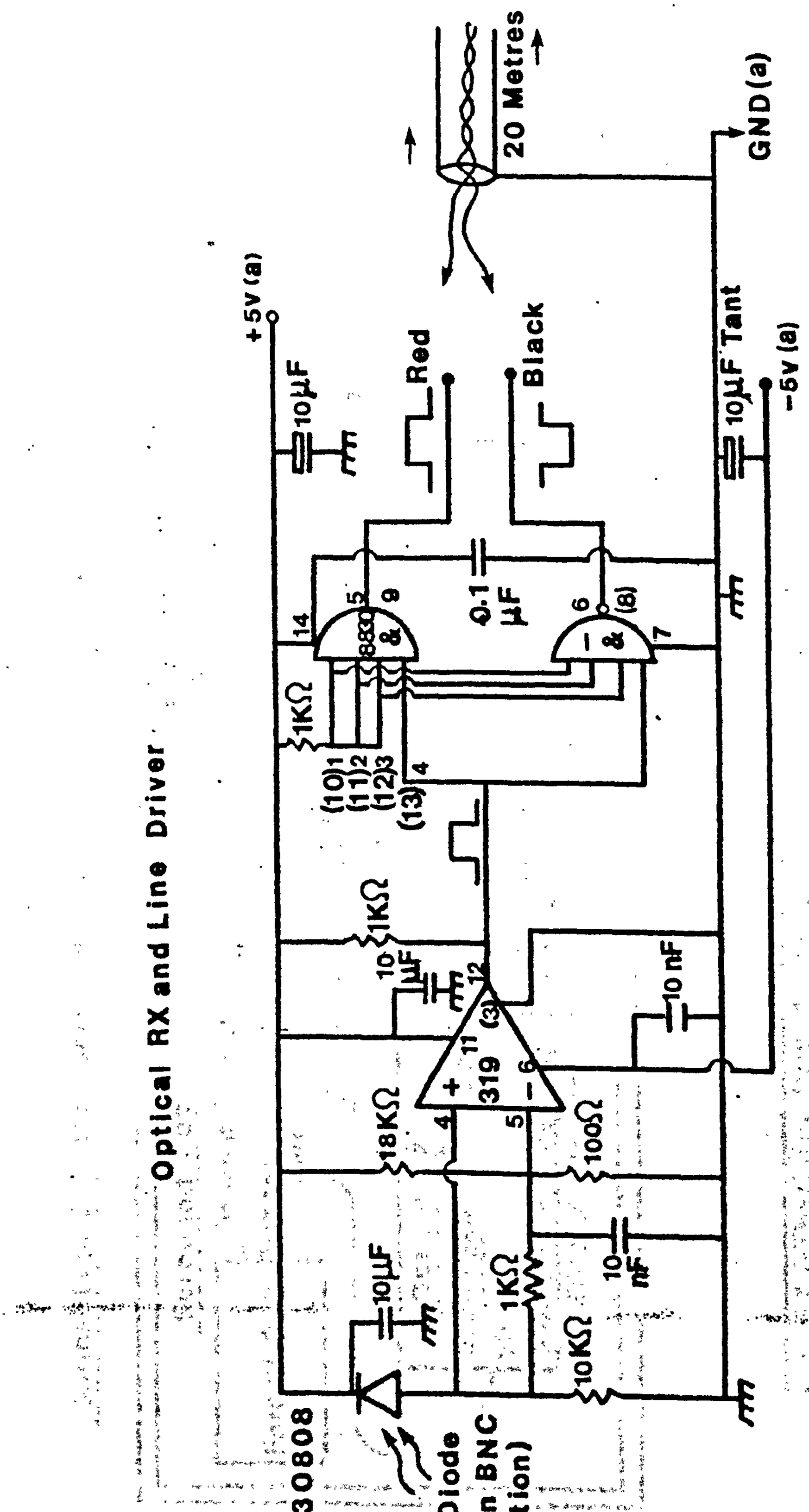

Figure 8 : Optical receiver and line driver

Optical RX and Line Driver

Optical Link Between Screened Room & Trigger Circuit

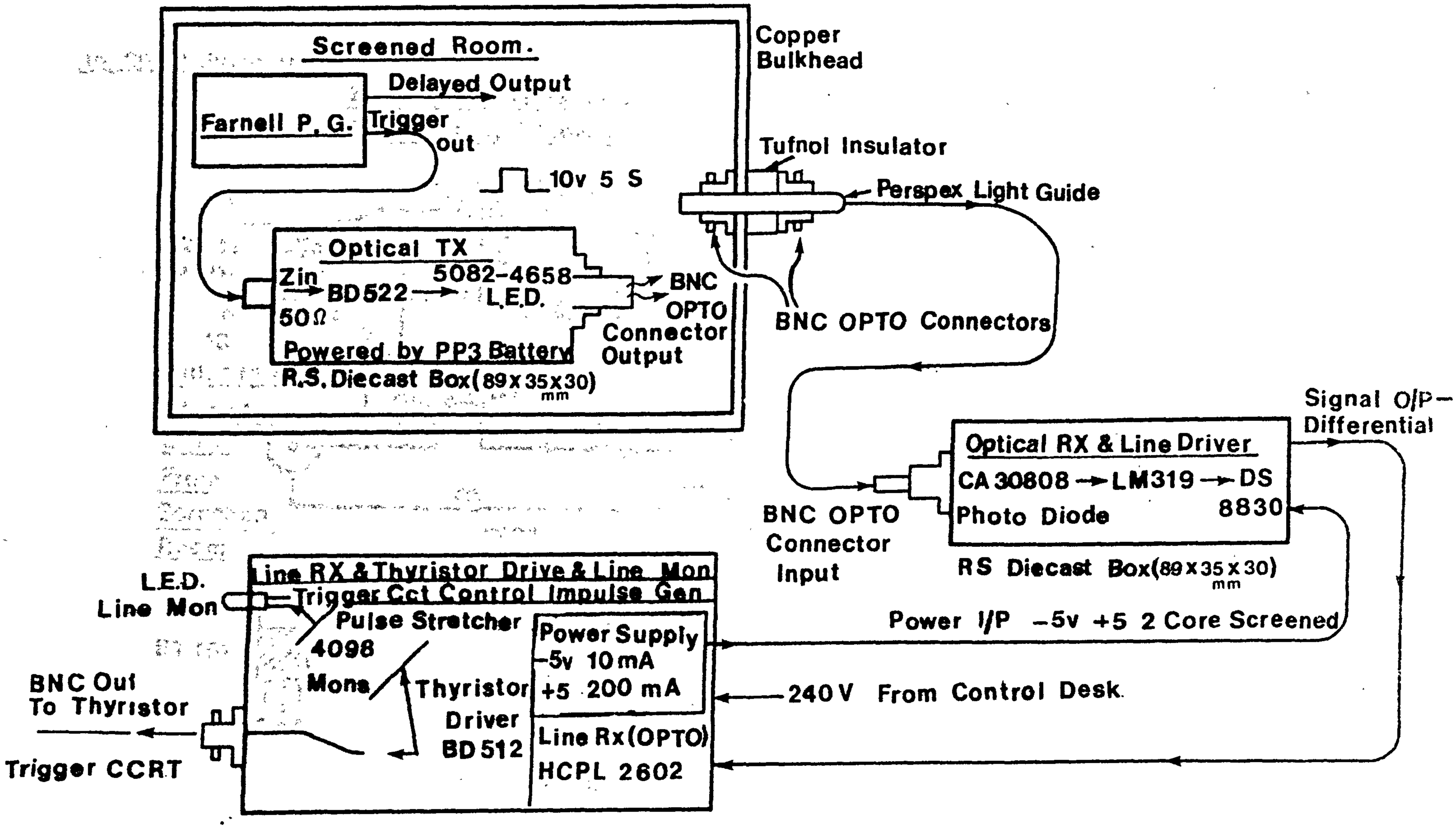

Figure 9 : Block diagram of optocoupler

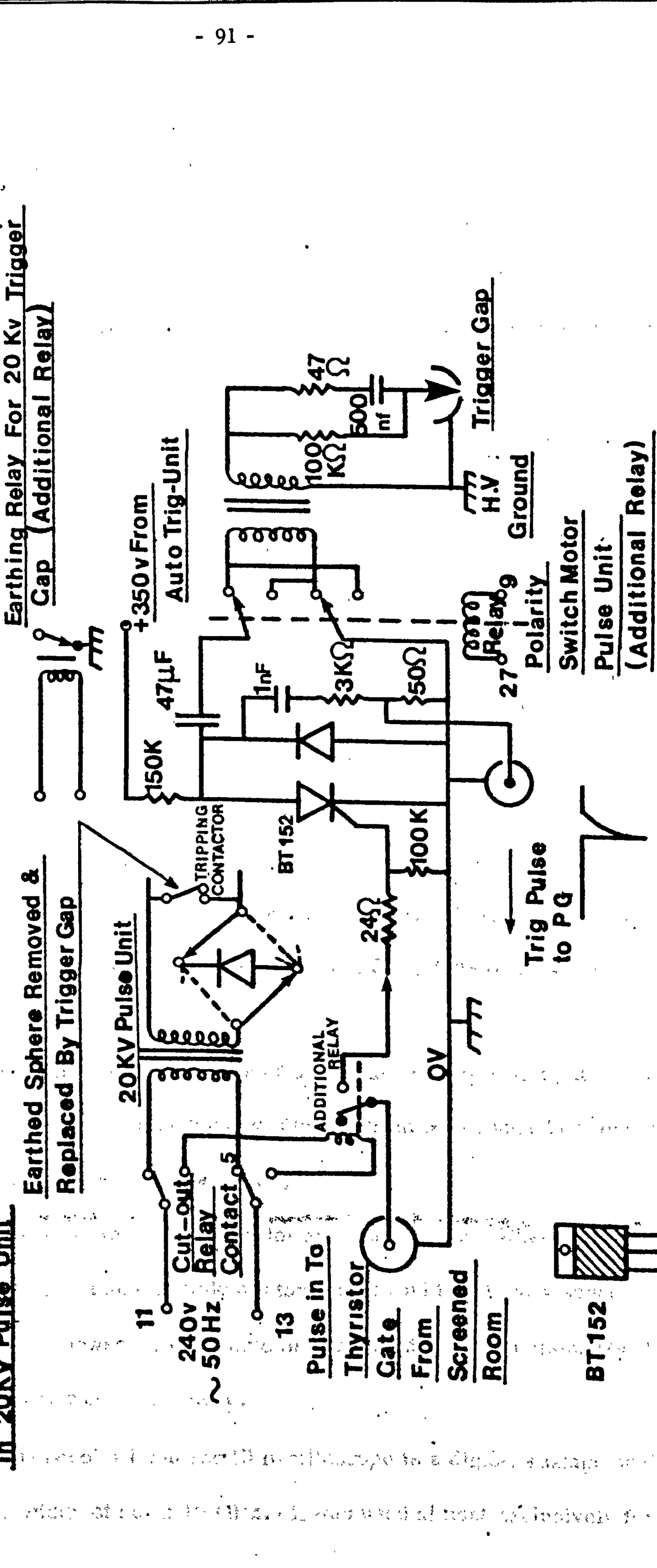

Figure 10 : Triggering arrangement for the thyristor that provides the trigger pulse for the impulse generator.

3.6 RECORDING EQUIPMENT

The recording equipment used was (a) Tektronix 7633 storage oscilloscope and (b) Nicolet Explorer III digital oscilloscope. Both oscilloscopes were earthed to the bottom of the capacitor voltage divider described in section (5).

The Tektronix 7633 oscilloscope was equipped with two type 7A16A vertical amplifiers with sensitivity of 5mV/ division to 5 V / division for a band width of 100 MHz. However, the bandwidth could be reduced to 20 MHz if required. The voltage rating of the amplifiers could be doubled by operating the oscilloscope on reduced scan. The range could be increased by a further factor of 2.5 by going into a range extended mode. The oscilloscope could be triggered internally or externally. On the internal it could be triggered on the left or the right channel. The time base used was a type 7B50A, it had a range of 50 ns /division to 5 sec/division sweep rate. This, however, could be increased first by a factor of two by operating in reduced scan mode, and extended down to 5 ns/division by going into a x10 mode of operation.

When the sweep rate was of the order of ms/division, it could be used in chop mode to display waveforms from both channels simultaneously with a reasonable degree of accuracy.

The rise time of the oscilloscope was 3.5 ns. When used in the fast variable persistence mode of storage, it could write at a speed of 150 divisions/μs. However, this could be increased to 2222 divisions/μs by operating in reduced scan mode.

(b) The Nicolet Explorer III oscilloscope is a digital storage device with a bandwidth of about 10 MHz. It was used almost exclusively for

luminosity measurements. The plug in used was a type 204A. It operates very much like a conventional oscilloscope (analogue). When a sweep trigger signal is received, the analogue to digital converter measures the signal at intervals (separated by amounts which depend on the selected sweep speed) and transfers the information to the buffer memory. The information is then transferred to the main frame memory and it is displayed on the screen. Information so obtained can then be transferred onto a disc memory, which can be held permanently to be retrieved at any time later. The discs are removable by opening the door of the front panel. The discs are divided up into eight tracks each of these having a capacity of 4096 data points. For any given waveform either half or quarter of the available memory space can be used. However, in this experiment whenever waveforms were stored all the available memory was used to store both waveforms that were captured during a given event. Once a waveform is captured and stored in memory, it can be expanded up to 64 times in both the horizontal and vertical directions. Also, the time and magnitude between any given set of points can be read off easily using the digital read out facility.

3.7 MEASUREMENT SYSTEM AND PROCEDURE

The photomultipliers and the field probe used is shown schematically in figure11. The system was used to determine the corona initiation voltage, and the growth of discharge in the interelectrode space. The photomultipliers were used to measure the discharge luminous extensions and the velocities of propagation in the regime $V_i(+) < V < V_B(+)$ and $p < p_c$. The measurements were made by imaging the discharge on to a 1 mm diameter moveable aperture placed in front of each photomultiplier, the magnification

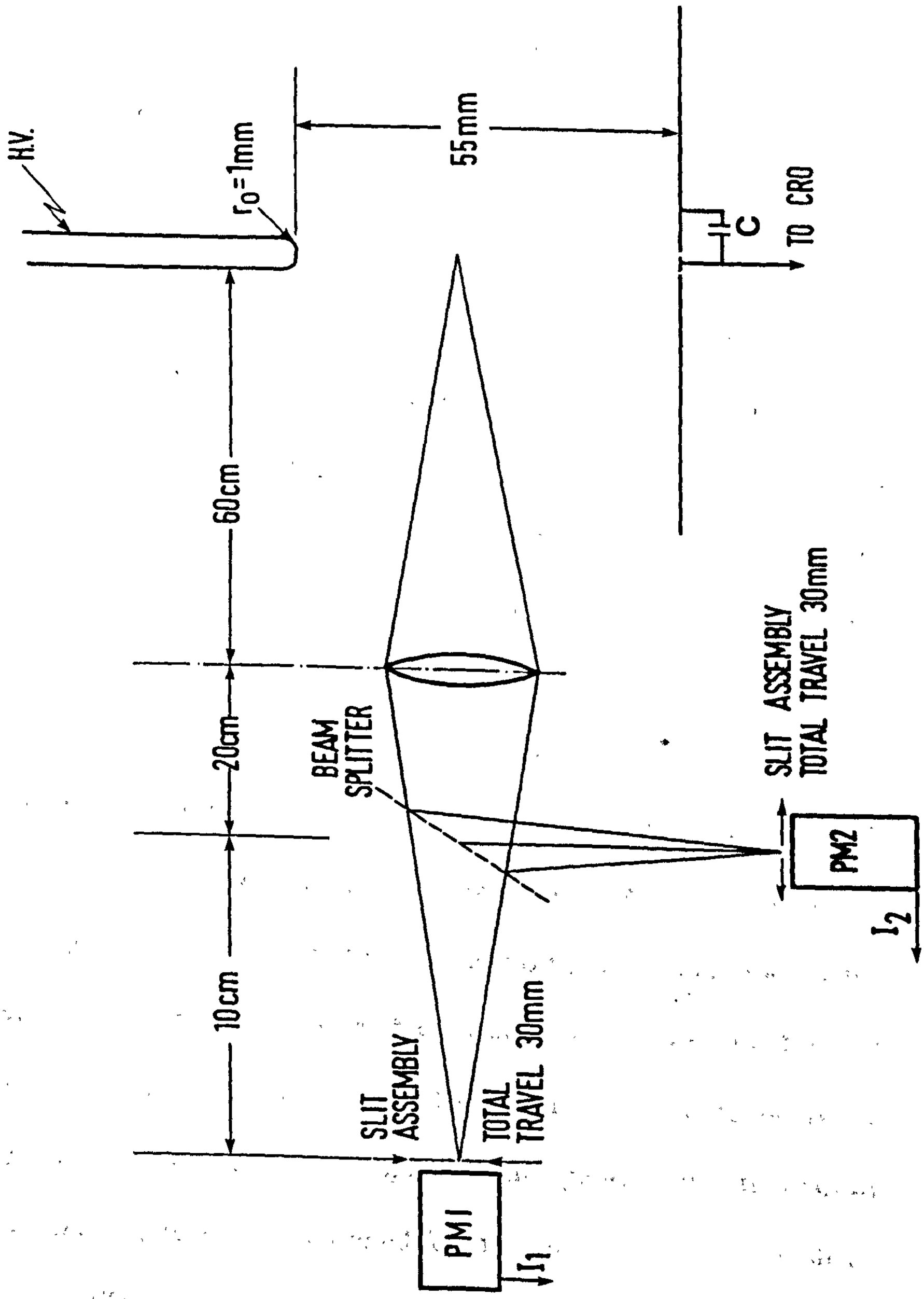

Figure 11 : The optical and field probe system used to study the predischarge development.

of the lens was 0.5. Each position of the pin hole aperture accessed a 2 mm diameter region along the axis of the discharge. The defining aperture of one photomultiplier was always positioned so as to measure the light level emanating from the tip of the highly stressed rod electrode, whilst the other was moved along the axis of the gap to access different points along the gap. At any given voltage V the ratio of (I_2/I_1) for different positions Z away from the point was measured. I_1 is the peak intensity of the initial corona pulse observed at Z = 0, the point electrode. I_2 is the same peak height of the first pulse as observed at different distances Z away from the point. For the majority of events the corona pulse was a single pulse and thus the ratio (I_2/I_1) accurately represents the ratio of the integrated intensity that would be obtained photographically. When the corona pulse was made up of more than one discrete pulse, then the value of I_1 was taken as the height of the first pulse and I_2 similarly referred to the height of the dominant pulse seen further into the gap. Comparison of (I_2/I_1) with the same ratio using the integrated photon flux for each corona pulse showed little difference in the measured luminous extension. A typical result of (I_2/I_1) versus Z is shown in figure12 . Each point represents the mean of ten voltage applications. From such curves it is possible to determine $Z = \ell$ at which (I_2/I_1) reduced to 0.5. This value of ℓ is taken as the mean luminous extension of the developing discharge at a specified voltage.

Figure 13 shows the two schemes used for measurement of luminosities and velocities . When making luminosity distribution measurements at different axial positions, the photomultipliers utilised 1000 Ω anode resistors feeding into the two channels of the Nicolet oscilloscope. When making velocity measurements the photomultipliers used 50 Ω anode resistors.

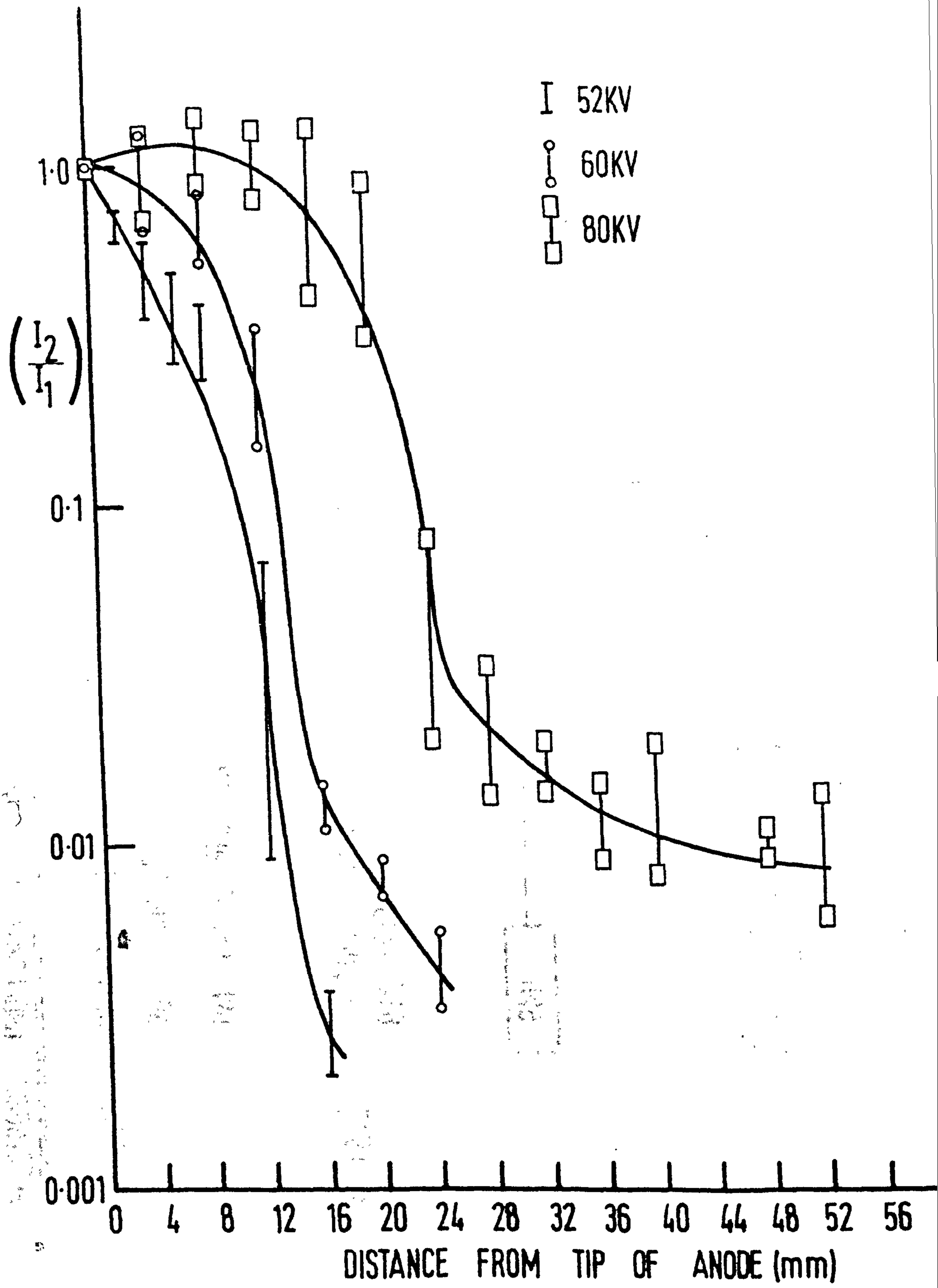

Figure 12 : Typical result of (I_2/I_1) versus the distance z from the anode

50% SF_6 50% N_2 2 bar

ELECTRONIC PROCESSING OF SIGNALS.

A. SLOW	20MHZ DIGITISER (NICOLET) 2024 SAMPLES / INPUT. PM ANODE RESISTORS 1KΩ	50ns/8 BIT (≃ 5MHZ BANDWIDTH)
B. FAST	100MHZ STORAGE SCOPE. P.M. ANODE RESISTORS 50Ω	TEKTRONIX 7633

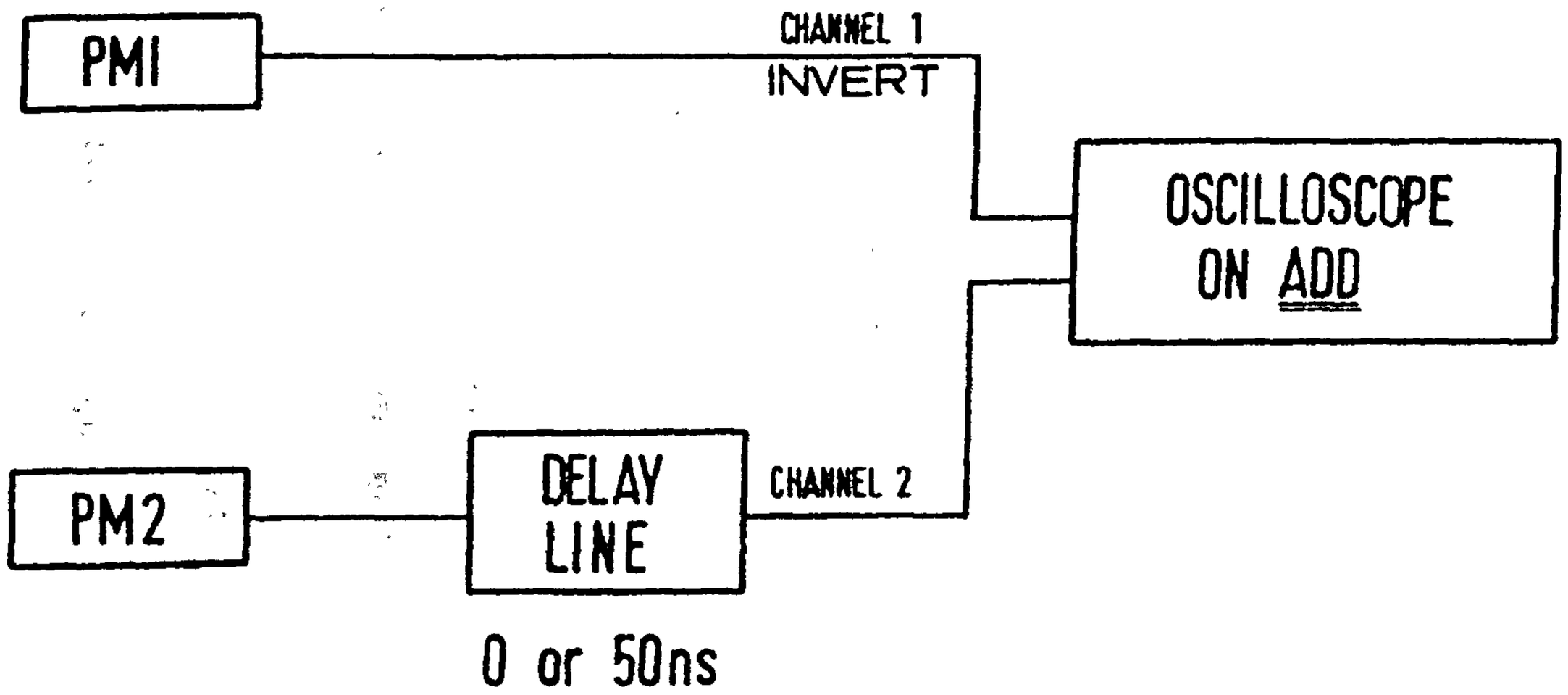

Figure 13 : Schematic of the measuring arrangements

At any specific voltage the photomultiplier 2 (PM2) was placed at a position such that it accessed á point in the interelectrode space, approximately equal to the luminous length corresponding to that level of voltage. The gap was subjected to the application of this voltage. Several such applications at the same voltage were made and the resulting oscillograms were recorded. This procedure was repeated by placing PM2 such that it accessed positions within and outside the limit of the luminous length. The voltage range used was $V_B > V > V_i$ at any given pressure.

3.8 FIELD PROBE MEASUREMENTS

3.8.1 Theory of Field Probe

The probe shown in figure11. was used to measure the field at the plane during corona discharge. This technique was first developed by Meek and Collins (1965). The technique involves the measurement of charge induced on a small probe mounted flush with the surface of the electrode and is based on the principle that the field is proportional to the flux density.

Consider a probe of area A with an electric flux of Ψ entering it.

$$\text{Since} \quad D = \epsilon_o E = \frac{\Psi}{A} \tag{3.1}$$

where D = electric flux density and ϵ_o is the permitivity of free space

and $\Psi = \int i \, dt$

where i is the displacement current in the probe, it follows that

$$E = \int \frac{i \, dt}{\epsilon_o A} \tag{3.2}$$

This integration can be performed in a practical situation using a capacitor C as shown in figure11, in the following manner,

$$E = \frac{C V}{\varepsilon_o A} \qquad (3.3)$$

as C, A and ε_o are constants the voltage can be calibrated directly in terms of E.

For the technique to be accurate specially in non-uniform field situations, as was the case in this experiment, the dimensions of the probe have to be small. In this case the diameter of the probe was 1 mm.

3.8.2 Probe Pre-amplifier - Line Driver

The probe signal obtained during the development of corona discharge was too small to be used for field measurements accurately. To overcome this problem a probe pre-amplifier- line driver was designed and installed by the staff of the Electronics Workshop in close consultation with the author. The pre-amplifier-line driver circuit was placed in a screened copper box, and is located at the base plate of the experimental chamber. The pre-amplifier-line driver circuit has a bandwidth of about 20 MHz and it conditions the probe signals and drives them along the 50 Ω cable. Figure14 shows the circuit diagram of the pre-amplifier-line driver. Figure15 shows schematic diagrams of what might be expected to be seen on the oscilloscope screen, during different phases of discharge development. Figure 15 (a) shows a signal in the absence of any corona activity. Under these conditions it will give an exact replica of the impulse voltage. Figure15 (b) shows what would be expected in the presence of a discharge at the anode, the time τ gives the duration of the discharge development. Figure15 (c) indicates that there is a decrement δ in the field probe signal, this is interpreted as the discharge crossing the gap and reaching the plane. The decrement is associated with charge neutralisations. The probe pre-amplifier-line

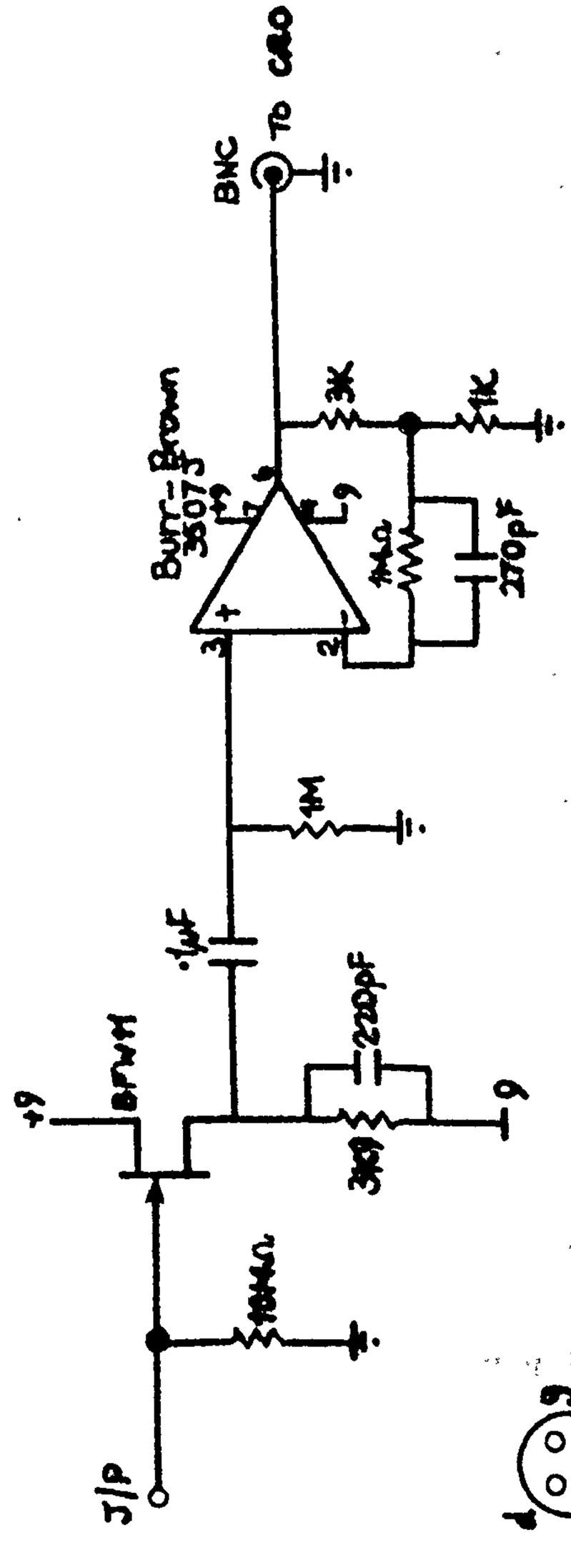

Figure 14 : Line driver for field probe

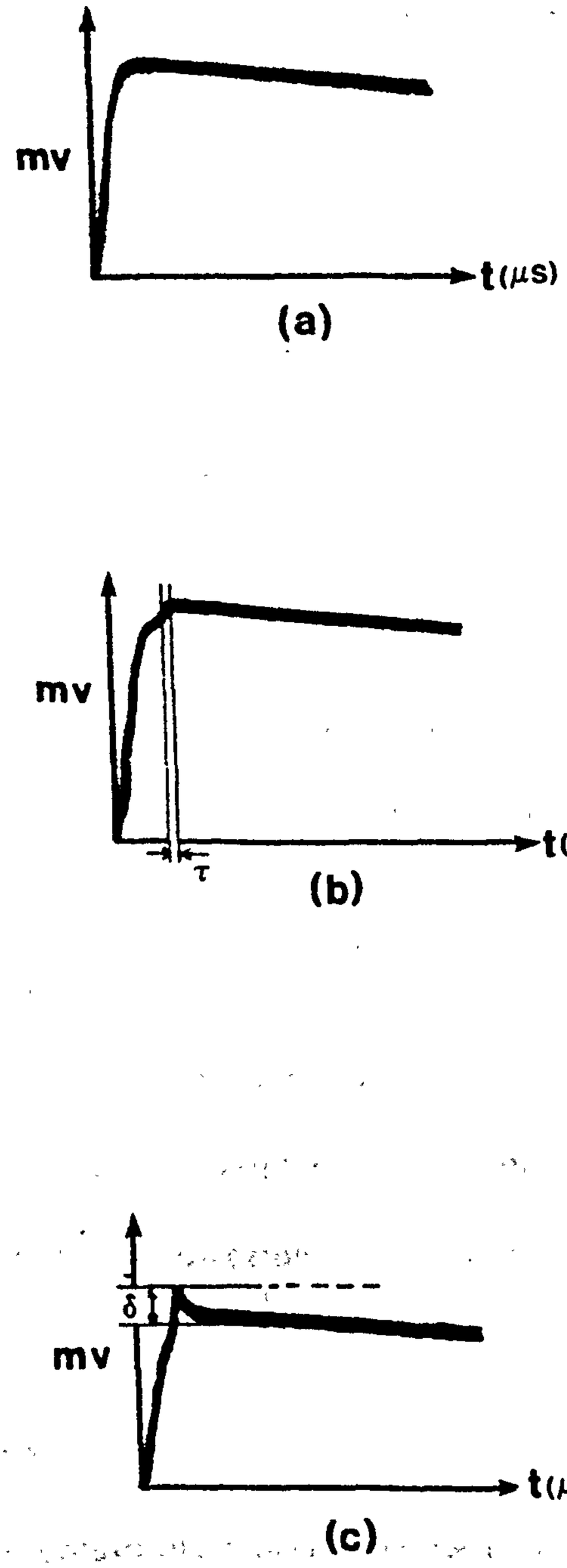

Figure 15 : Schematic of expected field probe signals

(a) undistorted field
(b) field signal in the presence of a discharge at the anode, τ gives the duration of discharge.
(c) field signal when the discharge crosses the gap and reaches the cathode.

driver was terminated at the oscilloscope with a 50 Ω resistor.

3.8.3 Method of Obtaining (Δ E/E)

3.8.3.1 Determination of E (geometric field)

The experimental chamber was evacuated down to a pressure of 2×10^{-2} torr and filled with SF_6 up to 10 bar, and allowed to stand for several hours. The corona initiation voltage under these conditions is far above the full range of voltages that were to be studied. Figure 16 shows a graph of the variation of the geometrical field as a function of voltage. The geometrical field is defined as : the field that exists in the absence of any corona activity at all. The crest value of the waveform was taken as the peak geometrical field.

Figure 17 shows typical oscillograms taken during discharge development. At the same time as the length ℓ was being determined, the step change ΔE in the cathode field was measured at the centre of the plane electrode for a given applied voltage. The step change ΔE was taken as the difference between peak field value in the presence of the discharge, and that obtained in the absence of any discharge activity (geometric field). Since it is a ratio that is involved, the calibration factor did not enter into the calculations.

3.9 INSTRUMENT RESPONSE

The method employed to obtain the instrument response of the two photomultipliers was as follows :

The impulse generator was connected up as described in section 2 so that a steady dc voltage could be placed on the tip of the rod electrode. The experimental chamber was evacuated and filled with nitrogen to a

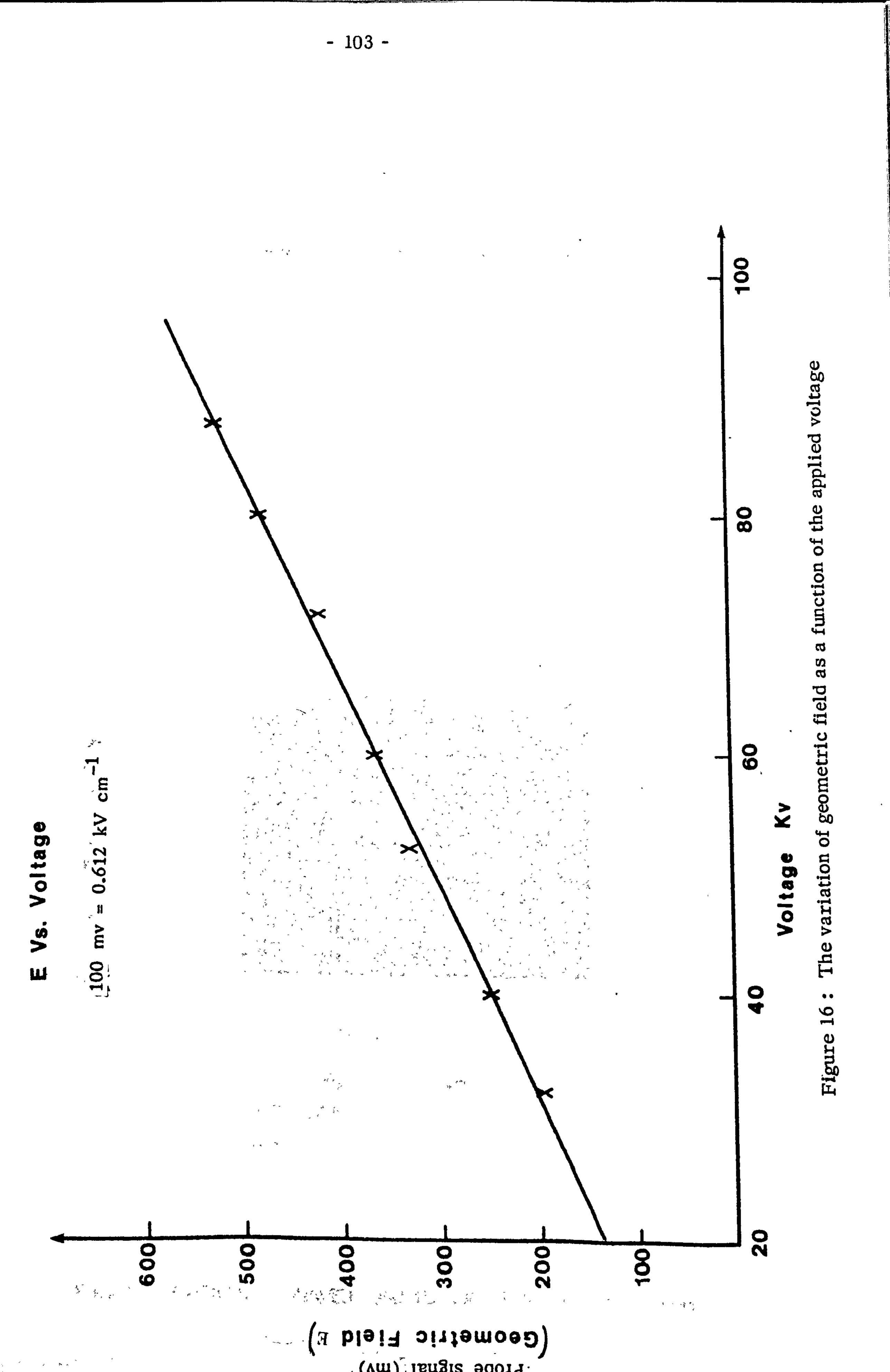

Figure 16 : The variation of geometric field as a function of the applied voltage

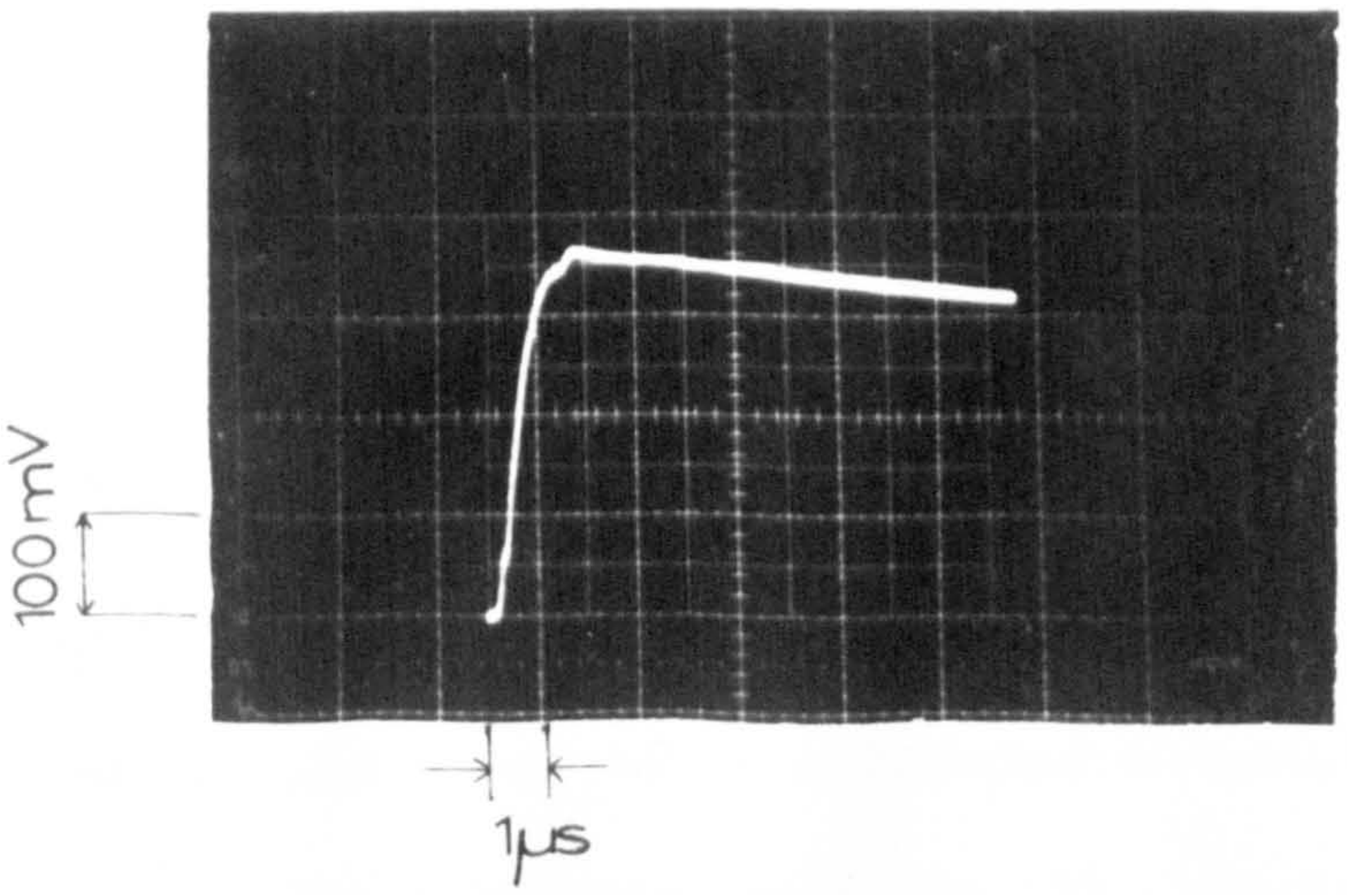

FIG. 17. TYPICAL WAVEFORMS OF FIELD AT THE CATHODE.

pressure of 1 bar. The voltage was switched on and increased gradually until it reached a steady value of about 30 kV/stage, and a steady glow discharge was seen. The photomultipliers, each in turn were then moved along the axis of the gap. Figures 18 and 19 show the response of the photo-multipliers as a function of distance from the tip of the electrode. The cut off as shown by these figures depicts that they are very sharp, thus indicating the fine focussing of the system.

3.10 IRRADIATION OF THE GAP

The figure 20 shows the method adopted for irradiation of the space around the tip of the high voltage electrode. The irradiation source used was a 50 mc, Cs_{137}, γ ray source. This method of irradiating the gap lent itself to flexibility in that it could be introduced and removed at will. It was considered necessary to irradiate the gap so as to provide sufficient numbers of initiatory electrons, and thereby reduce the possibility of erratic behaviour, when determining , in particular, the corona initiation voltage. When the source was in position, where it irradiated the gap, it was drawn out of the bottom of the lead castle and the γ rays were collimated through a 2 mm diameter hole that was bored along a radius of the upper half of the lead container. The area irradiated around the electrode tip was one of diameter 0.5 cm. The count rate monitored at a point diametrically opposite to the position of the collimating hole was 400 counts/sec. This level of intensity was confined to an area of diameter 1 cm.

3.11 DETERMINATION OF INITIATION VOLTAGE

The corona initiation voltage was determined using both the field probe positioned directly below the point electrode, and the photomultipliers. It

will be shown in the next section that the photomultipliers are about 10-15% more accurate than the field probe in detection sensitivity.

The method adopted for the determination of corona initiation voltage is as follows :

At a specified pressure for any given gas composition, the voltage was gradually increased, with the photomultiplier slits fixed at the tip of the point electrode. The voltage was increased in steps of 2 kV/stage until there were signals on the photomultipliers, this was taken as the corona inception voltage as detected by the photomultipliers and denoted by $V_i(+)$ (PM). The voltage was increased further until the field probe indicated a signal superimposed on the geometrical field, this was taken as the corona initiation voltage as indicated by the field probe and denoted by $V_i(+)$ (probe). In both cases the voltage was that which gave signals at every application of the impulse voltage. Also, the signals appeared at or near the crest of the voltage waveform. In the case of the voltage waveform with the long wave-tail (10,000 μs) only the field probe was used to determine the corona initiation voltage.

3.12 THEORETICAL ESTIMATION OF CORONA DETECTION

(a) At corona initiation voltage the discharge was approximated to a dipole placed at the tip of the electrode. The dimensions of the length of the dipole was obtained by using the formulae derived by Farish et al (1978) and Chatterton (1979). Essentially this formula gives the dimensions of a corona cloud surrounding the point electrode. In this calculation the length Rc1 was taken as the length of the dipole.

(b) In the second approach using the photomultipliers, the principle used

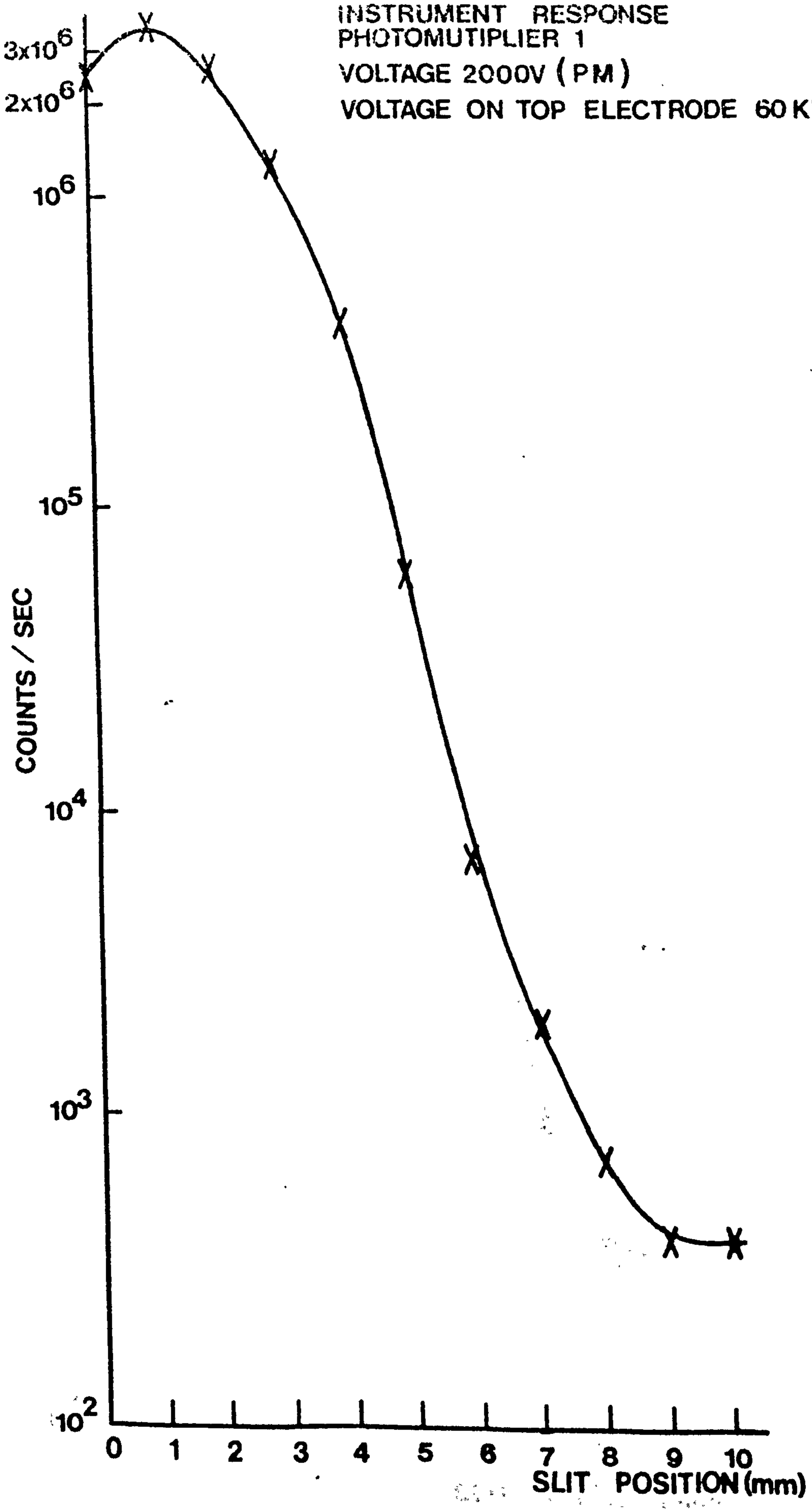

Figure 18 : Response of photomultipliers as a function of distance

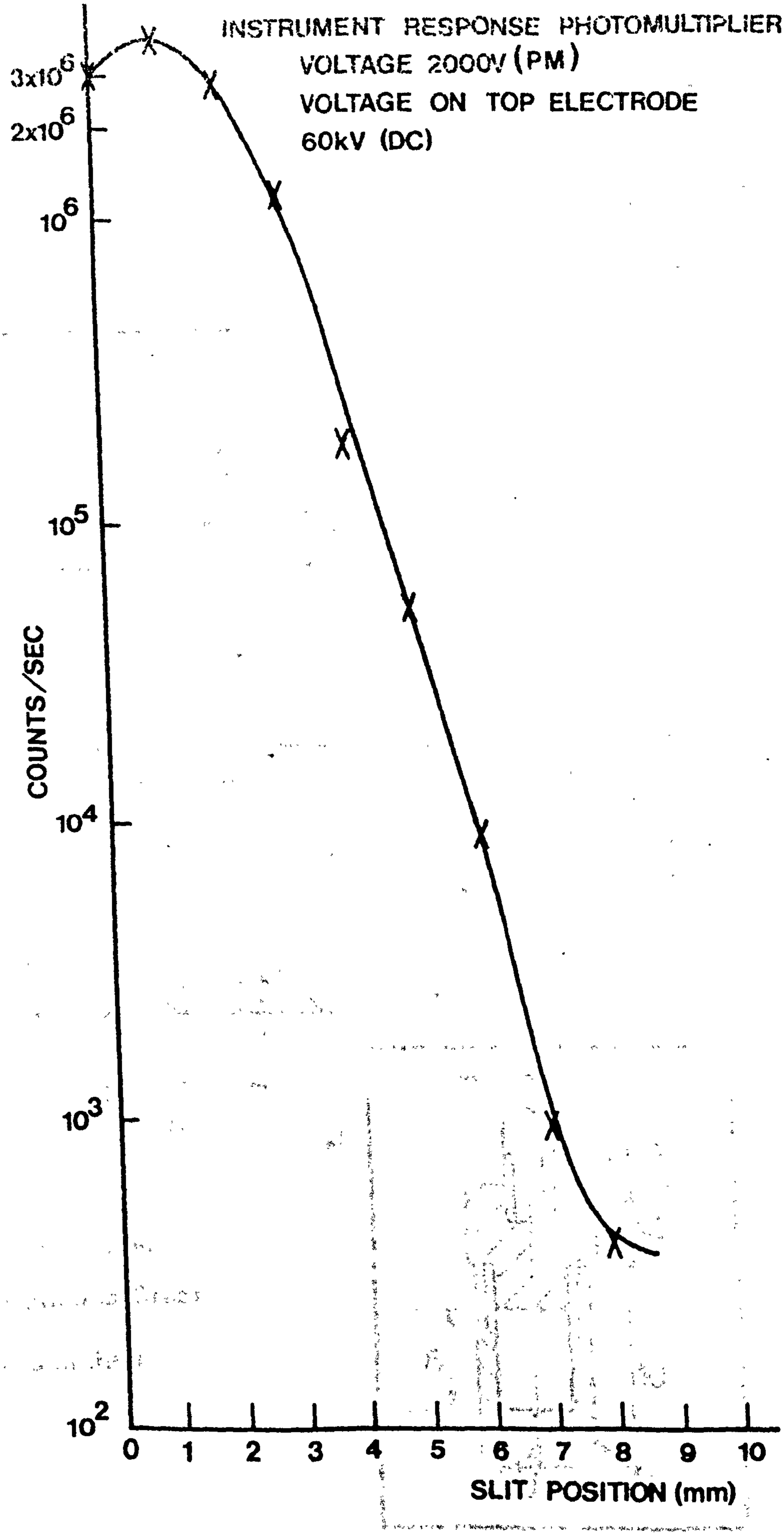

Figure 19 : Response of photomultiplier 2 as a function of distance

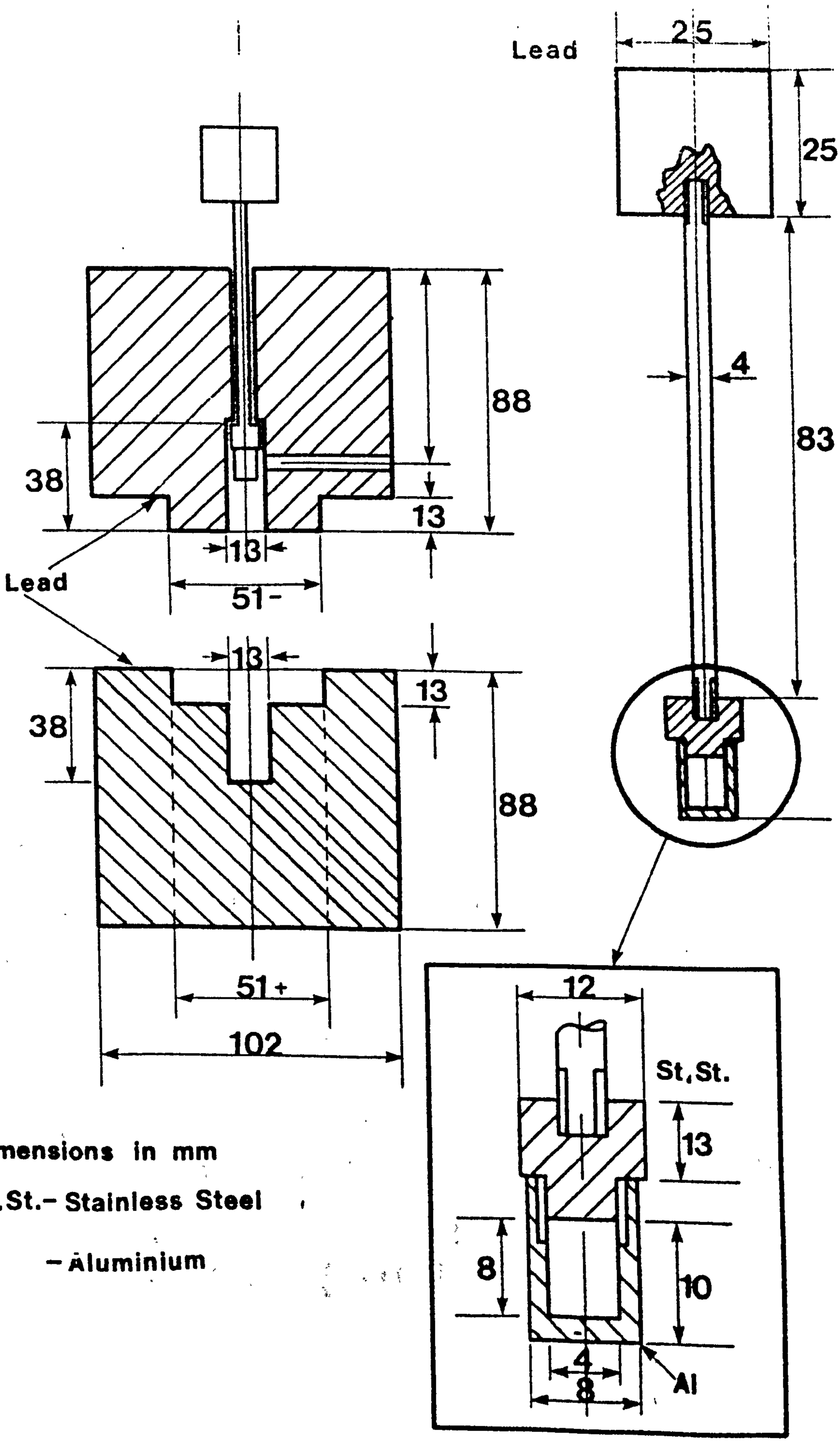

Dimensions in mm

St.St.- Stainless Steel

Al - Aluminium

Figure 20 : Details of irradiation source and the lead housing

is one where the light emanating at the tip of the high voltage electrode is detected and an attempt is made to estimate the level of activity.

The derivations for the two systems are as follows :-

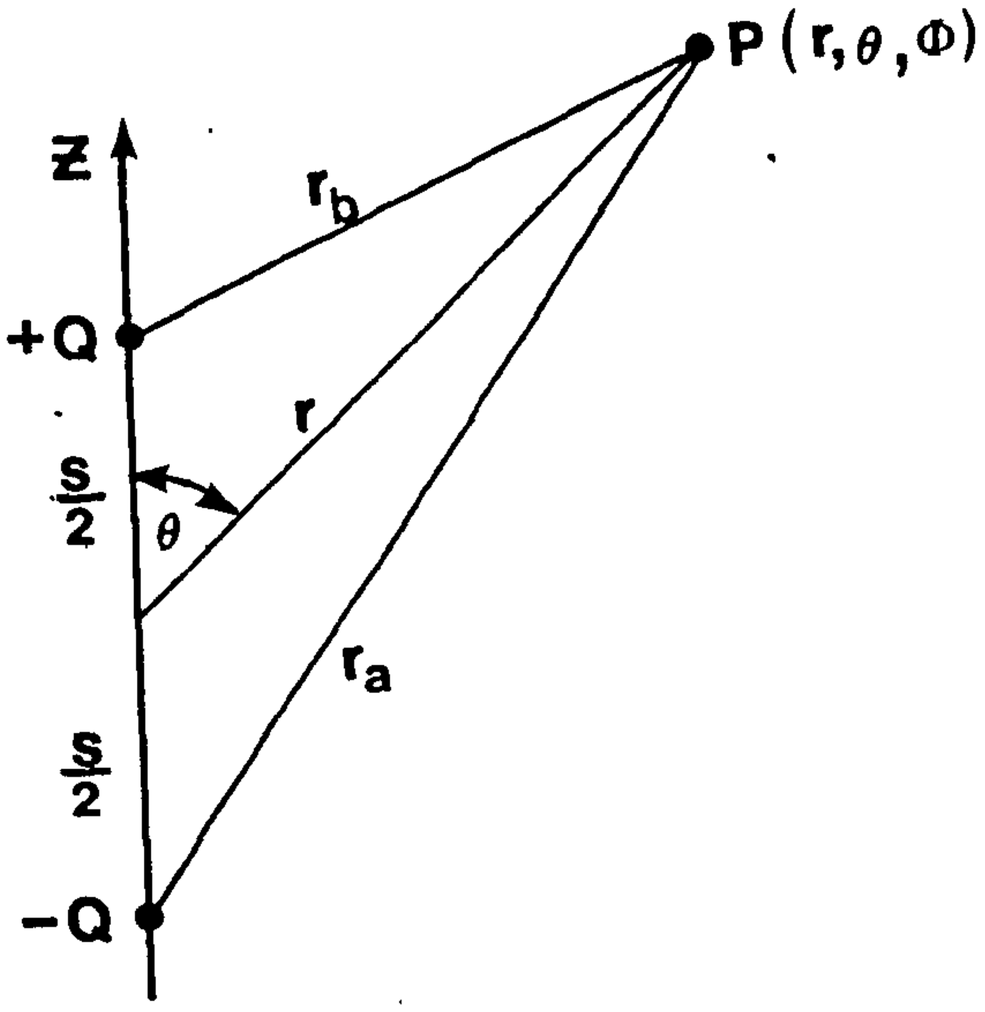

Figure 21

The two charges +Q and -Q form a dipole, the electrostatic potential at P is the sum of the potentials due to the individual charges. The distance s is small compared to r. Let the electrostatic potential at P be V and the electric field intensity E.

$$V = \frac{Q}{4 \pi \varepsilon_o} \left(\frac{1}{r_b} - \frac{1}{r_a} \right) \qquad (3.4)$$

where

$$r_a^2 = r^2 + \left(\frac{s}{2}\right)^2 + \frac{s}{r} \cos \theta \qquad (3.5)$$

$$\frac{r}{r_a} = \left(1 + \left(\frac{s}{2r}\right)^2 + \frac{s}{r} \cos \theta \right)^{\frac{1}{2}} \qquad (3.6)$$

expanding the right hand side of equation (3.6)

$$\left(\frac{r}{r_a}\right) = 1 - \tfrac{1}{2}\left(\frac{s^2}{4r2} + \frac{s}{r}\cos\theta\right) + \frac{3}{8}\left(\frac{s^2}{4r2} + \frac{s}{r}\cos\theta\right)^2 + \text{---} \qquad (3.7)$$

Neglecting terms of order higher than $\left(\frac{s}{r}\right)^2$

$$\left(\frac{r}{r_a}\right) = 1 - \frac{s}{2r}\cos\theta + \frac{s^2}{4r^2}\ \frac{3\cos^2\theta - 1}{2} \qquad (3.8)$$

similarly

$$\left(\frac{r}{r_b}\right) = 1 + \frac{s}{2r}\ \cos\theta + \frac{s^2}{4r^2}\ \frac{3\cos^2\theta - 1}{2} \qquad (3.9)$$

Hence by substitution in equation (3.4)

$$V = \frac{Qs}{4\pi\varepsilon_o r^2}\cos\theta\ \ (r^2 >> s^2) \qquad (3.10)$$

The dipole moment p = Qs, which is a vector whose magnitude in Qs, which is a vector whose magnitude in Qs and which is directed from the negative to the positive charge.

Figure 22

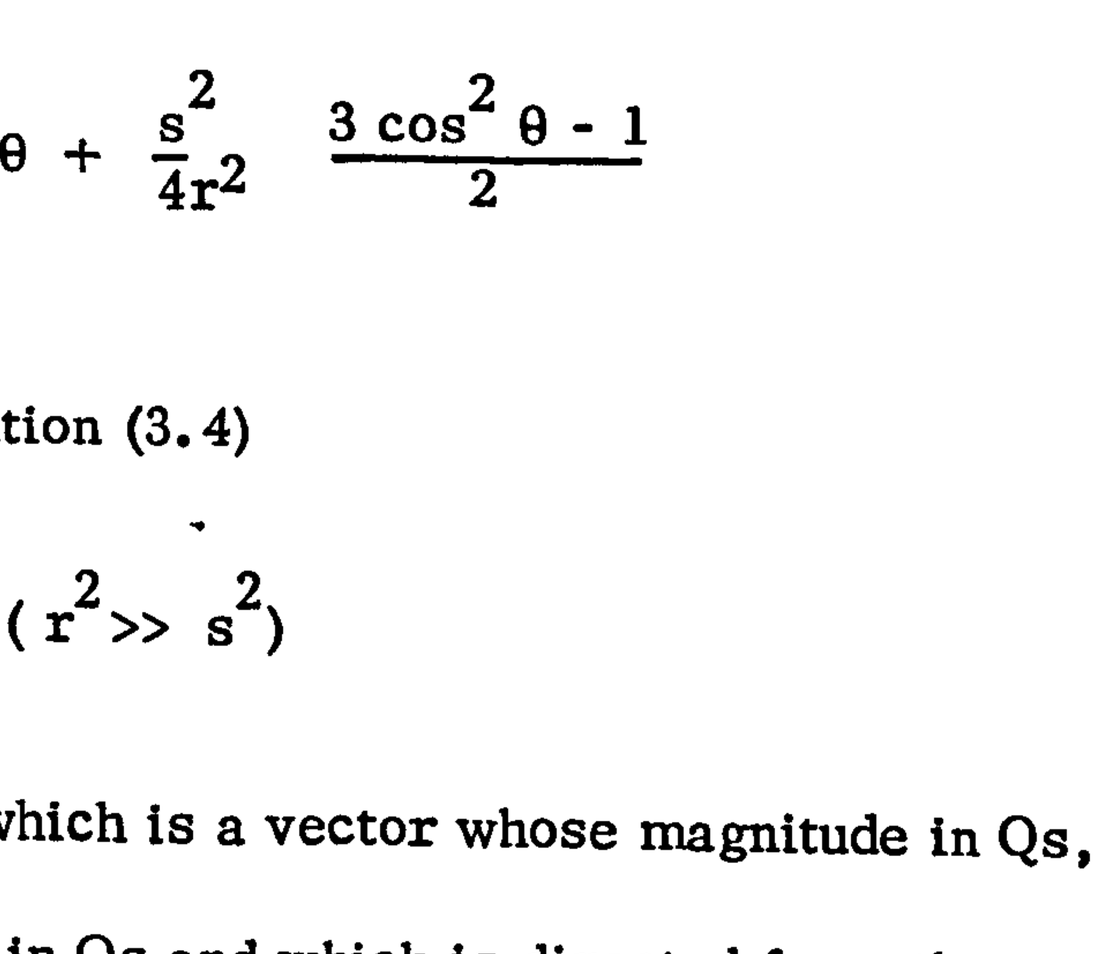

$$V = \frac{p \cdot r_1}{4\pi\varepsilon_o r2} \qquad (3.11)$$

i.e. $$V = \frac{p}{4\pi\varepsilon_o} \cdot \nabla\left(\frac{1}{r}\right) \qquad (3.12)$$

The components of E in spherical co-ordinates can be computed from the gradient of V.

$$E_r = - \frac{\partial V}{\partial r} = \frac{2p}{4\pi\varepsilon_o r^3} \cos\theta \qquad (3.13)$$

$$E_\theta = - \frac{1}{r} \frac{\partial V}{\partial \theta} = \frac{p}{4\pi\varepsilon_o r^3} \sin\theta \qquad (3.14)$$

$$E_\phi = - \frac{1}{r \sin\theta} \frac{\partial V}{\partial \phi} = 0 \qquad (3.15)$$

In this particular case $\theta = 0$

$$E = \frac{2p}{4\pi\varepsilon_o r^3} \qquad (3.16)$$

i.e. the field at the plane.

For SF_6

From Chatterton (1979)

$$r_c = r_o \left[1 + \left(\frac{k}{Bp\, r_o}\right)^{\frac{1}{2}}\right] \qquad (3.17)$$

where k = 18 and B = 2460

p = pressure, r_o the radius of the tip (r_o = 1mm)

at 1 bar,

$$r_c = 0.1 \left(1 + \left(\frac{18}{2460 \times 1 \times 0.1}\right)^{\frac{1}{2}}\right)$$

$$r_c = 1.27 \text{ mm}$$

$$x_c = r_c - r_o$$

$$x_c = 0.27 \text{ mm}$$

The extent to which the corona cloud grows at V_i, the corona initiation voltage, is r_c. The length of the discharge is then x_c, which is taken as the length of the dipole as in equation (3.16).

Using Goldman's equation

$$E = \frac{2V}{(r_o + 2d)\ \ell n\ (\frac{r_o + 2d}{r_o})} \qquad (3.18)$$

for $V = 40$ kV.

$$E = \frac{2 \times 40}{(0.1 + 2 \times 5.5)\ \ell n\ (\frac{1 + 2 \times 55}{1})}$$

$$E_1 = 1.5304 \text{ kV cm}^{-1}$$

when corona is present at the tip

$$x_c = 0.27 \text{ and } d = 55 - 0.27$$

$$d = 54.73 \text{ mm}$$

$$E_2 = \frac{2 \times 40}{(0.127 + 2 \times 5.473)\ \ell n\ (\frac{1.27 + 2 \times 54.73}{1.27})}$$

$$E_2 = 1.617 \text{ kV cm}^{-1}$$

$$\Delta E = 0.08658 \text{ kV cm}^{-1}$$

geometric field at 40 kV = 250 mV, let the size of the avalanche be A.

The signal Δ E at 40 kV is 10 mV

from equation (3.16)

$$\Delta E = \frac{2 \times 0.27 \times 10^{-3}\ e \times A}{\frac{4\pi \times 1}{4\pi \times 9 \times 10^{9}} \times 1 \times (55 \times 10^{-3})^3} \quad V\ m^{-1}$$

$$= \frac{2 \times 0.27 \times 10^{-3} \times 9 \times 10^{9}}{(55 \times 10^{-3})^3} \quad V\ m^{-1}$$

equating the values of E so obtained

$$\frac{1.5304 \times 10}{250} = \frac{2 \times 0.27 \times 10^{-3} \times 10^{9} \times 9 \times 1.9 \times 10^{-19} \times A \times 10^{-5}}{(55 \times 10^{-3})^{3}}$$

$$A = 0.99 \times 10^{12} = 10^{12}$$

$$A = 9 \times 10^{11}$$

The number of avalanches of size 10^8 are 10^4 at onset of corona.

Photomultiplier method

$$i_{eff} = \frac{G \times Q \times C}{\Delta t}$$

where G is the gain of the photomultiplier, Q the charge (= eN), C the capacitance at the oscilloscope, Δt the time interval during which C is charged, and N is the number of electrons produced in the photomultiplier

$$dV = \frac{G \times Q}{C}$$

if the efficiency of the photomultiplier is E, then

$$V = \frac{G \times E \times N \times 1.6 \times 10^{-19}}{C}$$

Let the avalanche size be A, and C = 300 pf.

Also, $$V = \frac{Q \times E \times G}{C} \; A \; (\frac{\delta}{\alpha}) \; (\frac{p_{quench}}{p}) \times e^{-\mu \ell} \times \frac{r^2}{4R^2} \times \text{loss}$$

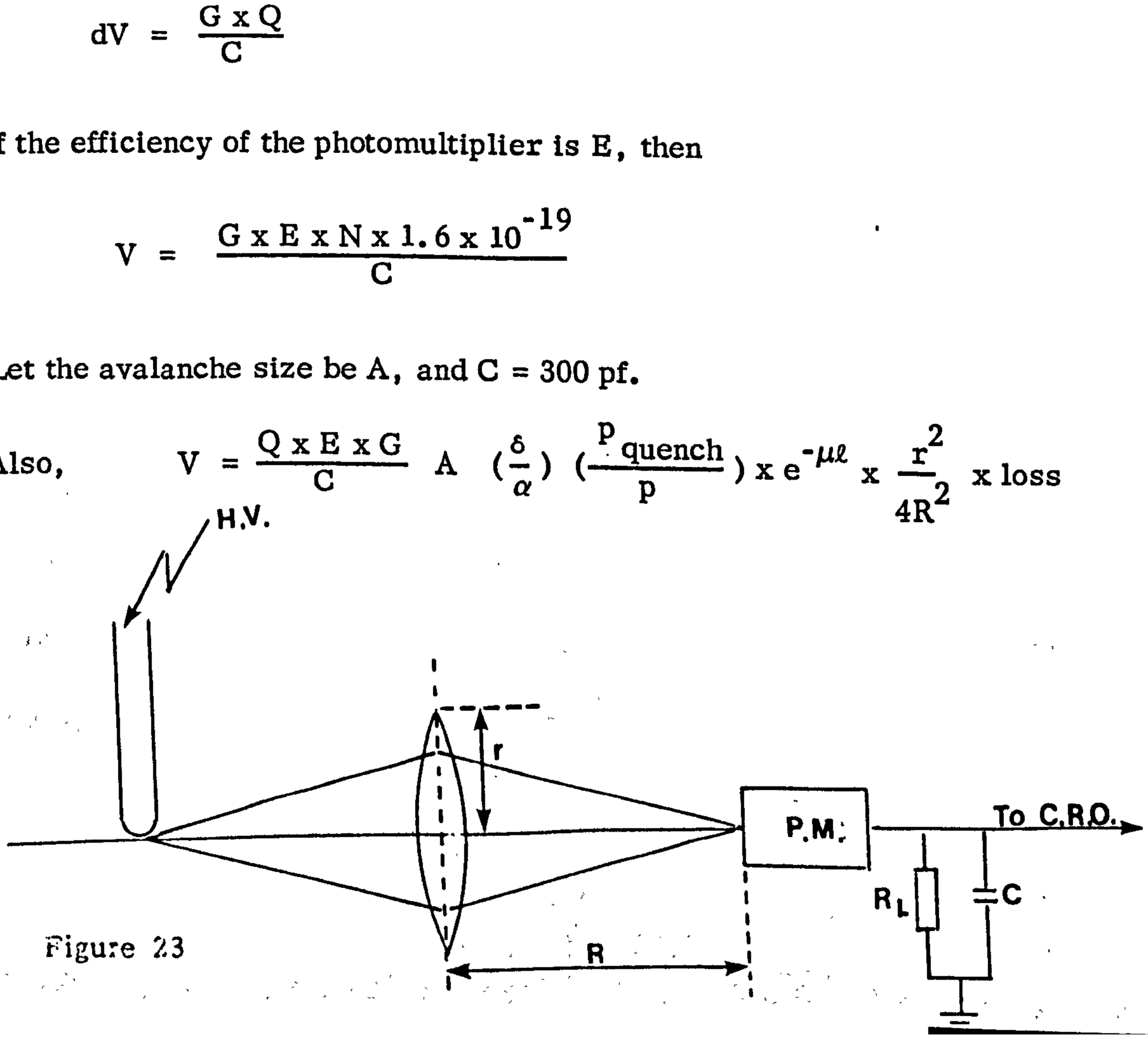

Figure 23

$R = 30$ cm, $\quad 2r = 7.5$ cm

$\left(\frac{\delta}{\alpha}\right) = 10^{-3} \qquad P_{quench} = 2.63 \times 10^{-3}, \qquad e^{-\mu\ell} = 1, \quad p = 2.63$

The value of $\left(\frac{\delta}{\alpha}\right)$, P_{quench} have been taken from Teich (1976)

$$V = 40 \times 10^{-3} = \frac{A \times 1.6 \times 10^{-19} \times 0.2 \times 10^{7} \times 10^{-3}}{300 \times 10^{-12}} \times 10^{-3}$$

$$\times \frac{(7.5/2)^2}{4 \times (30)^2} \times 0.8$$

$$A = 2.9 \times 10^{10}$$

The avalanche size is 3×10^{10}, i.e. the number of avalanches of size 10^8 are 3×10^2.

These calculations show that the photomultiplier detection sensitivity to be too low to detect a simple avalanche where $A \leqslant 10^8$ in SF_6 but any collective activity such as:: streamer extension, glow cloud or leader growth, should be easily detected. Hence in order to determine the corona onset voltage most reliance was placed on the photomultiplier system. From the foregoing it can be estimated that the minimum detector sensitivity for SF_6 to be $A \gtrsim 4 \times 10^9$ ionizations. The figure for the other gas mixtures is difficult to calculate but can be expected to be lower. At onset the signal detected in 10% SF_6 90% N_2 and 50% SF_6 50% N_2 were about three times those seen in SF_6. A typical example of the probe and photo-multiplier waveforms is shown in figure 24.

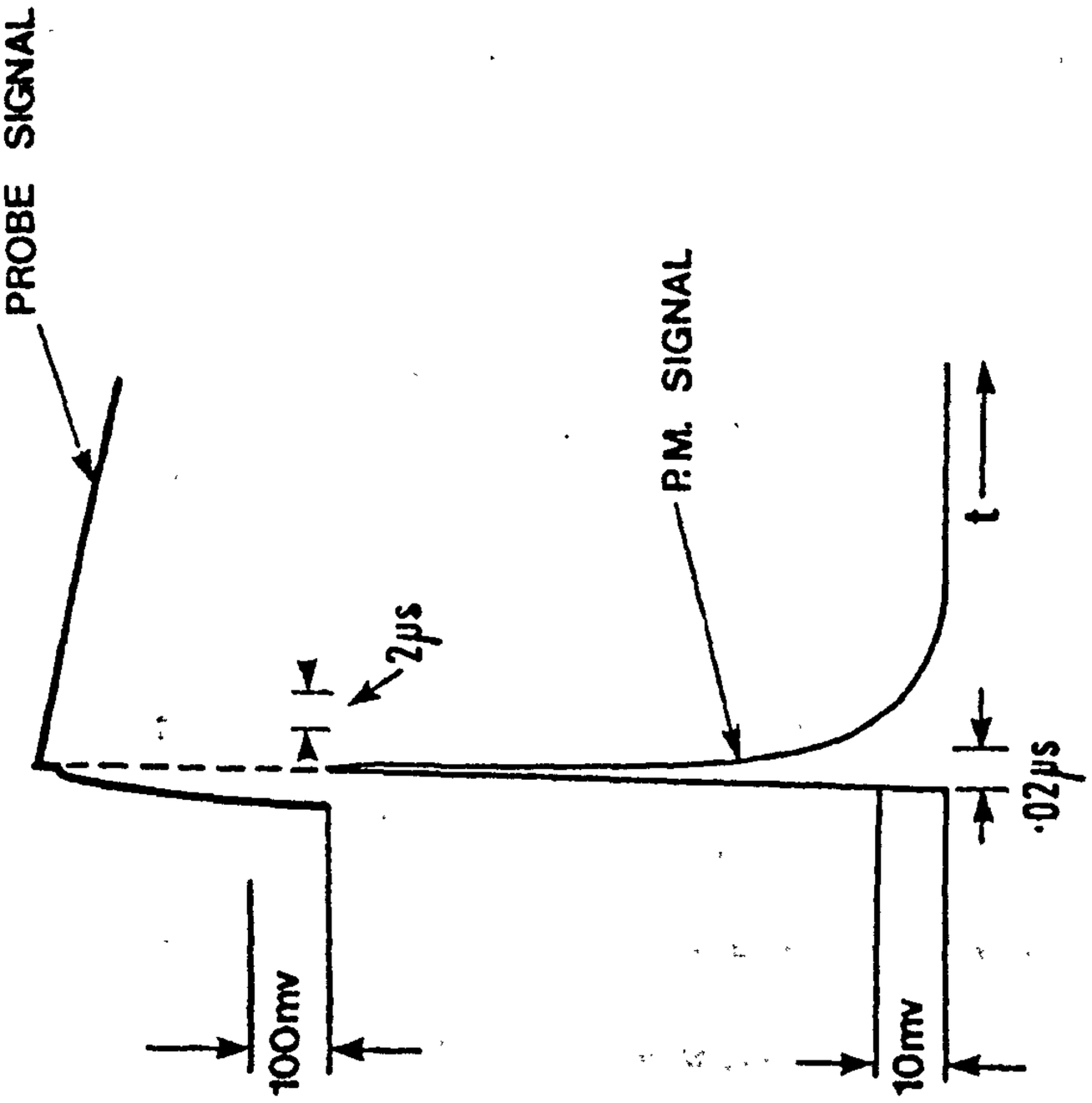

Figure 24 : An example of the field probe and photomultiplier (PM) signals at corona onset. 3 bar 10% SF_6 90% N_2 (tracing of actual recorded waveforms).

CHAPTER 4

RESULTS

4.1 INTRODUCTION

In this Chapter the results of the experiments performed during the project are presented. The sections are divided up into the different aspects of the discharge development irrespective of the composition of the gaseous medium. It is envisaged that by adopting this approach, repetition would be kept down to a minimum. Although what is presented here is not a full scale discussion, reference is made to the work of other authors from time to time. The calculation of electric field, and the field drop along the leader channel will be presented and discussed in the chapter to follow. The breakdown voltage and corona initiation voltage measurements for all gas compositions, and the different waveforms used are presented first. The theoretical determination of corona initiation voltage is also given in this Chapter as it is thought that it would be appropriate to deal with it here.

The velocity measurements are presented for two of the gas compositions studied, namely : 10% SF_6 90% N_2 and 50% SF_6 50% N_2. The velocity of discharge propagation in pure SF_6 will not be presented because of the difficulties of resolution of the waveforms.

4.2 BREAKDOWN VOLTAGE AND CORONA INITIATION VOLTAGE

4.2.1 Breakdown Voltage Measurement (V_B)

The experimental chamber was filled up with the required gas composition, after the electrodes were set and the chamber prepared as described in Chapter 3.

Throughout this project the maximum pressure to which the chamber was pressurised was 7 bar. At any given pressure for a specified gas composition the breakdown voltage was determined as follows :

The voltage of the impulse generator was increased gradually until the gap broke down spontaneously. The voltage was then reduced by about 20% and the gap was subjected to this reduced value of impulse voltage. If there was a breakdown at this reduced voltage when the impulse generator was fired then the voltage was further reduced until there was a withstand. If after the first reduction of voltage there was a withstand when the impulse generator was fired, then the voltage was raised by about 5% and the impulse generator was fired. This was repeated until there was a breakdown of the gap. Once a breakdown voltage was obtained at some voltage then the 50% breakdown voltage was determined by the up and down method described in Chapter 3. For each voltage determination thirty impulses were fired. The determination of corona initiation voltage was described in Chapter 3.

4.3 THEORETICAL DETERMINATION OF $V_i(+)$

The theoretical determination of $V_i(+)$ is based on the expression first derived by Nitta and Shibuya (1971). The constants required for the solution of equation (4.1) below were obtained from Aschwanden (1979), and Itoh et al (1979).

$$V_i = \left(\frac{E}{p}\right)_{lim} \; p.d. \; \frac{1}{f} \left[1 + \left(\frac{k}{B p r}\right)^{\frac{1}{2}}\right]^2 \qquad (4.1)$$

where d = gap spacing, f = a field enhancement factor, and r = radius of electrode tip, k is a constant equal to 18.

$$\bar{\alpha} = A\,E - B\,p \qquad (4.2)$$

$$\frac{\bar{\alpha}}{p} = A\left(\frac{E}{p}\right) - B \qquad (4.3)$$

where $\bar{\alpha} = (\alpha - \eta)$, A and B are constants.

Plots of $\bar{\alpha}$ versus (E/p) have been made by Aschwanden (1979) and Itoh et al (1979).

The $(\frac{E}{p})_{lim}$ is given by when $\bar{\alpha} = 0$ for the various mixtures and pure SF_6, in the above plots. The values of the field enhancement factor f were obtained from Ryan (1970) for the value of $(\frac{d}{r})$ used in this experiment. For SF_6

$$(E/p)_{lim} = 87.7 \text{ kV cm}^{-1} \text{ bar}^{-1}$$

$$B = 2236.36$$

$$A = 25.97$$

$$(d/r) = 55$$

$$f = 36.84$$

It may be seen from figures 4.1 to 4.6 that the agreement between experimental and theoretical values $V_i(+)$ is rather poor. The only case where agreement is good is for 10% SF_6 90% N_2 under an impulse waveform of 1/10,000 μs. In the case of pure SF_6 the experimental $V_i(+)$ values are about three times greater than the theoretical ones. Recent measurements of Anis and Srivastava (1981) confirm these results. Anis and Srivastava had used a voltage waveform with a rise time of 300 μs, the discrepancies are wide, however an explanation for such diagreement has not been forthcoming.

One of the major difficulties in the calculation of $V_i(+)$ in any gas or gaseous mixture is the lack of knowledge of the ionization and attachment coefficients at high pressure. There has been reasonably good agreement between experimental and theoretical values of ionization and attachment coefficients in mixtures of SF_6/N_2 under uniform field conditions and low pressure (Aschwanden 1979). However, Aschwanden has shown that there is a drastic deviation of the experimental values from those obtained theoretically above a certain value of (E/p). Bhalla and Craggs (1962),

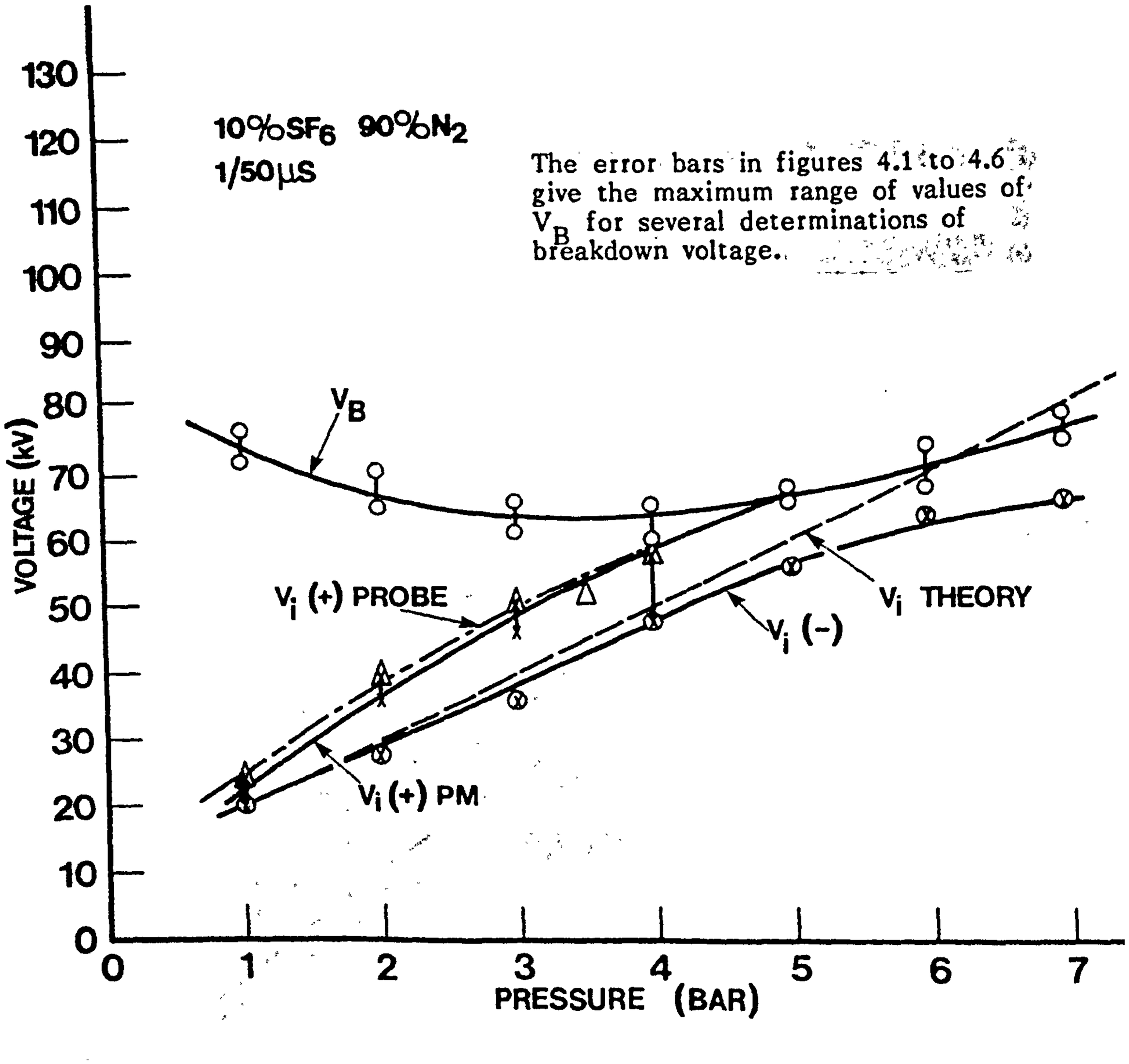

Figure 4.1 : Voltage versus pressure characteristics for the 10% SF_6 90% N_2 mixture using the 1/50 μs impulse waveform.

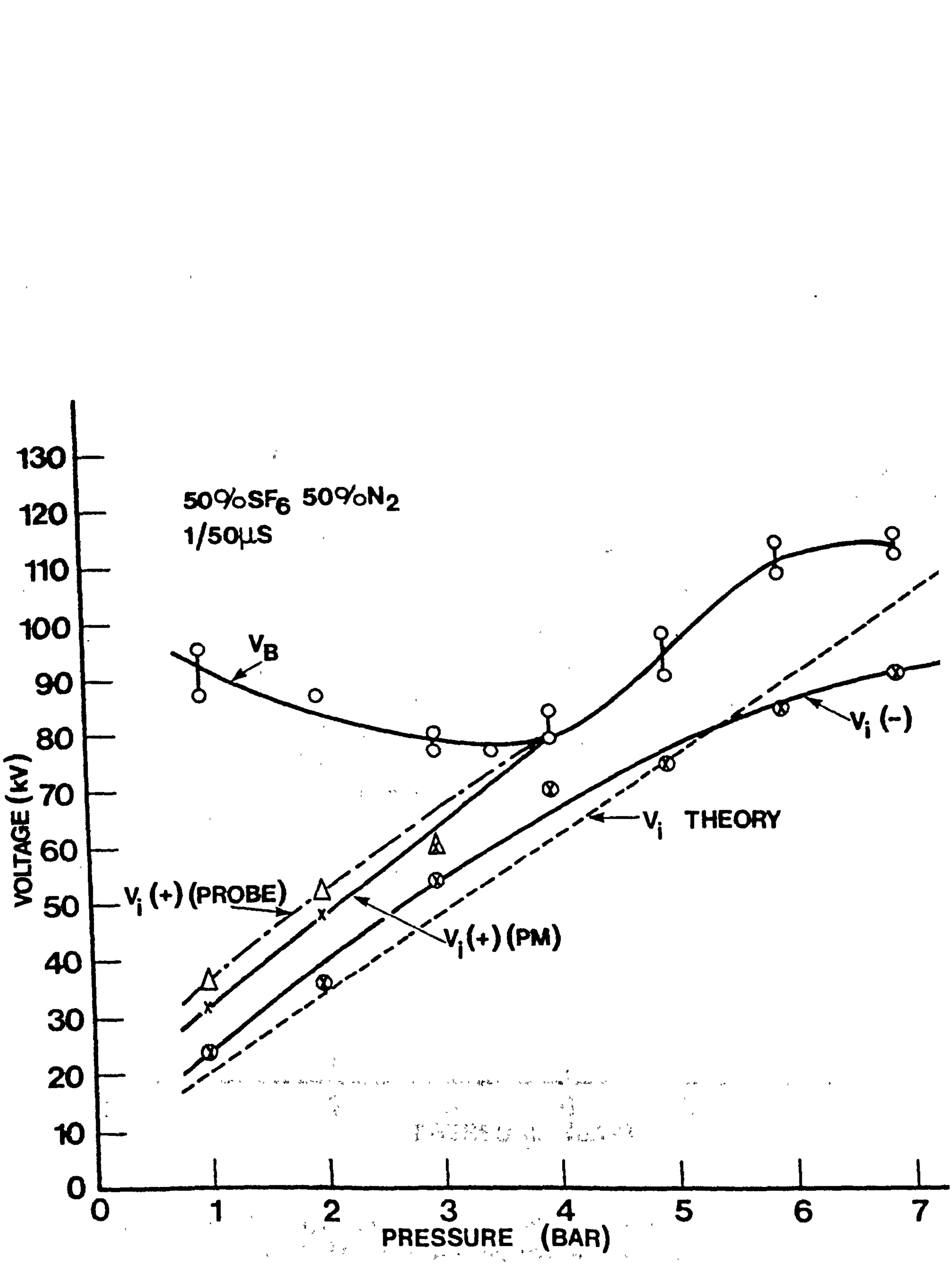

Figure 4.2 : Voltage versus pressure characteristics for the 50% SF_6 50% N_2 mixture using the 1/50 μs impulse waveform

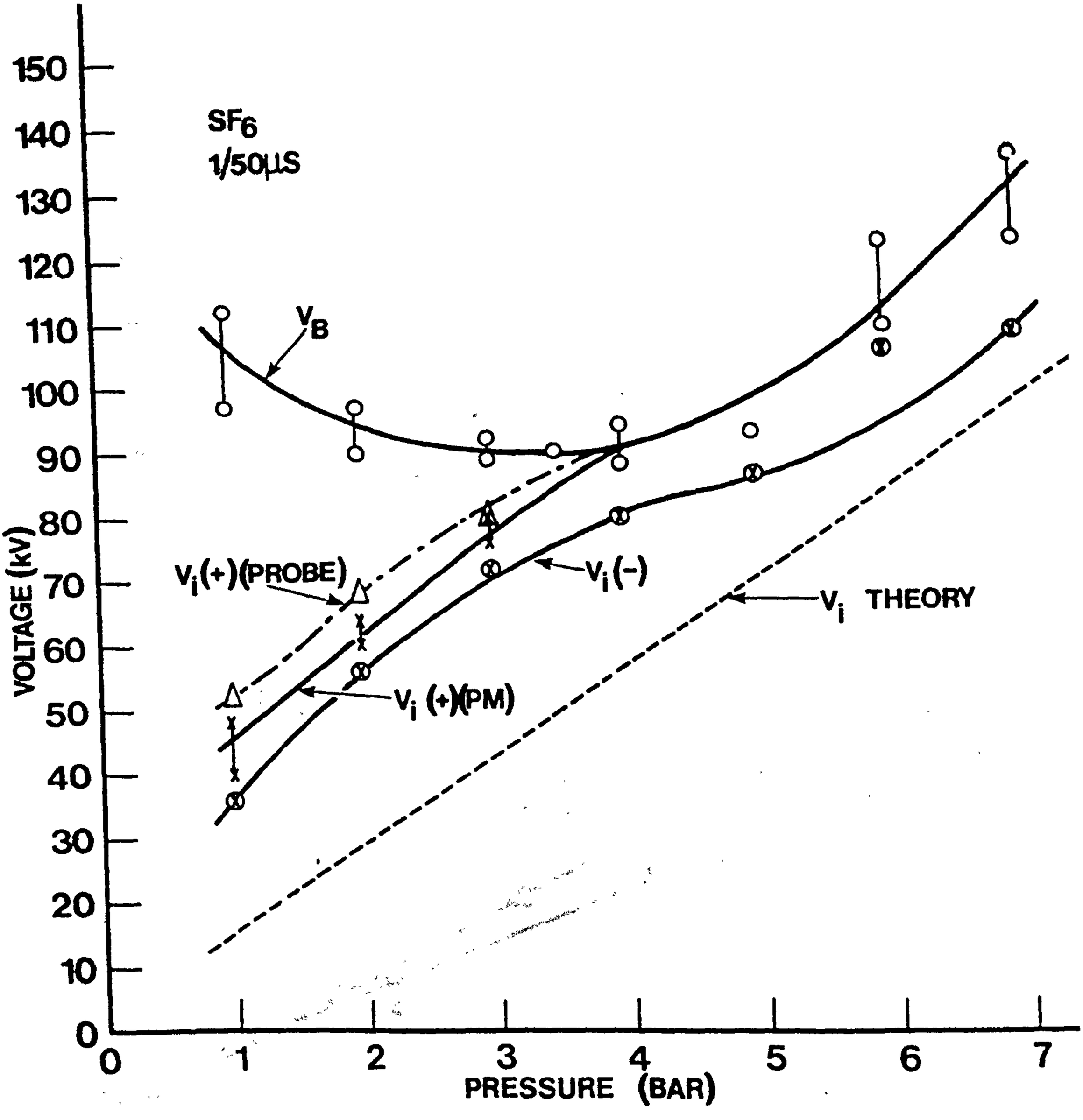

Figure 4.3 : Voltage versus pressure characteristics for SF_6 using the 1/50 μs impulse waveform.

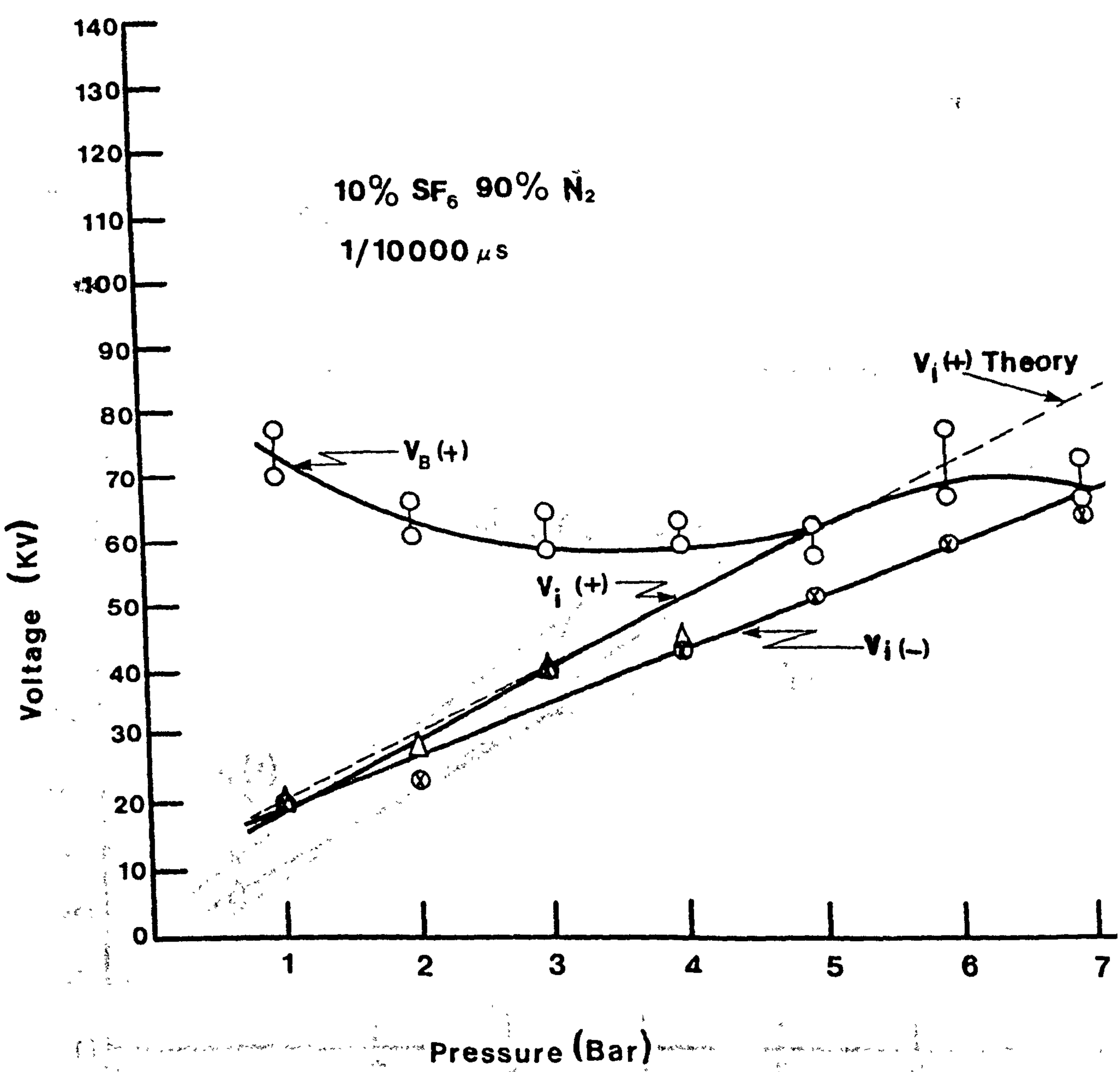

Figure 4.4 : Voltage versus pressure characteristics for the 10% SF_6 90% N_2 mixture using the 1/10,000 μs impulse waveform

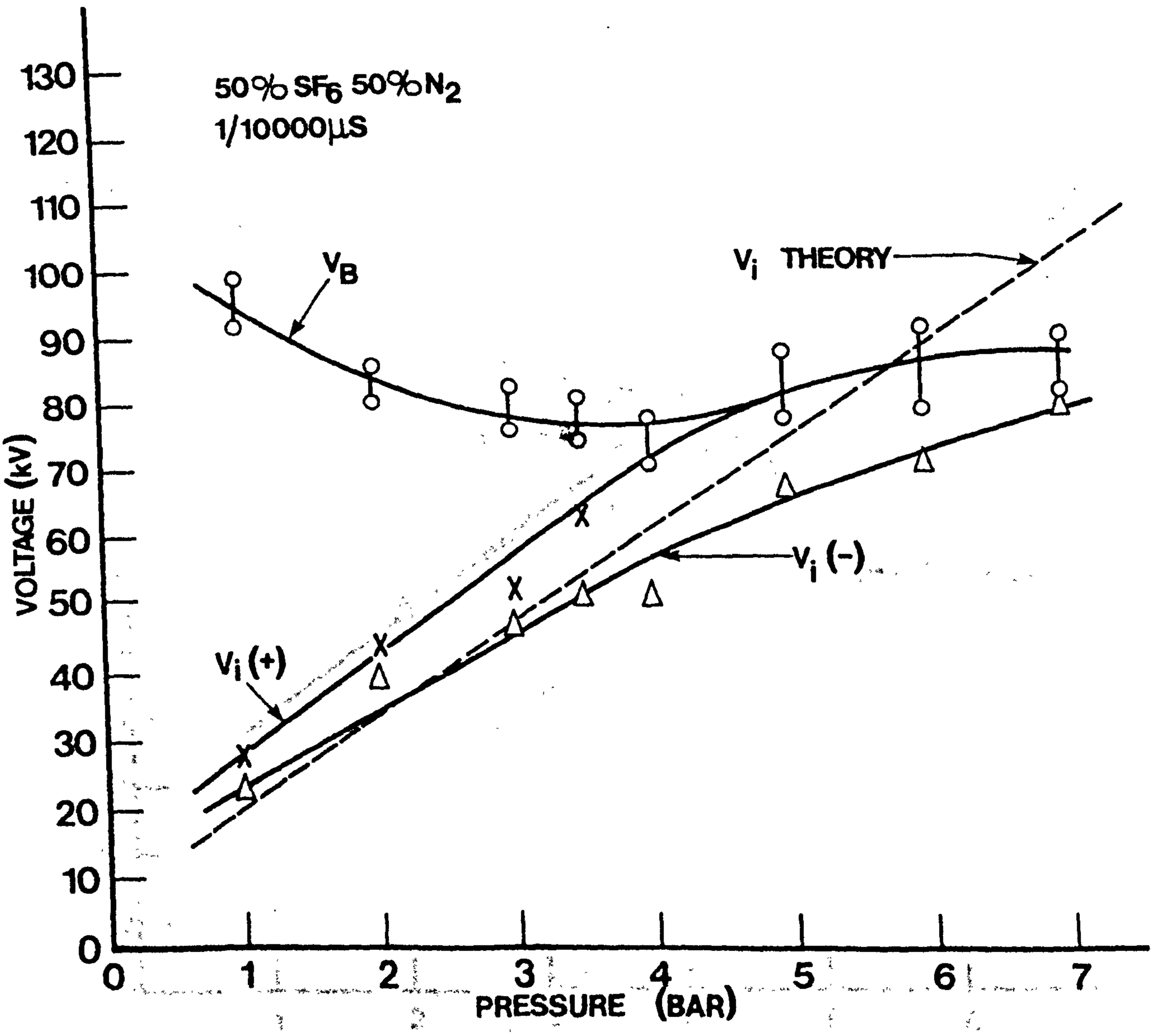

Figure 4.5 : Voltage versus pressure characteristics for the 50% SF_6 50% N_2 mixture using the 1/10,000 μs impulse waveform

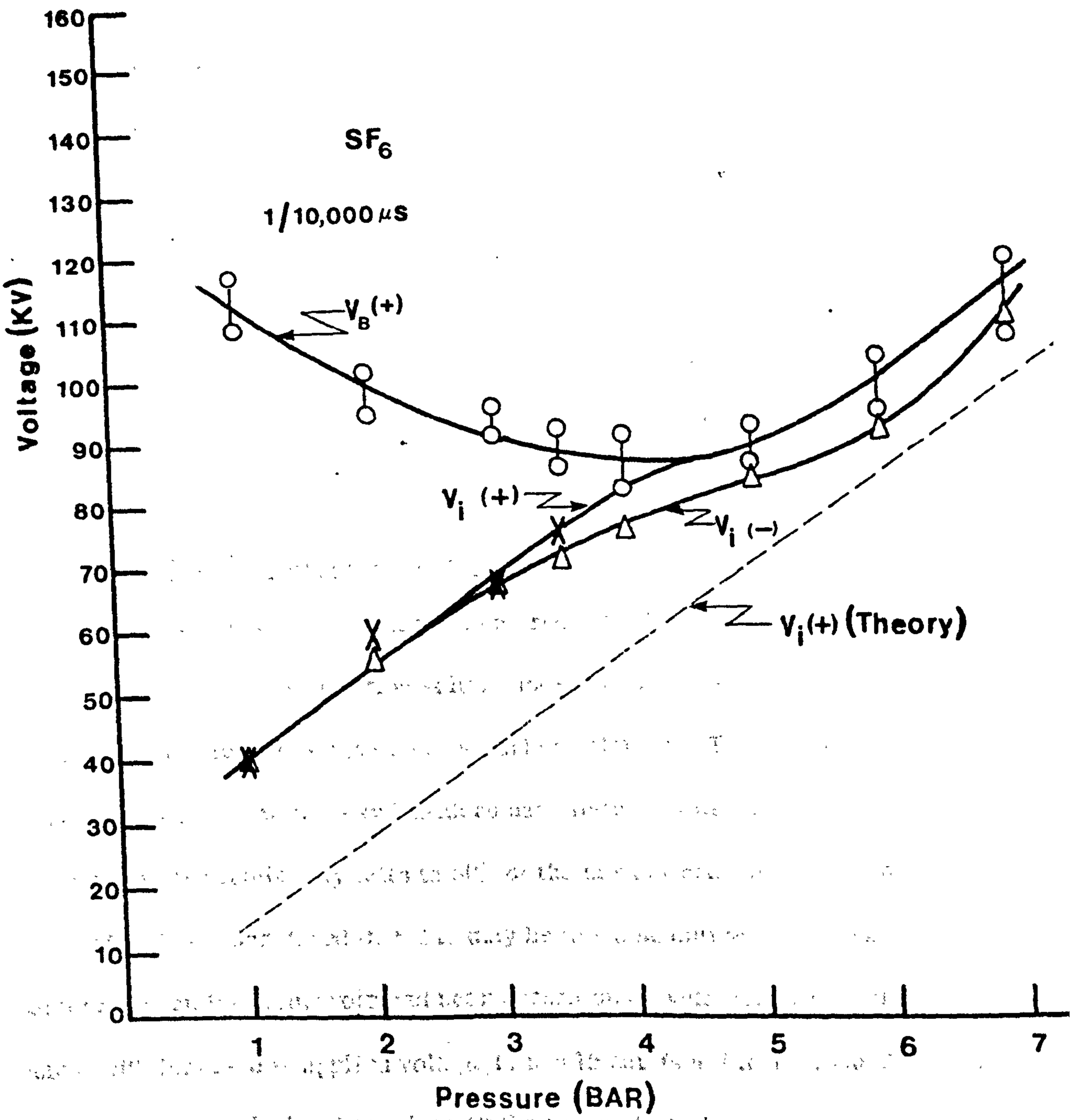

Figure 4.6 : Voltage versus pressure characteristics for SF_6 using the 1/10,000 μs impulse waveform

Karlsson and Pedersen (1972), Boyd and Crichton (1971), and Maller and Naidu (1976) have shown the measurements are not reliable above about 760 torr. The ionization and attachment processes in SF_6/N_2 mixtures under highly non-uniform fields may also be unreliable because of a lack of knowledge of the energy distribution, and the equilibrium of these coefficients under such conditions. This has to be appreciated when using the stated model for calculating corona initiation voltage in highly non-uniform fields where ionization and attachment take place in regions of high (E/p). The wide discrepancy between the theoretical and the experimental curves could be attributed to two possible reasons, (a) lack of initiatory electrons during voltage application and (b) insensitivity of the measuring system.

It has to be borne in mind, however, that the model used for $V_i(+)$ calculation assumes that no residual charge is present in the gap prior to initiation of the first streamer.

4.4 LUMINOSITY MEASUREMENTS

The peak value of the light pulses recorded by the photomultipliers increases as the corona inception voltage increases. This implies that the corona charge injected is higher at the higher voltages. The luminous extensions of the streamers and leaders have been obtained by taking the length where the luminosity falls to 50% of the normalised value at the point electrode. It is considered that this may be more sensitive than using a camera, specially at low voltages near corona onset voltage. The peak light output with increase in applied voltage is non linear (see Electra, No.35, 1974). Determination of ℓ has been done on the basis of discharge development along the axis of the gap. However, errors could be introduced due to the

fact that the discharge may not always develop along field lines and thus, not be axial. The determination of the leader lengths in long air gaps using image converter/intensifier cameras and photomultipliers (Electra, No. 35, 1974) have shown that there are large variations in the length determination. In the present experiments in compressed SF_6 and mixtures of SF_6 with N_2 there are large fluctuations in luminosity at each different position accessed down the interelectrode space as can be seen in figures 4.4.1 to 4.4.6. Due to this the length measurements determined using this technique also will be subject to similar variations. This may be because in SF_6 and mixtures of SF_6/N_2 under positive voltages, the streamer zone looks like a bunch of uniformly diverging streamer traces (Bortnik and Vertikov 1979). It can be seen from the experimental results that initial corona discharge near corona initiating voltage is highly localised near the tip of the rod electrode. This is particularly the case with SF_6, which is in agreement with the image converter photographs of Farish et al (1980). Voss (1979) has also shown that at low pressures with increase in voltage, the discharge is filamentary in nature. Farish et al (1979) have shown that under d.c. conditions the discharge in SF_6 goes from a purely "glow like" discharge at low pressure and low voltage through to a filamentary-glow discharge at higher voltages and higher pressure. The pressure range they had studied was between 0.2 barr and 1.6 bar. The results of relative luminosity extension presented in figures 4.4.1 to 4.4.6, and others like them, show that the longest extensions are for 10% SF_6 90% N_2 at a pressure of 1 bar. Measurements of luminous extensions have hitherto not been made in SF_6 and mixtures of SF_6/N_2, especially at pressures near the critical

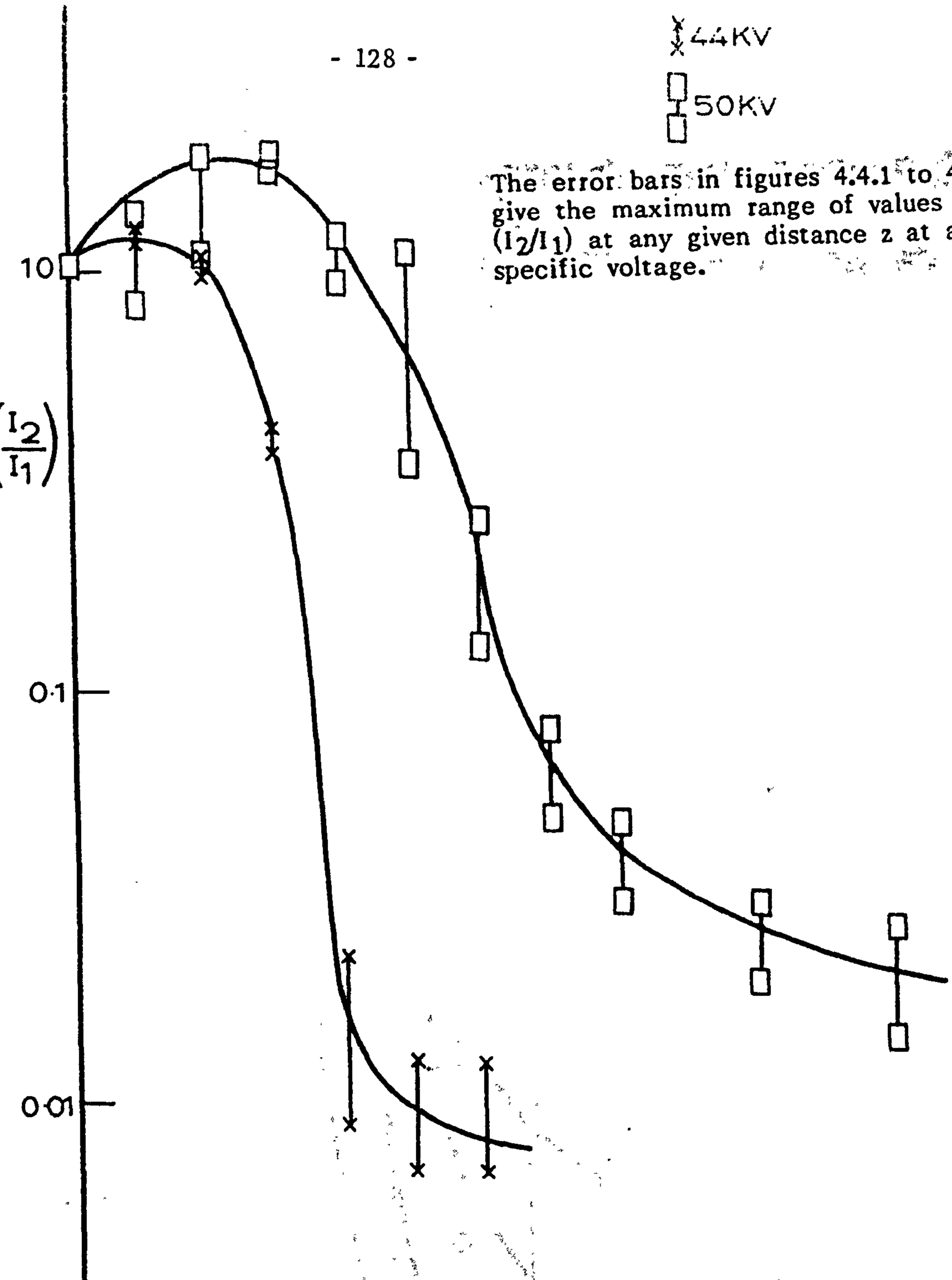

The error bars in figures 4.4.1 to 4.4.6 give the maximum range of values of (I_2/I_1) at any given distance z at a specific voltage.

Figure 4.4.1: The variation of (I_2/I_1) as a function of distance z from the anode for different voltages at a pressure of 1 bar in the 10% SF_6 90% N_2 mixture.

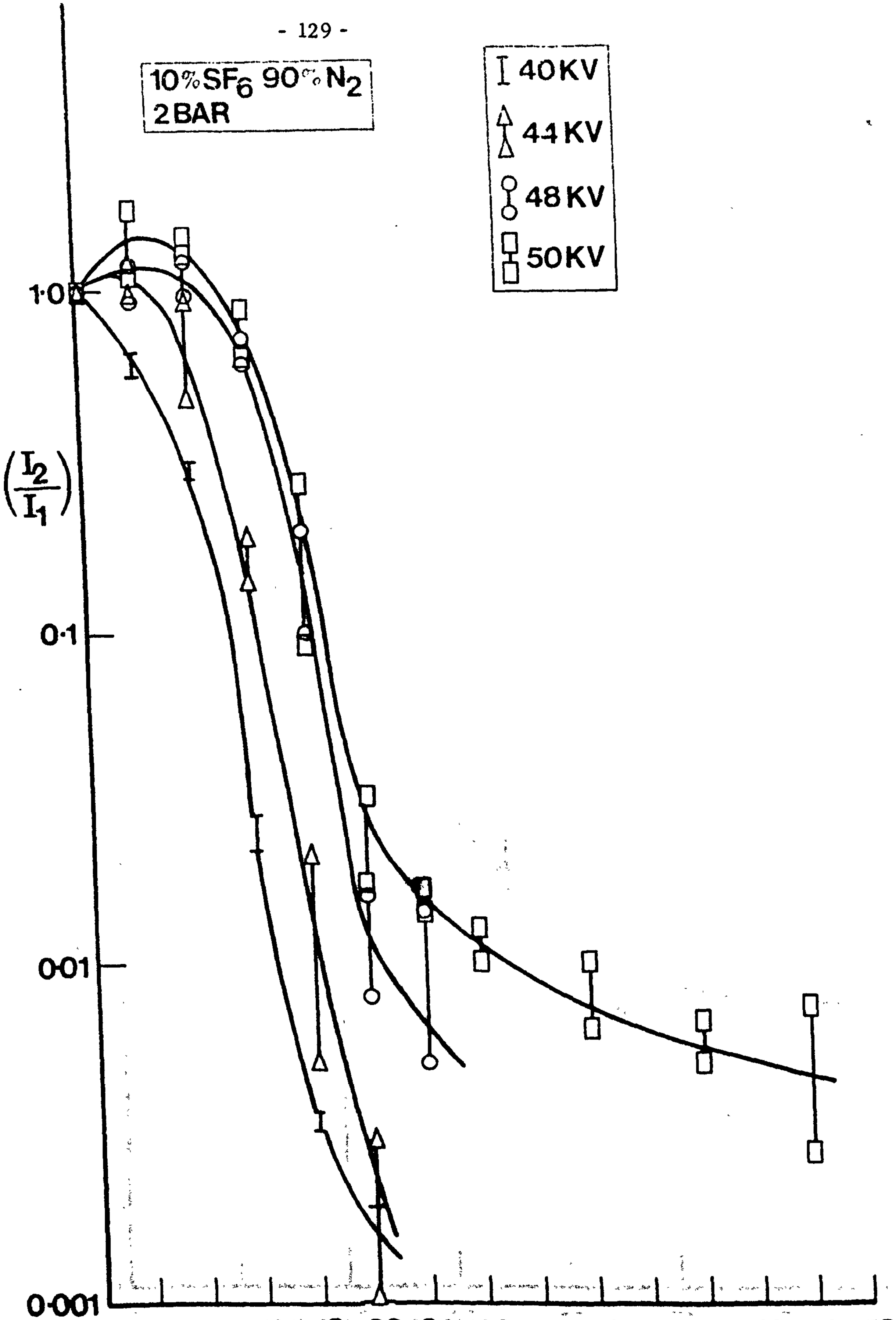

Figure 4.4.2 : The variation of (I_2/I_1) as a function of distance z from the anode for different voltages in the 10% SF_6 90% N_2 mixture at a pressure of 2 bar

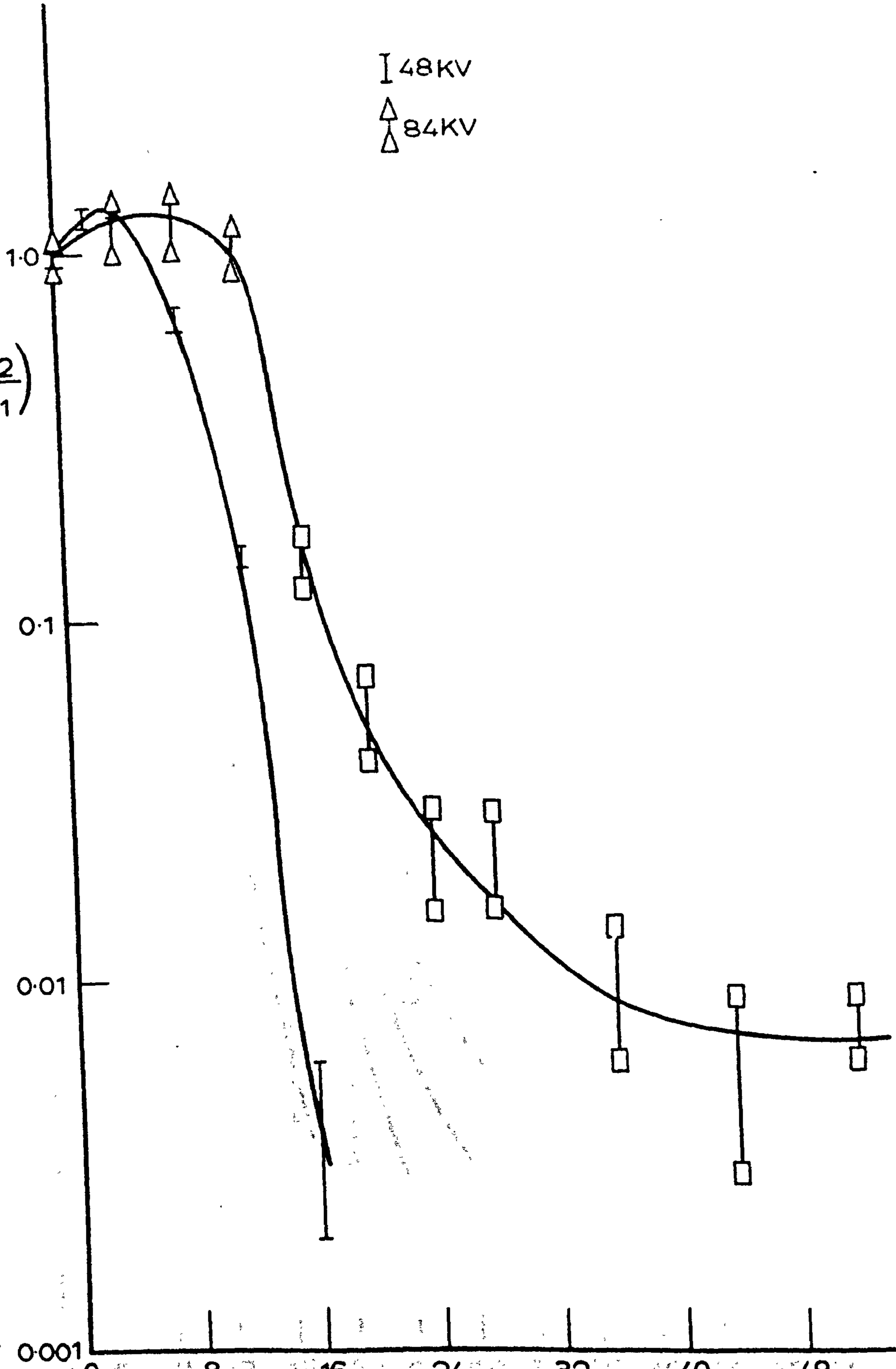

Figure 4.4.3 : The variation of (I_2/I_1) as a function of the distance z from the anode for different voltages, in 50% SF_6 50% N_2 at a pressure of 1.5 bar

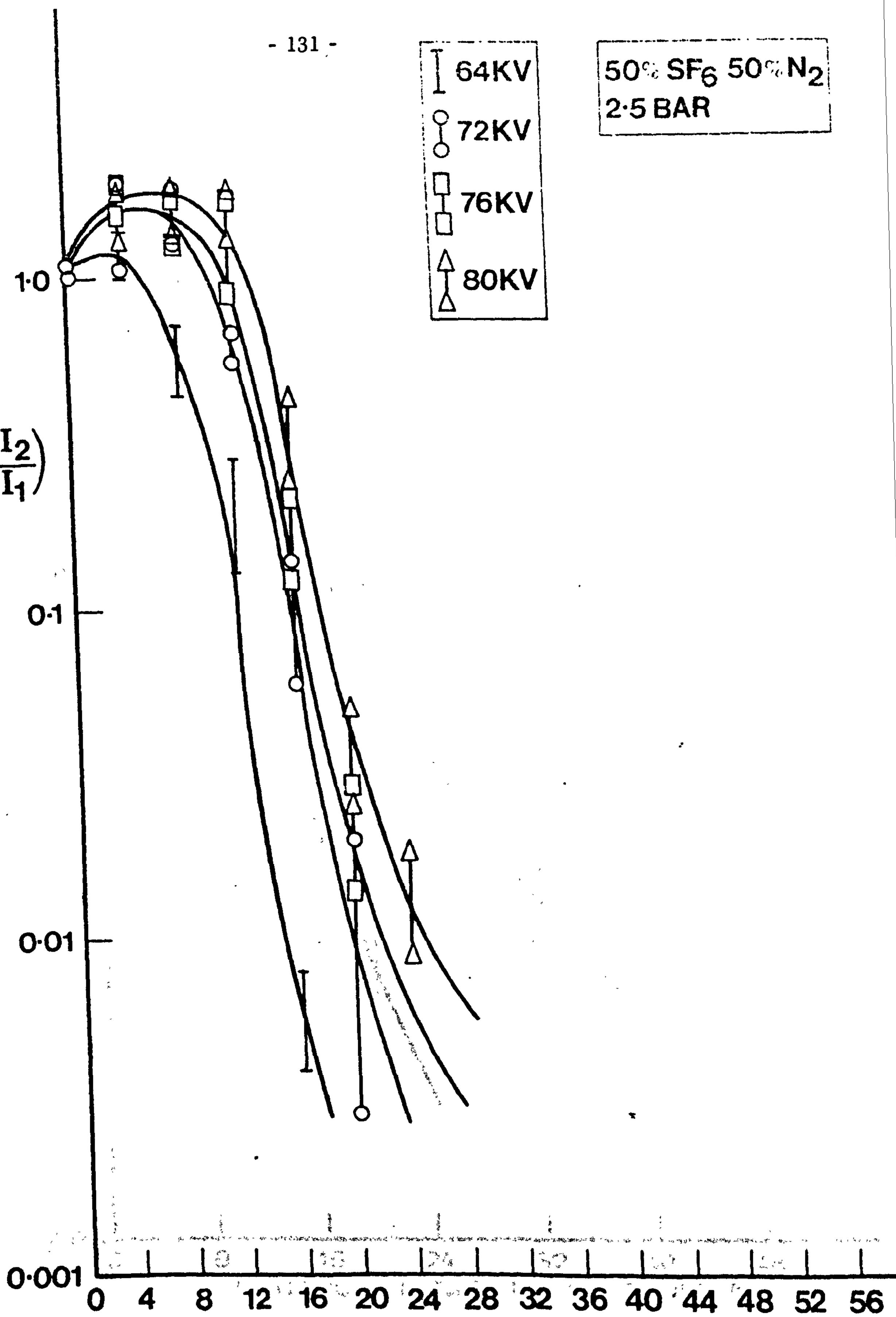

Figure 4.4.4 : Variation of (I_2/I_1) as a function of the distance z from the anode for different voltages in 50% SF_6 50% N_2 at a pressure of 2.5 bar

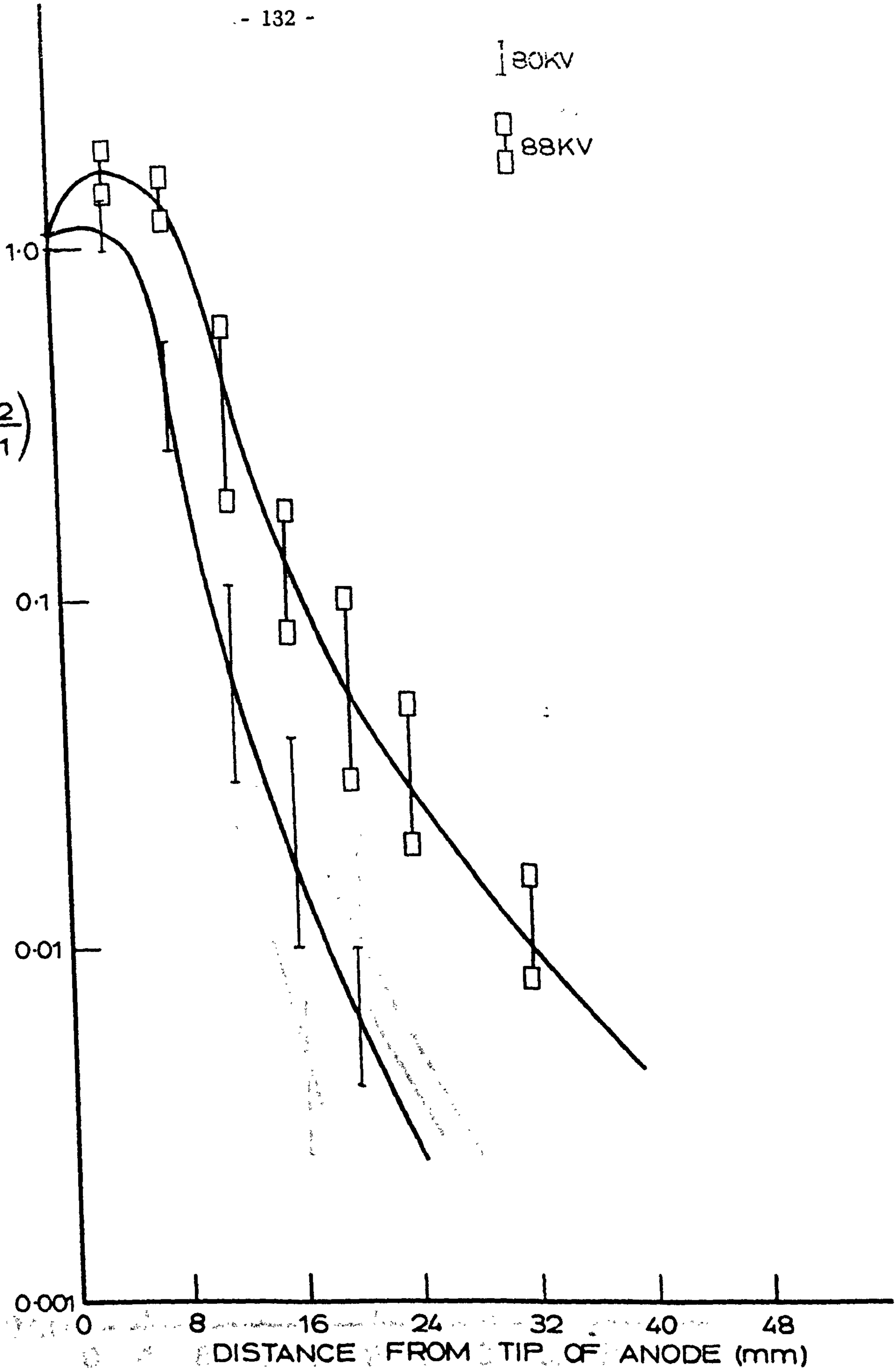

Figure 4.4.5 : The variation of (I_2/I_1) as a function of distance z from the anode for different voltages in SF_6 at a pressure of 2.5 bar

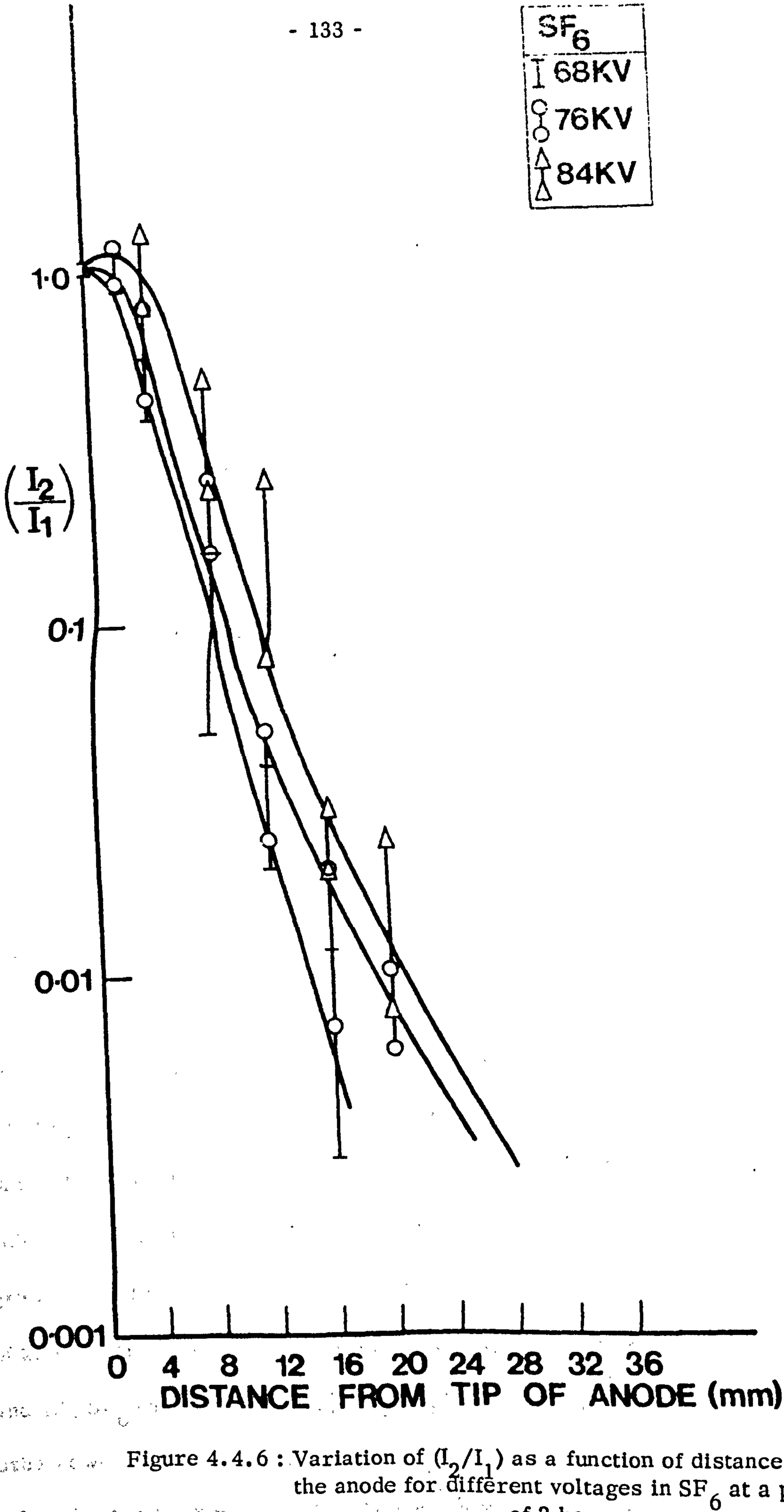

Figure 4.4.6 : Variation of (I_2/I_1) as a function of distance z from the anode for different voltages in SF_6 at a pressure of 2 bar

pressure. As such these results may be considered the first of their kind.

4.5 MEASUREMENTS OF LUMINOUS EXTENSIONS

The extent of luminous growth presented in figures 4.5.1 to 4.5.6 have been obtained from the results presented in the previous section, where the luminosity distribution along the interelectrode space was shown.

For the sake of brevity the three gas compositions, namely, SF_6, 50% SF_6 50% N_2, and 10% SF_6 90% N_2 will be referred to as : SF_6, 50% SF_6 and 10% SF_6 respectively.

By entrapolating the graphs of luminous extent versus voltage shown in figures 4.5.1 to 4.5.6 lengths corresponding to the breakdown voltages have been obtained. These lengths are called the instability lengths. It is assumed that the discharge grows to this length before the gap goes unstable and breakdown occurs.

The luminous extensions with voltage, in the three gas compositions at 1 bar depicted in figures 4.5.1, 4.5.3 and 4.5.6 indicate that in SF_6 and 10% SF_6 the growth is almost linear. As such it would be fair to assume that the graphs will remain linear when extrapolated. However, in the 50% SF_6 case the variation is quite complex; the discharge grows very slowly, in fact the growth up until 60 kV, which is 88% above the corona initiation voltage, is minimal. However, after this figure is reached the discharge grows exceedingly rapidly. It grows by nearly 13 mm over a voltage range of 20 kV. The effect of the presence of N_2 may be seen in the 50% SF_6 and 10% SF_6 cases. In the 50% SF_6 case when the voltage is 20% below the breakdown voltage the luminous extension is 13.4 mm, whereas for the 10% SF_6 case it is 20.8 mm at 22% below the breakdown voltage. As against

The error bars in figures 4.5.1 to 4.5.6 give the maximum and minimum values of the luminous length ℓ .

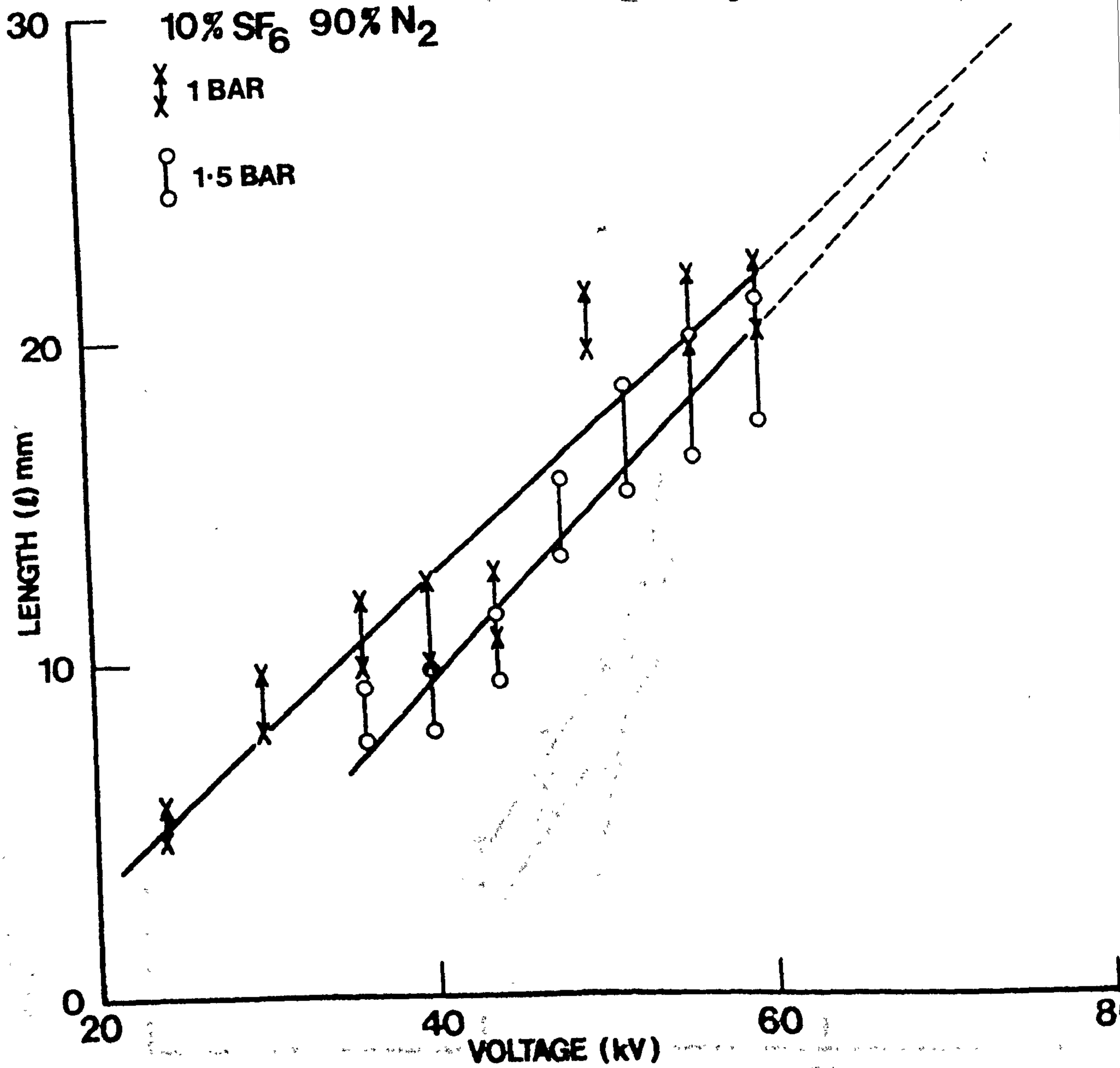

Figure 4.5.1 : The variation of the luminous length as a function of the applied voltage. The dotted lines indicate extrapolation to obtain the instability lengths corresponding to V_B

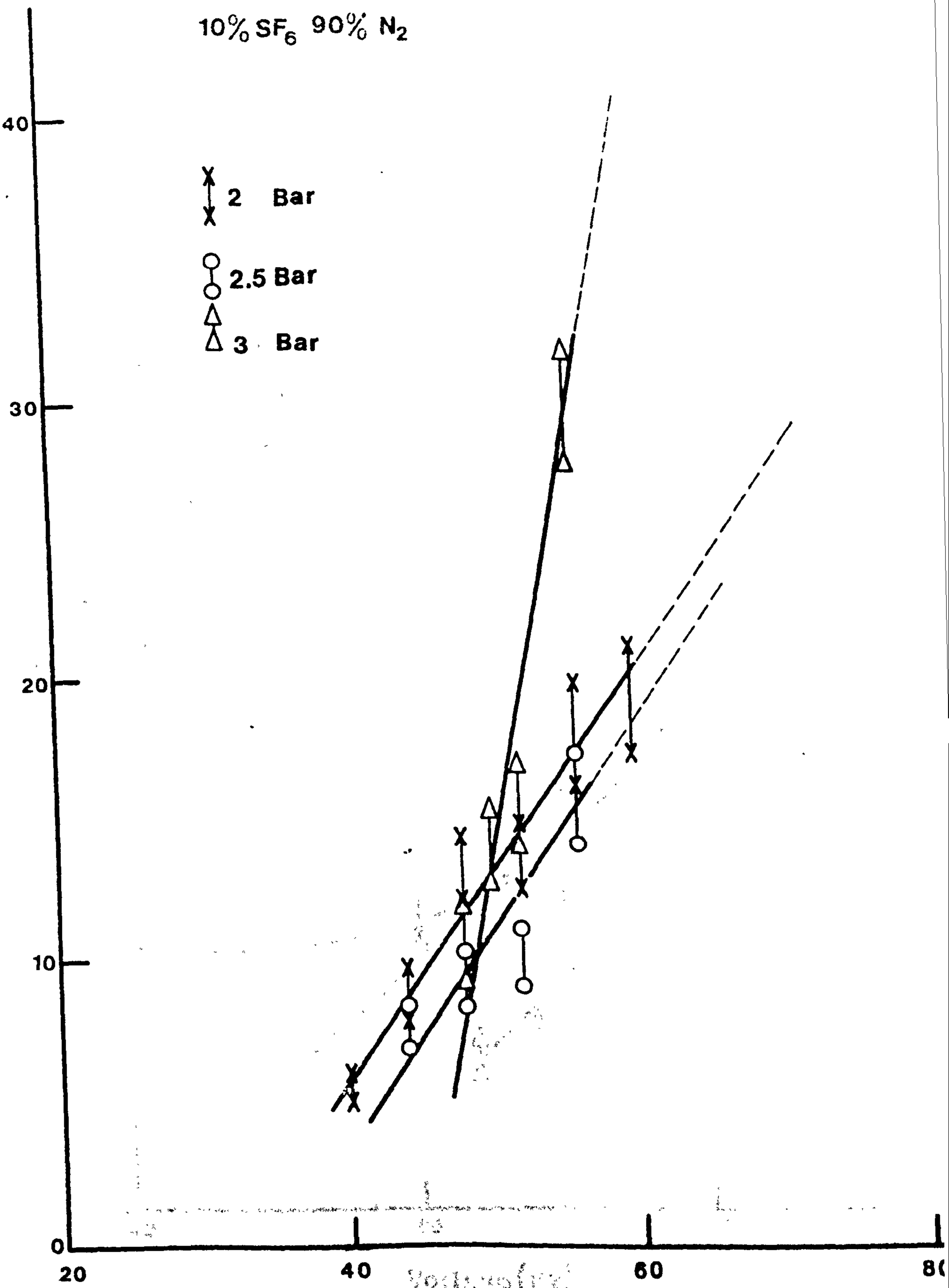

Figure 4.5.2 : The variation of the luminous length as a function of the the applied voltage. The dotted lines and indicate extrapolation to obtain the instability lengths corresponding to V_B

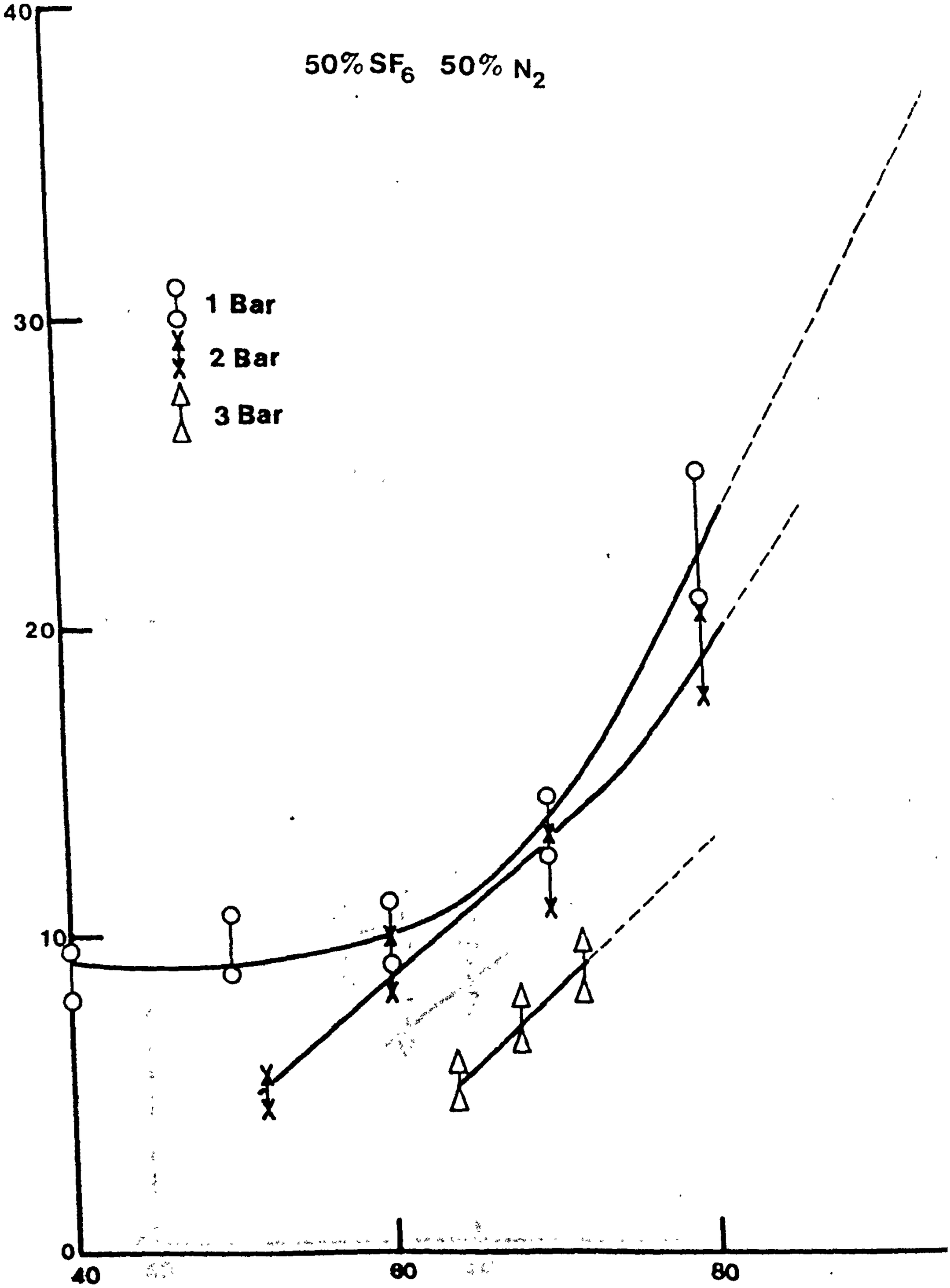

Figure 4.5.3 : The variation of luminosity length as a function of applied voltage. The dotted lines indicate extrapolation to obtain the instability lengths corresponding to V_B.

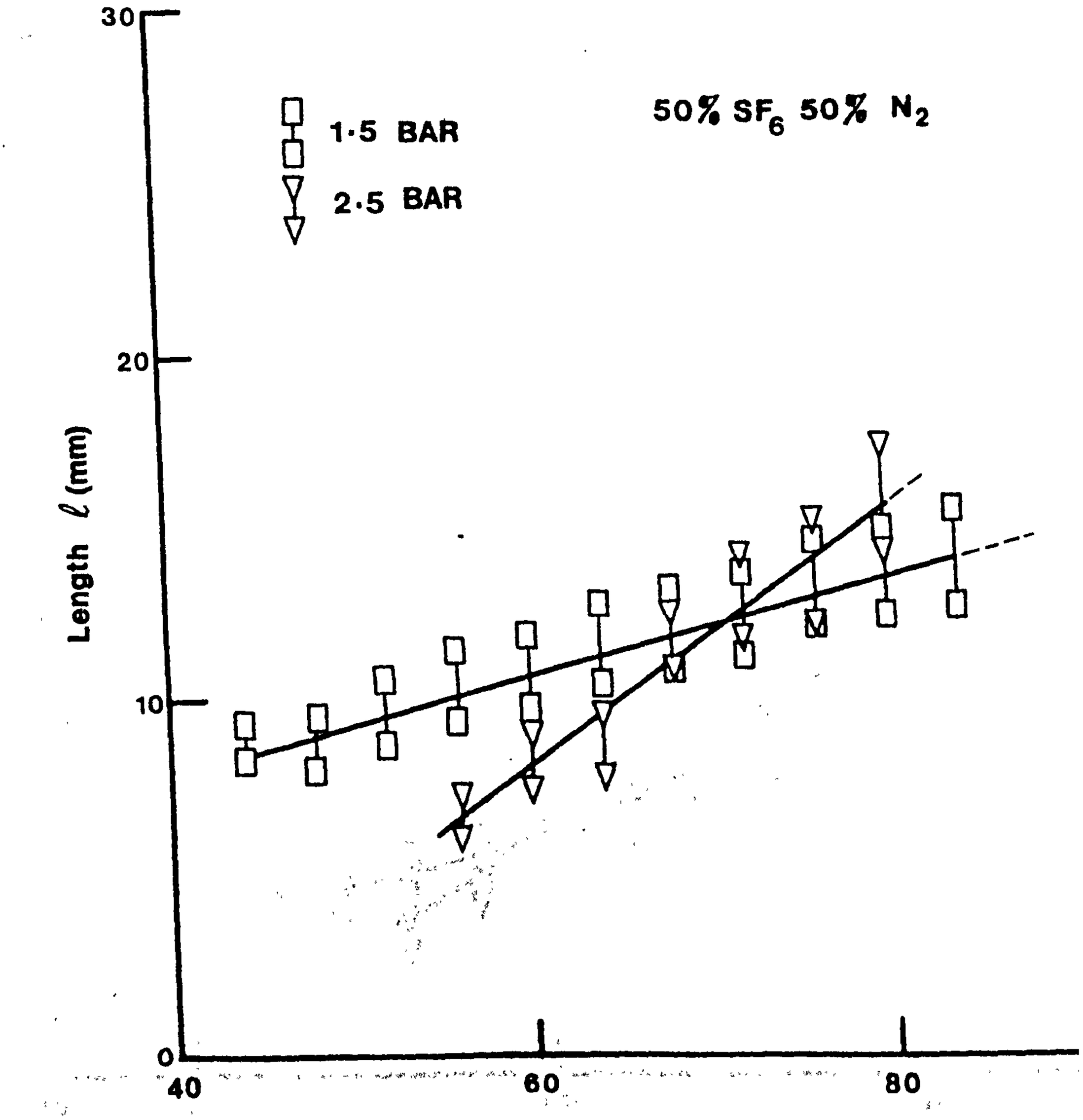

Figure 4.5.4 : The variation of the luminous length as a function of applied voltage. The dotted lines indicate extrapolation to obtain the instability lengths corresponding to V_B

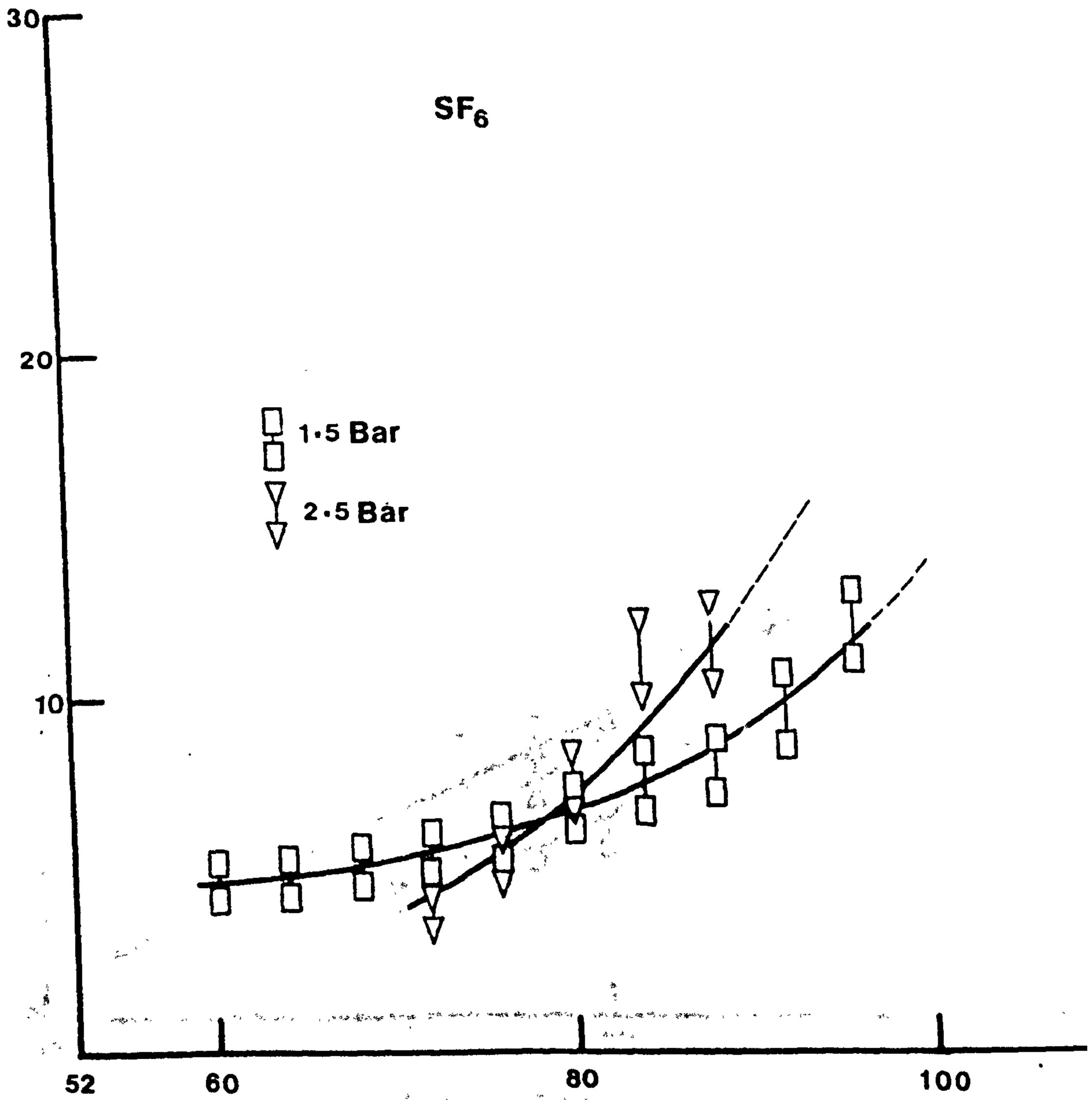

Figure 4.5.5 : The variation of luminous length as a function of applied voltage. The dotted lines indicate extrapolation to obtain the instability lengths corresponding to V_B.

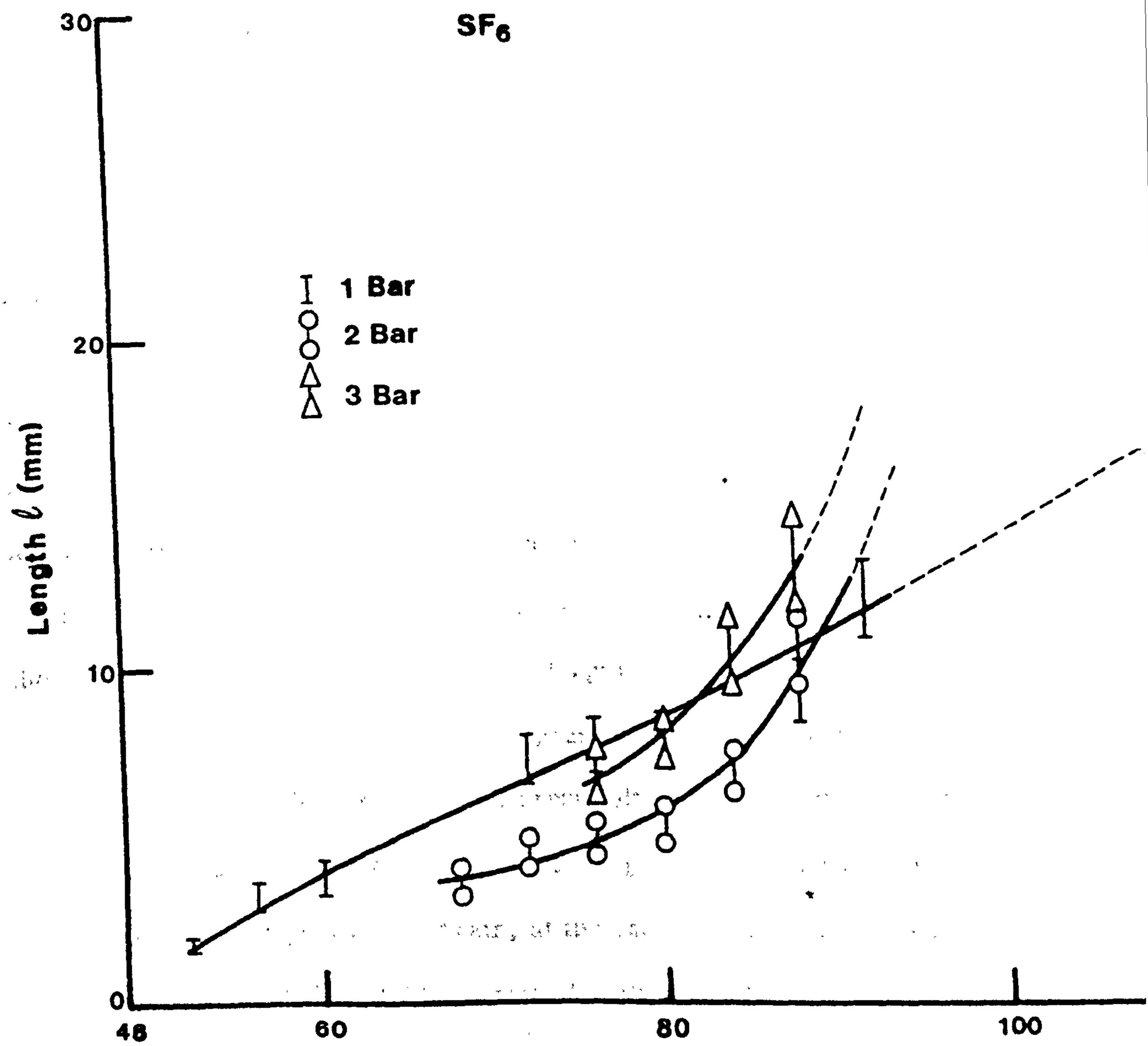

Figure 4.5.6 : The variation of luminous length as a function of applied voltage. The dotted lines indicate extrapolation to obtain the instability lengths corresponding to V_B.

these two, for SF_6 when the voltage is 5.8% below the breakdown voltage the luminous extension is 12 mm. The mean instability length at 1 bar for these three cases, namely, SF_6, 50% SF_6 and 10% SF_6 are 14 mm, 33.6 mm and 28.4 respectively. These figures seem somewhat inconsistent with the foregoing discussion. This is because for the 50% SF_6 case, as in the other two, the luminous growth was assumed to be linear beyond the voltages for which length measurements are available. This linearity may not entirely be true.

At the 1.5 bar the 10% SF_6 and 50% SF_6 compositions show that the luminous lengths vary linearly with voltage. In the SF_6 case the variation is non linear and the increment in length between 60 kV and 80 kV is very slight. The difference in length over that range of voltage is only 2 mm. It may be seen from figures 4.5.5, 4.5.4 and 4.5.1 that at 1.5 bar, the luminous extent in SF_6 is far more restricted than in the other two compositions. For instance, at a voltage level of approximately 70% above the corona inception voltage the luminous lengths in SF_6, 50% SF_6 and 10% SF_6 are 8 mm , 12 mm and 16.8 mm respectively. It has to be borne in mind, however, that these occur at different voltage levels although they are at a specified percentage above corona inception voltage pertaining to the different gas compositions. Again, at the same pressure of 1.5 bar the luminous length in SF_6 at 4% below the breakdown voltage is 12 mm and in 50% SF_6 it is 14 mm. However, in 10% SF_6 at 16% below the breakdown voltage the luminous length is 19.2 mm. The instability length in SF_6 is 13.6 mm, in 50% SF_6 it is 14.6 mm, and in 10% SF_6 it is 26.8 mm.

At 2 bar the development of the discharge is very similar to that at 1.5 bar. The variation of length with voltage is linear for 10% SF_6,

nearly linear for 50% SF_6 and non linear for SF_6. For both 50% SF_6 and 10% SF_6 there is accelerated growth of luminous length after about 72 kV and 80 kV respectively. At around 10% above the corona inception voltage the luminous lengths in 10% SF_6 and 50% SF_6 are respectively 5.6 mm and 5 mm. In SF_6 at 13% above corona initiation voltage the luminous length in SF_6 is 10.4 mm. For 50% SF_6 and 10% SF_6 when approximately 10% below the breakdown voltage the luminous lengths are 19 mm and 19.2 mm respectively. As may be seen from figures 4.5.3 and 4.5.6 although the pattern of variation in the two mixtures is different, the values are similar. These above values are related by percentage above corona initiation voltage, thus giving different levels of voltage. The mean instability length for SF_6 is 13.7 mm. The instability lengths for 50% SF_6 and 10% SF_6 are 23.4 mm and 26 mm respectively. It may be seen from figures 4.5.3 and 4.5.6 that at a pressure of 2 bar the discharge development is very similar in the 10% SF_6 and 50% SF_6 cases.

At 2.5 bar the discharge grows rapidly in all three gas compositions considered. In SF_6 the luminous length extends to 4 mm for a voltage only 3% above the corona initiation voltage. In 50% SF_6 for only 2% above corona inception voltage the luminous length is 6.8 mm, and the luminous extension in 10% SF_6 for a voltage 5% above the corona initiation voltage is 7.6 mm. In the 10% SF_6 and 50% SF_6 cases the variation of luminous length is linear with voltage. However, the rate of variation in SF_6 is non-linear yet again. When the voltage level in SF_6 is 5% below the breakdown voltage the luminous extent is only 11.6 mm. In 50% SF_6 when a voltage 2.5% below the breakdown voltage is reached, the length is 15.2 mm. However, in 10% SF_6 when a voltage 15% below the breakdown voltage is reached the luminous length

is 15.6 mm. In this instance there is an enormous difference between the 10% SF_6 case and the other two gas compositions considered. The instability length in SF_6 is 15.8 mm which is close to 16.4 mm, the value obtained in 50% SF_6. The instability length in 10% SF_6 is 23 mm, which is almost 1.5 times that in SF_6. The results at 3 bar are the most restricted of all the cases considered, this is because the separation between the corona inception voltage and the breakdown voltage is small. It may be seen from figures 4.5.2, 4.5.3 and 4.5.6 that the corona growth is quite extensive even at the very onset of corona. The luminous length at corona onset in SF_6 is 6.8 mm which is more than at any other pressure. For 50% SF_6 and 10% SF_6 at approximately 6% above the corona initiation voltage the luminous lengths are respectively 5.2 mm and 7.6 mm. The variation of luminous length with voltage is linear for the 50% SF_6 and 10% SF_6 cases. However, the variation in SF_6 is non linear. The variation in 10% SF_6 is exceedingly rapid. For instance, as may be seen from figure 4.5.2 the luminous length increases from 15.4 mm to 29.6 mm over a voltage of 4 kV. When the voltage is raised to a level of about 2% below the breakdown voltage in SF_6 the luminous extension is 13.2 mm. In 50% SF_6 at a voltage 6% below the breakdown voltage the luminous extension is 8.8 mm. In 10% SF_6 at nearly 7% below the breakdown voltage the luminous extension is 29.6 mm. In this instance at 3 bar the mean instability lengths in SF_6, 50% SF_6 and 10% SF_6 are respectively, 16.2 mm, 11.8 mm and 40 mm.

4.6 FIELD MEASUREMENTS

4.6.1 Introduction

The results of field measurements will be presented in this section. These results were obtained simultaneously with the luminosity measurements.

As such they will be discussed in conjunction with the results in the previous sections. The method employed for calculating ($\Delta E/E$) was discussed in Chapter 3, Section 8.3. As in the previous section, the three gas compositions, pure SF_6, 50% SF_6 50% N_2, and 10% SF_6 90% N_2 will be referred to as SF_6, 50% SF_6 and 10% SF_6 respectively.

4.6.2 ($\Delta E/E$) Variations with Voltage

The Variation of ($\Delta E/E$) with voltage at 1 bar is shown in figures 4.6.1, 4.6.3 and 4.6.5 for 10% SF_6, 50% SF_6 and SF_6 respectively. In 10% SF_6 near the corona initiation voltage the corona activity does not always take place on the crest of the voltage wave. In cases such as this the value of the geometrical field, obtained from figure16 in Chapter 3, is taken at the voltage corresponding to the position along the tail of the field waveform where corona activity distorts the waveform.

As against the luminosity extension results in the previous section, the variation of ($\Delta E/E$) versus voltage are all non linear for all three cases considered at 1 bar. The wide fluctuations of the values of ($\Delta E/E$) at any given level of voltage indicate that the discharge behaves in an irregular manner. This was shown in the luminosity distribution diagrams shown in section 4.5.

At 1.5 bar the discharge development follows an approximately linear pattern in SF_6, and 50% SF_6. However, in 10% SF_6 the development is highly non linear. This is in contrast to the variation of luminosity length with voltage. The development of the discharge in SF_6 at 1.5 bar is highly restricted and is similar to the luminous extension in SF_6. However, as the voltage is raised the value of ($\Delta E/E$) becomes comparable in SF_6 and

50% SF_6. It may be seen from figures 4.6.4 and 4.6.6 that the rate of increase of ($\Delta E/E$) versus voltage in 50 % SF_6 is far slower than that in SF_6. In 10% SF_6 at this pressure the variation of ($\Delta E/E$) versus voltage is exceedingly rapid after a voltage of 48 kV is reached. This is 60% above the corona inception voltage in 10% SF_6. At 60 kV in 10% SF_6, which is 16% below the breakdown voltage, the value of ($\Delta E/E$) is about twice that in either SF_6 or 50% SF_6.

At 2 bar the discharge develops in such a manner to make the ($\Delta E/E$) values exceedingly small, in all three gas compositions. In 10% SF_6 the value of ΔE right at onset is about 14 mV, and this does not occur at the crest of the field wave always. The geometrical field at 36 kV is 250 mV, which gives a value of 0.06 for ($\Delta E/E$). The values of ($\Delta E/E$) obtained for SF_6 and 50% SF_6 are comparable to the value in 10% SF_6. Although in SF_6 the values of ($\Delta E/E$) are available from 6% above the corona initiating voltage and in 50% SF_6 they are available from 8% above the corona inception voltage. In 50% SF_6 the value of ($\Delta E/E$) does not increase at all as the voltage is increased. This is in striking contrast to the other two compositions of SF_6 and 10% SF_6. Also, in 50% SF_6 at a voltage crest value of 52 kV, the field waveforms show corona activity away from the crest, along the tail of the waveforms. The graphs showing the variation of ($\Delta E/E$) versus voltage are given in figures 4.6.2, 4.6.3 and 4.6.5. At 2.5 bar the value of ($\Delta E/E$) is small in the three different compositions. In SF_6 at 76 kV, which is 9% above the corona inception voltage, the value of ΔE is 35 mV. In 10% SF_6 the value of ΔE at a voltage 5% above corona initiating voltage is about 22 mV. However, in 10% SF_6 when the corona activity occurs away from the crest of the field waveform, the voltage correspondingly is 42 kV and

the value of ΔE at this voltage is 14.3 mV. The value of ΔE in 10% SF_6 jumps up to 74 mV at 48 kV which is 14% above the corona initiating voltage. The variation of ($\Delta E/E$) with voltage is much slower in 50% SF_6 than in the other two compositions, this may be seen in figures 4.6.1, 4.6.4 and 4.6.6. The mean value of ΔE in SF_6 at 88 kV which is 5% below the breakdown voltage is 493.5 mV. In 10% SF_6 when the voltage is 15% below the breakdown voltage the mean value of ΔE is 176.8 mV. In contrast to these values given above in 50% SF_6 at a voltage of 80 kV, which is only 2.5% below the breakdown voltage the mean value of ΔE is 100.8 mV. At 3 bar as at 2.5 bar above the variation of ($\Delta E/E$) versus voltage is exceedingly steep in SF_6 and 10% SF_6. However, the variation of ($\Delta E/E$) with voltage in 50% SF_6 is rather complex. In 50% SF_6 near the onset of corona the field variations due to corona do not always occur at the crest of the voltage wave. The fact that these superimposed signals occur down the tail of the field waveform indicate that the corona inception voltage may in actual fact be lower than the 60 kV indicated in figure 4.2. However, the most consistent results of corona inception voltage as occurring at the crest of the field waveform indicated by the field probe is 60 kV. The photomultiplier signals too appear at a crest voltage of 60 kV. Hence this value is taken as the corona initiating voltage. In SF_6 at 76 kV, which is the corona onset voltage, the smallest value of ΔE is 22.8 mV. It may be seen from figure 4.6.5 that there is a wide fluctuation of the value of ($\Delta E/E$) at 76 kV. In the 10% SF_6 the value of ΔE at corona onset is 25 mV. Again in this case as in the 50% SF_6 the field waveform indicates the occurrence of corona away from the crest of the waveform. In the 10% SF_6 as the voltage is raised to a value

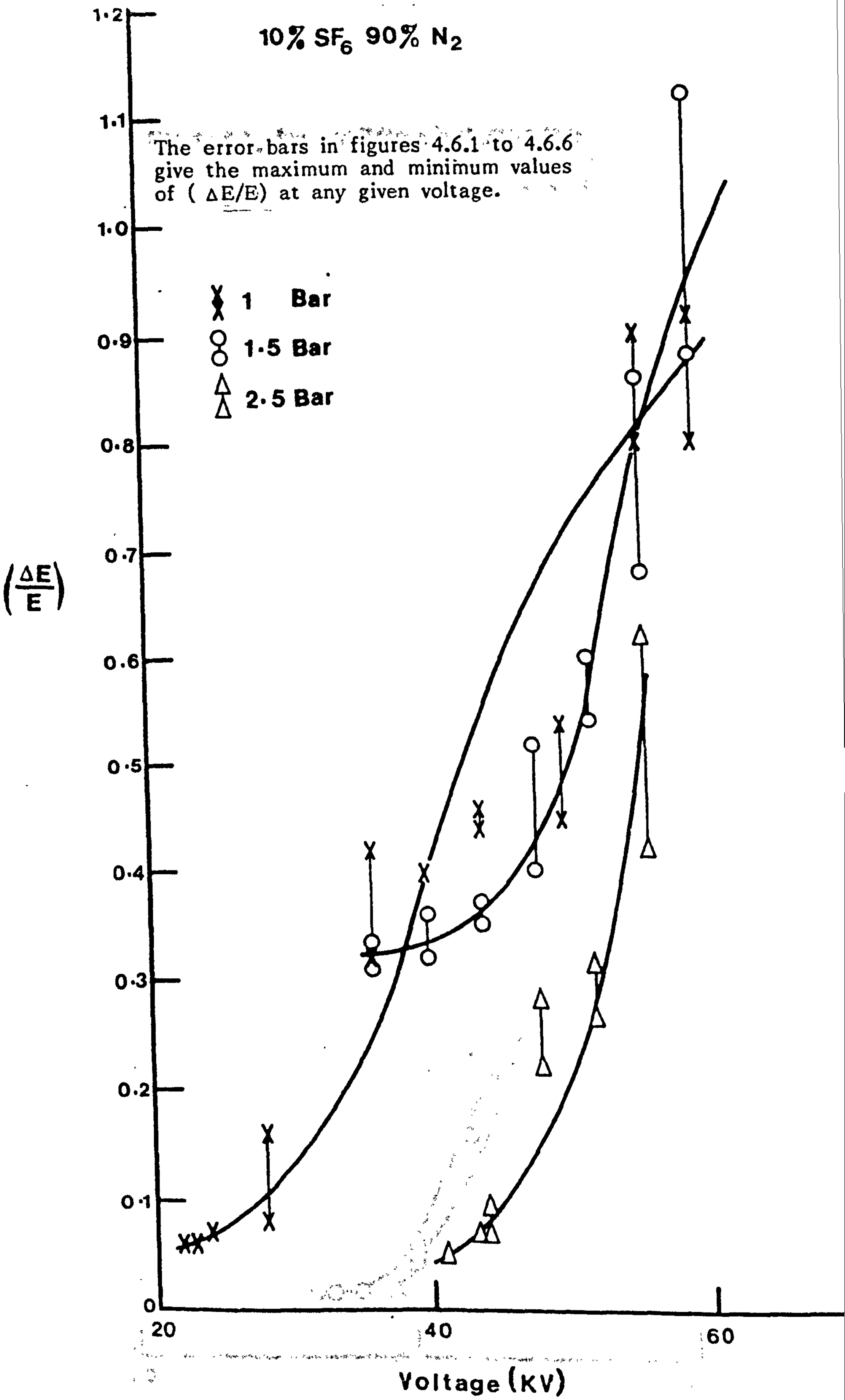

Figure 4.6.1 : The variation of ΔE/E with applied voltage for different pressures in the 10% SF_6 90% N_2 mixture

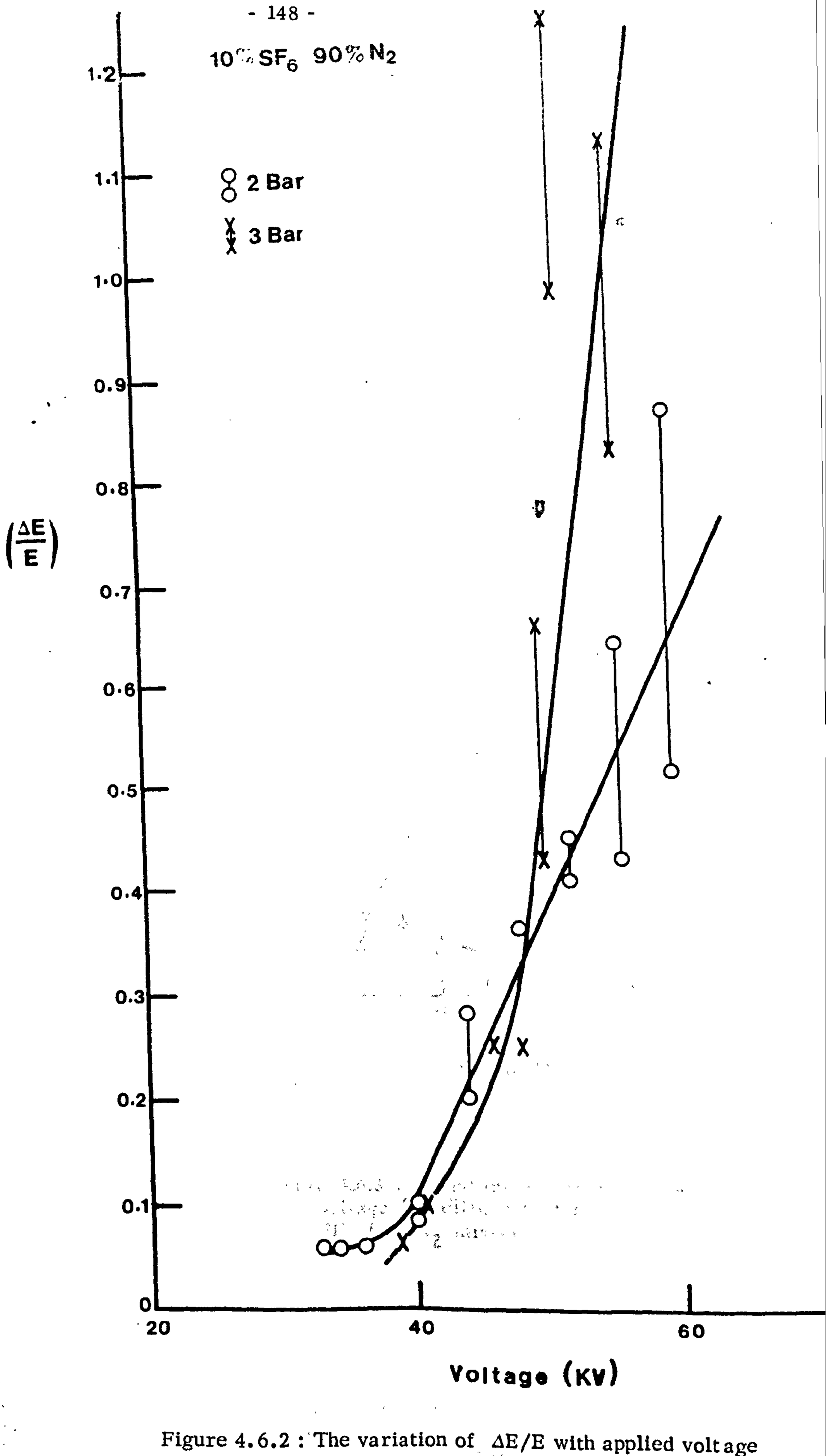

Figure 4.6.2 : The variation of $\Delta E/E$ with applied voltage for different pressures in the 10% SF_6 90% N_2 mixture.

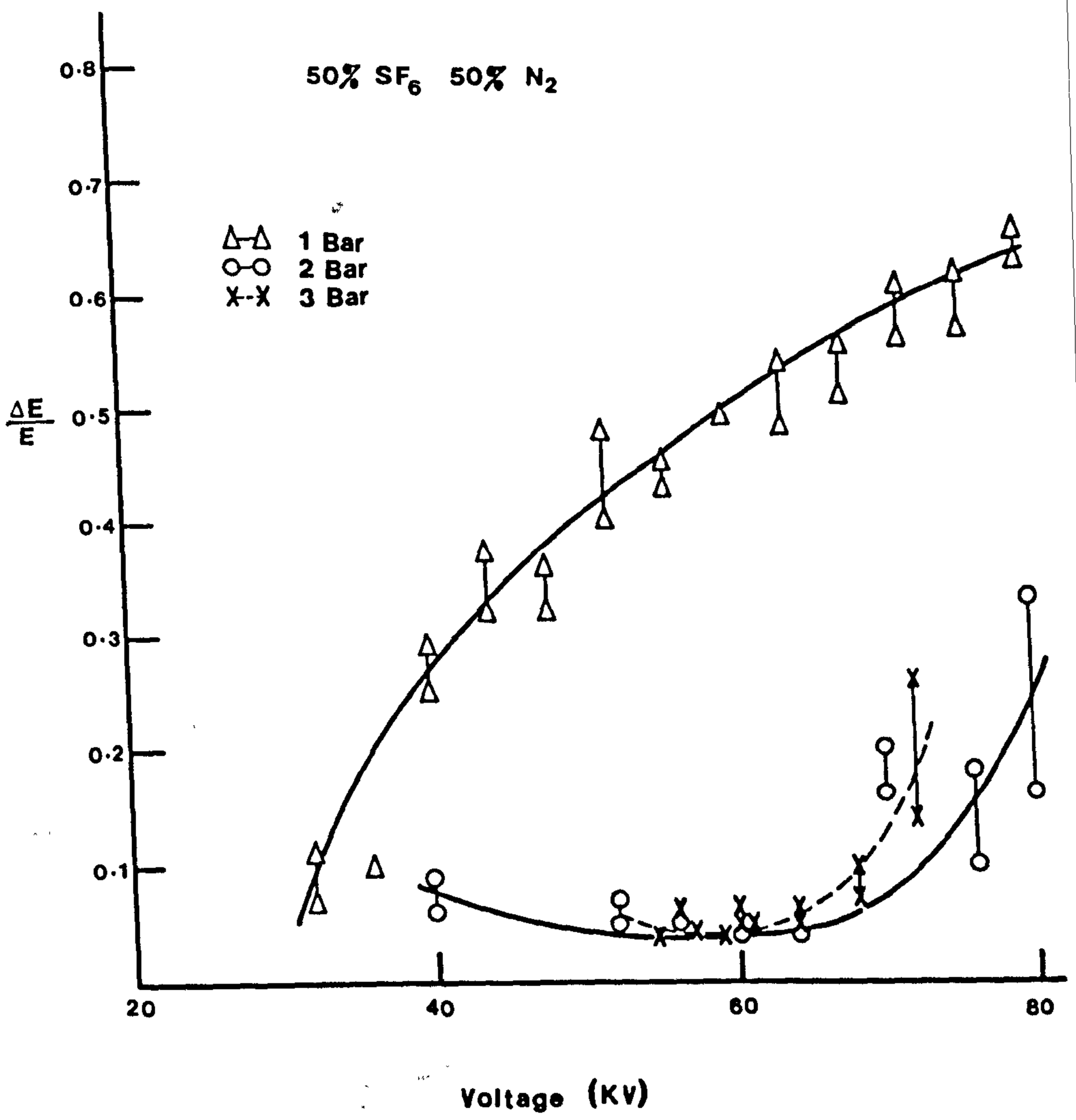

Figure 4.6.3 : Variation of $\Delta E/E$ with applied voltage for different pressures in the 50% SF_6 50% N_2 mixture

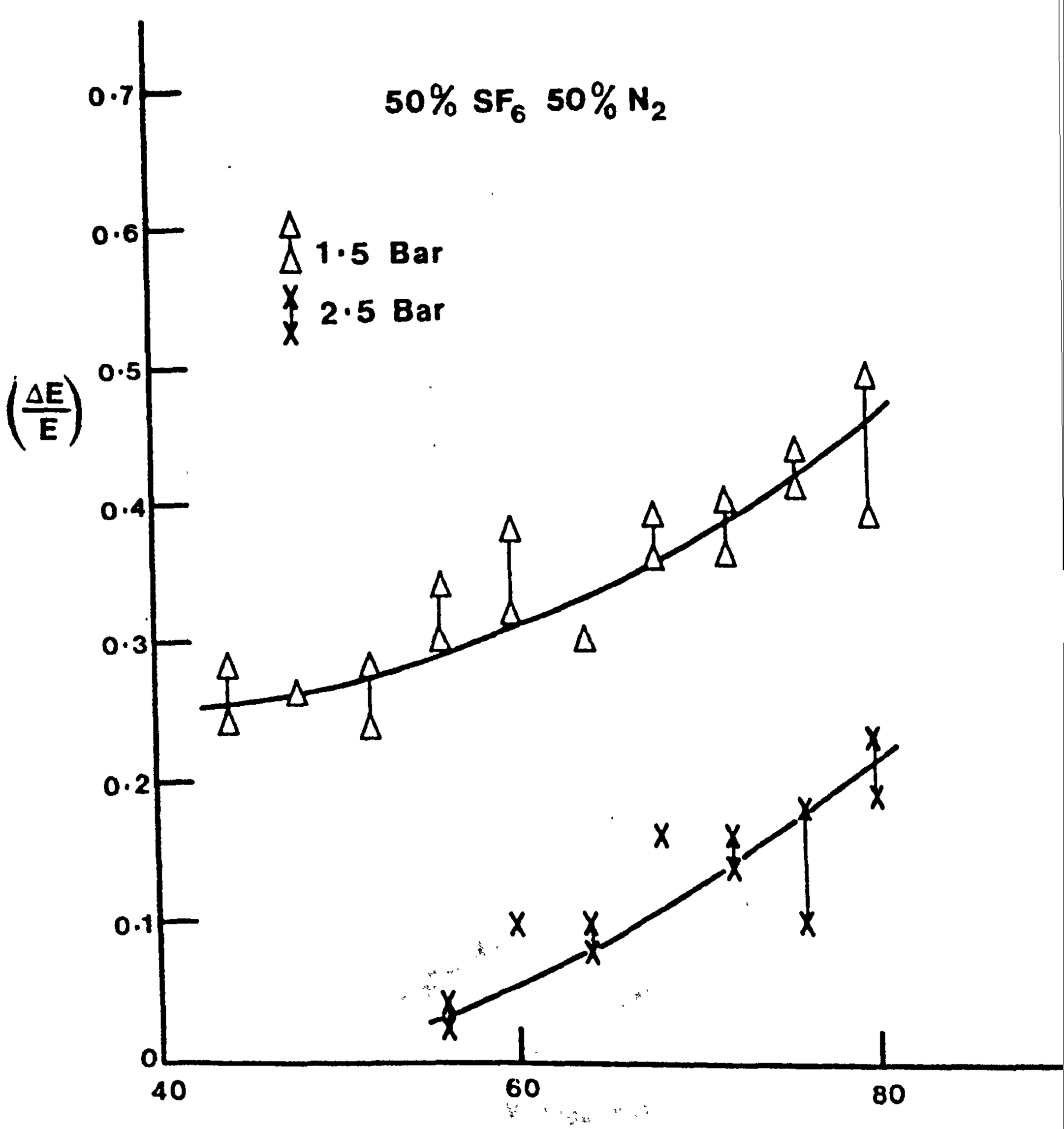

Figure 4.6.4 : Variation of $\Delta E/E$ with applied voltage for different pressures in the 50% SF_6 50% N_2 mixture

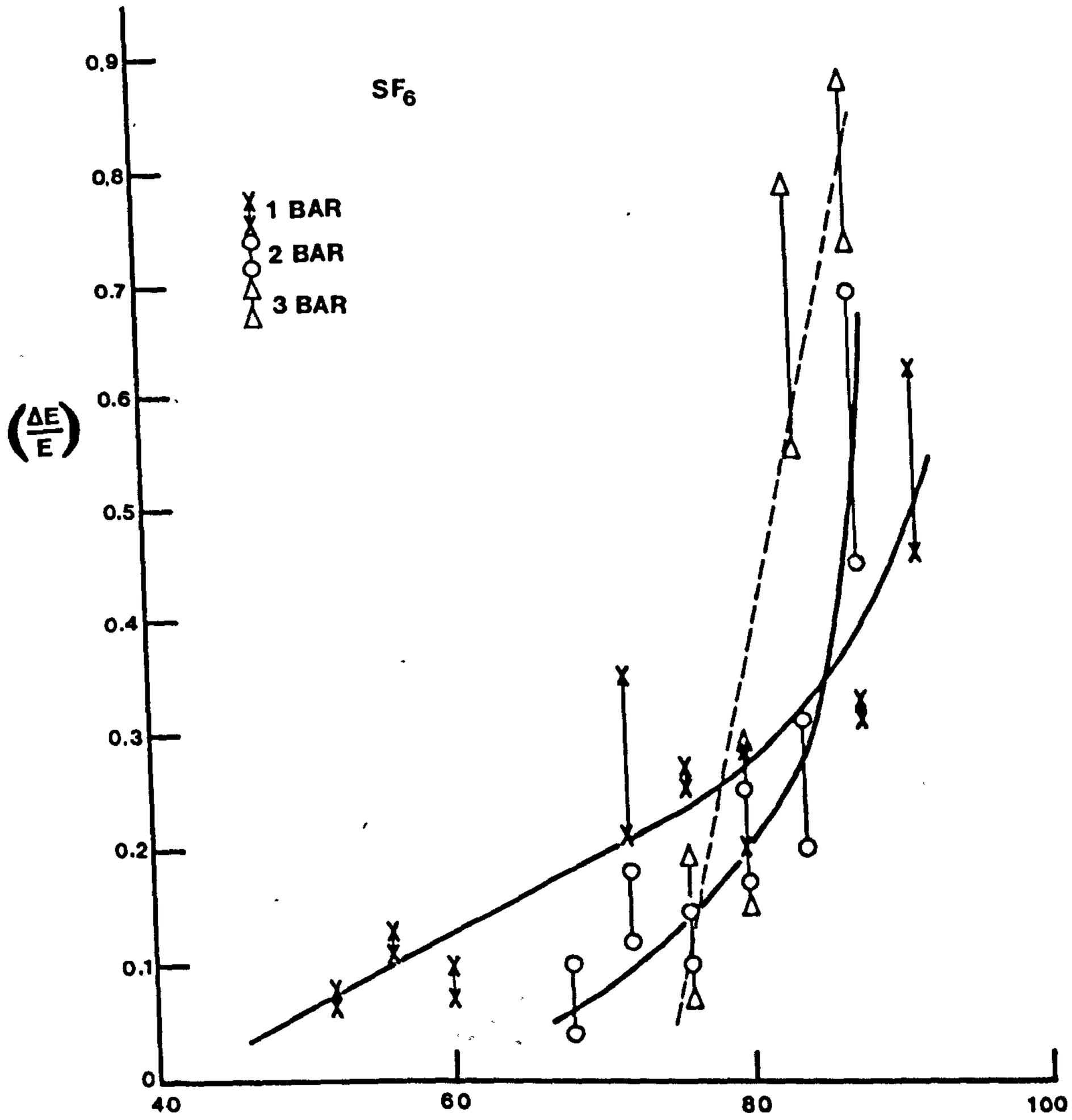

Figure 4.6.5 : Variation of $\Delta E/E$ with applied voltage for different pressures in SF_6

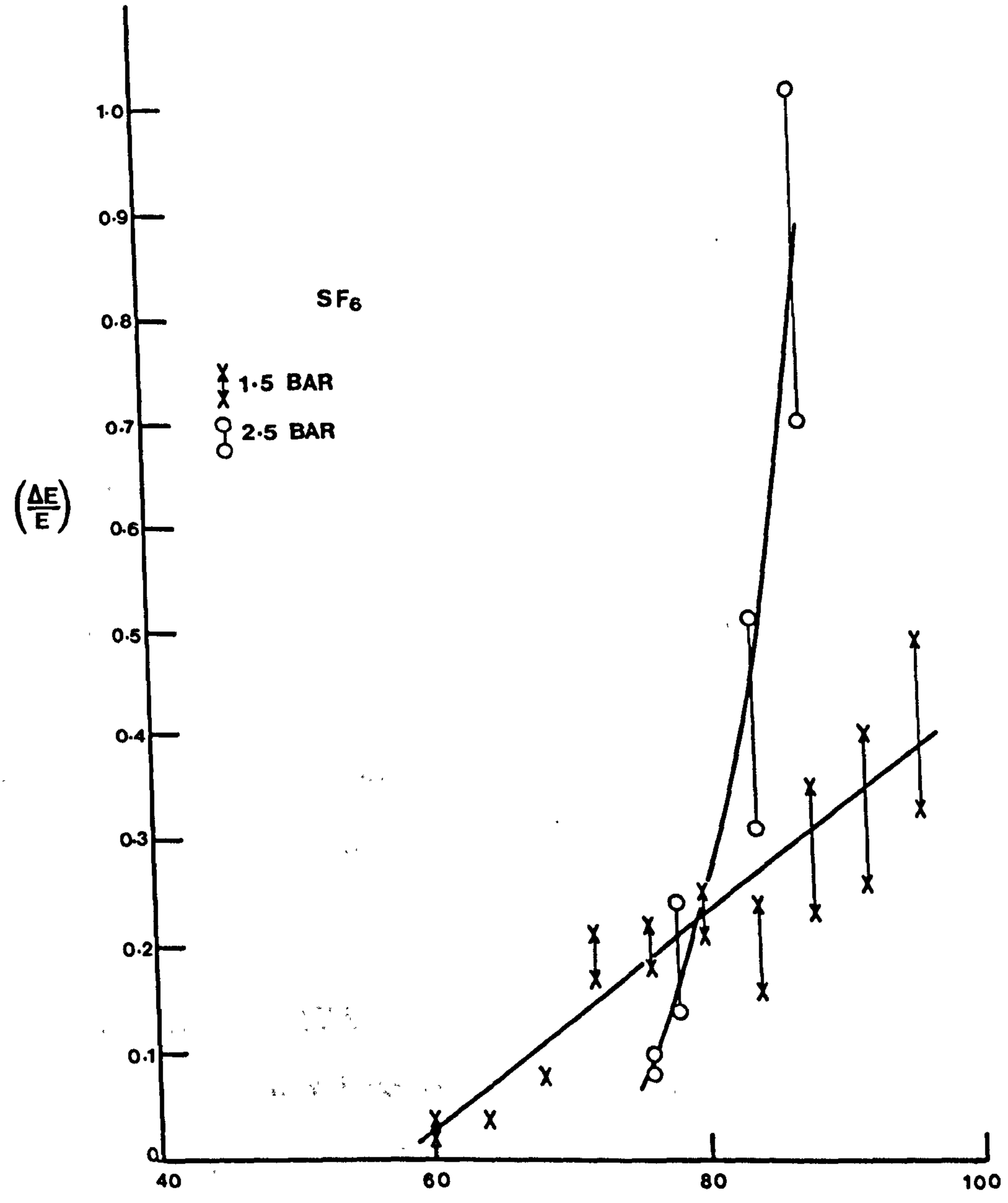

Figure 4.6.6 : Variation of $\Delta E/E$ with applied voltage for different pressures in SF_6

of about 7% below the breakdown value, the mean value of ΔE is 333 mV. In SF_6 at a voltage of 88 kV, 2% below the breakdown voltage the mean value of ΔE is 443.7 mV. Against these two cases is the 50% SF_6 where at 72 kV which is 6.5% below the breakdown voltage the mean value of ΔE is 86 mV. The variation of ($\Delta E/E$) with voltage are depicted in figures 4.6.2, 4.6.3, and 4.6.5 for 10% SF_6, 50% SF_6 and SF_6 respectively.

4.7 VELOCITY MEASUREMENTS

4.7.1 Introduction

The results of velocity measurements are presented in this section. The method employed for these measurements were discussed in Chapter 3, Section 8, a diagram of the measuring system was given in figure 13. Measurements pertaining to the 10% SF_6 and 50% SF_6 cases are given in the following section. Those in SF_6 will not be given, as these were exceedingly difficult to obtain using the present triggering arrangement. Also, those that were obtained are far too complex to decipher to give meaningful results. Thus, they have been omitted.

4.7.2 Variation of Velocity with Voltage

The variation of velocity with voltage is shown in figures 4.7.1 to 4.7.6. Also, a typical photograph of the photomultiplier traces used for determining the velocity of propagation is shown in figure 4.7.7 (a + b). One of the difficulties in this measurement has been to determine the voltage at which the discharge development changes from a streamer type of development to one that has leaders and streamers. Also, once delayed reilluminations are observed, as were seen by Pigini et al (1982), and shown

in Chapter 2, figure 2.11.5, it is not possible to differentiate between a leader tip propagation and a reillumination. As such, in this thesis the velocities determined beyond the reilluminating voltage (V_{Ri}) will not be ascribed to the velocity of the leader tip.

In all the cases considered the streamers propagate with velocities of the order of 10^8 cm sec^{-1}, and the reilluminating velocities are of the order of 10^6 cm sec^{-1}. When the reilluminations start to occur the conditions are optimum for the formation of leaders.

At 1 bar in 10% SF_6 the reilluminations do not develop until the voltage reaches 30% below the breakdown value. At this voltage and above there is prompt light relating to streamers and delayed light pulses indicating reilluminations. In 50% SF_6 reilluminations occur at a voltage 20% below the breakdown voltage. However, in this case the velocity of the fast component is of the order of 10^7 cm sec^{-1}, which may indicate the propagation of the stem.

At 1.5 bar the pattern of discharge development is quite different from that at 1 bar, in 50% SF_6 the reilluminations develop at a very late stage, until 80 kV which is 8% below the breakdown voltage the reilluminations are absent. In the 10% SF_6 case on the other hand, the reilluminations occur at a very early stage. The reilluminations occur at 48 kV which is 45% below the breakdown voltage.

The variation of velocity with voltage at 2 bar and 2.5 bar for 50% SF_6 and 10% SF_6 are depicted in figures 4.7.3 and 4.7.6 respectively. At 2 bar in 50% SF_6 the streamers start off at an average velocity of 1.75×10^8 cm sec^{-1} at 52 kV, which is 8% above the corona initiation voltage.

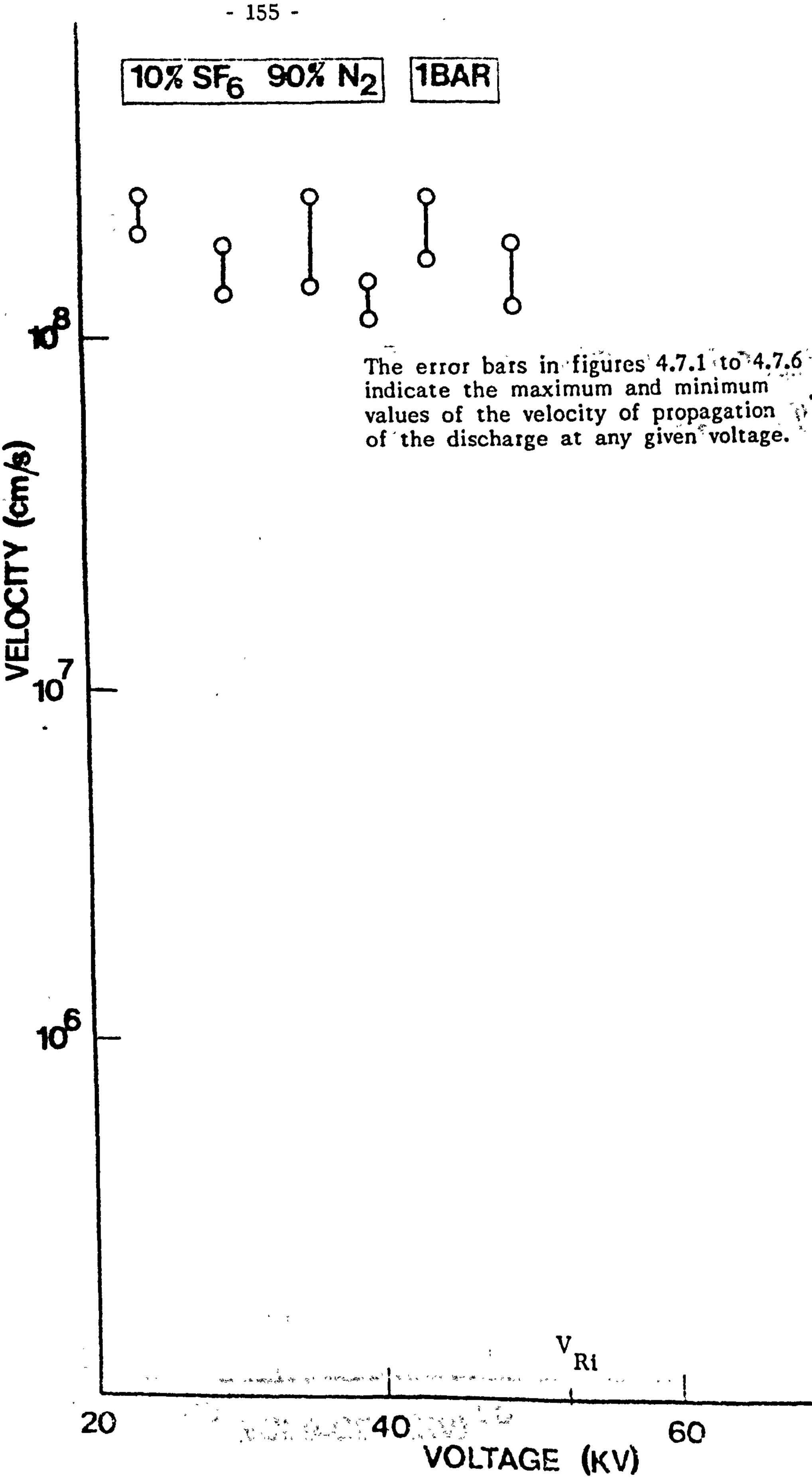

The error bars in figures 4.7.1 to 4.7.6 indicate the maximum and minimum values of the velocity of propagation of the discharge at any given voltage.

Figure 4.7.1 : The variation of velocity with applied voltage in 10% SF_6 90% N_2 at 1 bar. V_{Ri} indicates the onset of reilluminations.

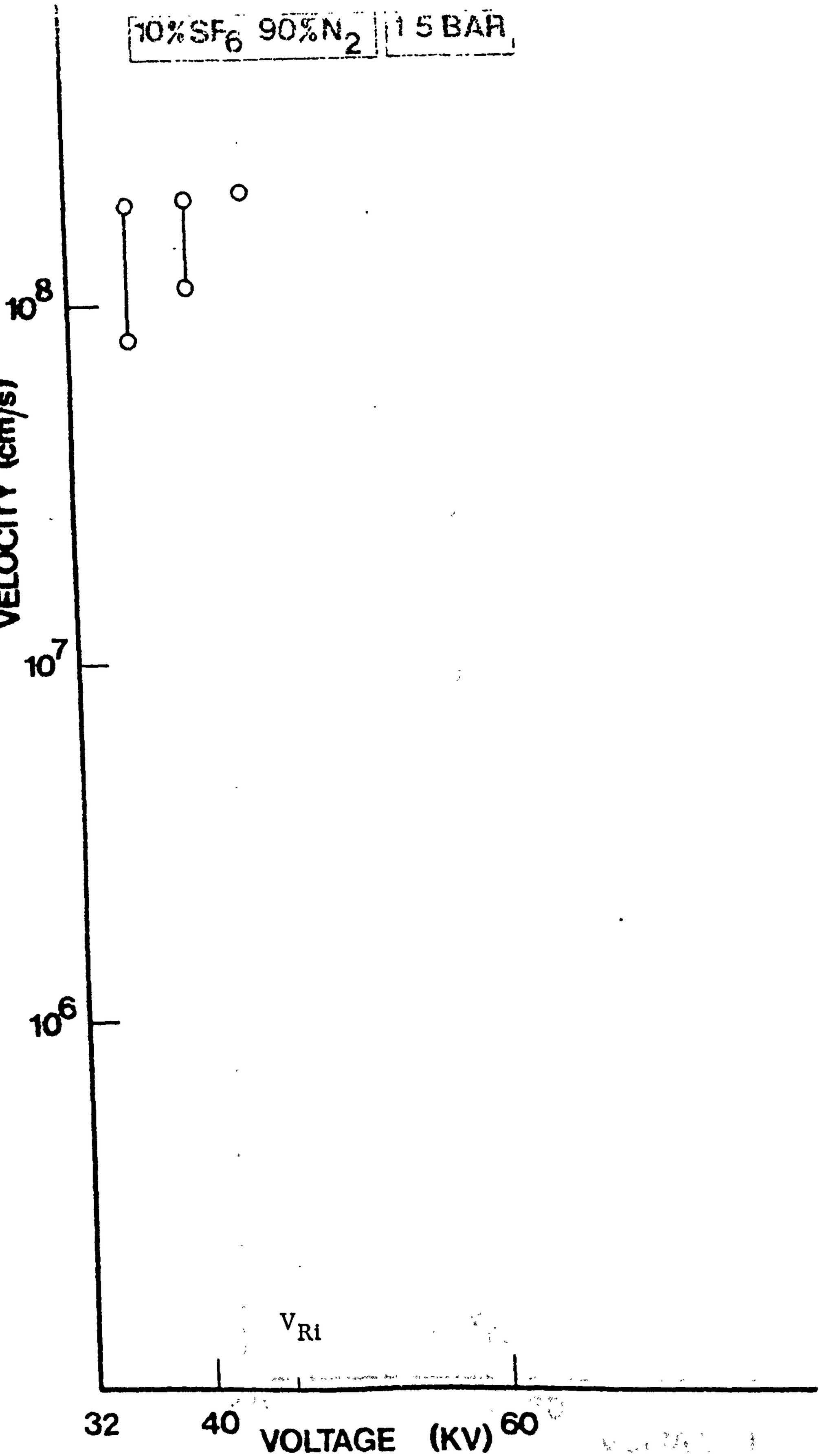

Figure 4.7.2 : The variation of velocity with applied voltage in 10% SF_6 90% N_2 at 1.5 bar. V_{Ri} indicates the onset of reilluminations.

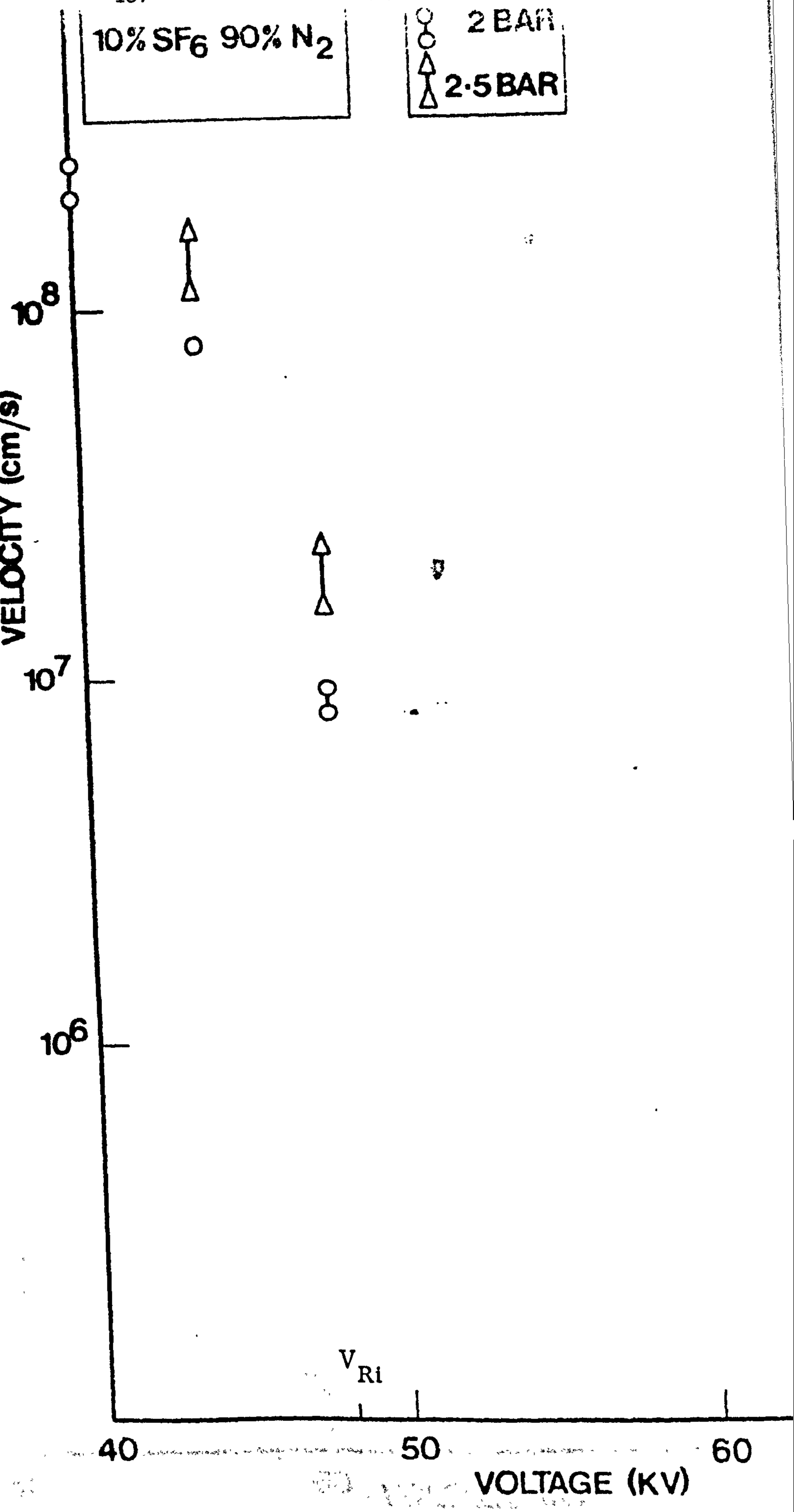

Figure 4.7.3 : The variation of velocity with applied voltage at 2 bar and 2.5 bar in 10% SF_6 90% N_2 V_{Ri} indicates the onset of reilluminations

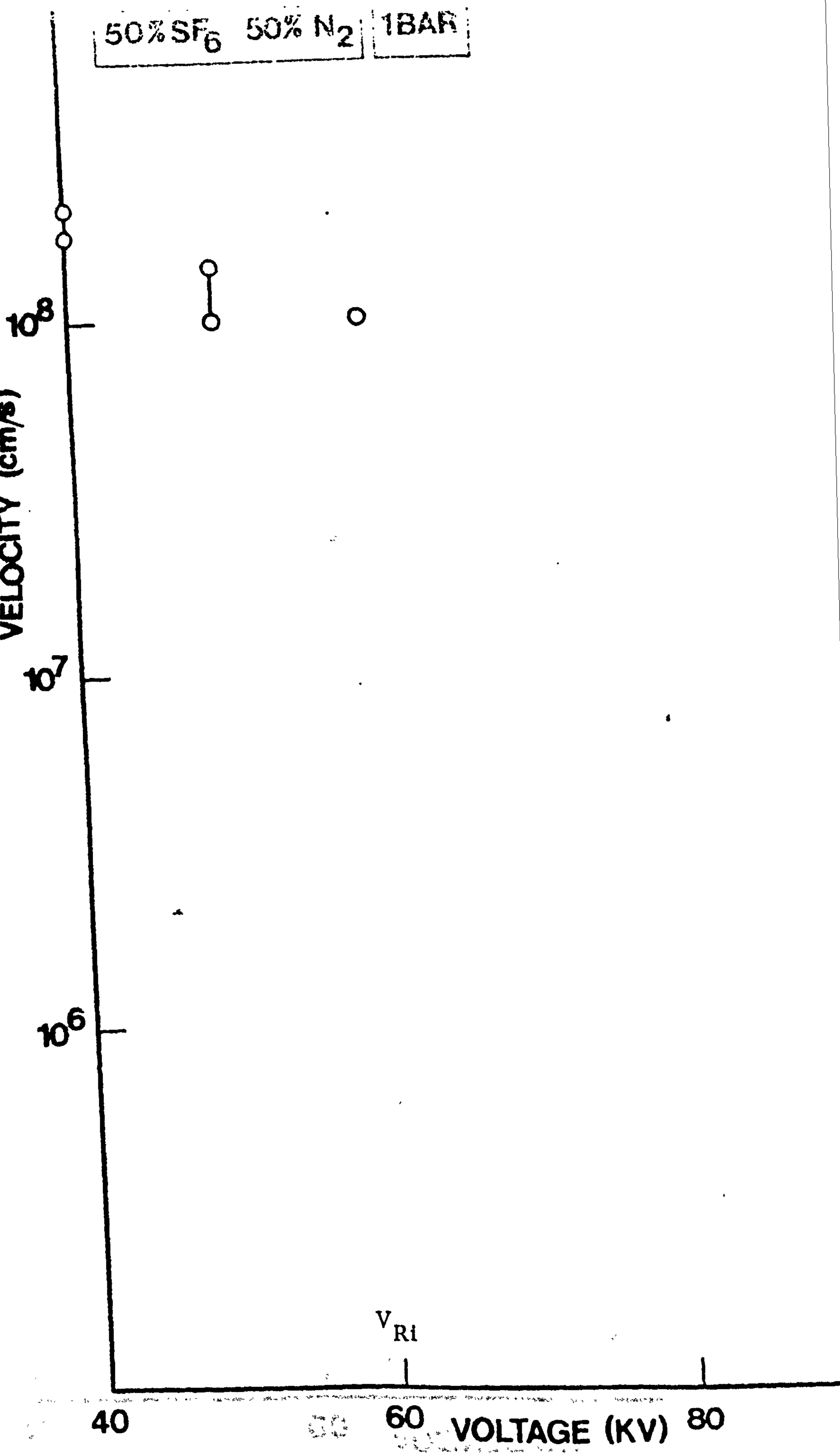

Figure 4.7.4. : The variation of velocity with applied voltage in 50% SF_6 50% N_2 at 1 bar. V_{Ri} indicates the onset of reilluminations

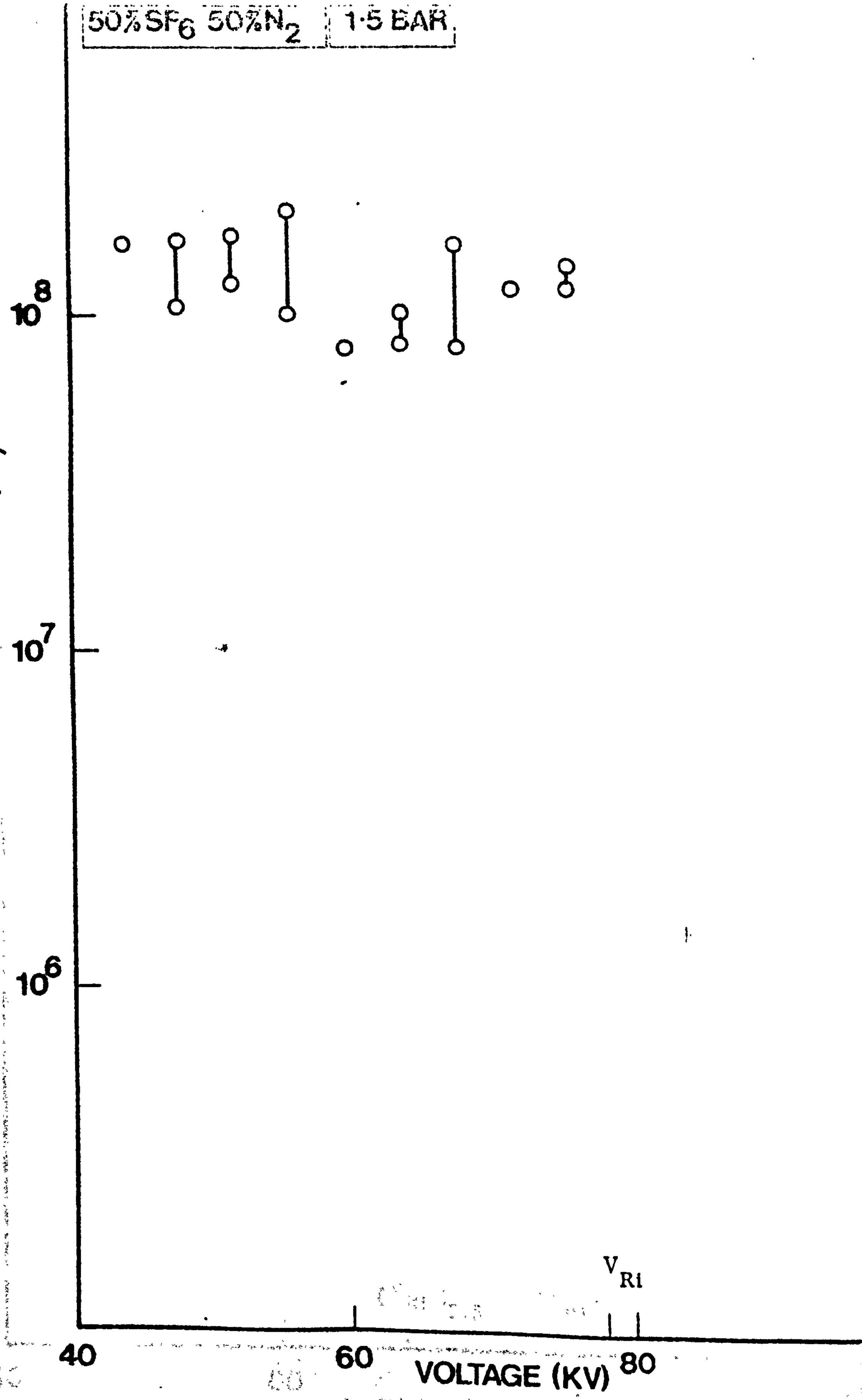

Figure 4.7.5. The variation of velocity with applied voltage in 50% SF_6 50% N_2 at 1.5 bar. V_{Ri} indicates the onset of reilluminations

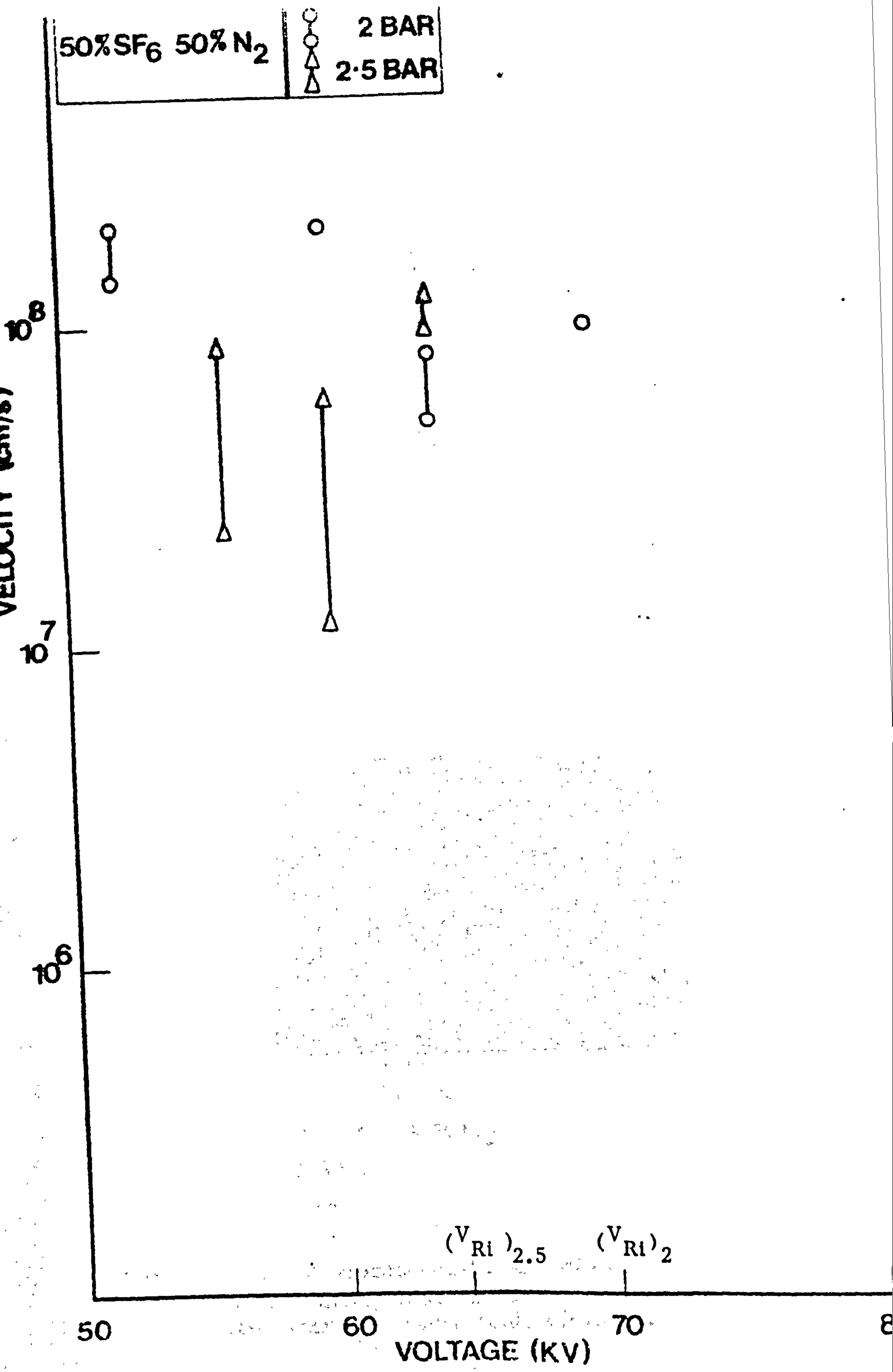

Figure 4.7.6 : The variation of velocity with applied voltage in 50% SF_6 50% N_2 at 2 bar and 2.5 bar. V_{Ri} indicates the onset of reilluminations

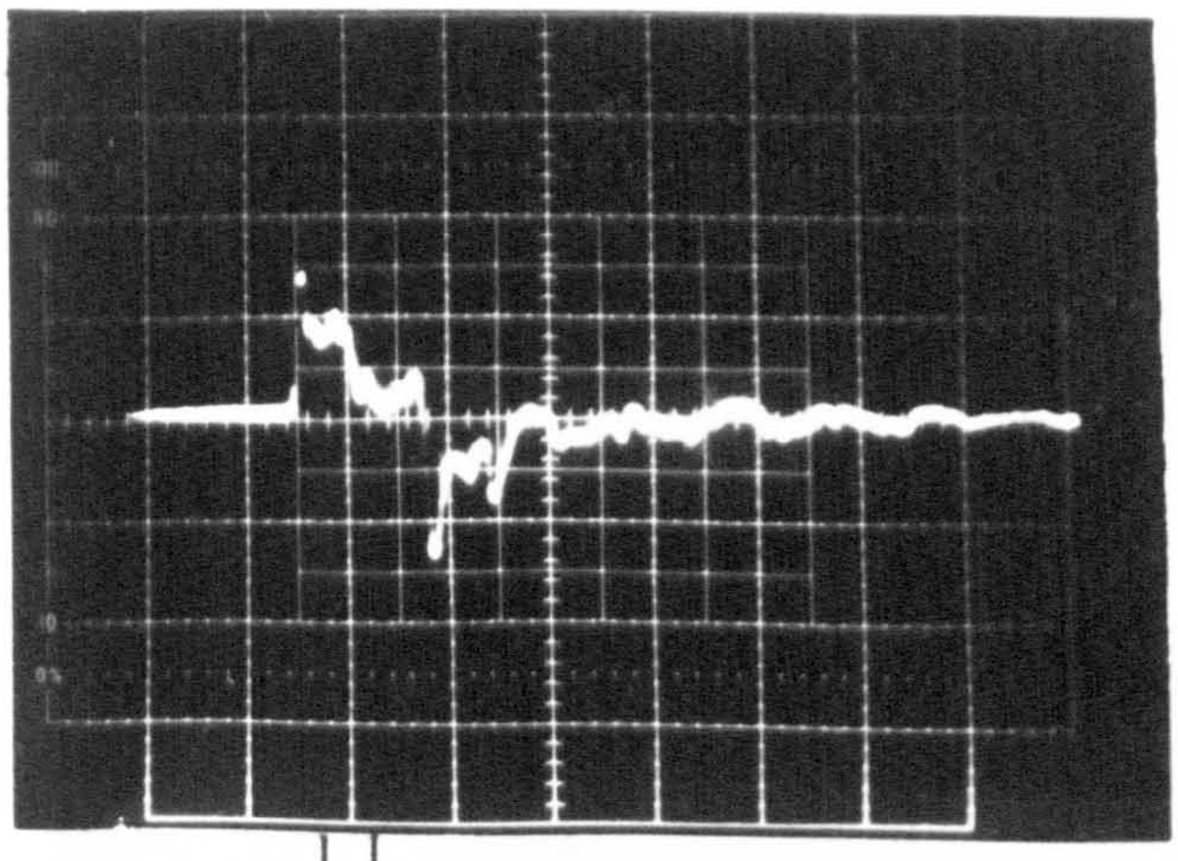

(a)

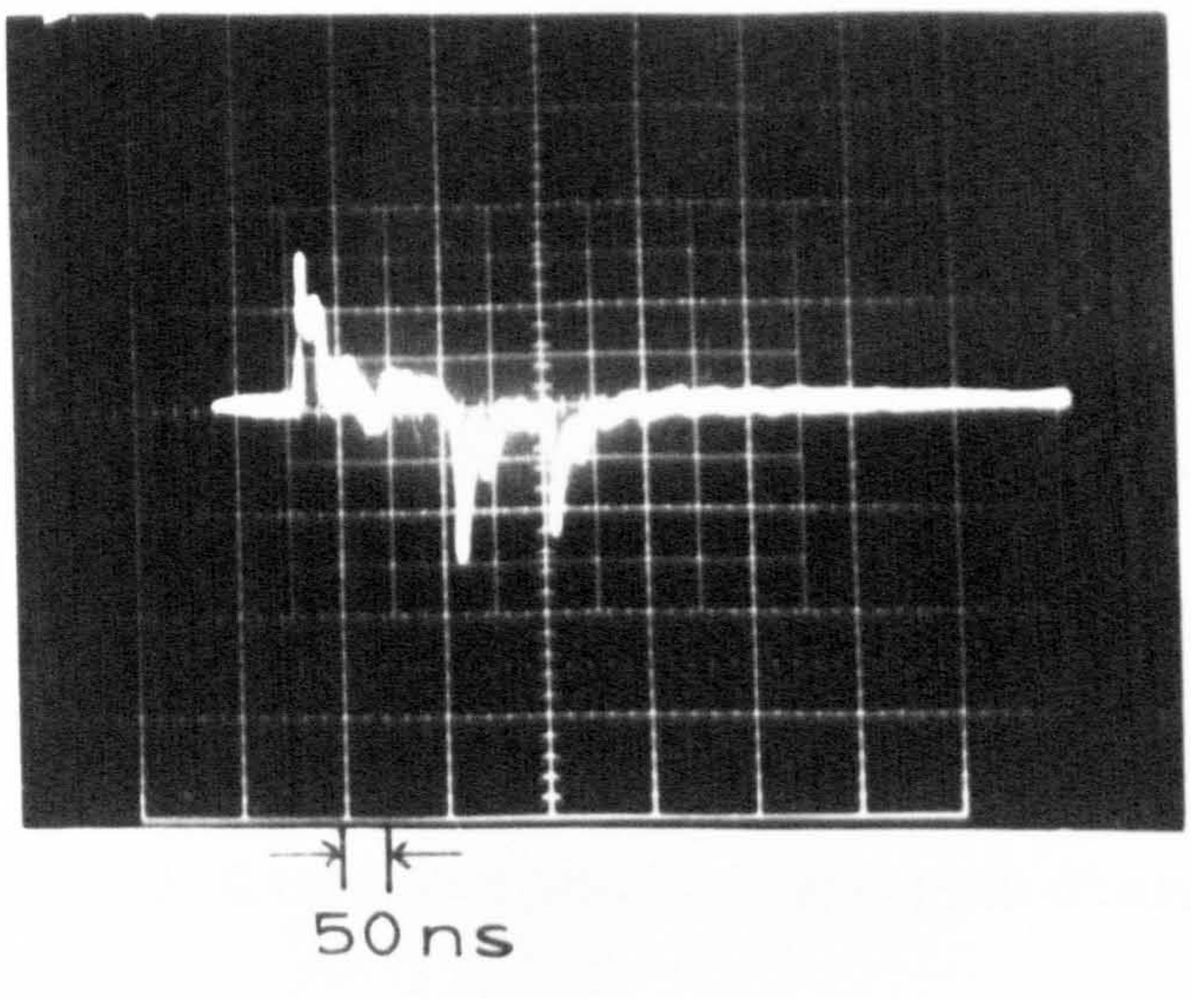

(b)

Fig. 4.7.7 Typical photographs of photomultiplier traces.
(a) Streamer discharge.
(b) Discharge with reilluminations.

At 64 kV the velocity falls to an average value of 6.67×10^7 cm sec^{-1}. Beyond this value of voltage there are reilluminations and thus the conditions for leader formation.

At 2.5 bar, in 10% SF_6, the velocity of propagation falls very quickly from 1.37×10^8 cm sec^{-1} at 44 kV, which is 5% above the corona initiation voltage to 1.9×10^7 cm sec^{-1} at 48 kV. Beyond this voltage at 52 kV there are reilluminations. In 50% SF_6 at this pressure the velocity of propagation at 56 kV is 5.6×10^7 cm sec^{-1}, which is lower than in most of the other cases. The reilluminations occur at 64 kV and beyond. The results at 2.5 bar for 50% SF_6 are given in figure 4.7.3.

4.8 STREAMER CROSSING VOLTAGE

The step change ΔE in the electric field was measured at the centre of the plane electrode for any specified voltage, as described before. The field oscillograms obtained were examined to determine whether the streamers had crossed the gap and reached the plane (cathode). Streamers on arrival at the cathode neutralise the induced charge on the probe and this is indicated on the field probe signal as a decrement in the field signal. Any charge reaching the plane also causes a reduction in the indicated field. Typical oscillograms pertaining to this condition are shown in figure 4.8.1. The voltage at which this effect first takes place is called the onset voltage V_c, for streamer crossing. Figure 4.8.2 shows the variation of streamer crossing voltage with pressure for the three gas compositions considered.

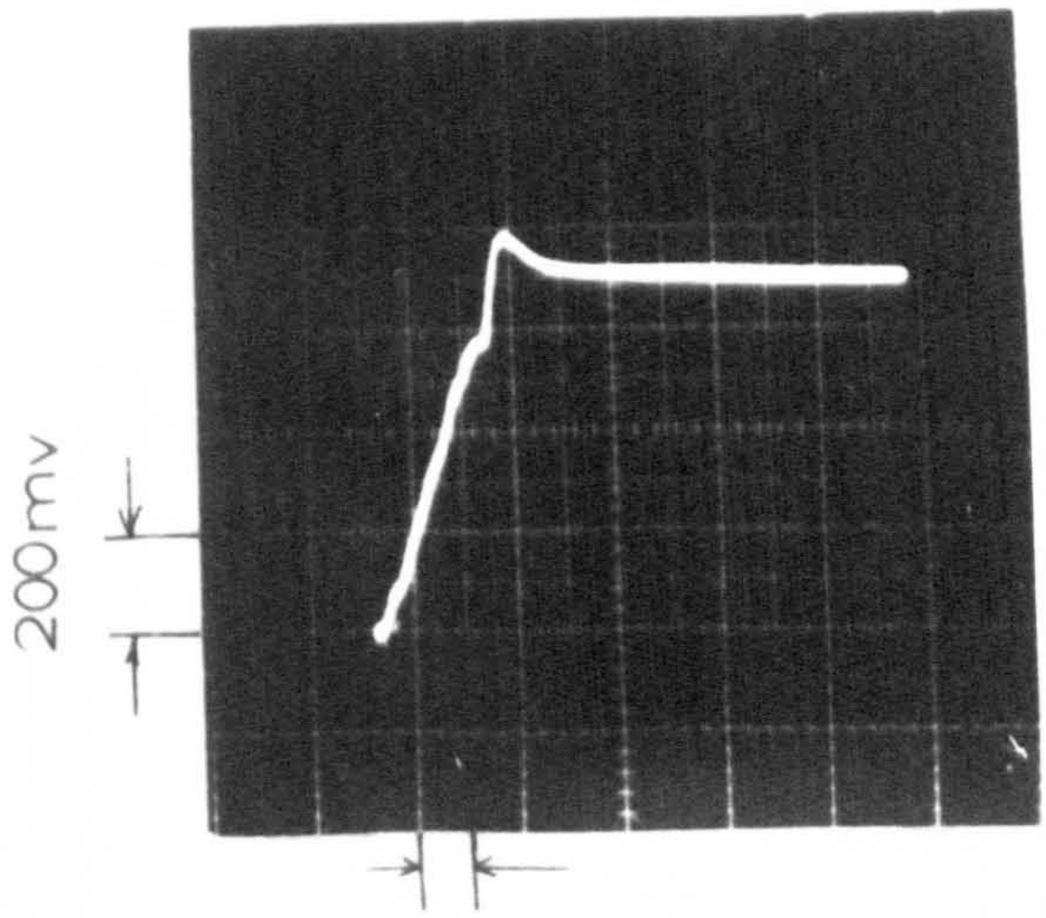

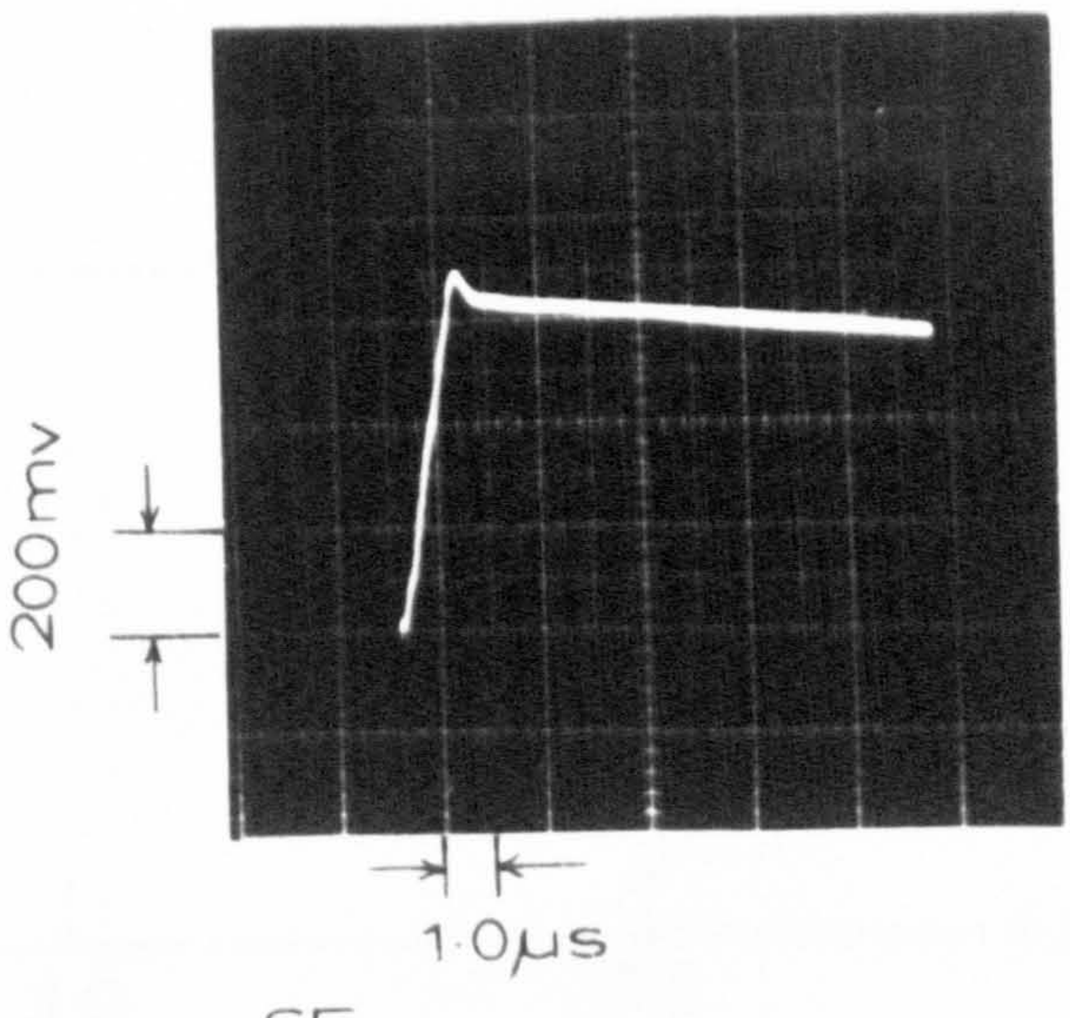

Fig. 4.8.1. Typical streamer crossing field probe signals.

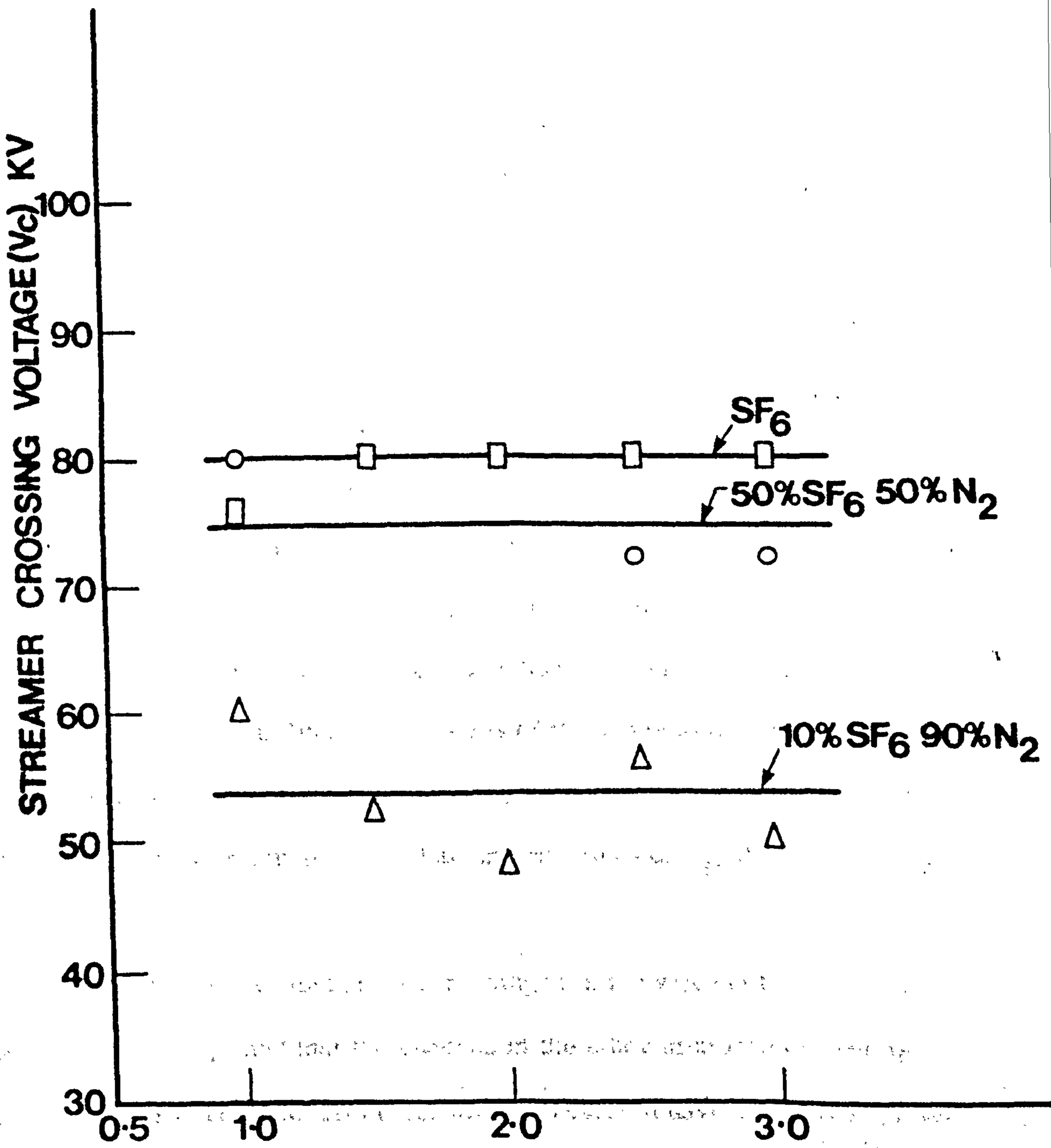

Figure 4.8.2 : The onset for streamer crossing voltage, V_c as a function of pressure

CHAPTER 5

DISCUSSION, CONCLUSIONS and SUGGESTIONS FOR FUTURE WORK

5.1 INTRODUCTION

The results presented in Chapter 4 will be discussed, with particular reference to the critical pressure, and the electric field within the discharge channel. An attempt will be made to determine the critical pressure using an extrapolation technique. The results are compared with the work of other authors. It will be shown that the cloud model is inoperative, at least under impulse voltages, such as used for the work in this thesis. An attempt has been made to establish the different regimes of operation with regard to leader formation both prior to and after streamers cross the gap. This will be done with particular emphasis on the d/r ratio and the field variations with increment in voltage. It will be shown that there is no simple relationship linking the radius of the anode to the critical pressure. An attempt will be made to explain the large discrepancy in SF_6 between the calculated, and the experimentally determined values of V_i, the corona onset voltage.

It will be shown that there are changes in the values of the internal leader fields in SF_6, and that the changes in the other mixtures are not as pronounced. The electric field calculations presented have been made within definite bounds of experimental conditions using an electrostatic model.

5.2 CRITICAL PRESSURE

The theoretical values of V_i for SF_6 using equation (4.3) in Chapter 4 have been shown to be in reasonable agreement with experimental

values in d.c. (Farish et al, 1977, Hazel et al, 1976). The agreement in mixtures of SF_6 with N_2 is much better (Farish et al, 1977). When one considers the present results it is clear that particularly for the SF_6 case the impulse determination of corona onset voltage and V_i (theory) is exceedingly poor. The initiation rate affects the issue in a strong way, this is confirmed by the fact that at low pressure $V_i(-)$ is close to V_i (theory). This is also confirmed by the fact that there is an improvement with the longer impulse wavetail. In general, one could suggest three possible reasons for this lack of agreement.

(a) The detection system used has insufficient sensitivity to detect corona onset. In the present results it is considered that the photomultiplier system should adequately sense any multiple avalanche ionization activity necessary for any corona/streamer to exist.

(b) There might be no initial electron available to start a primary avalanche (Anis and Srivastava, 1981).

(c) The primary avalanche even if formed may not be able to form a streamer or glow cloud since these both imply the need for photo induced secondary initiators which may also be in short supply. One could consider this another aspect of the primary initiation problem, but in principle, it is different from (b).

At the present time it is not possible to distinguish between (b) and (c). Anis and Srivastava (1982) have shown for SF_6 that by determining the corona onset low probability thresholds closer agreement is achieved between theory and experiment but in all cases there is lack of agreement with

with impulse voltages apparently due to lack of initiators of one sort or another. When SF_6 is mixed with N_2 the problem is less severe, as shown in figures 4.1,4.2 and 4.3 Chapter 4. The possible reason for this is that whilst the γ source may produce much the same ionization rate in the various gas compositions at the same pressures, the ion-ion recombination rate may differ markedly. Thus, one might suppose that negative SF_6 ions do not recombine so readily with nitrogen positive ions so causing higher negative ion densities to be present in the mixtures. Thus, if the initial electrons are formed by detachment from the negative ions, the initiation rate will be higher in nitrogen mixtures. In all cases agreement is better at higher pressures though in this case surface roughness effects may start to play a part.

In the present experiments the probe signals were observed to be small at onset even when $V_i \gtrsim 2\ V_i$ (theory) which occurs at low pressures. This observation has important consequences in two respects.

(i) It could be caused by a lack of suitable photon induced secondary initiators so preventing the corona cloud from growing to the expected radius (Chatterton, 1979).

(ii) Another explanation could be that the potential at the edge of the corona cloud is not close to the electrode potential.

In either case this suggests that the cloud model is not operative in the present experiment, even at the lowest pressure used. This reinforces the need to use the photomultiplier system to determine the corona onset voltage.

The next question to be raised is how can p_c be defined in the impulse case and should it necessarily have the same value as that

determined with d.c. Figure 5.2.1 (a) and (b) shows the situation for d.c. and impulse voltage application. In figure 5.2.1 (a) the d.c. corona onset is close to the theory and p_{cl} is clearly defined as the pressure beyond which direct breakdowns without prior corona occur. The agreement between theory and experiment (assuming the streamer onset model is correct and the drift coefficients known) depends even in the d.c. case on the number of secondary photo induced initiators. Thus, the value of k in equation (4.1) Chapter 4, and so the triggering avalanche size may need to change from one experiment to another. This factor is illustrated in figure 5.2.1 (a) by the definition of p_c the ultimate critical pressure as being the intersection of the extrapolated V_B, p curve and the V_i (theory) curve. Thus, even in d.c. p_c may be greater than the observed value p_{cl}, due to initiation linked effects. In figure 5.2.1 (b) for the impulse case the two critical pressures p_{cl} and p_c are defined again, p_{cl} is the highest pressure at which corona prior to breakdown is actually observed.

This pressure is expected to depend on the initiation rates, voltage pulse length and the exact statistics of breakdown and corona initiation . The fundamental limit p_c which could occur if sufficient initiators were available and which perhaps should correspond to p_c for d.c. with the same number of initiators cannot be easily determined. The approach adopted in this work is once again to linearly extrapolate the V_B curve for pressures below p_{cl} to intersect the V_i(theory) curve. In order to allow for the scatter of breakdown voltages a band of values for p_c naturally results as indicated. In each case $p_c \pm \Delta p_c$ was determined from the present results. The values of p_{cl} and p_c obtained from this approach are given in table 1. When

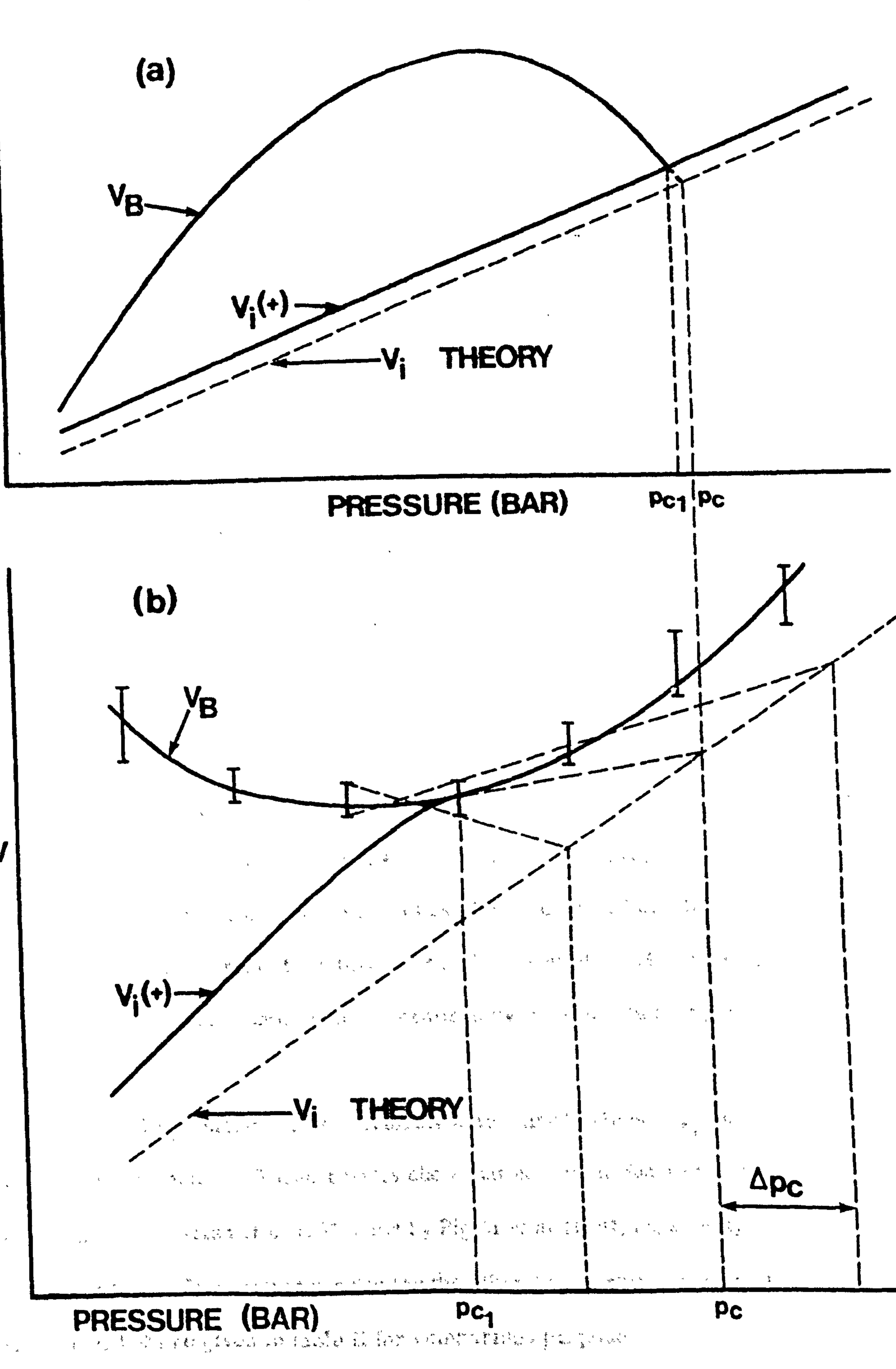

Figure 5.2.1 : Schematic representation and method of determining the critical pressures p_{c1} and p_c for

(a) d.c. voltages
(b) Impulse voltages

as in the mixture case V_i (theory) is close to V_i $p_{cl} \simeq p_c$ but for SF_6 with the 1/50 μs waveshape there is considerable difference.

Composition	1/50 μs		1/10,000 μs	
	p_{cl} (bar)	p_c (bar)	p_{cl} (bar)	p_c (bar)
SF_6	4 ± 0.5	6.25 ± 0.75	5 ± 0.5	6 ± 1.0
50% SF_6 50% N_2	4 ± 0.5	6 ± 1.0	5 ± 0.5	5.5 ± 0.5
10% SF_6 90% N_2	5 ± 0.5	5.5 ± 0.5	5 ± 0.5	5 ± 0.5

Table 1 : Values of p_{cl} and p_c determined from V_B and V_i curves

It may be seen that the SF_6 values for p_c are close to the values recently determined by Anis and Srivastava (1982) using the low probability onset determination techniques. Moreover, as has been suggested previously, p_c is not a strong function of mixture ratio. The present results show no measurable differences between p_c determined by the two different pulse shapes.

For SF_6 a summary of previously determined values of p_c is shown in figure 5.2.2 . These results show that no simple function such as proposed by Farish et al (1977) and by Pigini et al (1982) apparently links r with p_c. The earlier results for the other two mixtures are not so extensive, but are given in table II for comparison purposes.

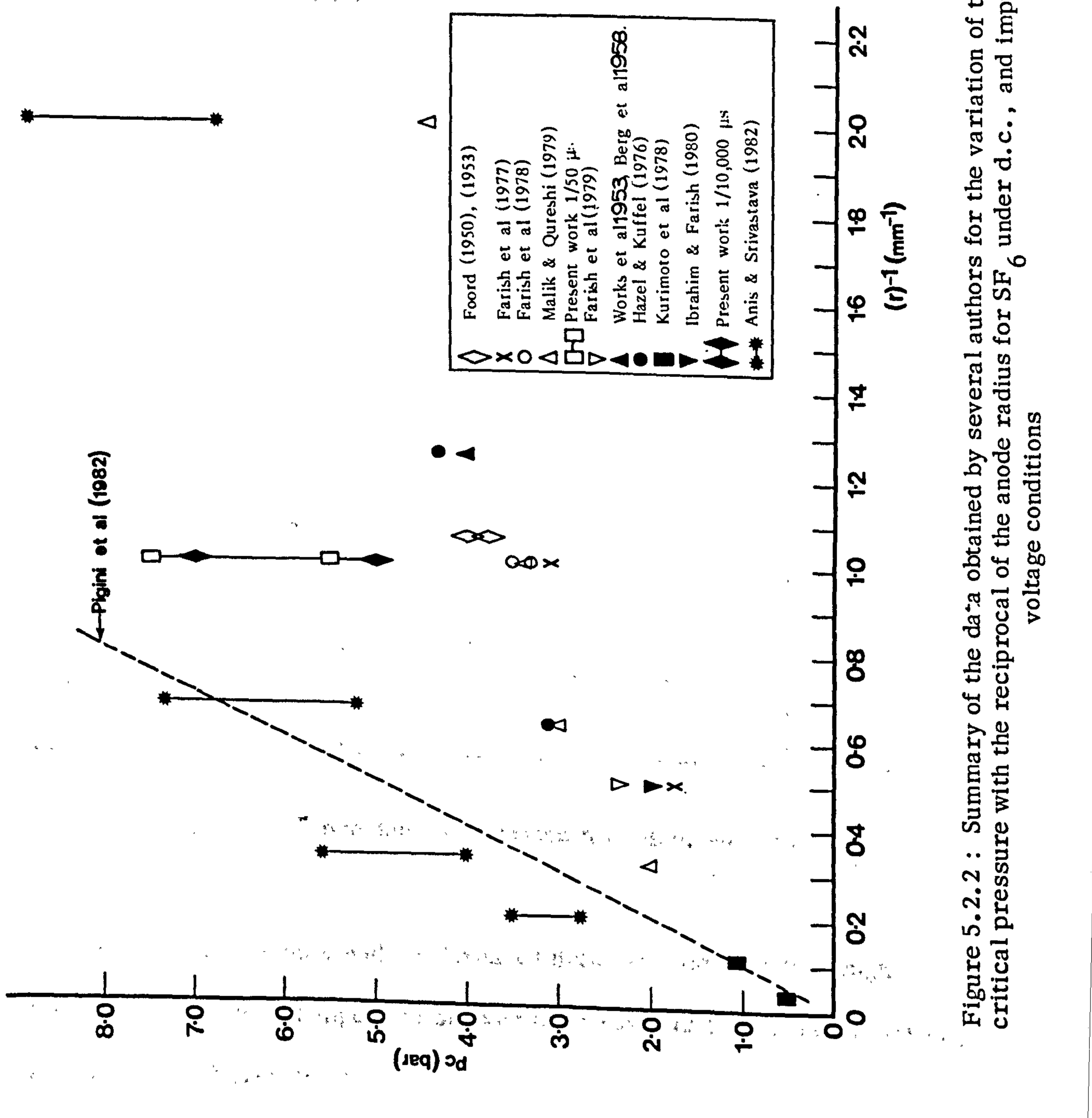

Figure 5.2.2 : Summary of the data obtained by several authors for the variation of the critical pressure with the reciprocal of the anode radius for SF_6 under d.c., a.c. and impulse voltage conditions

Authors	mixtures	voltage type	d/r	p_c (bar)	r (mm)
Farish et al (1977)	10% SF_6 90% N_2	d.c.	10	3.22	1.0
Farish et al (1978)	50% SF_6 50% N_2	d.c.	10	3.5	1.0
Farish et al (1979)	50% SF_6 50% N_2	d.c.	10	2.20	2.0
Farish et al (1979)	10% SF_6 90% N_2	d.c.	10	2.26	2.0
Foord (1950, 1953)	25% SF_6 75% N_2	d.c.	10.64	5.10	0.94
"	40% SF_6 60% N_2	d.c.	10.64	5.10	0.94
"	50% SF_6 50% N_2	d.c.	10.64	5.10	0.94
Nelson et al (1982)	50% SF_6 50% N_2	impulse 0.8 μs/ several ms	15	4.86	1.0
Nelson et al (1982)	50% SF_6 50% N_2	"	30	10.0	0.5

Table II : Summary of previous p_c obtained for mixtures of SF_6/N_2

These results again show wide differences between experiments though the present data would appear to support the results of Foord (1950), (1953), and Nelson et al (1982).

Earlier explanations of p_c (Chatterton, 1979) and Farish et al (1977) were linked to corona cloud models. However, work using photography (Farish et al, 1978, 1979) and the optical multichannel analyser measurements of Nelson et al (1982) have shown that the predischarge does

not have the correct shape to be explained by the cloud model. The present results confirm this in a number of ways :

Firstly, measurements of discharge extension as a function of voltage using the dual photomultiplier system, figure 11, Chapter 3, have shown that the discharge exceeds any prediction based on the cloud model (Chatterton, 1979). The figures 4.5.1 to 4.5.6. Chapter 4 show the discharge extension as a function of applied voltage for all three cases considered in the present work. When these curves are extrapolated to the breakdown voltage, the maximum discharge extension ℓ_{is} can be determined. Figure 5.2.3 shows such estimated values of ℓ_{is} as a function of pressure for all the gas compositions. The figure compares these results with the predictions of the cloud model (p_c = 6 bar : dotted curve) and so clearly confirms the expected lack of agreement.

Secondly, the cloud model cannot explain the field jumps that were observed using the field probe.

The only other candidate for explanation (Voss, 1979, Farish et al, 1978, Pigini, et al 1982) of the predischarge pattern in long SF_6/N_2 gaps invokes processes common to long air gap studies (Gallimberti, 1979). The central features to be considered are the relative possibilities of streamer formation, streamer crossing, leader formation and the occurrence of the so called final jump. As far as the streamers are concerned, the important dividing line in any geometry is the field distribution necessary to allow streamers to form and then proceed across the gap to reach the cathode. Streamer onset is normally calculated using equation (4.3), Chapter 4. The extent streamers propagate is not easy to estimate. One

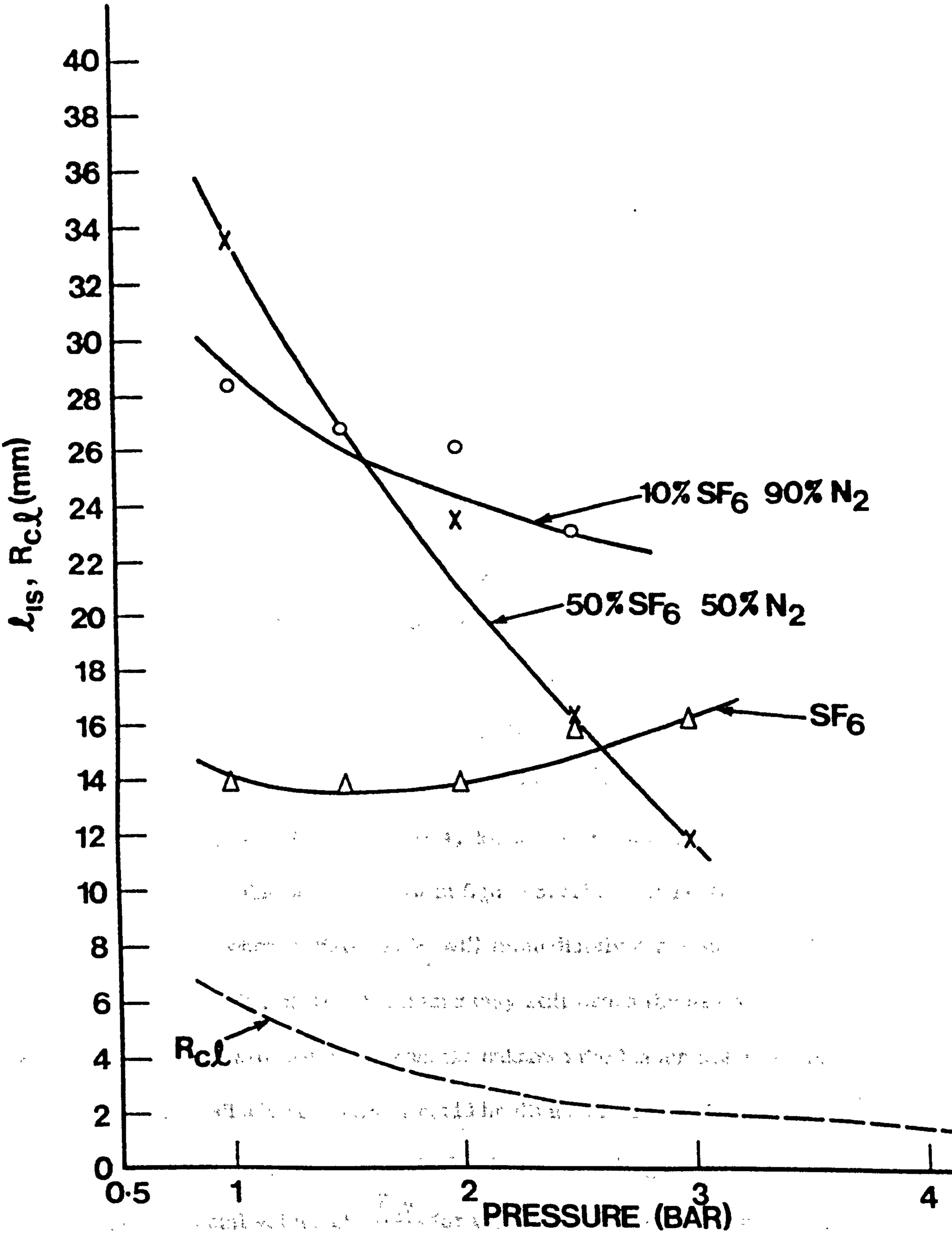

Figure 5.2.3 : Plots of the instability length l_{is} and the predicted maximum cloud radius R_{cl} as a function of pressure for the various gas compositions

could consider that the field at the cathode would be crucial since this would influence directly the effective size of streamers arriving and so directly the size of any charge injected back from the cathode. An alternative approach which could be justified since streamers do not appear to stop instantaneously even in zero field is to say that the average field in the intergap space is the deciding factor of ability of a streamer to penetrate and thus stimulate secondary processes. The average field to pressure ratio is considered to be the dominant quantity, in this discussion. The average field to pressure ratio $\frac{E_{av}}{p}$ necessary for streamer penetration has been estimated for SF_6 by Voss (1979), and Farish (1978). Figure 5.2.4 shows these results together with those estimated in the present work from the leader field determinations. If these results are correct, then it becomes clear immediately how the geometry of point plane gap can affect the type of predischarge activity present. The average field at corona onset can be calculated from equation (4.1), Chapter 4, for a variety of d/r and the results of such a calculation are shown in figure 5.2.5. It is clear that for $d/r < 5$ streamers when initiated at V_i will immediately cross the gap. At a somewhat higher value of d/r streamers may still cross the gap before a leader forms. This will depend on another unknown the leader onset voltage V_L. Thus, the predischarge activity could be divided into two simple regimes :

(1) $d/r < X_1$ (X_1 depends on the leader onset voltage and the experimental values of $\frac{E_{av}}{p}$ for which streamers cross the interspace and start secondary processes prior to leader/ secondary streamer formation (Marode, 1975(a)).

(2) $d/r > X_1$ for which leaders must form prior to any bridging of the gap by streamers.

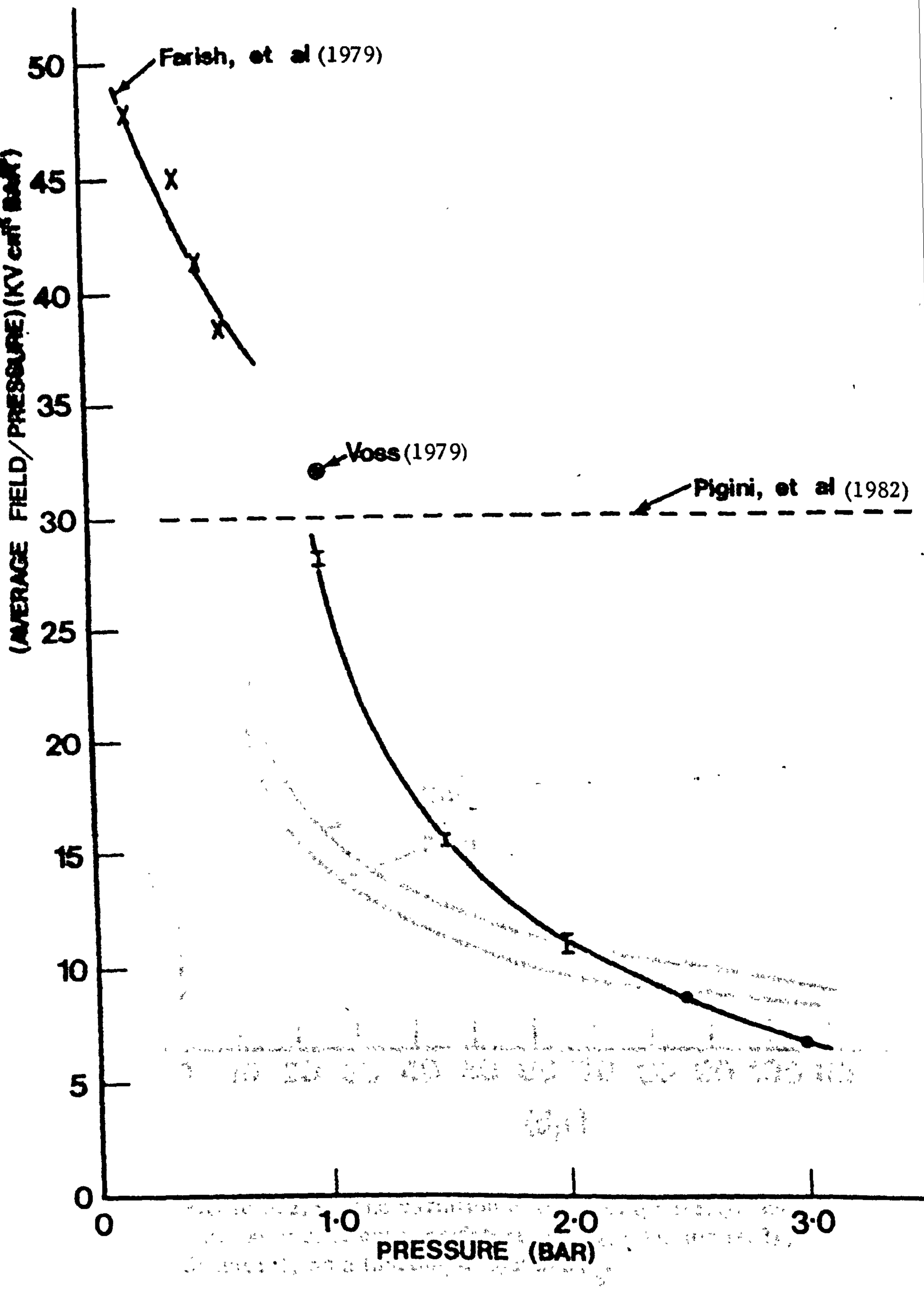

Figure 5.2.4 : The variation of the measured average field/pressure ratio with pressure for SF_6

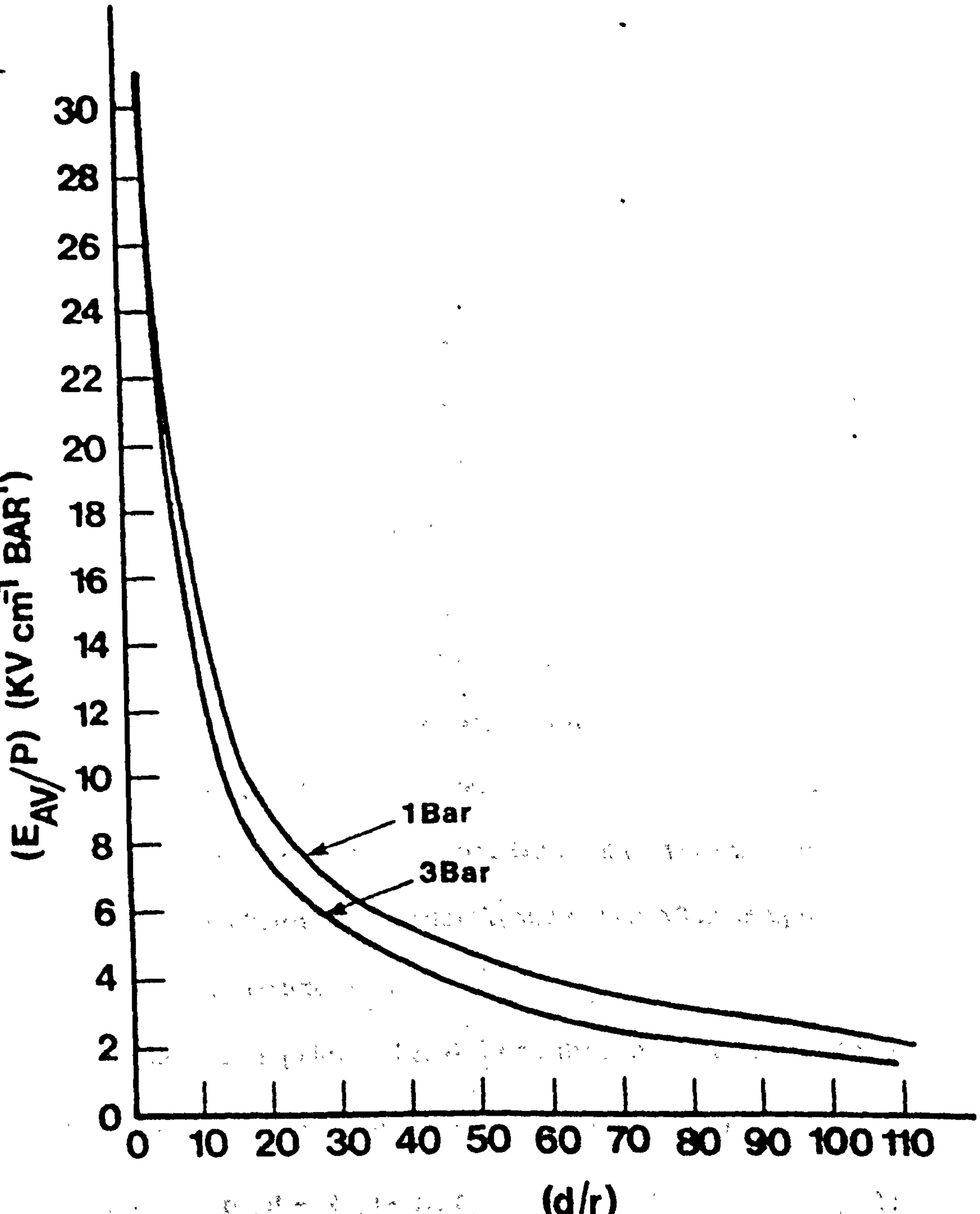

Figure 5.2.5 : The variation of the average field/pressure ratio at corona onset as determined by equation (4.3), Chapter 4, as a function of d/r in SF_6.

This dividing line may be dependent upon the pressure so that it is not possible to put an accurate value of X_1, but on the assumption that $\frac{E_{av}}{p} \simeq 20$ kV cm^{-1} bar^{-1} for SF_6 and $V_L \simeq 2\ V_i$ at low pressures then X_1 can be estimated to be approximately 15. Thus, many experimental determinations of p_c have been carried out in one or other of the two regimes. It would be surprising if the same theory describes the condition for p_c in both regimes so that the lack of a clear relationship in the results presented in figure 5.2.2 might be expected. For example, once leaders are formed, it would be surprising if tip radii would dominate the occurrence of p_c. In the present work where d/r = 55, it appears that leader properties should dominate the results for SF_6. The present results suggest that the leader properties dominate also in 10% SF_6 90% N_2 and 50% SF_6 50% N_2 mixtures.

It has to be stressed once again, however, that the results for $\frac{E_{av}}{p}$ presented in figure 5.2.4 suggest a strong dependence on p. Therefore, X_1 may vary in such a way that for a given geometry at low pressures a leader might form prior to streamer crossing, but as the pressure increases the streamers might cross before the leader forms thus further complicating the discharge regimes that control p_c.

Once a leader forms prior to breakdown, then the breakdown voltage might be given by the simplified Lemke formula (Waters, 1978, Voss, 1979).

$$V_B = \left(\frac{E_{av}}{p}\right) p\,(d - \ell_{is}) + E_\ell\, \ell_{is} \qquad (5.1)$$

where

$\frac{E_{av}}{p}$ = average field/pressure ratio necessary for streamer crossing and initiation of the secondary effects which cause breakdown.

ℓ_{is} = length of leader at point of final instability.

d = gap spacing

E_{ℓ} = Average leader field

Hence when this is the case (for $d/r > X_1$) the value of p_c is determined by the intersection of equation (5.1) and equation(4.3), Chapter 4. p_c can be expressed as :

$$p_c = \frac{E_{\ell} \times \ell_{is}}{(E/p)_{lim} (\frac{d}{f}) X - (\frac{E_{av}}{p}) (d - \ell_{is})} \qquad (5.2)$$

where $X = \left\{ 1 + (\frac{k}{B\ p\ r})^{\frac{1}{2}} \right\}^2$ which can be considered to be approximately constant.

Since many of the terms in equation (5.2) above may have unusual time, and pressure dependencies, p_c defined this way cannot be said to be unique independent of the rise time of the applied voltage pulse. Moreover, if the breakdown voltage is not decided by the need for streamers to cross so as to trigger leader instability then equations (5.1) and (5.2) will be incorrect. It is certainly possible that leaders could go unstable electrostatically, (Kurimoto et al, 1978) without involving streamer crossing. Evidence for this might be found in the low values of $\frac{E_{av}}{p}$ presented in figure 5.2.4. In the case of air in long gaps E_{ℓ} is known to be a function of the leader length ℓ and so possibly also of the age of the leader. For SF_6 there are no details yet but some indications suggest that leaders in this gas could have easily predictable properties (Neimeyer et al 1982). If this is the case and if ℓ_{is} and $\frac{E_{av}}{p}$ can be predicted then p_c will be capable of being assessed.

All previous results and the present work seem to suggest that there is little variation in p_c with the addition of nitrogen to SF_6. For

$d/r > X_1$, therefore one is forced to the conclusion that since $\frac{E_{av}}{p}$ will tend to increase with increase in SF_6 concentration then E_ℓ would have to decrease with addition of SF_6. To a first approximation this might be expected if the leader in SF_6 occurs in a dissociated column of weak SF_6 products (Pinnekamp, 1982) since nitrogen may be stronger electrically at the temperatures at which SF_6 dissociates.

When $d/r < X_1$ the situation is that the streamers cross albeit possibly out of some sort of glow prior to the formation of a secondary streamer or leader (Marode, 1975). The conducting cloud model seems unlikely to be of use (Voss, 1979, Nitta and Shibuya, 1971) though a full investigation of discharge extension for $p < 1$ bar has yet to be made. At the present time the leader instability processes and the limiting condition near p_c seem little understood in this d/r regime.

On the model presented here p_c will tend to change with d/r if it is accepted that there is a transition in the predischarge processes as d/r approaches X_1. Whilst detailed predictions of p_c variations with d/r await further knowledge of the leader instability processes a simplified application of equation (5.2) suggests that above X_1, p_c may increase. The results in figure 5.2.6 are a plot of p_c for SF_6 determined by other workers (Farish et al, 1977, and 1979, Foord, 1950, 1953, Malik et al 1979), together with with the present results, for a value of r approximately equal to 1 mm but with different d/r values. There is definitely a tendency for p_c to increase with d/r. The results for the other mixtures of SF_6 with N_2 are too scarce.

The value of p_c determined using d.c. voltages may actually be taken to be close to p_c determined with impulse voltages provided a plentiful supply of initiators is available. This is because at p_c no predischarge exists

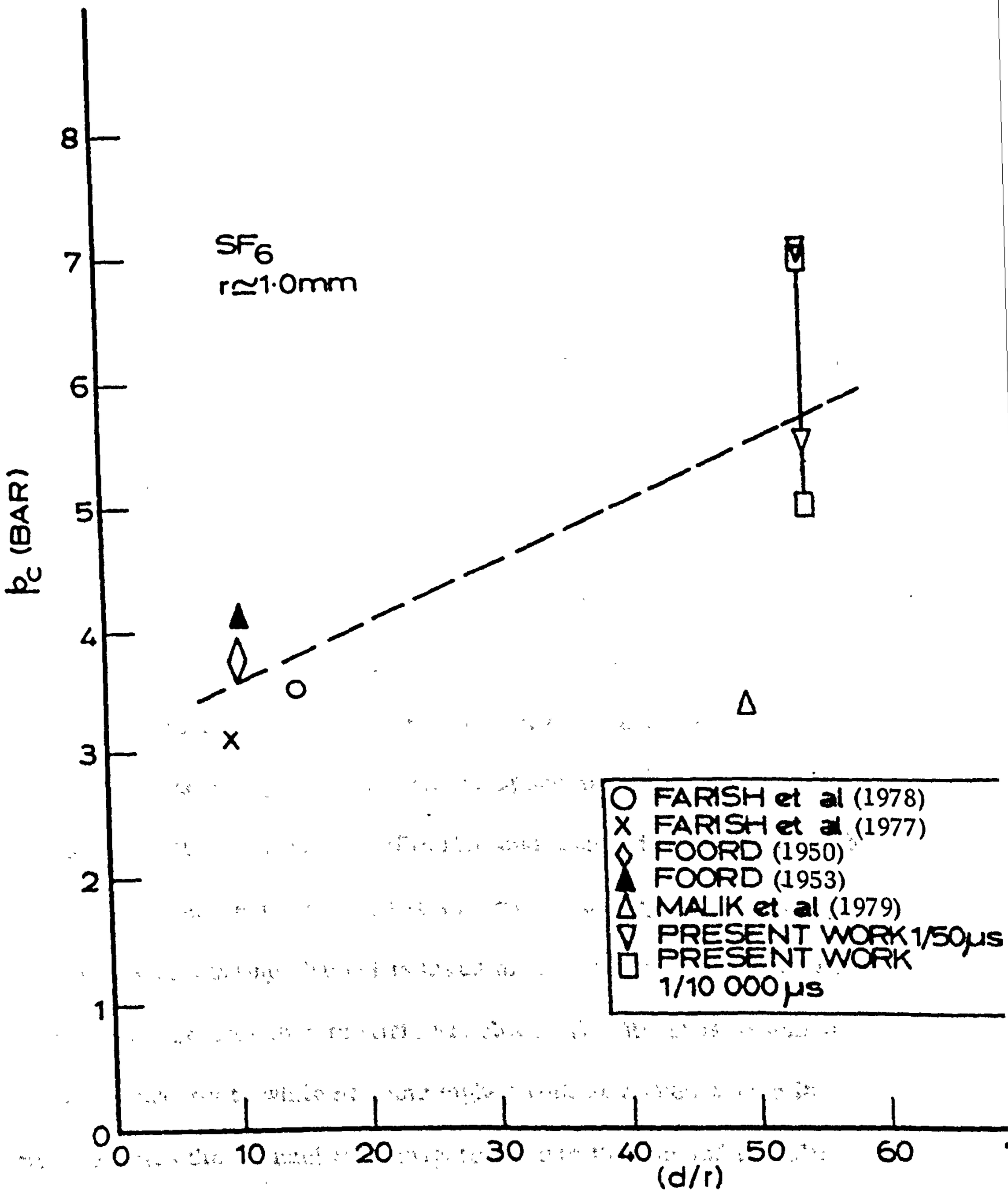

Figure 5.2.6 : The variation of the critical pressure with d/r for both d.c. and impulse voltage conditions in SF_6 for anode radius r ≃ 1mm

and so space charge cannot modify the potential distribution out in the gap and the development of the first avalanche to streamer to leader (for $d/r > X_1$) will take place in much the same way as for the impulse case when initiation and breakdown takes place on the peak of the voltage wave (Anis and Srivastava, 1982).

5.3 INTERNAL ELECTRIC FIELD ESTIMATIONS

The data for the luminous length ℓ and $\Delta E/E$ can be analysed in terms of discharge parameters if certain assumptions are made. The pre-breakdown discharge in SF_6 and mixtures of SF_6 and N_2 may be envisaged to have three stages :

(1) glow + streamers

(2) glow + stem + streamers

(3) glow + leader + streamers

These are illustrated schematically in figure 5.3.1 and the expected ($\Delta E/E$) for the different regions is indicated in figure 5.3.2. The assumptions in this representation are that the glow corona has an appreciable field drop over its extent or that it is not very extensive (Rodrigo and Chatterton, 1982, Farish et al, 1979). Once the stem forms (as is assumed in analogy to the situation in air) the narrow conducting channel is taken to have a reasonable conductivity and an extent much greater than the original glow. The stem is assumed to stay at this conductivity while at some higher voltage a sudden rise in conductivity enables the channel to propagate out into the gap and be called a leader. It is suspected that such motion in strongly attaching gases is accompanied by reilluminations (Gallimberti, 1979, Pigini et al, 1982). The limitations of the experiment necessitates that $\Delta E/E$ be greater than

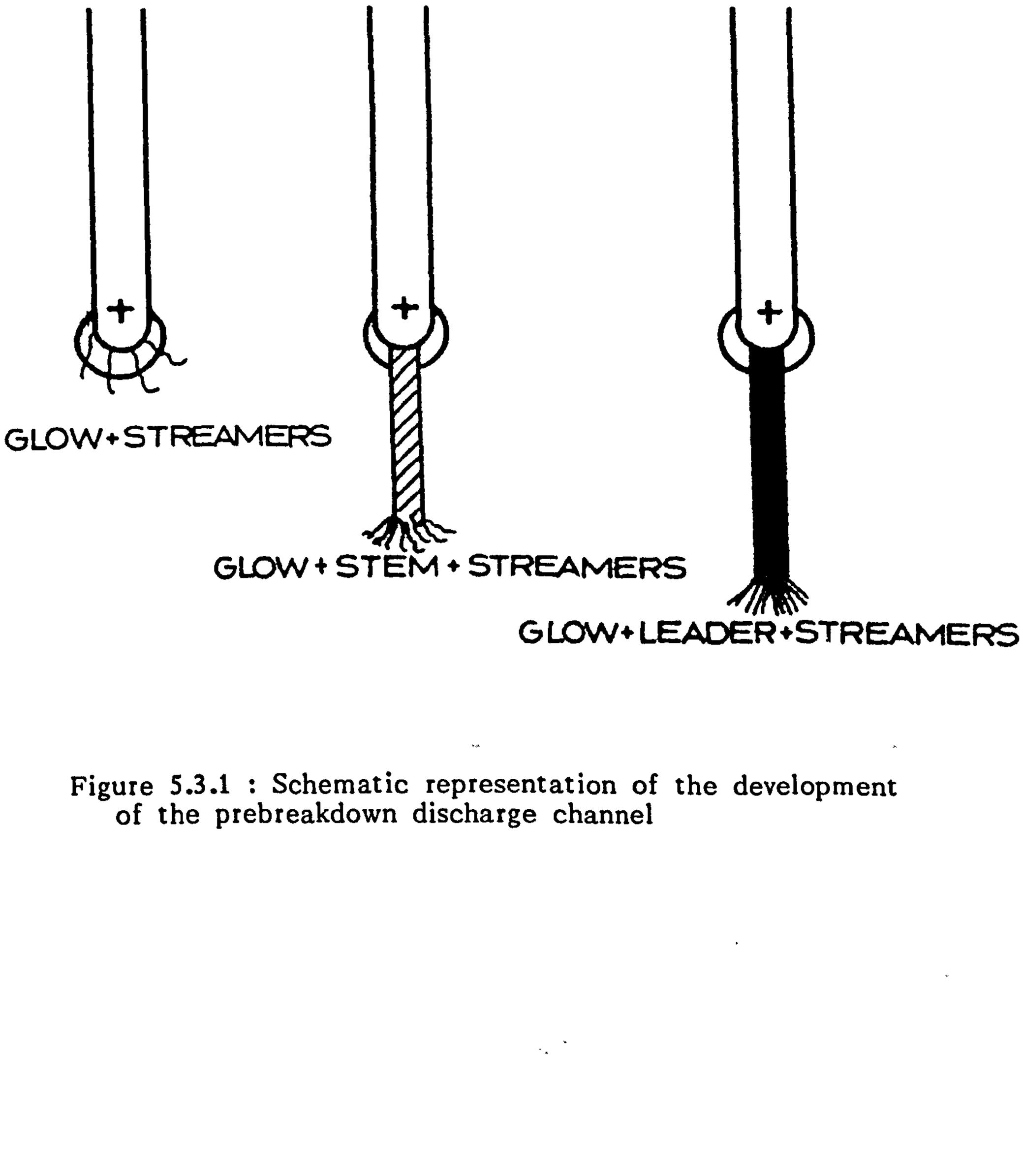

Figure 5.3.1 : Schematic representation of the development of the prebreakdown discharge channel

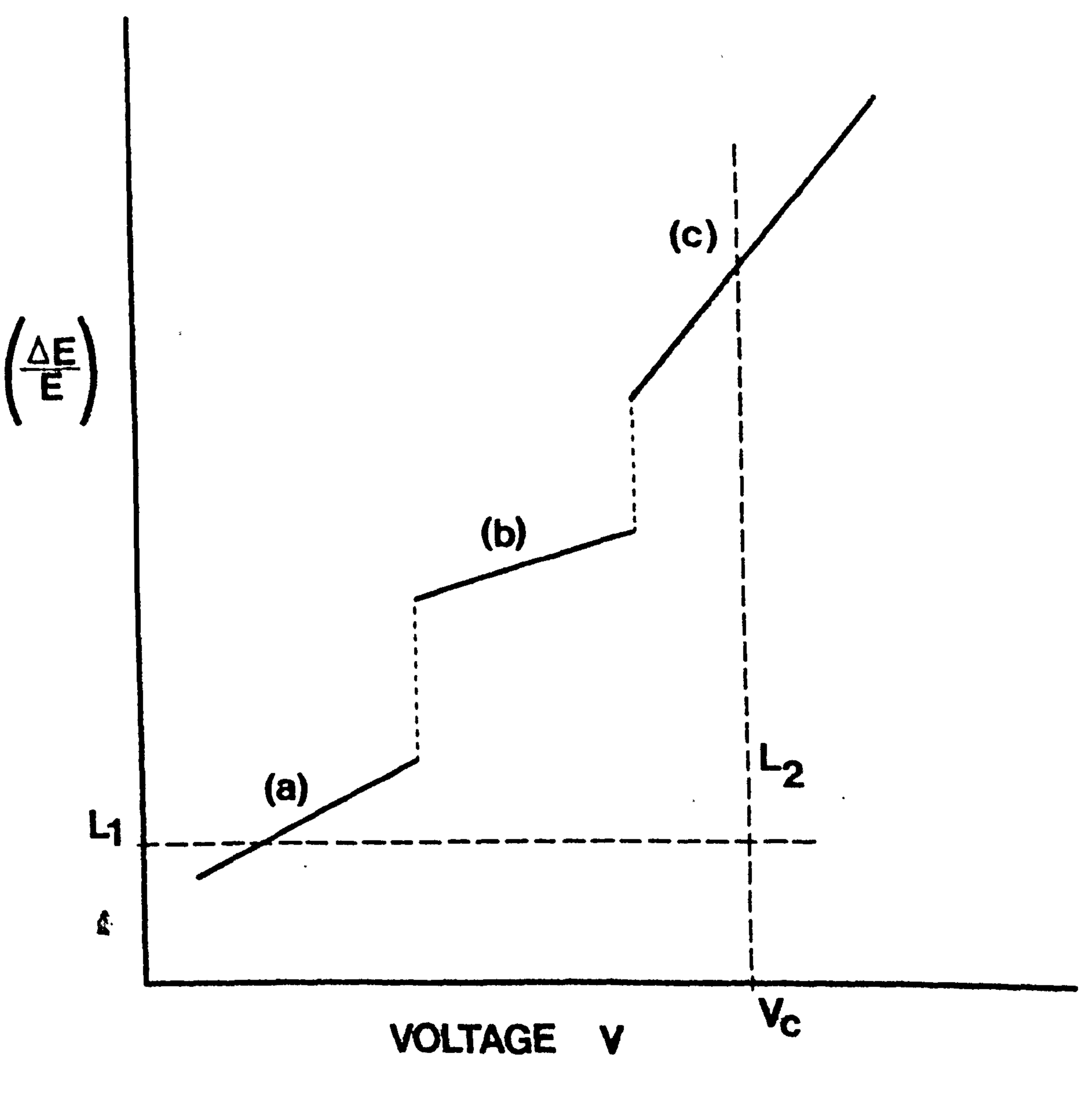

Figure 5.3.2 : The expected $\Delta E/E$ variation as a function of the applied voltage for the development of the discharge shown in figure 5.3.1.

0.05 to be measurable, and that V be less than V_c if the probe readings are to be accurate. These conditions are indicated by dotted lines L_1 and L_2 in figure 5.3.2 and define the experimental window. It is of course not known where the window will be looking in a specific experiment. In order to define our parameter space, use is made of the velocity determinations to define when the active leader is present. In the case of air, the first streamers that are formed at the onset of corona propagate into the interelectrode space at speeds of the order of 5×10^8 cm sec^{-1} (Gallimberti 1979). These streamers, as they propagate leave behind a positive space charge. The space charge distorts the field and drags in electron avalanches, that may be formed due to photoionization towards the high voltage electrode. A luminous zone is thus created close to the electrode which travel at a speed of about 10 times slower than the initial primary streamers. This luminous zone is called the secondary streamer or stem. The streamers that are formed around the stem create further ionization and the leader is launched from the stem. The leader elongates and propagates into the interelectrode space at a speed of about two orders of magnitude less than that of the primary streamers. In the case of SF_6 and its mixtures less information is available. First of all it is certain that as air is made more humid and so more attaching the average velocity of leader propagation increases and the actual development takes place in the form of rapid steps. The recent measurements of Pigini et al, (1982,) in SF_6 show a similar but more rapid stepping phenomena in which the mean leader extension velocity is $7 \pm 2 \times 10^6$ cm sec^{-1}. In the present work it is assumed that a leader is characterised by a velocity of less than 10^7 cm sec^{-1} and by reilluminations. The higher tip velocities

observed in some situations are assumed to correspond to the stem if such a phase exists in SF_6/N_2 mixtures. It is clear from a study of the photo-multiplier system in Chapter 3 that individual streamer tips are unlikely to be detected. The analysis in the present work assumes that the discharges are in region (b) or (c) in figure 5.3.2 and that the presence of the small glow region (Farish, 1979) can be neglected. The resulting analysis assumes that r_e the effective discharge tip radius is fixed and that in going from the stem to leader state the internal fields may drop.

The electrostatic model used to determine r_e and the discharge internal fields is shown in figure 5.3.3. In this model, it is assumed that the discharge is axial and has a length ℓ as shown. The electrode and discharge are then replaced by the equivalent paraboloidal point plane system illustrated. The gap length being given by $d^* = (d - \ell)$ and the voltage at the tip then being given by $V_{tip} = (V - E_\ell \times \ell)$ where V is the applied voltage and E_ℓ the internal electric field strength and r_e is the radius of curvature of the paraboloidal electrode at its apex. Then it can be shown using the known field distribution for a paraboloidal electrode system (Goldman and Goldman, 1978) that :

$$\frac{\Delta E}{E} = \left\{ \left(1 - \frac{E_\ell \times \ell}{V} \right) \right\} \left\{ \frac{(r_o + 2d)\, \ell n \left(\frac{r_o + 2d}{r_o} \right)}{(r_e + 2d^*) \ell n \left(\frac{r_e + 2d^*}{r_e} \right)} \right\} - 1 \qquad (5.3.1)$$

where

$(\frac{\Delta E}{E})$ = the ratio of the step field change to the undistorted electric field at the cathode.

E_ℓ = internal field strength

ℓ = length of discharge

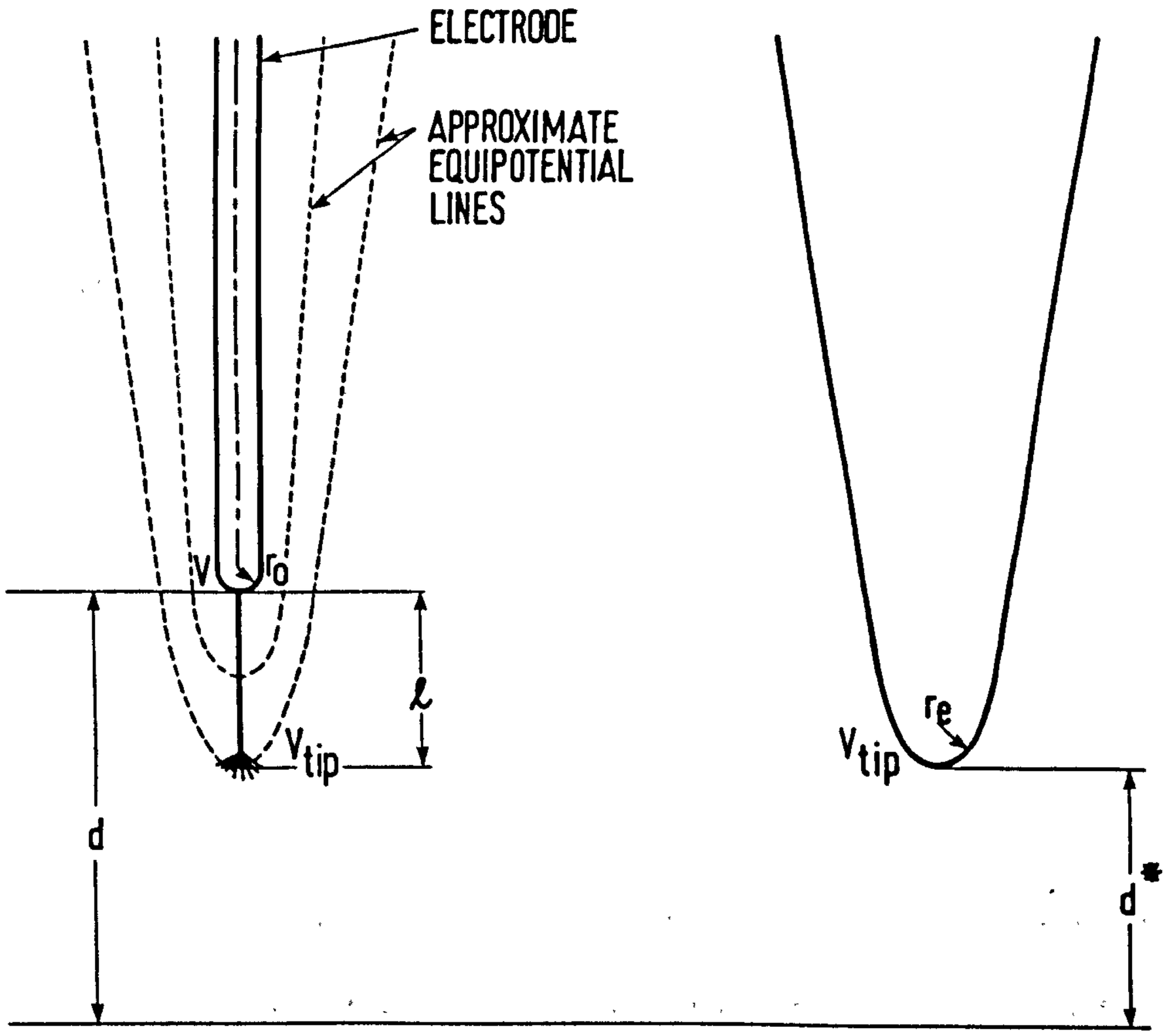

$$V_{tip} = V - \ell E_\ell$$

$$d^* = (d - \ell)$$

d = gap spacing

ℓ = luminous extent

V = applied voltage

Figure 5.3.3 : The paraboloidal point plane gap model used to calculate the electrostatic field at the cathode as a function of discharge extension.

V = applied voltage

r_e = the radius of curvature of the paraboloidal system at its apex.

r_o = radius of the electrode

d = gap length.

It must be stressed that the model assumes the electrode and any glow region will have little effect on the cathode field as computed above. The fact that the discharge will. not follow the same track from shot to shot is taken into account by averaging the measurements of ℓ and $\Delta E/E$ over ten voltage applications. More accurate electrostatic models can easily be visualised and applied to a situation where the discharge is photographed for each voltage application and a number of cathode probes employed. It is felt that the present approach is adequate for the current stage of knowledge of SF_6/N_2 prebreakdown discharge properties. To determine r_e and E_ℓ equation (5.3.1.) must be fitted to the experimental ($\Delta E/E$) results given in Chapter 4 using the different possibilities outlined in figures 5.3.1 and 5.3.2. As E_ℓ falls the accuracy of the method decreases. For good accuracy large variations in V and $\Delta E/E$ are required to provide adequate fitting sensitivity. In the present work, with an experimental gap spacing of 5.5 cms, the region of leader propagation below V_c was sometimes quite small leading to a poor sensitivity for determination. This, however, could be overcome if measurements at longer gap lengths could be carried out. In any situation a range of values of E_ℓ and r_e fit the measured curves. The results given quote the mean values determined together with the maximum possible excursions from the mean which would allow extreme forms of the calculated

curves to just lie within the experimental scatter of the measured values of $\Delta E/E$.

The results presented in Chapter 4 have been analysed using the procedure outlined above and a number of examples have been chosen to illustrate the different types of characteristics obtained. These are presented with the results for the velocity where appropriate. For the 10% SF_6 90% N_2 mixture complicated $\Delta E/E$, V curves were obtained and examples of these are shown in figures 5.3.4 and 5.3.5 together with the determined velocity up to the onset of delayed reilluminations. For the 1 bar results (figure 5.3.4) two distinct steps appear and the second of that corresponds to the restriking and presumed leader onset voltage (V_{Ri}). The lower step may correspond to the supposed glow phase suggested in figures 5.3.1 and 5.3.2, there is, however, some uncertainty. This phase was only detected in the 1 bar results for this mixtures, which could be expected to be the case, if the glow phase is much smaller than previously supposed (Farish et al, 1979). At 1.5 bar in the same mixture, figure 5.3.5, only one step is observed again roughly coincident with the onset of leader formation. In the 50% SF_6 50% N_2 no such steps are observed when the restriking onset voltage was reached and exceeded. An example of this type of result is shown in figure 5.3.6. Again at very low voltage a step can be seen which could be ascribed to a glow/stem phase transition. This type of event was once again only seen at 1 bar. No analysis of the two low voltage steps seen both in 50% SF_6 50% N_2 and 10% SF_6 90% N_2 mixtures was attempted through lack of knowledge of the exact electrostatic model to use for the glow/stem transition. These low voltage phenomena apparent only at the lowest pressures used will require further study. Figure 5.3.7 gives the results for 50% SF_6 50% N_2 at 1.5 bar,

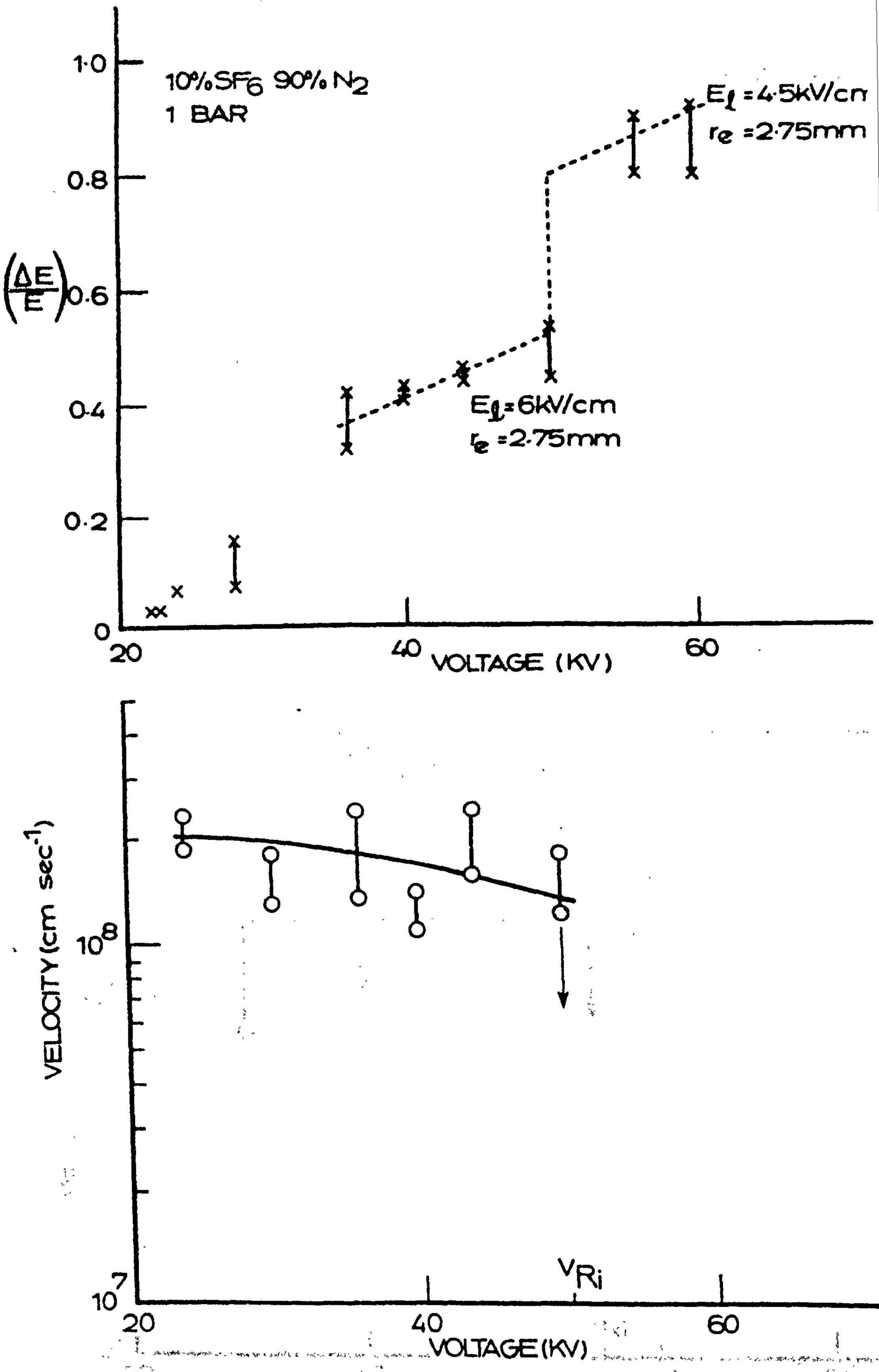

Figure 5.3.4. : The variation of $\Delta E/E$ and velocity with applied voltage. The dotted curves give the calculated values of $\Delta E/E$ for estimated values of E_l and r_e. 10% SF_6 N_2 at 1 bar

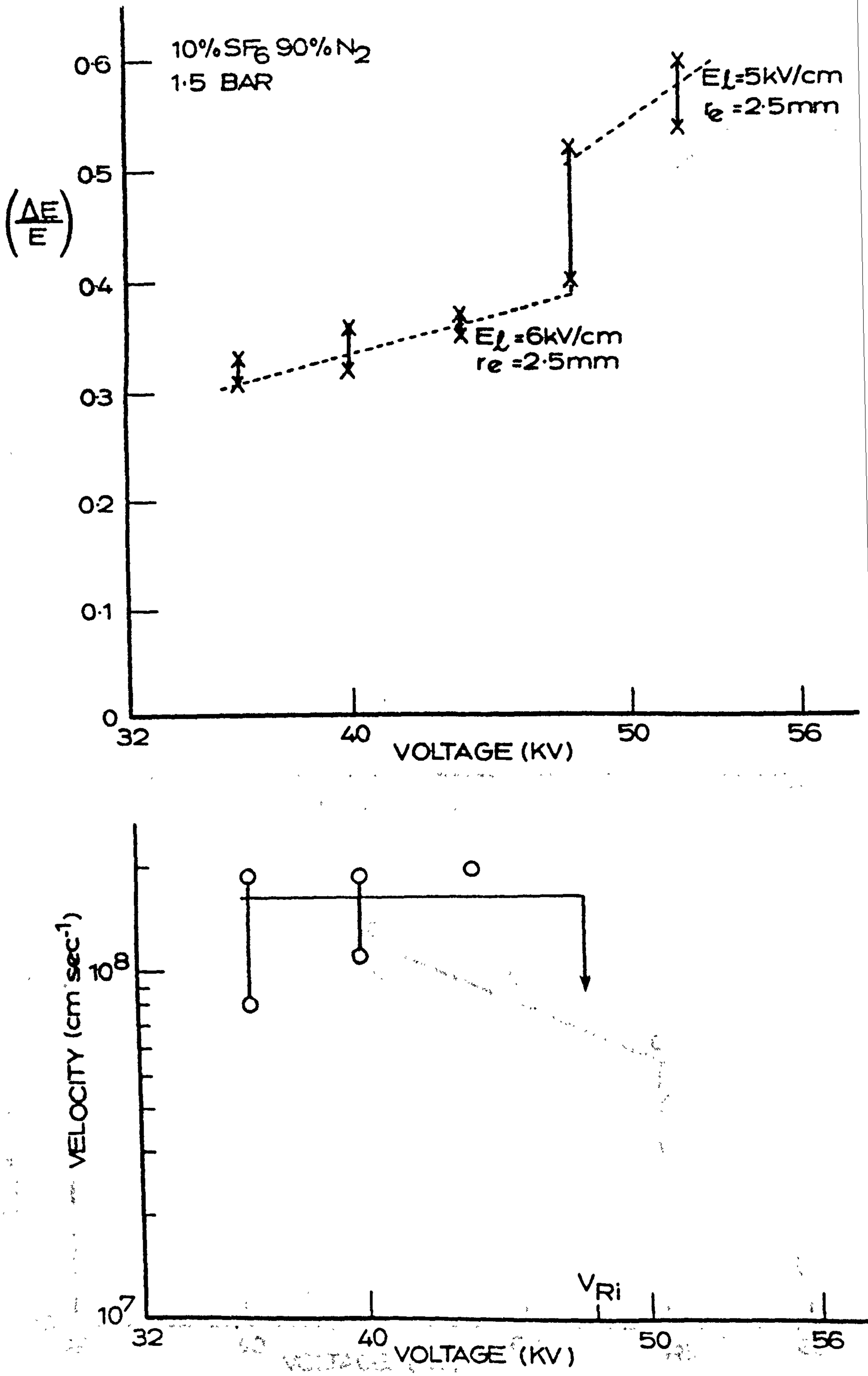

Figure 5.3.5. : The variation of $\Delta E/E$ and velocity with applied voltage. The dotted curves give calculated values of $\Delta E/E$ for estimated values of E_ℓ and r_e 10% SF_6 90% N_2 at 1.5 bar

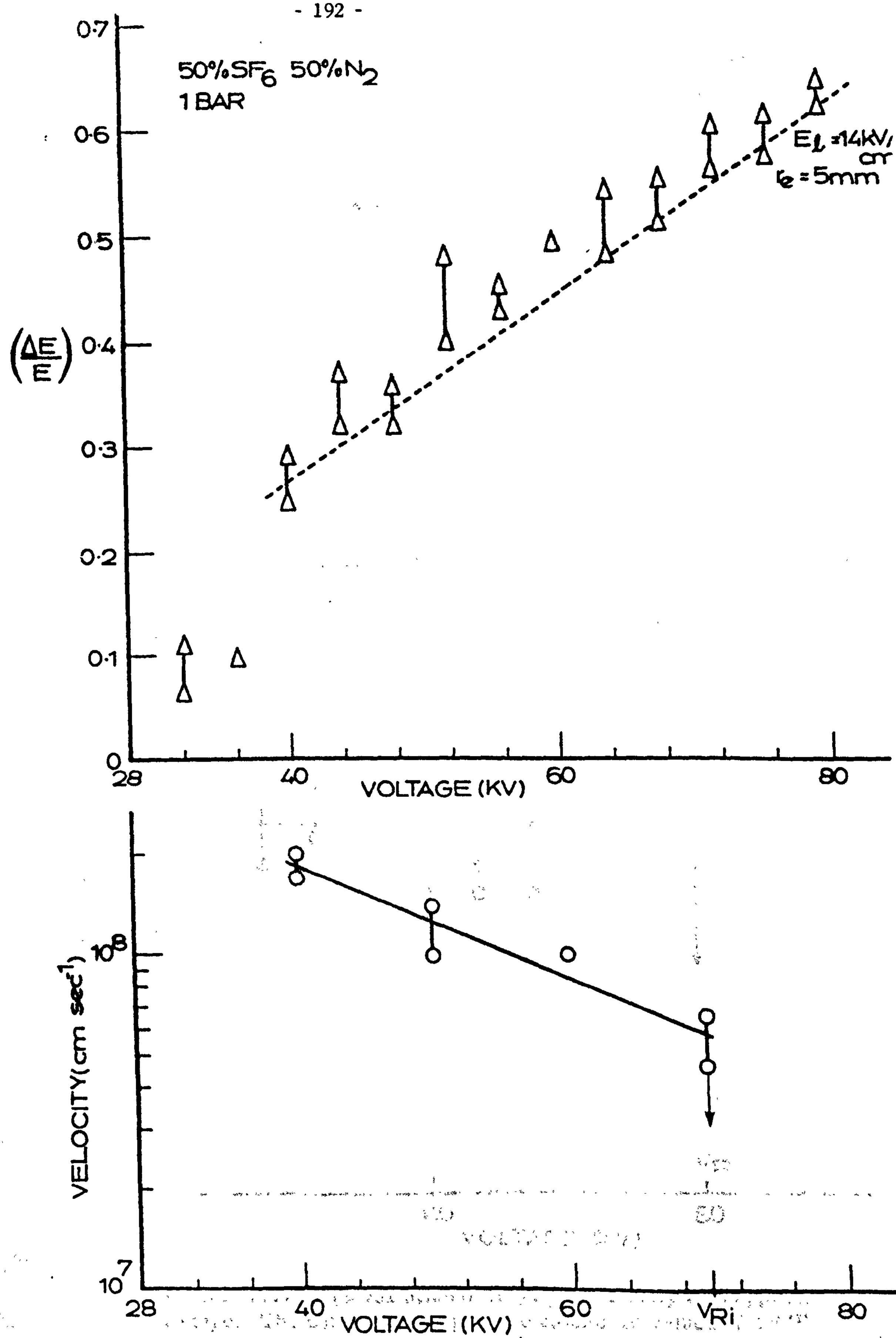

Figure 5.3.6 : The variation of $\Delta E/E$ and velocity with applied voltage. The dotted curves give the calculated values of $\Delta E/E$ for estimated values of E_ℓ and r_e . 50% SF_6 N_2 at 1 bar.

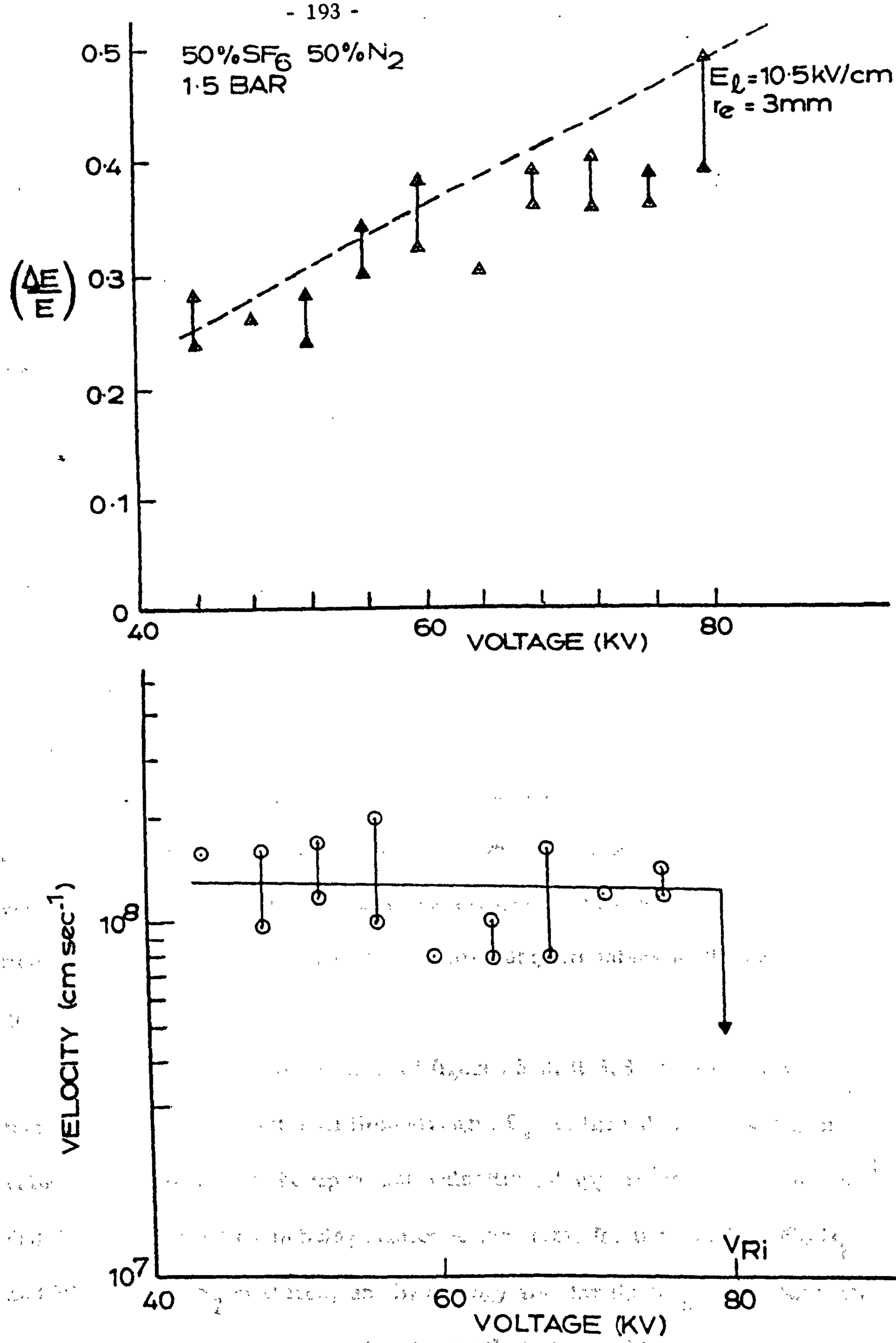

Figure 5.3.7 : The variation of $\Delta E/E$ and velocity with applied voltage. The dotted curves give the calculated values of $\Delta E/E$ for estimated values of E_ℓ and r_e. 50% SF_6 50% N_2 at 1.5 bar.

no steps were observed when the restriking voltage was reached and exceeded.

Using the techniques outlined previously the $\Delta E/E$, V curves were fitted to obtain estimates of E_ℓ and r_e. At any step at the restriking onset r_e was assumed to be constant and E_ℓ was allowed to jump to some new value and remain fixed at that value. In all cases the $\Delta E/E$, V curves were only analysed below the streamer crossing voltage V_c. In the case of SF_6 single steps in the $\Delta E/E$, V curves were observed as shown for example in figures 5.3.8 and 5.3.9 but the lack of velocity measurements did not allow a correlation with restriking to be made in this instance. The lower internal field state was assumed in this case to represent the leader by analogy with the other results. The higher field values being assumed to correspond to the stem state on the assumption that the glow phase was even less likely to be apparent than in the case of the mixtures. The resulting values of E_ℓ for the different pressures and gas compositions are given in figures 5.3.10, 5.3.11, and 5.3.12. A more complete tabulation being given in table III.

It is clear from the results of figures 5.3.10, 5.3.11 and 5.3.12 that in many cases the internal field strength E_ℓ is two valued. The higher values corresponding to the tip transit velocities of approximately 10^8 cm sec^{-1} and these are identified as being related to the stem, for the 10% SF_6 90% N_2 and 50% SF_6 50% N_2 mixtures, and by analogy also for the SF_6 case. As soon as reilluminations occur the leader apparently forms and the predischarge internal fields drop. It is assumed that the lower value of E_ℓ correspond to the leader state and the higher ones to the stem but more work will be

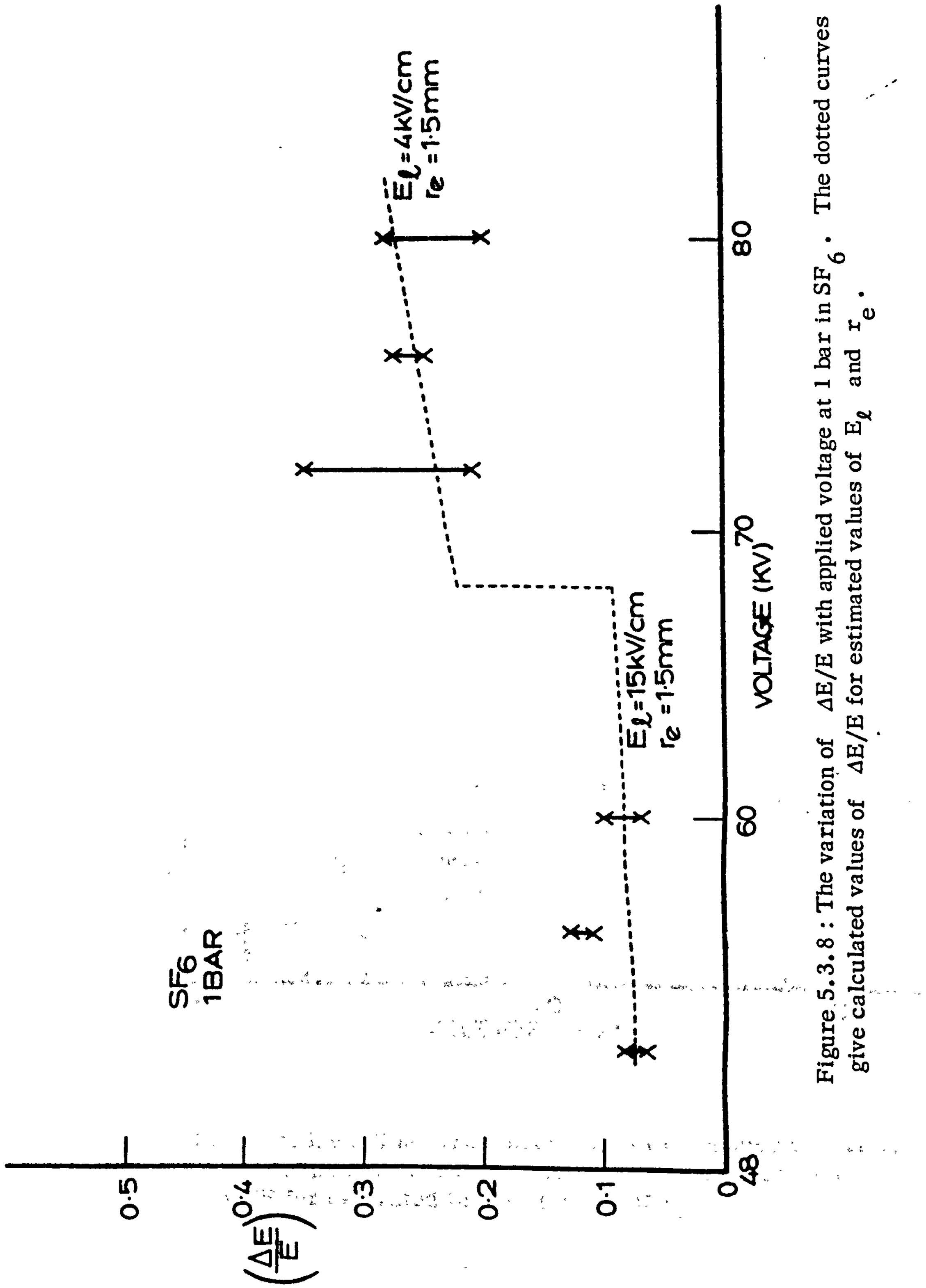

Figure 5.3.8 : The variation of $\Delta E/E$ with applied voltage at 1 bar in SF_6. The dotted curves give calculated values of $\Delta E/E$ for estimated values of E_l and r_e.

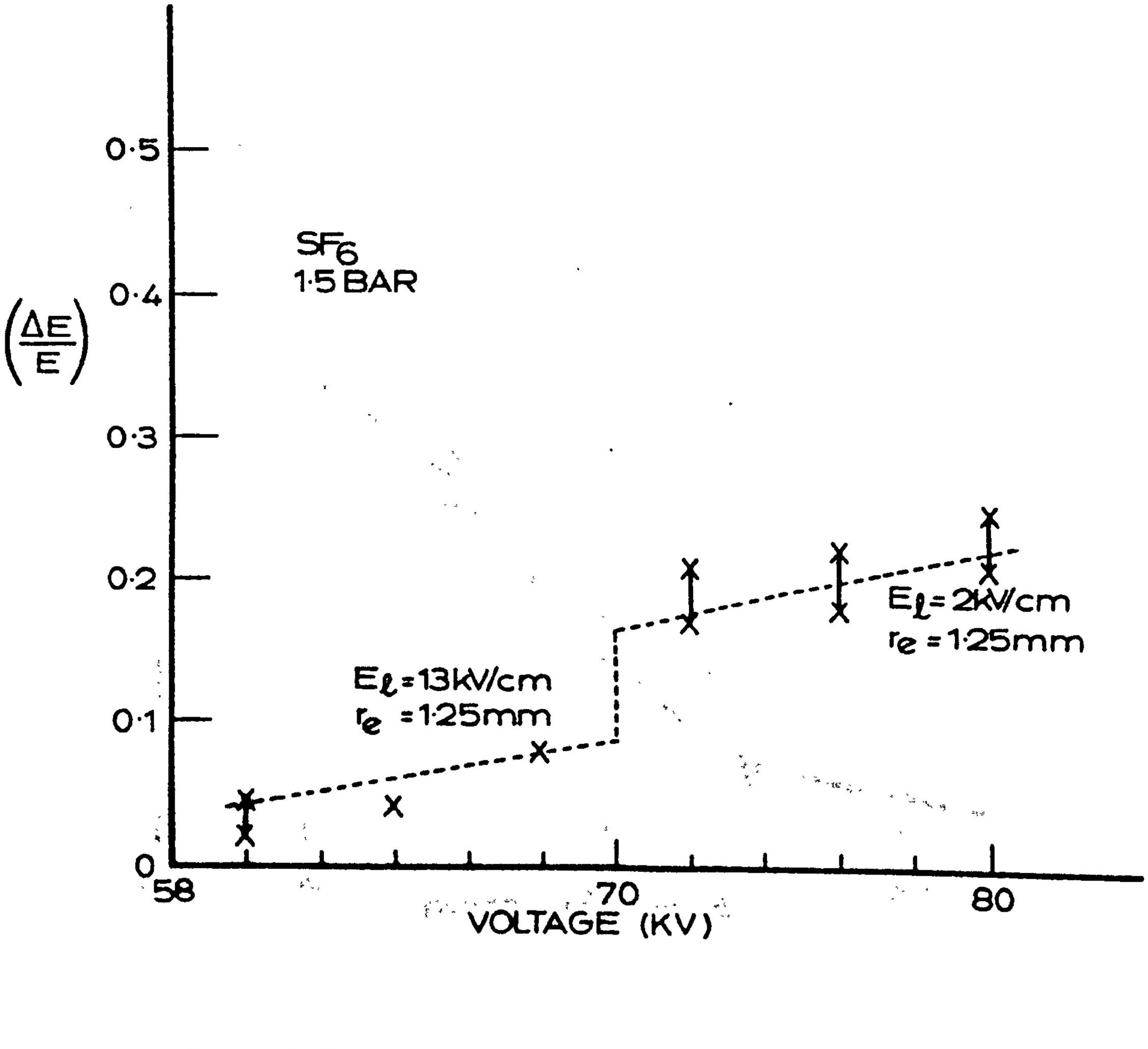

Figure 5.3.9 : The variation of $\Delta E/E$ with applied voltage at 1.5 bar in SF_6. The dotted curves give calculated values of $\Delta E/E$ for estimated values of E_ℓ and r_e.

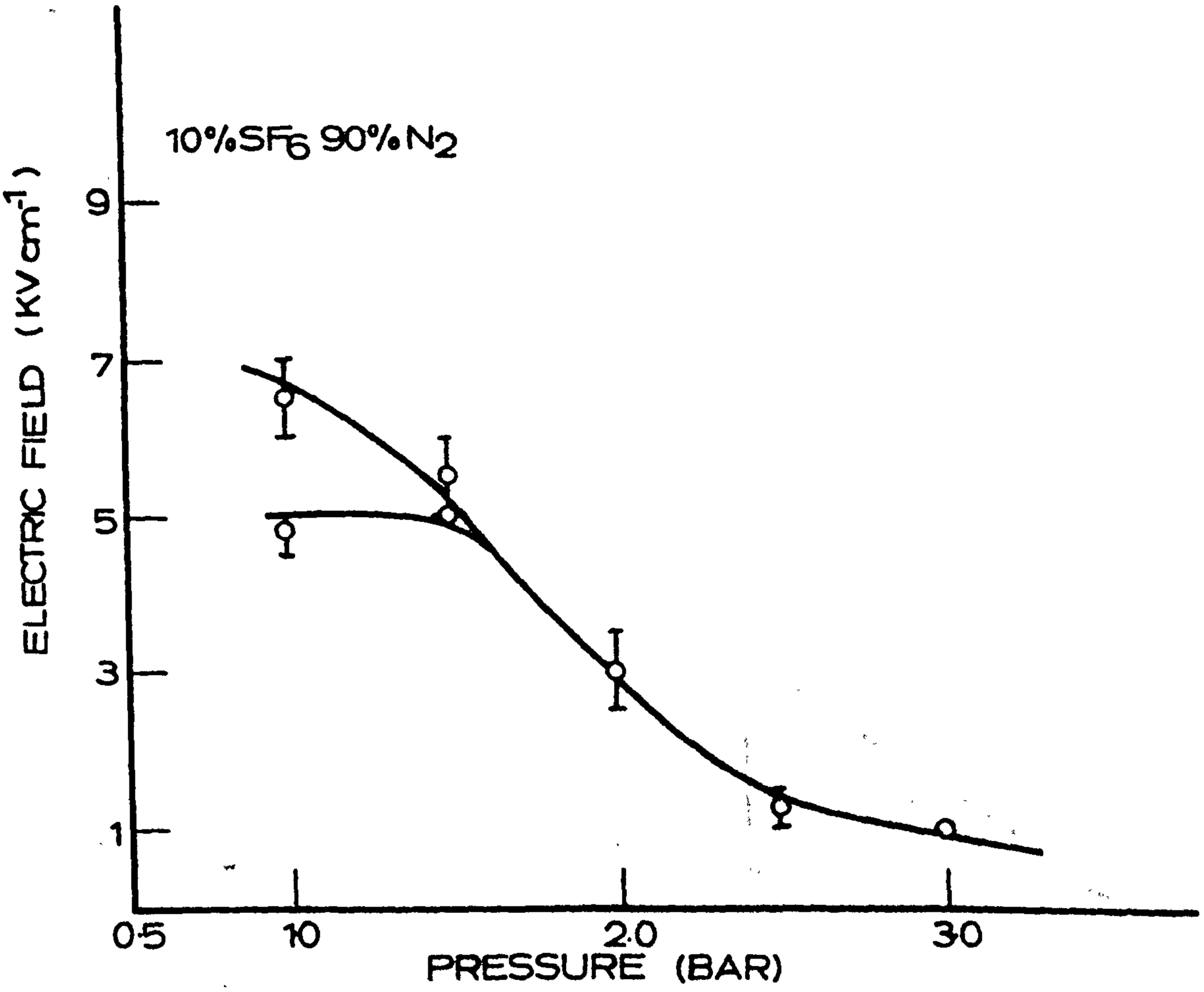

Figure 5.3.10 : The variation of prebreakdown discharge internal electric field with pressure in 10% SF_6 90% N_2 .

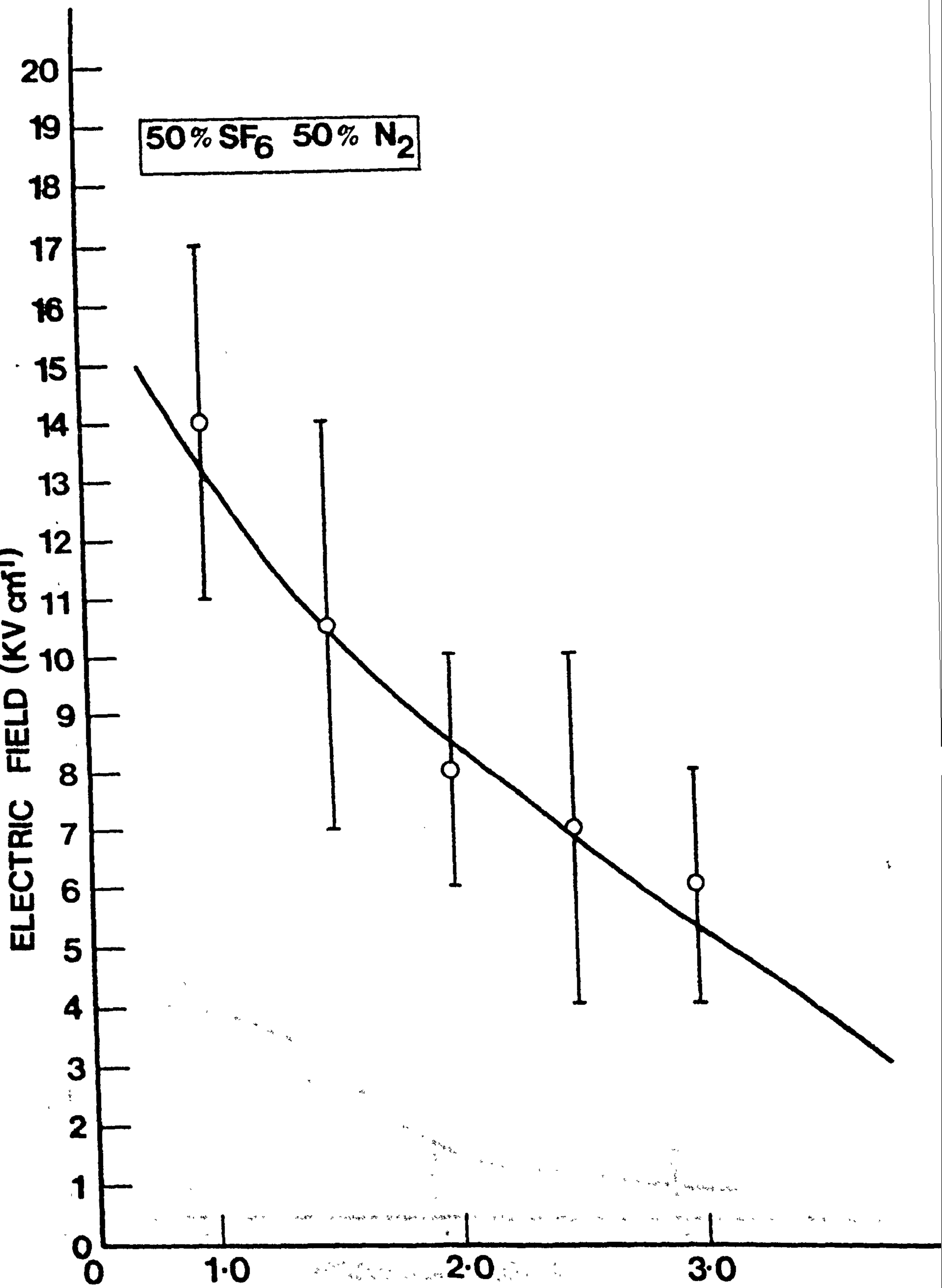

Figure 5.3.11 : The variation of the prebreakdown discharge internal field with pressure in 50% SF_6 50% N_2

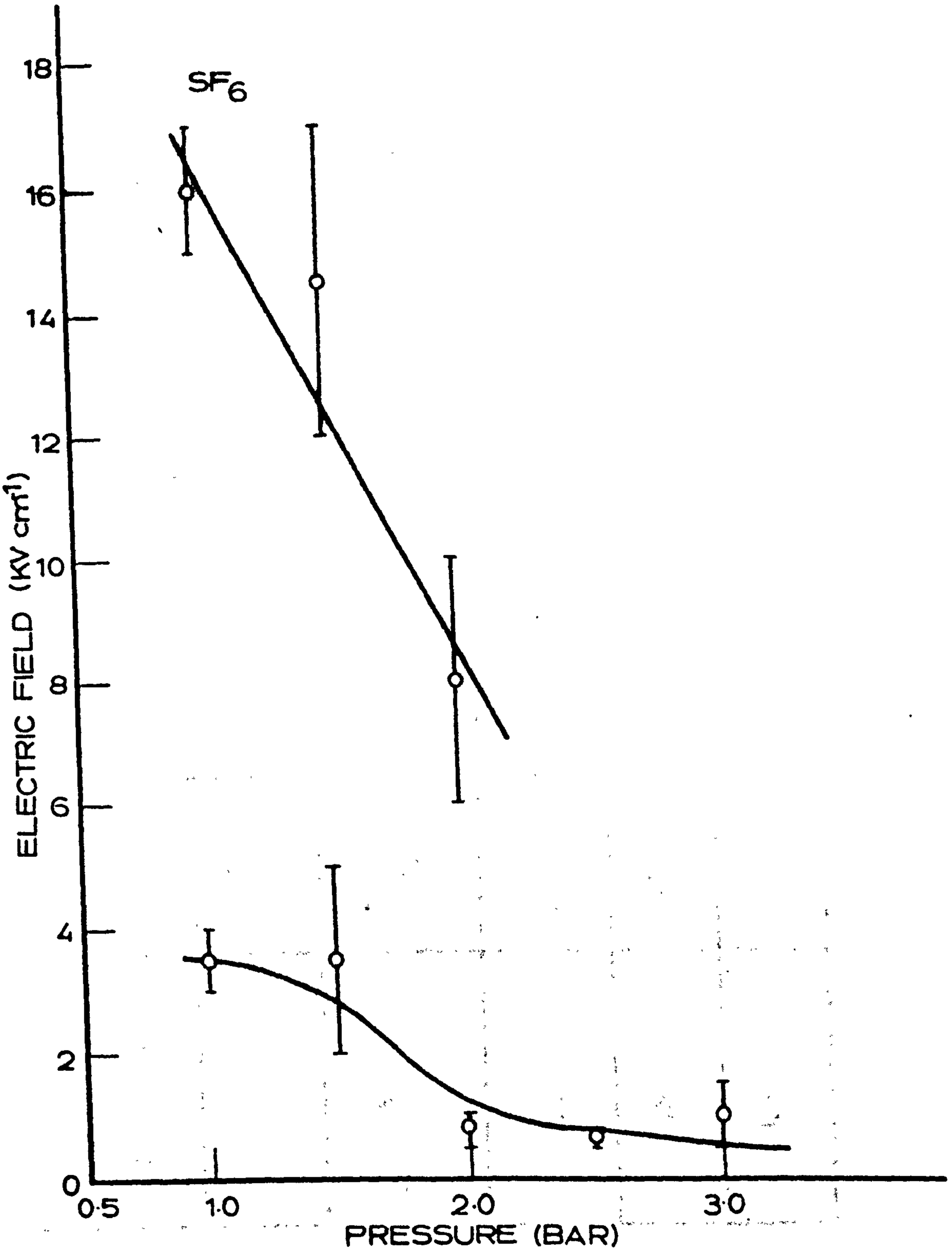

Figure 5.3.12. The variation of the prebreakdown discharge internal electric field with pressure in SF_6

PRESSURE (bar)	GASEOUS COMPOSITION					
	10% SF_6 90% N_2		50% SF_6 50% N_2		SF_6	
	E (kV/cm)	r_e (mm)	E (kV/cm)	r_e (mm)	E (kV/cm)	r_e (mm)
1.0	6.5± 0.5 4.74± 0.25	2.88± 0.13	14 ± 3	5 ± 0.5	16 ± 1 3.5± 0.5	1.5± 0.1
1.5	5.5± 0.5 5.0	2.5	10.5± 3.5	3.5± 0.5	14.5± 2.5 3.5 ± 1.5	1.28± 0.13
2.0	3 ± 0.5	1.38± 0.13	8 ± 2	1 ± 0.1	8 ± 2 0.75± 0.25	1.25
2.5	1.25± 0.25	1 ± 0.1	7 ± 3	0.95± 0.15	0.63± 0.13	1.05± 0.05
3.0	1.0	0.9	6± 2	1 ± 0.1	1.0± 0.5	1± 0.25

Table 3 : Summary of Results

required to fully prove this. In the case of the 50% SF_6 50% N_2 mixtures no distinction in the results could be ascertained between the leader and the stem state and so only one curve is given. It is not yet certain as to why this should be the case, but the higher leader/stem fields seen in this gas composition may mean that it is a favourable choice as a gas mixture in regimes where leader properties dominate the breakdown voltage. The values of E_ℓ obtained by earlier workers are given in table 4.

Gaseous composition	Pressure (bar)	leader field strength E (kV/cm)	Author
10% SF_6 90% N_2	1.0	3.5	Voss,(1979)
50% SF_6 50% N_2	1.0	7.5	Voss,(1979)
SF_6	1.0	11.3	Voss,(1979)
SF_6 (surface discharge)	1 - 10	1 - 2	Niemeyer et al, (1982)
SF_6	1.07	8 - 10	Kurimoto et al, (1978)

Table 4 : Summary of E_ℓ values obtained by earlier workers

For the case of the 10% SF_6 90% N_2 and 50% SF_6 50% N_2 mixtures results have only previously been obtained by Voss (1979), at 1 bar. His measurements using an anode probe seem to be slightly lower than the present values, and this is probably because his values were determined at the point of final instability. The results of the present work indicate the $\Delta E/E$ increase fairly rapidly above V_c (the limit of analysis) and this may signify that E_ℓ

is reducing close to the final instability voltage. No accurate measurements with the present cathode probe system are possible in this high voltage range. In the case of SF_6 the work of Kurimoto et al (1978) and Voss (1979) again at 1 bar do not seem to agree well with the present work. They do, however, seem to fit the mean of the high and low conductivity states and this may mean that these workers have measured a mean value though this seems surprising in view of the long leader lengths investigated by Kurimoto et al (1978). The recent surface discharge studies of Niemeyer and Pinnekamp (1982) give values of leader field in the range 1 - 2 kV/cm and independent of pressure. The results in the present work indicate a weak pressure dependence and a reasonable agreement with the values determined in the surface discharge experiments. Thus the evidence seems reasonably clear that leader fields are low in the case of SF_6 and 10% SF_6 90% N_2 but that some doubt exists as to the distinction between the leader and stem states for the 50% SF_6 50% N_2 mixture. Finally, it must be recognised that the possibility exists that leader properties for long lengths generated by slowly rising voltage waveforms (Kurimoto et al (1978) or close to the anode (Voss, 1979) may be different from the properties associated with the leaders studied in this work.

The leader fields determined in the present work when coupled with the voltage for onset of streamer crossing enable mean field to pressure ratio (E_{av}/p) to be determined for the streamer crossing condition in the space between the leader tip and the cathode. Such calculations have been performed for the three gas compositions and the results are shown in figure 5.3.13. The values determined appear to be pressure dependent and considerably below the values assumed by other workers (Pigini et al, 1982) at the onset of the final jump. Extending the present results to the final jump

state may increase the values of (E_{av}/p) but not significantly. The reason for these low values at breakdown may mean that as the leader fields drop the extra amount of feedback needed from the streamers arriving at the cathode to complete the instability is reduced. Thus, the size of the streamers guiding field could fall as seen in figure 5.3.13. In section 5.1 of this Chapter, the streamer crossing point was considered as a possible limiting condition that determined V_B and so p_c. However, other processes could equally well determine leader instability. One such alternative explanation could be linked to some sort of electrostatic instability (Kurimoto et al, 1978 , Rodrigo and Chatterton, 1982). This instability can be linked to the concept that as the leader extends it may go into a situation where each extension increases the field at its tip.

5.4 CONCLUSIONS

The corona onset voltage determined with impulse voltages are difficult to compare with theoretical values due to the lack of initiatory electrons. Adding nitrogen to SF_6 lessens this problem. The critical pressure p_c was determined in this work by extrapolation technique. These values are close to those obtained by Anis and Srivastava (1982), who used extreme value statistics to determine p_c. Direct measurement of p_c with impulse voltages is difficult. Explanations for p_c have to be found which depend on the value of d/r rather than that of r for the geometry investigated. More detailed knowledge of the leader instability processes is needed, than is currently available, for a more accurate model for the prediction of p_c.

The measurement of leader and stem fields as a function of pressure have indicated that the leader fields are lower than the stem

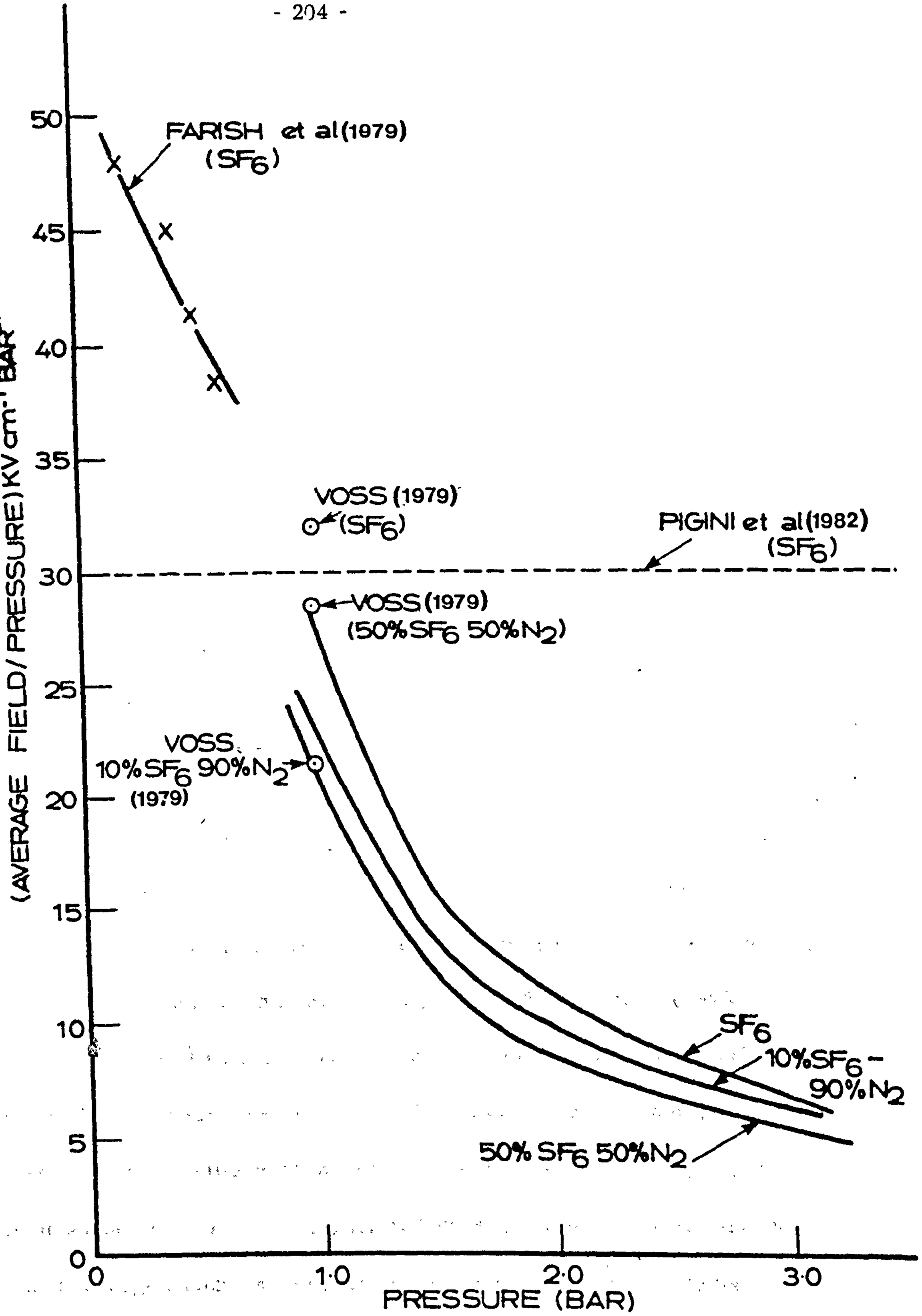

Figure 5.3.13 : The variation of the average field/pressure ratio as a function of pressure for the different gaseous compositions. The present results refer to the space between the leader tip and the cathode plane.

fields except in the case of 50% SF_6 50% N_2. There is reasonably good agreement between the leader fields in the present work and the surface discharge measurements of leader fields in SF_6 carried out by Niemeyer and Pinnekamp (1982). The velocity measurements indicate that in both the 10% SF_6 90% N_2 and 50% SF_6 50% N_2 the secondary streamer or stem propagates at about 10^8 cm sec^{-1}. The fact that both E_ℓ and r_e decrease with increase in pressure suggests that the final instability condition of theleader could be brought about by an electrostatic instability without necessarily involving streamer crossing. However, the prediction of this ultimate instability condition will require detailed knowledge of the variation of E_ℓ and r_e with pressure, which are not as yet available.

5.5 SUGGESTIONS FOR FUTURE WORK

The most useful line of research that could be pursued would be to study the development of predischarge phenomena in a longer gap of between 100 and 150 mm in length, with both lightning and switching impulse voltages. This would enable the discharge channel to be studied under different regimes of voltage. More cathode probes, which are biased as used by Tassicker (1974) would enable the range of field measurements to be extended close to the point of final instability. These probes, together with an anode probe as used by Voss (1979) would help to measure the field of the discharge channel accurately and by careful measurements the transition from the state of stem to leader could be determined accurately.

By incorporating high speed image converter/intensifier photography into the experimental set up with the photomultipliers the optical

characteristics could be studied in detail. Streak photography will reveal the exact nature of the discharge channel as it propagates into the inter-electrode space. These measurements together with the time related photomultiplier records would enable very accurate measurements of the velocity of propagation of the discharge channel.

A separate study, however, incorporating Schlieren photography with spectroscopic studies would help to estimate the electrostatic radius of the discharge channel. These above mentioned measurements would go a long way to help formulate an accurate electrostatic model for prediction of the electric field strength in a discharge channel, and hence predict the critical pressure with a higher degree of confidence in SF_6 and mixtures of SF_6 with N_2 than is currently available.

REFERENCES

AHEARN, A.J. and HANNAY, N.B.
"The formation of negative ions of sulphur hexaflouride", J. Chem. Phys., Vol. 21, No. 1, Jan, 1953, pp. 119-124.

ALEKSANDROV, G.N.
"Mechanism of corona-to-spark transition in long air gaps", Sov.Phys.Tech.Phys, Vol. 10, No. 7, January; 1966, pp. 948-951.

ALEKSANDROV, G.N.
"Growth of a spark discharge in a wide air gap", Sov.Phys.-Tech.Phys., Vol. 14, No. 4, Oct. 1969 (a), pp. 560-567.

ALEKSANDROV, G.N.
"Peculiarities of spark discharge development in long air gaps", 9th Int. Conf. on Phenomena in ionized gases, Bucharest, 1969 (b), p.283.

ANIS, H. and SRIVASTAVA, K.D.
"Pre-breakdown discharges in rod-plane gaps in SF_6 under positive switching impulses", IEEE. Trans. on Elec.Insul., Vol. EI-16, No.6, Dec. 1981, pp.552-563.

ANIS, H. and SRIVASTAVA, K.D.
"Breakdown of rod-plane gaps in SF_6 under positive switching impulses", IEEE.Trans. PAS Vol. 101, No.3, March,1982, pp. 537-546.

ASCHWANDEN, Th.,
"Ionization and attachment coefficients in SF_6/N_2 mixtures", 3rd Int.Symp. on H.V.E., Milan, 1979, paper No. 31.12.

AZER, A.A. and COMSA, R.P.
"Influence of field non-uniformity on the breakdown characteristics of sulphur hexafluoride", IEEE. Trans. on Electr.Insul. Vol. EI-8, No.4, Dec.1973, pp. 136-142.

BAKKEN, JON, ALFRED,
"Determination of characteristic voltages in impulse and switching surge testing", IEEE. Trans., PAS, Vol.86, No.8, Aug. 1967, pp. 962-968.

BEATTIE, J.
Ph.D. Thesis, University of Waterloo, 1975.

BERG, D. and DAKIN, T.W.
"Electron attachment in sulphur hexafluoride", J.Chem.Phys., Vol. 25, 1956, p.179.

BERG, D. and WORKS, C.N.
"Effect of space charge on electric breakdown of sulphur hexafluoride in non-uniform fields", AIEE. Trans. Vol. 77, pt. III, Oct. 1958, pp.820-823.

BERGER, S.
"Onset of breakdown voltage reduction by electrode surface roughness in air and SF_6", IEEE. Trans., PAS, Vol. 95, No.4, July/Aug. 1976, pp.1073-1079.

BHALLA, M. S. and CRAGGS , J.D.
"Measurement of ionization and attachment coefficients in sulphur hexafluoride in uniform fields", Proc.Phys.Soc., Vol. 80, 1962, pp.151-160.

BLACKETT, J., MATTINGLEY, J.M. and RYAN, H.M.
"Breakdown voltage estimation in gases in semi-empirical concept", Int. Conf. on Gas Discharges, London, Sept., 1970, pp. 293-297.

BLAIR, D.T.A. and WHITTINGTON, H.W.
"Absorption of radiation in a Townsend discharge", Int.Conf. on Gas Discharges, London, 1970, pp.1-5.

BLAIR, D.T.A., MACLEOD, N.M. and ORR, J.S.
"Radiation in the vacuum ultraviolet from discharges in gas mixtures", 4th Int. Conf. on Gas Discharges - Swansea, Sept. 1976, IEE. Conf.Pub., No. 143, pp.401-403.

BORTNIK, I.M. and VERTIKOV, V.P.
"Discharge development in SF_6", 3rd Int.Symp. on H.V.E., Milan,1979, paper No. 32.11.

BORTNIK, I.M. and COOKE. C.M.
"Electrical breakdown and the similarity law in SF_6 at extra high voltages", IEEE. Trans., PAS., Vol. 91, No.5, 1972, pp.2196-2203.

BOYD, H.A. and CRICHTON, G.C.
"Measurement of ionization and attachment coefficients in SF_6", Proc. IEE., Vol. 118, No. 12, Dec. 1971, pp. 1872-1877.

CARRARA, G. and THIONE, L.
"Switching surge strength of large air gaps : A physical approach", IEEE. Trans., PAS 95, 1976, pp. 512-520.

CHALMERS, I.D., DUFFY, H. and TEDFORD, D.J.
"The mechanism of spark breakdown in nitrogen, oxygen and sulphur hexafluoride", Proc. Roy. Soc,, Lond., 1972, A.329, pp.171-191.

CHATTERTON, P.A.
"A model for the breakdown of SF_6 in the presence of positive impulse corona", 3rd Int. Symp. on H.V.E., Milan, Aug. 1979, Paper No. 31.07.

COOKE, C.M.
"Ionization, electrode surfaces and discharges in SF_6 at extra high voltages", IEEE. Trans., PAS, Vol. 94, No.5, Sept./Oct., 1975, pp.1518-1523.

COOKSON, A.H.
"Electrical breakdown for uniform fields in compressed gases", Proc. IEE., Vol. 117, No.1, Jan. 1970, pp. 269-280.

DAVIES, A.J., DAVIES, C.S. and EVANS, C.J.
"Computer simulation of rapidly developing gaseous discharges", Proc. IEE., Vol. 118, No.6, June 1971, pp. 816-823.

DAWSON, G.A. and WINN, W.P.
"A model for streamer propagation", Zeits. fur Physik, Vol. 183, 1965, pp.159-171.

DUTTON, J.
In Meek, J.M. and Craggs, J.D. (Eds.), "Electrical Breakdown of Gases", John Wiley and Sons, Chapter 3, 1978.

DUTTON, J., HARRIS, F.M., and JONES, G.J.
"Ionization, attachment and breakdown in SF_6", Nature, Vol. 227, Aug.15, 1970, pp. 702-703.

FARISH, O., DAVIDSON, R.C., and TEDFORD, D.J.
"Corona stabilization and the critical pressure in SF_6 and in SF_6/N_2 mixtures", Proc. Conf. on Insulation Dielectric Phenomena, Colonie, N.Y., 1977.

FARISH, O., IBRAHIM, O.E. and KORASLI, C.
"Corona stabilization and breakdown in SF_6 and SF_6/N_2 mixtures", 5th Int. Conf. on Gas Discharges, Liverpool, Sept., 1978, IEE. Conf. Pub., No. 165, pp.. 320-324.

FARISH, O., IBRAHIM, O.E. and KURIMOTO, A.
"Prebreakdown corona processes in SF_6 and SF_6/N_2 mixtures", 3rd Int. Symp. on H.V.E., Milan, 1979. Paper No. 31.15.

FOORD, T.R.
"Positive point-to-plane spark breakdown of compressed gases", Nature, Oct. 1950, Vol. 166, pp. 688-689.

FOORD, T.R.
"Some experiments on positive point-to-plane corona and spark breakdown of compressed gases", Proc. IEE., Vol. 100, Part 2, No. 78, Dec. 1953, pp. 585-590.

GALLIMBERTI, I.
"The mechanism of the long spark formation", Journal de Physique, Colloque C7, Supplement au No. 7, Tome 40, Juillet 1979, Vol. 2, (Invited papers), pp. 193-250.

GALLIMBERTI, I.
" A computer model for streamer propagation". J.Phys.D · Appl.Phys., Vol. 5, 1972, pp. 2179-2188.

GEBALLE, R. and REEVES, M.L.
"A condition on uniform field breakdown in electron attaching gases", Phys.Rev., Vol. 92, No. 4, Nov. 1953, pp. 867-868.

GOLDMAN, M. and GOLDMAN, A.
"Corona Discharges",
in Gaseous Electronics, Vol. 1, Eds. Hirsh, M.N. and Oskam, H.J., Academic Press, N.Y., 1978, Chapter 4, pp. 219-290.

GORYUNOV, B.A.
"Dielectric strength of compressed sulphur hexafluoride and the electrode material and surface structure", Sov.Phys.Tech.Phys., Vol. 20, No.1, July, 1975, pp. 66-67.

HARRISON, M. and GEBELLE, R.
"Simultaneous measurement of ionization and attachment coefficients", Phys. Rev., Vol. 91, No. 1, July 1953, pp. 1-7.

HAZEL, R. and KUFFEL, E.
"Static field anode corona characteristics in sulphur hexafluoride", IEEE., Trans., PAS., Vol. 95, No. 1, Jan/Feb., 1976. pp. 178-186.

HEPWORTH, J.K., KLEWE, R.C. and TOZER, B.A.
"A model of impulse breakdown in divergent field geometries", J.Phys.D:; Appl. Phys., Vol. 5., 1972, pp. 730-740.

HEPWORTH, J.K., KLEWE, R.C., and TOZER, B.A.
"Calculation of electron avalanche growth towards an isolated sphere", Proc. 10th Int. Conf., on Phenomena in Ionized Gases, Oxford, 1971, pp.153.

HERTIG, G.E. and INGMAN, R.W.
"Fundamentals for the determination of EHV switching surge ratings", IEEE. Trans., PAS, Vol. 84, March, 1965, pp. 236-243.

HICKAM, W.M. and FOX, R.E.
"Electron attachment in sulphur hexafluoride using monoenergetic electrons", J.Chem. Phys., Vol. 25, No. 4, Oct. 1956, pp. 642-647.

HOWARD, P.R.
"Insulation properties of compressed electronegative gases", Proc. IEE., Vol. 104A, 1957, pp 123-138.

HUTZLER, B. and HUTZLER-BARR, D.
"Leader propagation model for predetermination of switching surge flashover voltage of long air gaps", IEEE. Trans., PAS, Vol. 97, No. 4, July/Aug., 1978, pp. 1087-1096.

IBRAHIM, O.E., and FARISH, O.
"Impulse breakdown and prebreakdown corona processes in SF_6 and SF_6/N_2 mixtures", In Christophorou, L.G. (ed.) "Gaseous Direlectrics II", Pergamon Press, 1980, N.Y., pp. 83-91.

ITOH, H., SHIMOZUMA, M., TAGASHIRA, H. and SAKAMOTO, S.
"Measurement of the effective ionization coefficient and the static breakdown voltage in SF_6 and nitrogen mixtures", J.Phys.D.: Appl.Phys., Vol., 12, 1979, pp. 2167-2172.

JONES, B.
"Switching surges and air insulation", Phil.Trans., Roy.Soc.Lond., A275, 1973, pp.165-180.

JONES, B. and ROSS, J.N.
"Simultaneous measurement of current and light in long sparks", 4th Int.Conf. on Gas Discharges, Swansea, Sept., 1976, IEE., Conf. Pub., No. 143, pp.291-294.

KARLSSON, P.W. and PEDERSEN, A.
"Inherent limitations in uniform field discharge data for SF_6", IEEE. Trans., PAS. Vol. 91, 1972, pp.1597-1601.

KAWAGUCHI, Y., SAKATA, K., and MENJU, S.
"Dielectric breakdown of sulphur hexafluoride in nearly unform fields", IEEE. Trans., PAS. Vol. 90, 1971, pp. 1072-1078.

KAGAGUCHI, Y. and MENJU, S.
"Breakdown characteristics of SF_6 in coaxial cylindrical electrodes", Elect.Eng. in Japan Vol. 90, No.5, 1970, pp. 197-203.

KEKEZ, M.M. and SAVIC, P.
"Subnanosecond schlieren study of the spark channel tip - part 1", Int.Conf. on Gas Discharges and their applications, Edinburgh, 1980, IEE. Conf., Pub., No. 189, pp.221-223.

KEKEZ, M.M. and SAVIC, P.
"A hypersonic interpretation of the development of the spark channel in gases", J.Phys.D.: Appl. Phys., Vol. 7, 1974, pp. 620-628.

KLINE, L.E. and SIAMBIS, J.G.
"Computer simulation of electron avalanches and streamers", Proc. IEEE. Vol. 59, 1971, pp. 707-709.

KLINE, L.E.
"Calculations of discharge initiation in overvolted parallel-plane gaps", J.Appl.Phys., Vol. 45, No. 5, May 1974, pp. 2046-2054.

KLINGBEIL, R., TIDMAN, D.A. and FERNSLER, R.F.
"Ionizing gas breakdown waves in strong electric fields", Phys. of Fluids, Vol. 15, No. 11, Nov. 1972, pp. 1969-1973.

KOPPTIZ, J.
"Nitrogen discharges of large cross section at high overvoltage in a homogeneous field", J.Phys.D.:Appl.Phys., Vol. 6, 1973, pp. 1494-1502.

KUFFEL, E. and ABDULLA, M.
"High voltage engineering", Pergamon Press, Oxford, 1979.

KURIMOTO, A., AKED, A., and TEDFORD, D.J.
"Prediction of the critical pressure in positive point/plane V_{50}, V_c/ pressure characteristics in air and SF_6", 5th Int. Conf. on Gas Discharges, Liverpool, 1978, IEE. Conf. Pub., No. 165, pp. 324-327.

KURIMOTO, A., DALE, S.J., AKED, A. and TEDFORD, D.J.
"Impulse discharge characteristics in long non-uniform field gaps in low pressure SF_6", Int. High Voltage Symp., Zurich, Sept, 1975, pp.349-354.

LES RENARDIERES GROUP,
Research on long air gaps, Electra, No. 35, 1974.

LLEWELLYN-JONES. F.
"Ionization and breakdown in gases", (Methuen), London, 1957.

LOEB, L.B.
"Streamer breakdown and sparking thresholds", Phys. Rev., Vol. 81, 1951,pp. 287.

LOEB, L.B. and MEEK, J.M.
"The mechanism of the electric spark", Stanford University Press, 1941.

LOEB, L.B.
"Electrical coronas their basic physical mechanisms", Univ. of California Press, Berkeley, 1965.

LOEB, L.B.
"Ionizing waves of potential gradient", Science, Vol. 148, No. 3676, June 1965, pp. 1417-1426.

LOEB, L.B.
"Basic processes of gaseous electronics", Univ. of California Press, 1961.

McALLISTER, I.W.
"The influence of electrode macroscopic curvature upon surface roughness effects in compressed SF_6", Archiv. fur Electrotechinic, Vol. 62, 1980, pp. 43-49.

MACALPINE, J.M.K. and COOKSON, A.H.
"Impulse breakdown of compressed gases between dielectric covered electrodes", Proc. IEE., Vol. 117, No. 3, 1970, pp. 646-652.

MALIK, N.H. and QURESHI, A.H.
"Non-uniform field breakdown in SF_6 and its mixtures with helium and nitrogen", 3rd. Int.Symp., on H.V.E., Milan, 1979, paper No. 31.03.

MALLER, V.N. and NAIDU, M.S.
"Sparking potentials and ionization coefficients in SF_6", Proc. IEE., Vol. 123, No. 1, Jan. 1976, pp. 107-108.

MARODE, E.
"The mechanism of spark breakdown in air at atmospheric pressure between a positive point and a plane. 1. Experimental : Nature of the streamer track", J.Appl.Phys., Vol. 46, No. 5, May, 1975a, pp.2005-2015.

MARODE, E.
"The mechanism of spark breakdown in air at atmospheric pressure between a positive point and a plane. II. Theoretical : Computer simulation of the streamer track", J.Appl.Phys., Vol. 46, No.5, May 1975(b), pp.2016-2020.

MASETTI, C., PIGINI, A. and PARMIGIANI, B.
"Influence of electrode characteristics on SF_6 corona inception conditions", Int.Conf. on Gas Discharges, A., IEE. Conf.Pub., No. 189, Edinburgh, 1980, pp.213-216.

MATTINGLEY, J.M. and RYAN, H.M.
"Potential and potential-gradient distributions for standard and practical electrode systems", Proc. IEE. Vol. 118, No. 5, May 1971, pp.720-732.

MEEK, J.M. and CRAGGS, J.D.
"Electrical breakdown of gases", Clarendon Press, Oxford, 1953.

MEEK, J.M. and COLLINS, M.M.C.
"Measurement of electric fields at electrode surfaces", Electronics Letters June 1965, Vol. 1, No. 4, pp. 110-111.

MEEK, J.M.
"A theory of spark discharge", Phy.Rev. Vol. 57, Apr.1940, pp.722-728.

MEEK, J.M.
"A theoretical determination of breakdown voltage for sphere gaps", J. of the Franklin Institute, Aug. 1940, Vol. 230, pp.229-242.

MEEK, J.M.
"The electric spark in air", JIEE., Vol. 89, part 1, 1942, pp.335-356.

McDANIEL, E.W.
"Collision phenomena in ionized gases", John Wiley and Sons, N.Y., 1964.

NASSER, E.
"Fundamentals of gaseous ionization and plasma electronics", John Wiley and Sons, N.Y., 1971.

NARBUT, P., BERG, D., WORKS, C.N., DAKIN, T.W.
"Factors controlling electric strength of gaseous insulation", Trans., AIEE., Vol. 78, Part 3, 1959, pp. 545-550.

NELSON, J.K., CHATTERTON, P.A., and BLOMQUIST, N.H.
"Corona stabilization in SF_6/N_2 mixtures under impulse conditions", in Christophorou, L.G. (ed.), Gaseous Dielectrics III, Pergamon Press, 1982, pp. 68-75.

NIEMEYER, L. and PINNEKAMP, F.
"Surface Discharge in SF_6", in Christophorou, L.G. (ed.) Gaseous Dielectrics III, Pergamon Press, 1982, N.Y., pp. 379-385.

NITTA, T. and SHIBUYA, Y.
"Electrical breakdown of long gaps in sulphur hexafluoride", IEEE. Trans., PAS. Vol. 90, June, 1971, pp. 1065-1071.

NITTA, T., YAMADA, N., FIJUIWARA,
"Area effect of electrical breakdown in compressed SF_6", IEEE. Trans., PAS. Vol. 93, No. 2, 1974, pp.623-629.

PEDERSEN, A.
"Criteria for spark breakdown in sulphur hexafluoride", IEEE. Trans., PAS. Vol. 89, No. 8, Nov/Dec. 1970, pp. 2043-2048.

PEDERSEN, A.
"Calculation of spark breakdown or corona starting voltages in non-uniform fields", IEEE. Trans., PAS. Vol. 86, No. 2, Feb. 1967, pp.200-206.

PEDERSEN, A.
"The effect of surface roughness on breakdown in SF_6", IEEE. Trans., PAS. Vol. 94, No. 5, Sept./Oct. 1975, pp. 1749-1754.

PENNEY, G.W. and HUMMERT, G.T.
"Photoionization measurements in air, oxygen and nitrogen", J.Appl.Phys., Vol. 41, No. 2. Feb. 1970, pp. 572-577.

PERLIN, A.S.
"Electrical discharge in nitrogen and sulphur hexafluoride in a uniform field", Sov.Phys.-Tech. Phys., Vol. 17, No. 5, Nov. 1972, pp.813-817.

PIGINI, A., RIZZI, G., and THIONE, L.
"influence of the gap geometry and impulse shape on leader characteristics", Electra, No. 53, 1977, pp. 51-60.

PIGINI, A., RIZZI, G., and BRAMBILLA, R.
"Dielectric behaviour of SF_6 in non-uniform fields near critical pressure", 7th Int. Conf. on Gas Discharges, London, 1982, pp. 203-206.

PINNEKAMP, F. (Private communication).

POLLOCK, H.C. and COOPER, F.S.
"The effect of pressure on the positive point-to-plane discharge in N_2, 0_2, CO_2, SO_2, SF_6, C Cl_2F_2, A, He, and H_2. Phy. Rev., Vol. 56, July, 1939, pp. 170-175.

RAETHER, H.
Zur entwicklung von kanalentladung, Arch. Electrotech Vol. 34, 1940, pp. 49-56.

RAETHER, H.
"Electron avalanches and breakdown in gases", Butterworths, London, 1964.

RAMSDEN, S.A. and SAVIC,.P.
"A radiative detonation model for the development of a laser-induced spark in air", Nature, Vol. 203, No. 4951, Sept. 19, 1964, pp. 1217-1219.

REES, J.A.
in Meek, J.M. and Craggs, J.D. (eds.), "Electrical Breakdown of Gases", John Wiley and Sons, Chapter, 1, 1978.

REIN, A., ARNESEN, A., and JOHANSEN, I.
"A statistical approach to the streamer breakdown criterion in SF_6", IEEE. Trans., PAS, Vol. 96, No.3, May/June, 1977, pp. 945-954.

REININGHAUS, W.
"Calculation of streamers in gaseous discharges", J.Phys.D.:Appl.Phys., Vol. 6, 1973, pp. 1486-1493.

RODRIGO, H. and CHATTERTON, P.A.
"Measurement of impulse positive point predischarge growth in 50% SF_6 50% N_2 gas mixtures.", 7th Int. Conf. on Gas Discharges, London, 1982, pp. 207-210.

ROSS, J.N.
"The diameter of the leader channel using Schlieren photography", Electra, No. 53, 1977, pp. 71-73.

RUHLING, F.
"Leader properties derived from channel diameter measurements", Electra, No. 53, 1977, pp. 67-73.

RYAN, H. McL.
"Electric field of a rod-plane spark gap", Proc. IEE., Vol. 117, No.1, Jan. 1970, pp. 283-284.

SAVIC, P. and KEKEZ, M.M.
"Subnanosecond Schlieren study of the spark channel tip - part III", Int. Conf. on gas discharges and their applications, Edinburgh, 1980, Pub. No. 189, pp. 224-227.

SHIBUYA, Y., YAMADA, N., NITTA, T.
"Electrical breakdown and prebreakdown dark current in compressed SF_6", 2nd. Int. Conf. on Gas Discharges, London, 1972, IEE. Conf. Pub., No. 90, pp. 320-324.

SUZUKI, T.
"Transition from the primary to the arc in positive point-to-plane corona", J.Appl.Phys. Vol. 42, No. 10, Sept. 1971, pp. 3766-3777.

SUZUKI, T.
"The determination of the diffusion rate of SF_6 into nitrogen", Trans. IEEE. Elect.Insul., Vol. EI-17, No. 1., Feb. 1982, pp. 34-38.

TAKUMA, T., WATANABE, T., KITA, K., and AOSHIMA, Y.
"Discharge development of long gaps in SF_6 gas", Int. Symp. on H.V.Tech., Munich, 1972, pp. 386-390.

TASSICKER, O.J.
"Boundary probe for measurement of current density and electric-field strength - with special reference to ionized gases", Proc. IEE., Vol. 121, No. 3, March, 1974, pp. 213-220.

TEICH, T.H. and BRANSTON, D.W.
"Light emission from electron avalanches in electonegative gases and nitrogen", Int. Conf. on Gas Discharges, London, Sept., 1972, IEE. Conf. Pub. No. 90, pp. 335-337.

TOWNSEND, J.S.
"Electricity in gases", Clarendon Press, Oxford, 1915.

VOSS, W.
"Discharge development of non-uniform gaps in SF_6-N_2 gas mixtures", 3rd. Int. Symp. on H.V.E., Milan, 1979, paper No. 31-13.

WARD, A.L.
"Calculations of electrical breakdown in air at near-atmospheric pressure", Phy. Rev. vol. 138, No. 5A, May 1965, pp. A1357-A1362.

WATANABE, T. and TAKUMA, T.
"The breakdown voltage and discharge extension of long gaps in nitrogen - SF_6 and air-SF_6 gas mixtures", J.Appl.Phys., Vol. 48, Aug. 1977, pp. 3281-3287.

WATERS, R.T.
"Fluxmeter measurements in rod-plane and sphere-plane gaps", Electra, No. 53, 1977, pp. 73-85.

WATERS, R.T.
in Meek, J.M. and Craggs, J.D. (eds.), "Electrical Breakdown of Gases", John Wiley and Sons, Chapter 5, 1978.

WATERS, R.T.
"Breakdown in non-uniform fields", Proc. IEE., Vol. 128, Pt. A, No. 4, May, 1981, pp. 319-325.

WORKS, C.N. and DAKIN, T.W.
"Dielectric breakdown of sulphur hexafluoride in non-uniform fields", AIEE Trans., Vol. 72, Part 1, Nov. 1953, pp. 682-689.

WRIGHT, J.K.
"A contribution to the theory of impulse corona and the long spark", Proc. Roy. Soc., A Vol. 280, 1964, pp. 23-36.